EXPERIMENTAL TESTING, ANALYSIS, AND STRENGTHENING OF REINFORCED CONCRETE PIER CAPS BY EXTERIOR POST TENSIONING

Presented to
The Academic Faculty

By

Curtis John O'Malley

In Partial Fulfillment
Of the Requirements for the Degree
Doctor of Philosophy in Civil Engineering

Georgia Institute of Technology

August, 2011

EXPERIMENTAL TESTING, ANALYSIS, AND STRENGTENING OF REINFORCED CONCRETE PIER CAPS BY EXTERIOR POST TENSIONING

Approved by:

Dr. Bruce R. Ellingwood, Co-Advisor
School of Civil and Environmental Engineering
Georgia Institute of Technology

Dr. Lawrence F. Kahn
School of Civil and Environmental Engineering
Georgia Institute of Technology

Dr. Abdul-Hamid Zureick, Co-Advisor
School of Civil and Environmental Engineering
Georgia Institute of Technology

Dr. Kenneth M. Will
School of Civil and Environmental Engineering
Georgia Institute of Technology

Dr. Russell T. Gentry
School of Architecture
Georgia Institute of Technology

Date Approved: 5/2/2011

I dedicate this thesis to my wife Dr. Laura Jacobs-O'Malley, for all her help and encouragement throughout graduate school, as well as to my parents John and Marlyne, and brothers Ryan and Mark for their encouragement throughout my education.

ACKNOWLEDGMENTS

The research presented herein was funded by the Georgia Department of Transportation.

I would like to thank my advisors Dr. Bruce Ellingwood, and Dr. Abdul-Hamid Zureick, whose help and advice made this research possible. I would also like to thank my committee member for their direction; Dr. Kenneth Will, Dr. Lawrence Kahn, and Dr. Russell Gentry.

I would also like to thank my fellow graduate students at Georgia Institute of Technology, who assisted in this experimental research; Naiyu Wang, Laura Jacobs, Andrew Bechtel, Robert Moser, Jonathan Hurff, Kennan Crane, Amal Ray Jayapalan, Carlyn Krapf, Christine Allen, Masahiro Kurata, and Tim Wright.

TABLE OF CONTENTS

LIST OF FIGURES

LIST OF TABLES

SUMMARY

Condition assessment of existing concrete bridge pier caps shear capacity using the simplified procedure for non-prestressed sections of the AASHTO LRFD Bridge Design Specification has caused the Georgia Department of Transportation (GDOT) to post a large number of bridges in the State of Georgia. Posting of bridges disrupts the free flow of goods within the region served by the bridge and has a negative economic impact. To prevent structural deterioration, diagonal cracking or failure of concrete pier caps in shear, the GDOT employs an in situ strengthening technique that utilizes an external vertical post-tensioning system. However, the fundamental mechanics of this system and its effectiveness under service load have not been examined previously.

This research examines the behavior of reinforced concrete pier caps that utilize the above strengthening system in a combined analytical and experimental program. In the experimental part of the study, two groups of full-scale reinforced concrete deep beam specimens were tested. The first group consisted of six deep beam tests with shear span/depth ratios of approximately 1.0, which is typical of bridge pier caps; of these six tests, two included the external post-tensioning system. In the second group, nine deep beam tests were performed that included a segment of the column representing the pier; four of those tests included the external post-tensioning system. The tests revealed that the shear capacity computed using the AASHTO LRFD Bridge Design Specifications strut and tie provisions provided a conservative estimate of the specimen capacity in all but one case when compared to the experimental results. However, the AASHTO strut and tie provisions were found to provide a much closer assessment of the load carrying mechanism in the pier cap than the general shear provisions, in that they were able to predict the load at which yielding of the tension reinforcement occurred as well as the angle of the compression strut. The presence of the column segment in the second group had a significant impact on the failure mechanism developed in the specimen near

ultimate load. The stress concentration at the reentrant corner between the pier cap and column interface served as an attractor for the formation of diagonal shear cracks, a mechanism not observed in previous deep beam tests in shear. The research has led to recommendations for improving the design of pier caps and the external post-tensioning system, where required, based on mechanics which is consistent with the results of the experimental program.

This research program demonstrated that the behavior of a composite pier cap and column differed significantly from the behavior of a deep beam or even a non-composite pier cap and column. This observation is significant since the majority of existing experimental data on the behavior of deep beams has been obtained from tests conducted on simply supported deep beams in either three or four point bending. In contrast, this program showed that failures of the pier cap specimens were governed by the interaction of the pier cap and column. In addition, the success of the external post tensioning system was due to its ability to shift the location of the diagonal compression strut away from the reentrant corner at the pier cap and column interface. It was concluded from the pier cap tests that for any rehabilitation or strengthening technique to be effective at increasing the strength and/or ductility of similar pier caps it must address the presence of the stress concentration at the reentrant corner where the pier cap and column meet. Any strengthening technique that is focused only on increasing the shear resistance of the pier cap would have a minimal effect on the ultimate capacity of the pier cap-column assembly.

CHAPTER 1. **INTRODUCTION**

1.1 Background

Of the approximately 9,000 bridges listed in the State of Georgia's Bridge Inventory Management System (BIMS) Database (as of October, 2005), over 2,000 bridges were listed as being posted to limit the maximum permitted truck loading. The economic costs of posting a bridge are related to the number of vehicles affected by the posting and the amount of time lost to detours. These costs can be quite large, especially along roads having large volumes of truck traffic. Problems arising from deteriorated bridge infrastructure are not unique to Georgia, but are prevalent throughout the United States.

Thirty percent of GDOT bridges in the BIMS database list their design live load as H-10 or H-15 loads (Figure 1.1), which are both less than half of the current legal loads stipulated for today's roads and highways. An additional nine percent of GDOT bridges are recorded to have been designed with the HS-15 or H-20 load (Figure 1.1), which are between fifty-five and seventy-five percent of the current legal loads stipulated for today's roads and highways. The transition in Georgia to the current design loads HS-20 (Figure 1.2) and HS-20-44 (Figure 1.2 and 1.3) was an incremental process beginning in approximately 1945, with new bridges in industrial or developed regions, while lighter design loads continued to be used for bridges in less developed regions of the state. The HS-20-44 design load represents the typical HS-20 load in conjunction with an alternate military loading comprised of two 12-ton axial loads 4 feet apart (Figure 1.3). Due to extensive urban development and expansion over the years, the HS-20-44 design load now is required for the entire State of Georgia. Figure 1.4 shows the percentage of bridges currently in service that were design in each decade over the last 100 years. Over one third of the bridges currently in service were constructed during the 1950 and 1960's when smaller design load were in used. In addition less internal shear

reinforcement was required during this time frame than is currently required, by the AASHTO LRFD Bridge Design Specifications (2007). The changes to the shear reinforcement requirements in the bridge design specifications are outlined in Chapter 4. While the design loads are used to design new bridge structures, the actual posting of a bridge structure generally is determined based on the state's legal loads. The legal loads represent the allowable vehicle weights and configurations; for Georgia, these legal loads are represented by Figure 1.5. The fact that the HS-20 and legal loads are twice as heavy as the H-15 load for which many structures were designed prior to the 1960's (Figure 1.4), coupled with the deterioration of bridge structures during their years of service and limited budgets for repair or replacement of transportation infrastructure in many states, has forced the posting of many bridge structures.

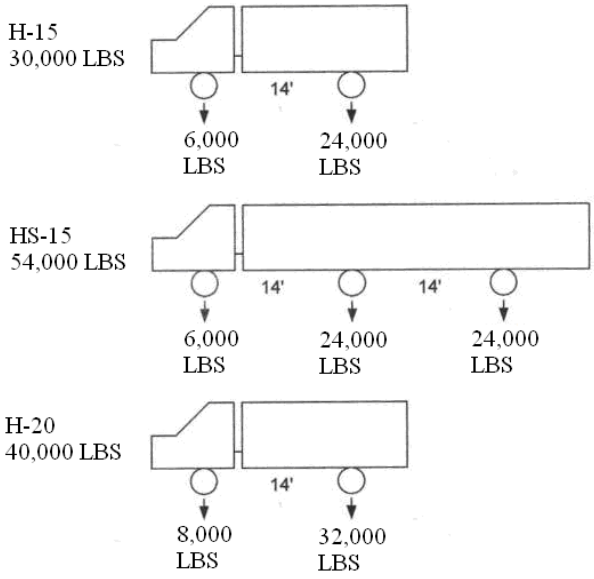

Figure 1.1 Design loads used prior to HS-20 loading vehicle (Tonias and Zhao, 2007)

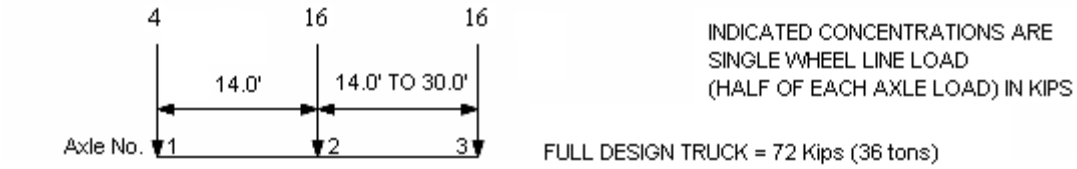

Figure 1.2 HS-20 rating vehicle (AASHTO 1994)

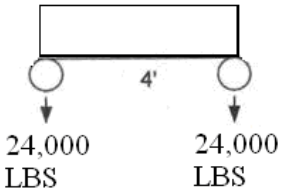

Figure 1.3 HS-20-44 (HS-20+mod) additional load case (Tonias and Zhao, 2007)

For the purposes of reporting bridge ratings in BIMS, a bridge structure is broken into three categories. These are 1) the superstructure consisting of the girders, 2) the deck consisting of the deck pavement and sidewalks, and 3) the substructure consisting of the foundation, piers, piles, pier caps, and abutments. The focus of this dissertation is on the pier caps in the substructure. The GDOT provided a database of the results of analyses performed on the substructure components of 5,715 Georgia bridges. Of these 5,715 bridges, 805 (or 37% of the total number of posted bridges in the state) were found to require posting due to perceived deficiencies in the shear resistance of one of the bridges pier caps. These 805 pier caps were found to be deficient when evaluated using the *AASHTO Manual for Condition Assessment of Bridges* (1994), despite the fact that many had apparently performed adequately over the past several decades. Thus, shear capacity of pier caps represents a very significant concern in terms of bridge rating.

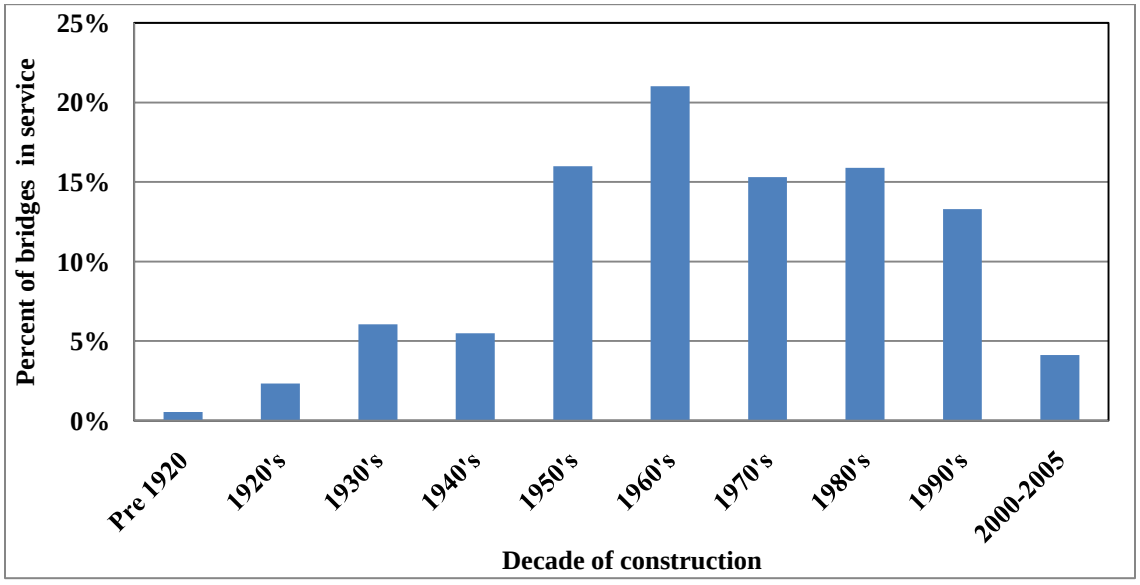

Figure 1.4 Bridges constructed by era (GDOT, 2005)

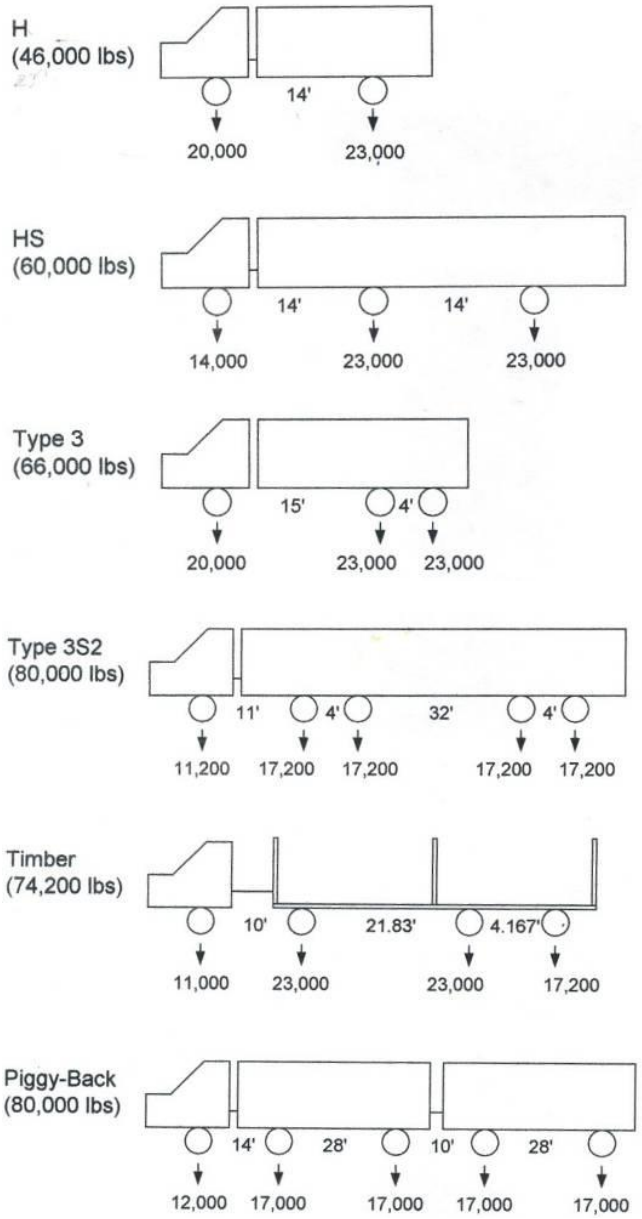

Figure 1.5 Georgia legal loads (GDOT, 2005)

A prior GDOT-sponsored research study (Ellingwood, et. al., 2009) focused on improving the overall bridge rating process through a combination of experimental, analytical and statistical analyses. Recent findings (Ellingwood, et. al. 2009) suggested that Article 5.8.3.4.1 AASHTO (1994) shear resistance estimate of reinforced concrete pier caps is likely to underestimate the shear resistance of typical bridge pier caps. The

ratings using AASHTO (1994) Article 5.8.3.4.1 were found to underestimate the shear resistance of three reinforced concrete pier caps (GDOT bridges 085-0018[1], 083-0016[2], 097-0032[3]) when compared to the results of a nonlinear finite element analyses of the pier caps, validated by a field load test of bridge 085-0018 (Ellingwood, et. al. 2009).

Tang and Tan (2004) found that for ratios of shear span to beam effective depth (a/d) from 0.27 to 0.81, the shear resistance predicted by ACI is between 29 and 51 percent of the reported experimentally determined shear resistance. Recognizing this conservatism has the potential to greatly reduce the number of bridges posted within the State of Georgia and allow the reallocation of funds for repair and replacement to those bridges in the worst condition.

1.2 Research objective and scope

The research described in this dissertation consists of an experimental study to evaluate the effectiveness of the state of Georgia's strengthening technique through a combination of experimental and analytical analysis. The GDOT strengthening technique consists of external post-tension stirrups applied to the region of the pier cap that is found to be deficient by a GDOT bridge rating analysis in terms of its shear capacity. A bridge pier cap is determined to have a shear strength deficiency based on a rating analysis of the pier cap performed by a GDOT bridge engineer. A bridge pier cap can also be determined to be deficient by the presence of diagonal cracking of the pier cap observed by a GDOT bridge inspector. This study evaluated the capacity of the test specimens using the strut and tie analysis as per Article 5.6.3 of the AASHTO LRFD Bridge Design Specifications 2007. The test specimens included both specimens that did and did not meet the internal shear reinforcement requirements of AASHTO (2007)

[1] 085-0018 is a multi span four steel girder bridge supported by a reinforced concrete pier cap designed in 1963

[2] 083-0016 is a multi span five steel girder bridge supported by a reinforced concrete pier cap designed in 1959

[3] 097-0032 is a multi span four steel girder bridge supported by a reinforced concrete pier cap designed in 1960

Article 5.13.2.3, which are required to evaluate a beam with the provisions of Article 5.6.3. Specimens that did not meet the minimum shear reinforcement requirement of AASHTO 2007 were included in the study to determine if Article 5.6.3 could be used to evaluate existing pier caps that do not meet current specifications. Two types of specimens were tested: "deep beam" specimens consisting of 24 in. deep beams, and "pier cap" specimens that consisted of a 36 in. deep beam and an 18 in. long column stub. These two specimen types were tested to identify any effect that the interface between the beam and the column had on the behavior and failure of the structure. A system intended to strengthen damaged pier caps using exterior post-tensioned stirrups was also evaluated during this study. This strengthening technique was evaluated in terms of the increase in the pier cap shear capacity as well as reduction of crack propagation.

The focus of this study was on those pier caps where the shear span was equal to or less than the depth of the pier cap. The research was conducted in two experimental phases, designed to gauge the behavior of pier caps and evaluate the effectiveness of the proposed external post-tensioning system at increasing the load carrying capacity of the specimens. The first phase consisted of six deep beam tests on three specimens intended to validate the experimental procedures. The second phase was intended to assess the behavior of full size pier caps, and evaluate the performance of the post-tensioning system on pier caps specimens with various levels of internal shear reinforcement.

1.3 Organization of dissertation

Chapter 2 of this thesis summarizes current practice as it pertains to the shear strength assessment of deep reinforced concrete beams. Previous work on reinforced concrete deep beam and short shear span testing, as well as the various pertinent code provisions, is considered. This work was used to identify the key parameter of this study such as shear span to depth ratio, reinforcement ratio, overall depth and amount of shear reinforcement.

Chapter 3 presents the design and implementation of the first set of experimental tests. This initial study was undertaken to validate the experimental and instrumentation techniques utilized for the remainder of the research effort. This initial set of experiments highlighted the need for further consideration of the beam-column interface. The experiments in Chapter 3 also evaluate the effect of various anchorage techniques on the capacity and behavior of the specimen. The three techniques evaluated were 180 degree hooked bars, bars with threaded Lenton Terminators, and bars with anchorage provided by welding steel plates to their ends.

The design of the second set of experimental tests is presented in Chapter 4, as well as the instrumentation scheme, and procedures followed during each test. The chapter presents the analysis conducted to reduce the pier cap structure to a single span simply supported beam with a column stub. The experiments were designed to evaluate the effectiveness of the external post-tensioning system on pier caps with and without internal shear reinforcement.

Chapter 5 describes the experimental results of the pier cap specimens and effect of external post-tensioning on the behavior of such specimens.

Chapter 6 discusses the various AASHTO analysis techniques used to analyze the pier cap and deep beam specimens, and highlights the strengths and shortcoming of each.

Chapter 7 presents the results, conclusions and recommendations based on the experimental and analytical work performed in this study.

CHAPTER 2. STRUCTURAL BEHAVIOR AND RESEARCH ISSUES

2.1 Behavior of deep reinforced concrete beams in shear

Typical reinforced concrete pier caps have shear span-to-depth ratios (a/d) below 1.5 and may be classified as deep beams. Kani (1964) found that over a range of a/d from 2.5 to 1.0, the load transfer mechanism in beams transitioned from "beam behavior" to arch behavior where the load was transferred through the specimen by a concrete arch in compression. Kani's (1964) tests show that the capacity of the arch mechanism is larger than the beam mechanism when the a/d ratio is "small" (less than 2.5). In a later study, Kani (1967) observed that the mechanical behavior and the resulting failure load of RC beams loaded in shear changed drastically with the magnitude of the member's depth, and that, "the 48 in. beams, when compared to the corresponding 6 in. beams, have a reduced safety factor of up to 40 percent." Kani concluded from his studies that the three primary factors important to deep beam behavior were longitudinal reinforcement ratio, a/d ratio, and member depth, and suggested a strength reduction factor keyed to these member parameters. In order for any mechanics-based modeling technique to provide a consistent factor of safety, then, it must account for the effects of these three factors when computing the resistance of the member.

The ACI-ASCE Committee 426 (1973) approach of modeling beams in shear, which utilizes the "truss analogy," forms the basis of the shear model presented in the load factor design portion of the fifteenth edition of the Standard Specifications for Highway Bridge Design (AASHTO, 1992) and in the AASHTO LRFD Bridge Design Specifications (2004), summarized in Eq. 2.1-2.3:

$$V_n = V_c + V_s + V_P \qquad \text{Eq. 2.1}$$

$$V_c = 0.0316\beta\sqrt{f_c'}\,b_v d_v \qquad \text{Eq. 2.2}$$

$$V_s = \frac{A_v f_y d_v (\cot\theta + \cot\alpha)\sin\alpha}{s} \qquad \text{Eq. 2.3}$$

$V_P =$ shear resistance due to prestressing (kips)
$\beta =$ Factor indicating ability of diagonally cracked concrete to transmit tension as specified in Article 5.8.3.4
$f_c^{'} =$ concrete compression strength (ksi)
$b_v =$ effective width (inches)
$d_v =$ shear depth (inches)
$A_v =$ area of shear reinforcement (inches^2)
$f_y =$ yeild strength of tension reinforcement (ksi)
$\theta =$ least angle between the diagonal compression strut and tension reinforcement (degrees)
$\alpha =$ angle betwen tension steel and shear steel (degrees)
$s =$ spacing of shear reinforcement (inches)

The governing assumption in flexure that plane sections remain plane does not hold true in the tied arch behavior exhibited by deep reinforced concrete members, Tan and Cheng (2006) claim that, "Arch action is not a shear transfer mechanism as defined by ACI Committee 426 (1973), 'it does not transmit a tangential force to a nearby parallel plane.' Thus, the conventional definition of ultimate shear strength of V/(bd) is inappropriate for deep beams, where V is the ultimate shear force, b the beam width and d the effective depth." As a result, methods like equation 2.1-2.3 which do not account for the a/d ratio and longitudinal reinforcement ratio, are based on an assumed failure mode other than the arch behavior exhibited by beams with a/d ratios less than 2.5. As a result of assuming the wrong failure mechanism, the mechanics behind such strength assessment methods do not represent the mechanics of deep beams with a/d ratios less than 2.5.

In summarizing the past 40 years of shear behavior research, Collins (2007) found that the assumption that the shear resistance of members without stirrups, as defined by Eq. 2.4:

$$V_c = 2\sqrt{f_c'}\, b_v d_v \qquad \text{Eq. 2.4}$$

$f_c^{'} =$ concrete compression strength (psi)
$b_v =$ effective width (in.)

$d_v = \text{shear depth (in.)}$

"Can lead to unsafe designs and can lead engineers to make decisions that inadvertently increase the chances of a brittle shear failure." Collins (2007) recommends the use of the Modified Compression Field Theory (MCFT), as an alternative to the Committee 426 approach, to ensure that structures that experience an overload "fail in a ductile flexural mode rather than a brittle shear mode." The Modified Compression Field Theory (MCFT) was developed by Vecchio and Collins (1986) to address flaws in existing shear capacity models. The MCFT is a mechanics based model where stress strain characteristics were developed for cracked concrete in terms of average stress and average strains. The method is similar to the compression field theory except that it includes the tensile stresses within the concrete regions between cracks (Vecchio and Collins 1986). A form of the MCFT method has been adopted in the AASHTO LRFD Bridge Design Specifications (2004), Article 5.8.3.4.2. The MCFT identifies the point at which the breakdown in beam action occurs, and not the capacity of "the remaining arch" (Kani 1967) that forms in deep beams once shear cracking occurs.

The strut and tie method (STM) differs from the MCFT in that it treats the concrete and steel reinforcement separately. The reinforcement is treated strictly as tension ties and the concrete as compression struts. The regions where these struts and ties intersect are referred to as nodal zones. Using this model, it is possible to break down any reinforced concrete structure into a series of tension and compression members that transfer the applied loads through the member to the supports. Both the Tang and Tan (2004) and Tan and Cheng (2006) studies recommended their own variations of the strut and tie model (STM), each of which was intended to account for the size effect and tied arch behavior of deep reinforced concrete beams.

The STM proposed by Tang and Tan (2004) differs from the STM presented in Article 5.6.3 (AASHTO LRFD 2007) in that it utilizes a Mohr-Coulomb failure criterion

to relate the interaction of the transverse tensile strain that causes splitting of the concrete struts and the compressive strain that causes crushing of the concrete struts. Tang and Tan (2004) utilized the results of three experimental studies - Tan (1995), Smith and Vantsiotis (1982), and Kong et al. (1970, 1972a, b) - to evaluate their model against the ACI 318-99 code (ACI 1999), the 1994 CSA code (CSA 1994), and CEB-FIP MC90 (CEB-FIP 1993). In their study, the safety factors used in each method were set equal to unity. Both the CSA and CEB codes have adopted a form of the STM that does not account for the interaction of compressive strain and transverse tensile strain in the diagonal compression strut; that interaction is included in Tang and Tan's model. The experimental studies to which the analysis models were compared included deep beam specimens with internal web reinforcement in the horizontal, vertical, and diagonal directions as well as specimens without internal web reinforcement. Tang and Tan demonstrated that their model produced estimates of structural capacity that were well correlated to the experimental data. In all three experimental studies, the mean of the ratio of experimental to computed capacity was between 1.1 and 1.32 and the COV in that ratio was between 0.086 and 0.116. Tang and Tan's method was shown to have a lower mean and COV than the traditional ACI approach or the CSA method in all three studies. However, they were lower than for the CEB method only when the beams utilized in Kong's experimental work were considered.

Tan and Cheng (2006) subsequently found that the primary cause of the size effect exhibited by deep reinforced concrete beams was that the calculation of shear resistance based on V/(bd), does not account for the tied arch behavior of deep reinforced concrete beams and that the STM can properly account for that behavior. They also discovered secondary causes of the size effect that included the geometry and boundary conditions of the struts. Their modifications to the STM were then able to account for these secondary size effects. Tan and Cheng evaluated their modified STM against earlier experimental work [Tan (2003), Tan et al. (1999), and Kani (1967)], showing that

their method resulted in a lower mean and COV as compared to both the CSA, and unmodified STM; however they did not compare their STM to either ACI or AASHTO procedures.

A comparison of seven of the most common reinforced concrete shear resistance models was done by Somo and Hong (2006), where each method was used to evaluate members from an experimental database of 1146 beams including members both with and without web reinforcement. This study provided a basis of comparison between the different analytical methods using the largest possible collection of experimental results. The mean and COV of the ratio of experimental to predicted capacity computed for each analytical model differed from the results of other studies that utilized smaller sets of experimental beams, which included the experimental results used to develop each method (Tang and Tan 2004, Tan and Cheng 2006). The seven methods analyzed by Somo and Hong (2006) included:

1) The ACI method where V_c is defined by Eq. 11-3 of ACI 318-05

$$V_n = V_c + V_s \qquad \text{Eq. 2.5}$$

$$V_c = \left(\sqrt{f_c'} \Big/ 6 \right) b_w d \qquad \text{Eq. 2.6}$$

$$V_s = min \left(\begin{matrix} A_v f_{yv} d \Big/ s \\ 2\sqrt{f_c'} b_w d \Big/ 3 \end{matrix} \right) \qquad \text{Eq. 2.7}$$

f_c' = concrete cylinder compression strength (MPa)
b_w = web width (mm)
d = shear depth (mm)
A_v = area of shear reinforcement (mm^2)
f_{yv} = yeild strength of shear reinforcement (MPa)
s = spacing of shear reinforcement (mm)

2) The ACI method where V_c is defined by Eq. 11-5 of ACI 318-05

$$V_n = V_c + V_s \qquad \text{Eq. 2.8}$$

$$V_c = min\begin{pmatrix} b_w d\dfrac{\left(\sqrt{f_c'}+120\rho_w min\left(1,{}^{V_u d}/_{M_u}\right)\right)}{7} \\ 0.3 b_w d\sqrt{f_c'} \end{pmatrix} \qquad \text{Eq 2.9}$$

$$V_s = min\begin{pmatrix} {}^{A_v f_{yv} d}/_{s} \\ 2\sqrt{f_c'} b_w d/_{3} \end{pmatrix} \qquad \text{Eq. 2.10}$$

f_c' = concrete cylinder compression strength (MPa)
ρ_w = longitudinal reinforcement ratio
V_u = web width (N)
M_{u} = web width (Nmm)

3) The CSA simplified method

$$V_n = V_c + V_s \qquad \text{Eq. 2.11}$$

$$V_c = 0.2\lambda\phi_c\left(\sqrt{f_c'}\right)b_w d \qquad \text{Eq. 2.12}$$

$$V_s = min\begin{pmatrix} \left(\frac{260}{1000+d}\right)0.2\lambda\phi_c\sqrt{f_c'} b_w d \\ 0.1\lambda\phi_c\sqrt{f_c'} b_w d \end{pmatrix} \qquad \text{Eq. 2.13}$$

Or

$$V_s = min\begin{pmatrix} {}^{\phi_s A_v f_{yv} d}/_{s} \\ 0.8\lambda\phi_c\sqrt{f_c'} b_w d \end{pmatrix} \qquad \text{Eq. 2.14}$$

f_c' = concrete cylinder compression strength (MPa)
λ = low density concrete factor
ϕ_c = 0.6 cast in place concrete, 0.65 precast concrete
ϕ_{s} = 0.85 for reinforcing steel

4) The MCFT, as defined by the R2K computer software program (Bentz 2000)

5) The shear friction model, as defined by (Loov 1998) and (Peng 1999)

$$V_{af} = \begin{pmatrix} 0.93\left(f_c'\right)^{0.22} b_w h\sqrt{{}^{h}/_{a_{cle}}} \\ 1.93\left(f_c'\right)^{0.11}\sqrt{{}^{b_w h A_v f_{yv} d_s}/_{s}} - A_v f_{yv} \end{pmatrix} \begin{matrix} without\ stirrups \\ with\ stirrups \end{matrix} \qquad \text{Eq. 2.15}$$

f_c' = concrete cylinder compression strength (MPa)
d_s = effective length of stirrups (mm)
a_{cle} = distance between point load and inner edge of bearing (mm)

6) The shear friction model, as revised by Loov, (Somo and Hong 2006)

$$V_{af} = min\{V_{45} \tan\theta + \varphi_s f_{yv} n\} \quad \text{Eq. 2.16}$$

$$V_{45} = \beta_v \lambda \varphi_c \sqrt{f_c'} b_w h V_{cf} + A_v f_{yv} n \quad \text{Eq. 2.17}$$

$$\beta_v = 0.36(30/f_c')^{0.25}(500/h)^{0.25} \quad \text{Eq. 2.18}$$

f_c' = concrete cylinder compression strength (MPa)
λ = effective length of stirrups (mm)
ϕ_c = concrete resistance factor
ϕ_s = steel stirrup resistance factor
n = number of stirrups cutting the failure plane
θ = angle of inclination of the failure plane

7) Zsutty's method (Zsutty 1968 and 1971)

$$V_{rZ} = V_s + V_{cZ} \quad \text{Eq. 2.19}$$

$$V_{cZ} = \begin{cases} 5.343\left(f_c' \rho_w\right)^{1/3} (d/a)^{4/3} b_w d & a/d < 2.5 \\ 2.137\left(f_c' \rho_w d/a\right)^{1/3} b_w d & a/d \geq 2.5 \end{cases} \quad \text{Eq. 2.20}$$

f_c' = concrete cylinder compression strength (MPa)
ρ_w = concrete resistance factor

Somo and Hong (2006) concluded that the method with the lowest COV is Zsutty's method when all beams are considered and that the R2K method is slightly better in terms of COV for beams with web reinforcement. Zsutty's method is based on a regression analysis that includes all three of the specimen parameters found to be important by Kani (1967): the a/d ratio, overall depth, and reinforcement ratio. Somo and Hong (2006) found that the mean of the ratio of experimental to predicted capacity in all seven methods was reduced when Kani's tests, which comprise 28% of the experimental database, are ignored. However, they do not provide sufficient data on the specific beams that were included in their study to identify the key differences between

the specimens tested by Kani and all other experiments; nor do they state any reason for excluding these experimental results from the data set. However, since all seven models produce lower COVs when Kani's experimental work is ignored, it is possible that the missing parameter, or parameters (a/d ratio, reinforcement ratio, or depth) in these mechanics models is founded in one of the member parameters heavily present in Kani's tests. The study by Somo and Hong does not specify which beams from each set of experiments were used in their assessment of the seven analysis techniques, so it is not possible to identify which of the three parameters is heavily present in Kani's tests. A possible cause of the observed difference is in accounting for the a/d ratio. Somo and Hong (2006) found that all of the models performed better when the a/d ratio was greater than 2; in many of Kani's tests, a/d is less than 2. However, Somo and Hong (2006) do not quantify exactly what range of a/d ratios or total heights are considered in their experimental database, or which studies had beams with a/d ratios less than 2.

2.2 Deficiencies in the current experimental database

NCHRP Report 549 (Hawkins et al. 2005) deals with simplified shear design provisions and identifies several deficiencies in the current state of research with regard to the behavior of concrete members subjected to shear. Hawkins et al. (2005) noted a lack of detailed information in the existing experimental literature about the performance of reinforced concrete members prior to shear failure. Current analytical methods were developed from laboratory tests aimed at determining only the ultimate shear resistance. As a result, most experimental work is not useful for evaluating member behavior, other than at ultimate capacity, or for determining the validity of behavior models over a complete range of loads. Consequently, it is uncertain whether pier caps evaluated using such behavior models will perform adequately at their intended legal load levels. It is worth noting that the formation of inclined cracking may occur at loads less than the legal loads. Therefore, a study of the behavior of reinforced concrete pier caps prior to

reaching the ultimate limit state of resistance is warranted to evaluate the performance of existing methods such as STM, and those used by AASHTO. While the appropriate remediation measure should depend on the safety margin against ultimate failure under the rating load, this margin is currently impossible to determine from the current AASHTO analysis models or their supporting databases. Hawkins et al. (2005) also identified gaps in the existing experimental work on shear behavior of members noting, in particular, a lack of data on behavior of large members, members with support conditions other than simply supported, members which support continuous loads, and members in which failure occurred in regions of the beam other than adjacent to the supports.

The pier caps that make up the focus of the present study fall into two of the four categories identified by Hawkins as lacking sufficient experimental work. Typical pier cap designs consist of members with depths and widths between 24 and 36 in. and as such fall into the category of large members. Additionally these members are often continuous over the piers or columns that support them, putting them in the second area of limited study. The pier cap test specimens also differ from previous deep beam experimental studies due to the inclusion of a composite column, in which the reentrant corner introduced a discontinuity in the region of maximum shear.

2.3 Recent experimental testing

Aguilar et al. (2002) compared four reinforced concrete deep beams designed using the ACI 318-99 code and the strut and tie provisions from Appendix A of the ACI 318-02 code. While provisions found in these codes differ from those found in the AASHTO specifications, they are based on the same theory. Therefore, the results of this experimental testing gives some insight into the type of behavior that can be expected when comparing AASHTO's simplified shear design procedure (article 5.8.3.4.1 AASHTO 2004) to the strut and tie design (article 5.6.3 AASHTO 2004). Each of the

beams tested by Aguilar et al. (2002) was unique in its design; the first was detailed using Eq. 2.1 (ACI 318-99) and anchored the tension reinforcement with threaded anchors. The other three beams were all designed using the strut and tie method as defined in Appendix A of ACI 318-02. One beam used threaded terminators, one used hooked ends, and the third used hooked ends but omitted most of the shear reinforcement. The ultimate capacity of each of the beams was within 6% of each other except for the beam designed by the STM with threaded anchors; however, the effective depth of this beam was 2 ½-inches less than that of any of the other designs. While size effects result in a reduction in the ratio of computed to experimental capacity when comparing shallow beams (12 inches) to deep beams (36 inches), this effect is negligible when comparing 28 5/8 to 31 1/8 inch beams. In the case of these test specimens where the shear span was constant and the depth reduced, the reduced angle of inclination of the compression strut resulted in a larger percentage of the force in the compression strut in the horizontal direction. Consequently the yield strength of the horizontal tension reinforcement was reached at a lower load which accounts for the reduced capacity of the specimen. Aguilar et al. (2002) found that the strut and tie method produced a prediction of ultimate resistance that was closer to the experimental capacity than the empirical equations of ACI 318-99 (Eq. 2.1). The specimen where most of the shear reinforcement was eliminated only resulted in a 1% decrease in capacity. This indicated the inaccuracy of any empirical method that defines a shear resistance component V_s, such as Eq. 2.3, when considering the behavior of deep beams with short shear spans.

The specimens tested as part of the study by Aguilar et al. (2002) exhibited concrete crushing in the region of flexural compression in addition to the diagonal shear cracking. Since the capacity and behavior of the nodal regions limit the capacity of the diagonal compression strut, for the purposes of this study, it is necessary to replicate the pier cap boundary conditions as accurately as possible.

2.4 External post-tensioning retrofit

Replacing all bridges with apparent pier cap deficiencies is not feasible from a cost standpoint, especially when the remainder of the structural elements in many of the bridges are performing adequately. Thus, it is necessary to devise techniques for strengthening these deficient structures. The current strengthening technique employed by the GDOT for increasing the shear resistance of pier caps is an external post-tensioning system. This method consists of mounting a pair of steel channels on the top and bottom of the deficient pier cap and using them to anchor a pair of post-tensioned threaded rods (Figure 2.1).

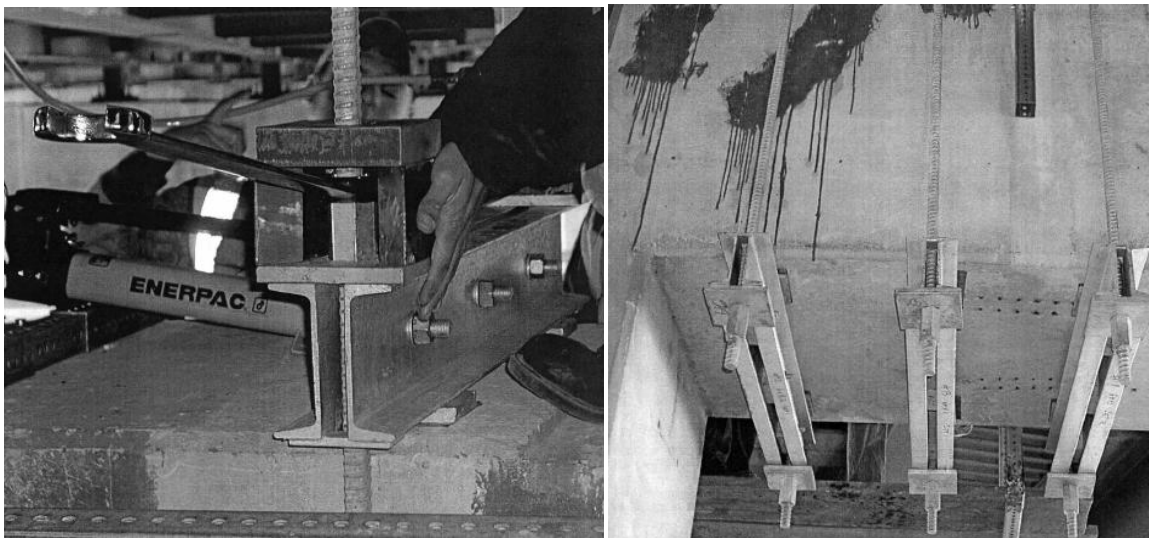

Figure 2.1 Post-tensioning system installation (GDOT, 2005): Top view of pier cap (left), Bottom view (right)

The post-tensioning system acts as an exterior stirrup that effectively reduces the inclined tension strains carried by the concrete in the beam by inducing compressive strains into the beam throughout its height. While this concept is theoretically sound, an experimental program is needed to develop and validate analytical tools for assessing the performance of this technique, and recommend improvements. The work of Zhang et al. (2004), while done on externally bonded fabric, found that as the a/d ratio decreased, the effectiveness of vertical reinforcement decreased. This observation can be justified by

examining the mechanics by which the load is carried from the girder through the pier cap and into the supporting column. As the column and girder get closer together, the load path becomes nearly vertical. As a result, the direction of principal compression stress within the pier cap will approach vertical and the direction of principal tension stress will approach horizontal. In this case, the addition of an external post-tensioning force will do little to reduce the tensile strains and, in the case of extremely small a/d ratios, may even increase the principal compression and tension strains. Zhang et al. (2004) did find external reinforcement to be effective if it was either horizontal or inclined.

A recent GDOT pier cap repair project included the use of this post-tensioning system. The design utilized 1 in. dia. ASTM A733 Grade 150 threaded bars, and C6x10.5 ASTM A572 Grade 50 channels (Figure 2.1). Two pairs of channels were bolted together to form the horizontal legs of the post-tensioned system, while the threaded bars were tensioned between them to form the vertical legs of the assembly (Figure 2.2). The post-tensioning system was designed by computing the total factored live and dead load shear V_u across the pier cap. The total post-tensioning force required was computed by subtracting the shear resistance provided by the concrete V_c (Eq. 2.2) and the internal stirrups V_s (Eq. 2.3) from the factored load V_u. The post-tensioning force was then divided out among the external post-tensioning bars within the shear span.

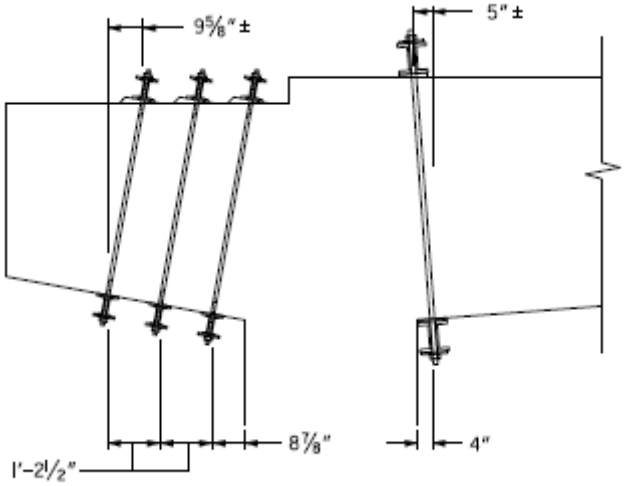

Figure 2.2 Post-tensioning system (GDOT, 2005)

Considerable experimental work focused on strengthening reinforced concrete pier caps for lateral loading has already been undertaken. Among the methods employed in these studies are post-tensioning of the reinforced concrete pier cap (Bollo, 1990), where retrofit techniques were tested on a three span segment of an existing bridge, including post-tensioning of each pier cap and external column shear reinforcement. The study presented in this report however focused solely on increasing the vertical shear resistance of the pier cap, rather than the lateral resistance for the pier cap and column structure. While the study by Bollo did not achieve a significant increase in lateral stiffness it did increase the strength of the structure and the displacement ductility. Since one of the key objectives of this pier cap retrofit study is to develop methods for increasing pier cap shear resistance, the Bollo study offers experimental justification for exploring the effect of post-tensioning of the pier cap on the vertical shear resistance of reinforced concrete pier caps. A second study by Saatcioglu (2003) evaluated the shear strengthening of rectangular and circular reinforced concrete bridge columns using post-tensioning strands. This method succeeded in increasing the ductility and lateral drift capacity of the reinforced concrete columns to the point where shear no longer governed the capacity of the column. Furthermore, external pre-stressing of concrete members is

recognized as a viable seismic shear strengthening retrofit, but one that requires further research according to the Federal Highway Administration's (FHWA) Seismic Retrofitting Manual (1995).

2.5 Serviceability evaluation of retrofitted and un-retrofitted pier caps

Based on the findings of Aguilar et al. (2002), it can be expected that changing the internal or external shear reinforcement of a deep beam, such as a pier cap, will not result in an increased ultimate capacity. However, the pier cap tests in this work include a segment of the column in addition to the pier cap itself. The addition of the column makes it possible to shift the compression node at the beam-column interface up into the column resulting in a larger effective depth, which could increase the specimen capacity. However the introduction of the composite column segment also creates a stress concentration that could reduce the capacity of the compression strut. Application of the post-tensioning retrofit shifts the compression strut away from the stress concentration at the corner of the beam column interface, preventing it from reducing the capacity of the compression strut. It is also under investigation whether the creation and widening of shear cracking can be delayed through post-tensioning of the shear span. Schiessl and Raupach (1997) found that with sufficient cover and concrete quality, cracks smaller than 0.3 to 0.5 mm did not affect long term corrosion rates of steel reinforcement.

CHAPTER 3. **DEEP BEAM EXPERIMENTS**

Three deep beam specimens were designed and tested in the first phase of the experimental program to examine the performance in shear of deep members with shear span to depth ratios (a/d) of 1.26 to 1.29. The primary purpose of these tests was to validate the proposed testing procedures intended to be used in a later phase of the program through comparison to previously established work and to establish instrumentation and experimental testing protocols before undertaking the pier cap testing presented subsequently in Chapter 4. The tests presented in this chapter were also intended to evaluate three different means of providing the anchorage necessary to develop the yield strength of reinforcement in pier cap specimens with short a/d ratios. Three anchorage techniques were considered: 180 degree hooked bars, bars welded to a 1 inch steel plate, and a proprietary threaded anchor system (Lenton Terminators). Two of the tests conducted in this section also included an external post-tensioning system currently in use by the Georgia Department of Transportation (GDOT) as a means of rehabilitating damaged pier caps.

3.1 Deep beam specimen design

The specimens discussed in this chapter were modeled after typical reinforced concrete pier caps constructed for the GDOT during the 1950s and 1960s. The key pier cap details collected from examining GDOT drawings are presented in Table 3.1. In the drawings reviewed, the spacing of the shear reinforcement in the shear span of the pier cap varied between 6 and 18 inches.

Table 3.1 Typical pier cap details circa 1950-60's

	Depth (inches)	Width (inches)	f'_c (ksi)	Tension Reinforcement	
				Ratio	Bar size
Typical Range 1950-1960	**30 - 48**	**30 - 48**	**3 - 3.5**	**0.85 - 1.25%**	**No. 9 - No. 11**

Kani's (1967) experimental work showed that beams with the same depth and reinforcement ratio but with different widths behave similarly. Accordingly, the widths

of the three deep beam specimens were reduced to 12 inches. The test specimens were designed to be loaded asymmetrically and each end's shear capacity tested independently (Figure 3.1 and 3.2), with a different stirrup configuration at each end. The first end (designated E1) of each beam had internal shear reinforcement provided by three No. 3 stirrups spaced 12 inches on center in the test shear span (Figure 3.1). The shear span is defined here as the distance from the center of the support to the center of the load plate. The second end (designated E2) of the beam had no internal shear reinforcement (Figure 3.2).

One 10 foot 6 inch long beam was used to test each anchorage type, with tests being performed on both ends of some specimens. The design details of each of the specimens are presented in Table 3.2. The specimen ID identifies the anchorage type: welded plate (WP), 180 degree hook (H), and Lenton Terminator (LT).

Table 3.2 Specimen details

	w (in)	h (in)	d (in)	a/d	f'_c (ksi)	Shear reinf.	Longitudinal reinforcement	
Specimen ID						f_y (ksi)	ρ	f_y (ksi)
WP	12	24	21	1.26	3.5	40	1.24%	60
LT	12	24	21	1.29	3.5	40	1.24%	60
H	12	24	21	1.29	3.5	40	1.24%	60

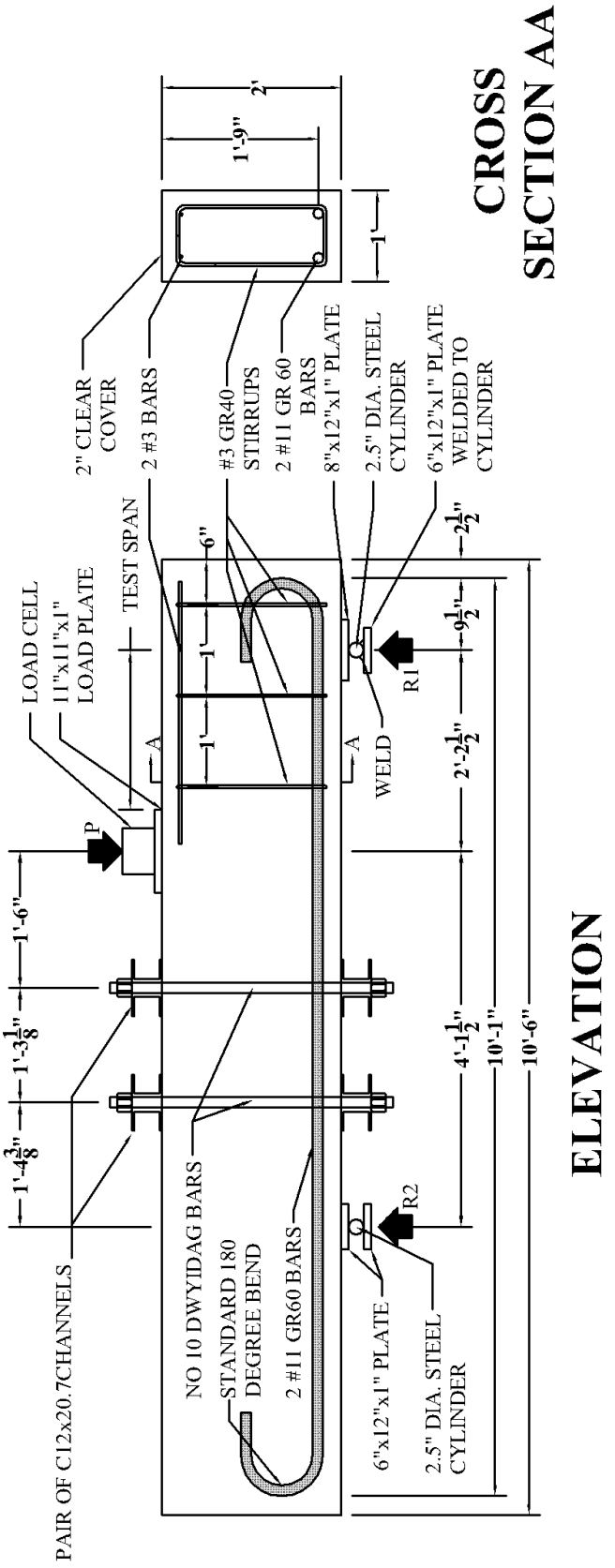

Figure 3.1 Test configuration end E1

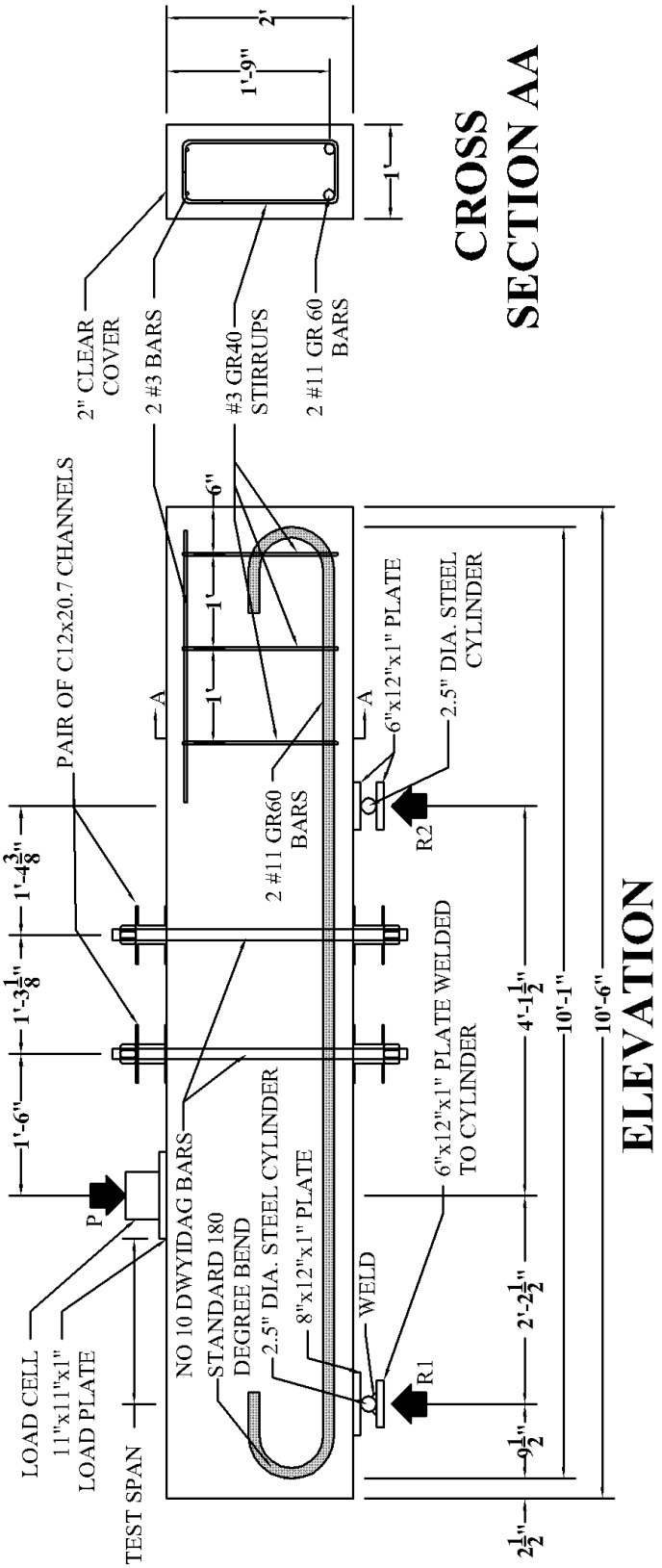

Figure 3.2 Test configuration end E2

3.2 Deep beam specimen material properties

Tests were performed on the tension reinforcement and the concrete used in the construction of the three specimens to determine material strength and stiffness. During the tension tests the strain in the bar was measured by an extensometer, and used in conjunction with the applied load to compute the elastic modulus of the No. 11 bars used as tension reinforcement E_s = 28,890 ksi**.** The average yield stress of the two bars tested was 68.8 ksi (68.81, 68.69). Concrete cylinder compression tests and split cylinder tests were performed on the day of each experiment in order to determine the properties of the concrete for use when comparing the analysis results with the experimental behavior of each specimen. The concrete compression and tension strength on the day of each test are presented in Table 3.3. The tests are labeled WP, LT or H depending on the anchorage type, E1 or E2 depending on the end of the specimen being tested, and PT if the specimen was post-tensioned prior to testing.

Table 3.3 Material properties

Test ID	f'_c (psi)		f_t (psi)		f_y (ksi)
	Cylinder test	Average	Cylinder test	Average	
WP-E1	3150	3,580	526	490	68.8
	3752		452		
	3471		-		
	3957		-		
WP-E1-PT	4161	3,830	474	407	
	3854		340		
	3472		-		
WP-E2	3427	3,320	382	393	
	3025		404		
	3504		-		
LT-E1	4095	3,710	462	455	
	3604		447		
	3426		-		
H-E1	3263	3,420	496	506	
	3301		517		
H-E1-PT	3686		-		

3.3 Deep beam specimen test procedure

The specimens were designed to be simply supported and loaded asymmetrically so that one end experienced higher shear and failed first, allowing for the beam to be rotated and the second end tested. The test spans labeled in Figures 3.1 and 3.2 are the spans in which the specimen failure was designed to occur. However, during the experiments, more damage than was expected was observed in the end of the specimens between the load "P" and support reaction "R2" in Figure 3.1 and 3.2, resulting in a need to alter the geometry of the test configuration from the initial design. As a result, each test maintained a shear span to depth ratio (a/d) of 1.26-1.29 in the test shear span, and altered the length of the span between "P" and "R2".

Prior to each test, the center segment of the beam was externally reinforced in an attempt to limit the level of damage experienced by the specimen outside of the intended test region. The external reinforcement was comprised of No. 10 DYWIDAG bars[4] positioned vertically on each side of the beam and anchored to a pair of channels on the top and bottom of the beam. Each set of DYWIDAG bars was post-tensioned to carry the anticipated shear experienced by the beam between the load "P" and the support "R2". A statics analysis of the beam shows that for the structure shown in Figure 3.1 an applied load of 185 kips would result in a reaction at the left support "R1" of 65 kips. As a result, the vertical force required of each pair of DYWIDAG bars in order to carry the full shear in the span was 65 kips. Therefore, each of the two DYWIDAG bars were post-tensioned to 32.5 kips of force prior to loading the specimen. The 1 ¼ inch DYWIDAG bars were post-tensioned to 17.3% of their ultimate strength. The 1 ¼ inch bar were used because they were readily available at the Georgia Institute of Technology along with the equipment to post-tension them. The 17.3% of ultimate strength does not represent a target percentage of the ultimate strength of the bar but was used in the case of these

[4] DYWIDAG bars refers to reinforced concrete post-tensioning bar system developed by the German construction company Dyckerhoff & Widmann AG

experiments because it resulted in the desired total post-tensioning force, additionally the force in the bars was monitored so any changes in the post-tensioning would be known.

3.4 Deep beam specimen instrumentation design

The design of the instrumentation for the deep beam tests was aimed at identifying an effective means of monitoring the performance of deep members for use during the pier cap tests presented subsequently in Chapter 4. In order to model the load carrying mechanisms of the deep beam specimens and validate the strut and tie method's (STM) ability to predict the capacity of the specimens, several response quantities needed to be measured. The first response parameter monitored was the strain in the horizontal tension tie comprised of two No. 11 reinforcing bars, as shown in Figure 3.1. The second parameter was the angle of the compression strut. Additionally, an attempt was made to monitor the strain profile through the depth of the specimen. Since the purpose of the instrumentation was to identify the most appropriate instrumentation techniques for the subsequent pier cap tests, the instrumentation was changed from one test to the next. This section details the instrumentation technique used for the first test. The section describing each successive test will identify any differences in the instrumentation layout from the first test.

The instrumentation used during the first experiment included strain gauges mounted on the reinforcing bars (SG_s), and on the surface of the concrete (SG_c). The gauges on the reinforcing bars were installed by grinding the surface of the bars, epoxying the gauges and then coating the gauge with a wax waterproofing. The concrete surface mounted gauges were installed by grinding the surface, leveling it with epoxy, and epoxying the gauge to the leveled surface. Figure 3.3 shows the location of the gauges on the bars and on the concrete surface. Gauges SG_c 1-9 were mounted on one face of the beam while 10-18 were mounted on the opposite face; similarly gauges SG_s 1-4 were mounted on one bar and 5-8 are mounted on the other. The strain gauges mounted

on the bars were located to monitor the strain in the bar beneath the load "P" (SG location 1) and the development of the bar through the shear span (SG location 2). The surface mounted rosettes, consisting of a horizontal and two diagonal strain gauges, were used to compute the direction of principal strain throughout the testing process and to define the angle of the primary compression strut.

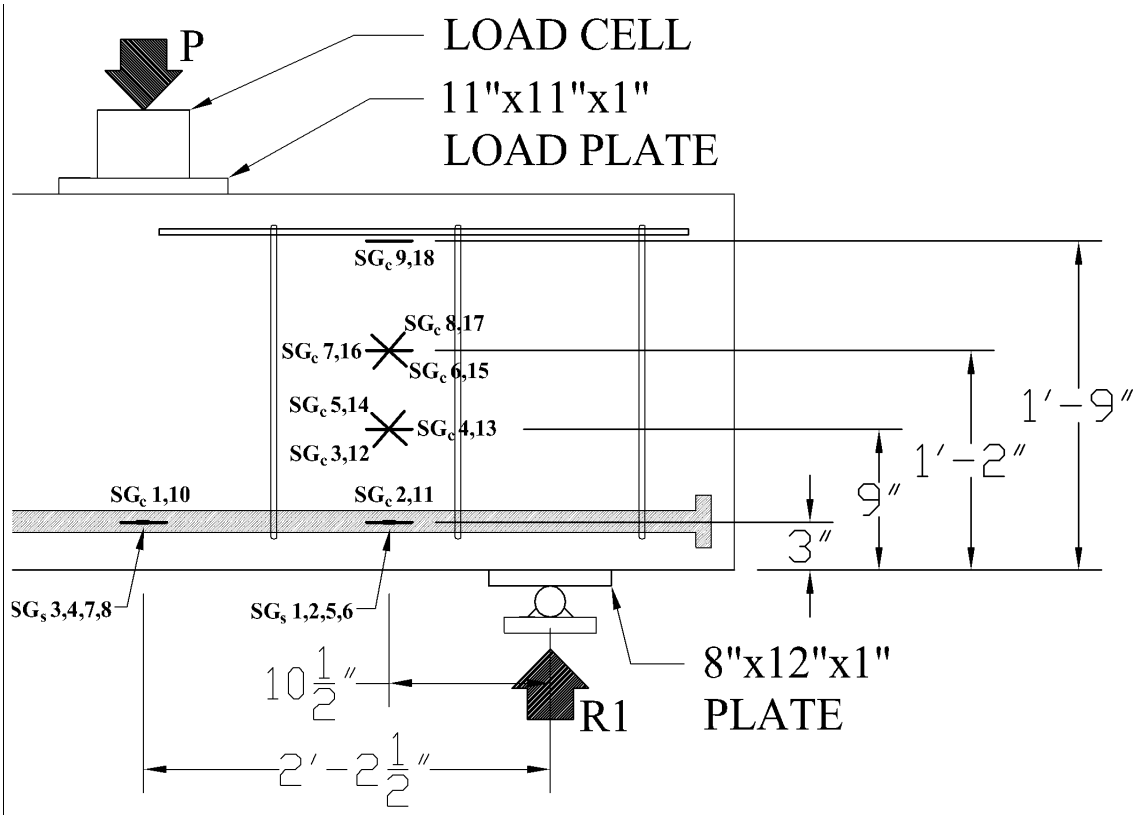

Figure 3.3 Experiment WP-E1 and WP-E1-PT SG locations

Surface-mounted linear variable differential transformers (LVDTs) were also used during the first experiment in many of the same locations as the strain gauges in order to identify the most effective, efficient, and reliable way of monitoring the beams behavior. The location of these gauges is illustrated in Figure 3.4. During the first experiment the LVDTs were attached by drilled mechanical anchors. A string potentiometer and a dial gauge were also mounted below the specimen directly under the load "P" to measure the displacement of the specimen.

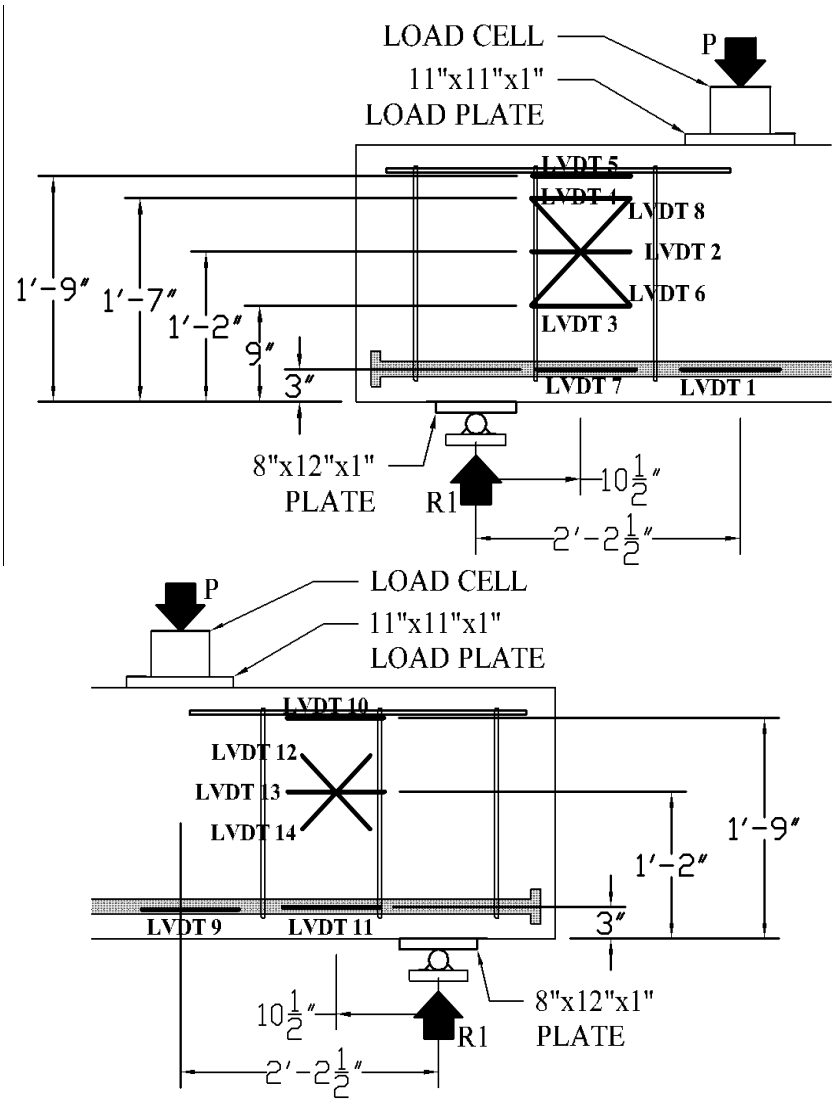

Figure 3.4 Experiments WP-E1 and WP-E1-PT LVDT locations

3.5 Test WP-E1

The first experiment, WP-E1, was performed on the beam with rebar anchorage provided by a single steel plated welded to the end of both No. 11 bars (Figure 3.5). The test end (E1) of the beam included No. 3 stirrups at 12 inch spacing. The beam was loaded to 202 kips, corresponding to a shear "R1" of 131 kips. The strain in the tension reinforcement when the test was stopped was of 0.002, which is below the yield strain of 0.00238. Due to the significant cracking of the specimen, and the intention to retest the specimen with the post-tensioning system the test was stop at a shear of 131 kips, before

the damage to the specimen was too severe to rehabilitate. This test provided a damaged specimen, which subsequently was rehabilitated and retested in Test WP-E1-PT.

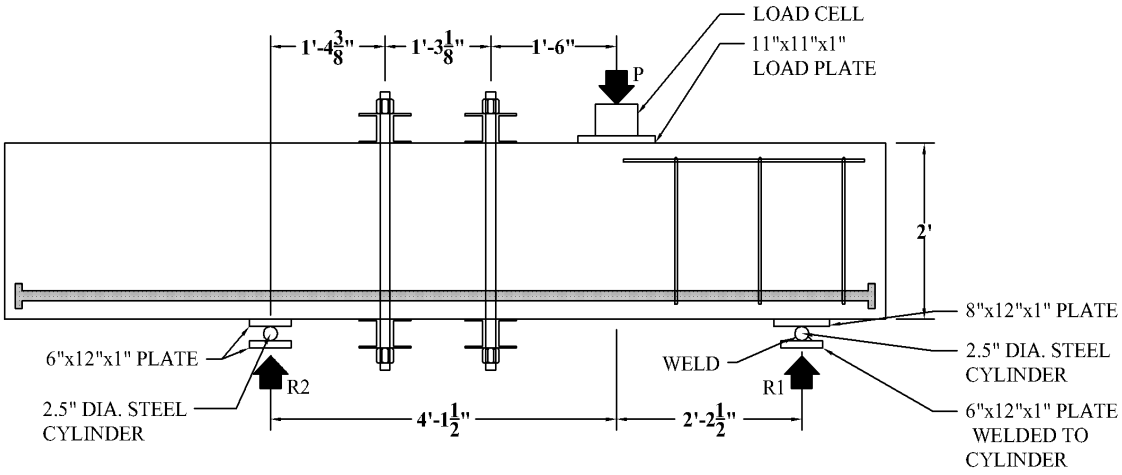

Figure 3.5 Experiment WP-E1 configuration

3.5.1 Instrumentation used during test WP-E1

The instrumentation used is outlined in Figure 3.3 and 3.4. During this test the noise levels in the response of the LVDTs and potentiometer were larger than the measured response. As a result, the filtering process was enhanced for future tests.

All measured and computed responses in this section (displacement, strain, angle of inclination of the compression strut, and crack width) are plotted against the shear in the test span "R1" (Figure 3.5), as defined by the shear transferred through the specimen between the applied load "P" and the support "R_1." For test WP-E1, the shear V is related to the applied load "P" through the geometry of the test setup shown in Figure 3.5 (Eq. 3.1).

$$V = R_1 = P\frac{49.5\ in.}{76\ in.} \qquad \text{(Eq. 3.1)}$$

3.5.2 Displacement of the specimen during test WP-E1

The shear in the test span is plotted against the deflection measured by the dial gauge below the location of the load plate in Figure 3.6. Figure 3.6 shows the displacement of the specimen and the permanent set but not the unloading, due to the fact

that the load was released too quickly to take reading during the unloading. The change in slope of the displacement response in Figure 3.6 that occurs between a shear of 40 and 60 kips coincides with the observed shear cracking of the specimen. Once this shear crack forms, the specimen experiences permanent set and does not return to its initial position after unloading. In this test, the permanent set was 0.07 inches.

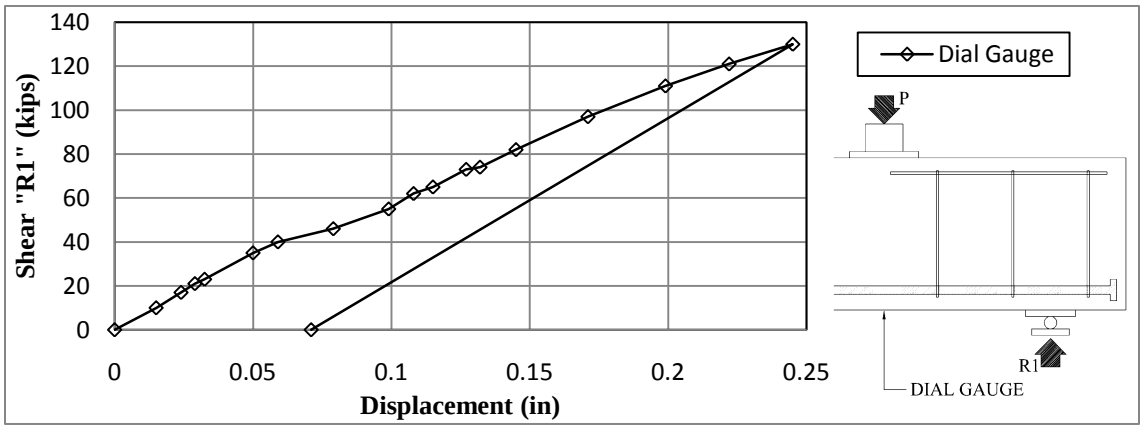

Figure 3.6 WP-E1 displacement response

3.5.3 Strain in the longitudinal reinforcement during test WP-E1

The average measured strain in the tension reinforcement at SG location 1 (SG 3, 4, 7, and 8 Figure 3.3) and SG location 2 (SG 1, 2, 5, and 6 Figure 3.3) in Figure 3.7 and the strain response during the experiment is plotted in Figure 3.8. These average strain measurements show that once diagonal shear cracking of the specimen occurs, constant strain is developed in the horizontal tension reinforcement from beneath the load "P" to the support "R1". This finding is in agreement with the behavior assumed by the strut and tie method, in which it is assumed that tension ties develop and carry a constant force between adjoining nodes (AASHTO 2007 Article 5.6.3). Since the reinforcing bars that make up the tension tie in question remained elastic throughout this test, the force in the bar can be computed using the average measured strain, elastic modulus, and area of the bars.

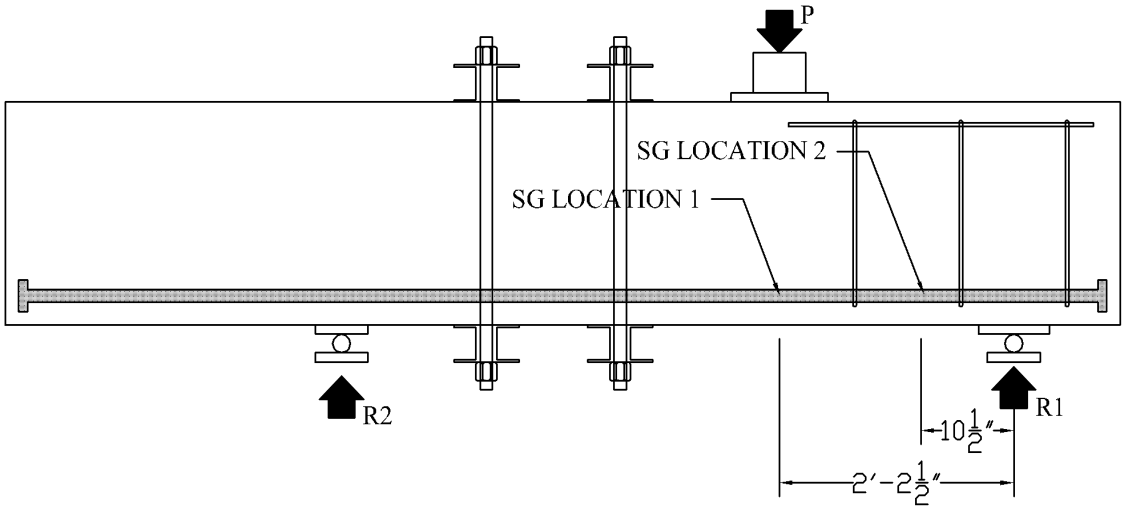

Figure 3.7 Tension reinforcement strain gauge locations

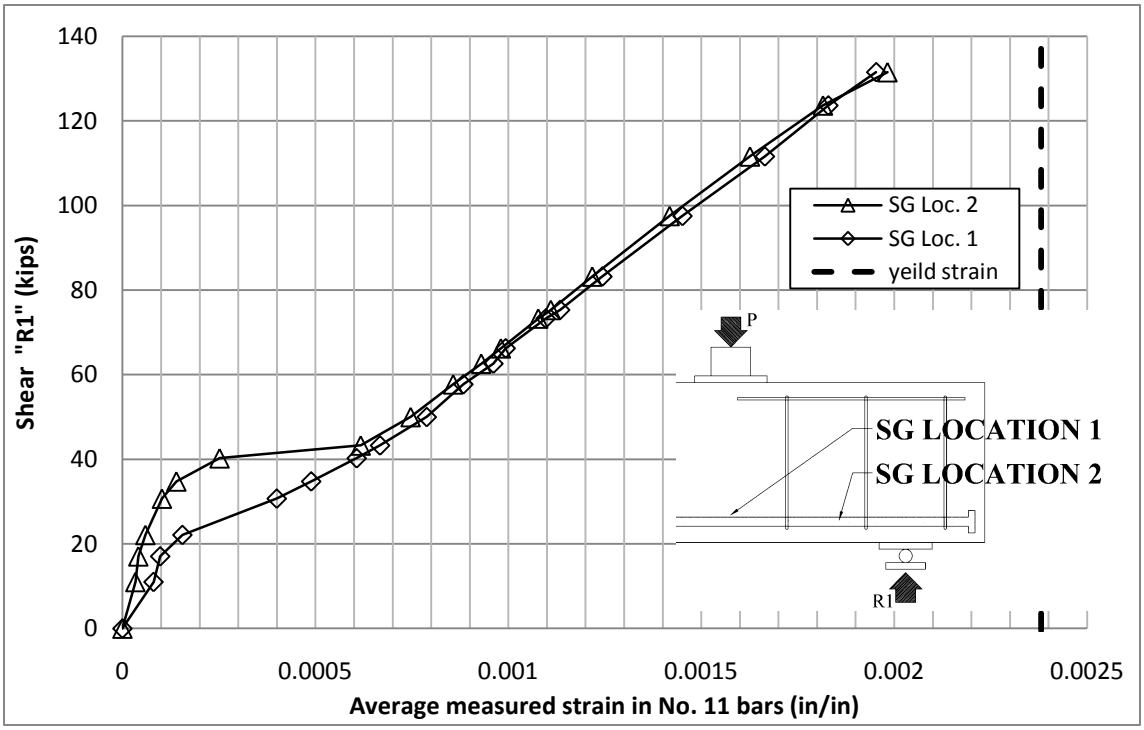

Figure 3.8 WP-E1 average strain measurements in tension reinforcement

3.5.4 Angle of inclination of the compression strut during test WP-E1

The angle of inclination of the compression strut was computed from the measured responses with two approaches. The first approach utilized the three strain readings from SG and LVDT rosettes to compute the angle of principal compression

strain. During the first experiment there was a problem with the LVDT instrumentation so only the SG rosette responses were used to compute the principal compression strain angle. The second approach was to compute the angle of the compression strut directly from statics, using the shear in the span "R1" and the force in the tension reinforcement "T" (Eq. 3.2). The force in the tension reinforcement was computed from the measured strain in the reinforcement at SG location 1 and SG location 2 (Figure 3.7) as follows:

$$T = \epsilon_{SG} E A_s \qquad \text{(Eq. 3.2)}$$

$\epsilon_{SG} = average\ measured\ strain\ in\ the\ reinforceing\ bar$

$E = 28{,}890\ ksi\ (Section\ 3.2)$
$A_s = area\ of\ No.11\ rebar = 1.27\ in^2$

There were four strain gauge rosettes mounted on the specimen (Figure 3.3). Two sets of strain gauge rosettes were placed on each side of the specimen, the first 9 inches and the other 14 inches from the bottom of the beam. Equation 3.3 was used to compute the angle of principal compression from the three strain components with respect to longitudinal plane of the specimen. The results of this analysis are illustrated in Figure 3.9.

$$\theta = \frac{1}{2}\tan^{-1}\left(\frac{\varepsilon_A - 2\varepsilon_B + \varepsilon_C}{\varepsilon_A - \varepsilon_C}\right) + 45° \qquad \text{(Eq. 3.3)}$$

$\varepsilon_A = strain\ gauge\ at\ 45°\ (paralell\ to\ compression\ strut)$
$\varepsilon_B = horizontal\ strain\ gauge\ reading$
$\varepsilon_C = strain\ gauge\ at\ -45°\ (perpendicular\ to\ compression\ strut)$

The angle of principal compression strain was also computed using the average strain measured in the tension reinforcement at locations 1 and 2 (Figure 3.7). This average strain was computed by averaging the measured strain in each of the No. 11 reinforcing bars. The principal compression strain angle was computed from the average

strain at each location, using Eq. 3.4, in which V is the shear in the test span, E_s is the elastic modulus measured during bar tests (E=28,890 ksi), A_s is the area of the tension reinforcement, and ε_s is the average measured strain in the tension reinforcement. The angle of principal compression strain computed using these measurements is presented in Figure 3.10.

$$\theta = \tan^{-1}(V/(\varepsilon_s E_s A_s)) \quad \text{(Eq. 3.4)}$$

V =Shear in the test span ("R1")
A_s = Area of longitudinal reinforcement
E_s = Elastic modulus of longitudinal reinforcement
ε_s = Average measured strain in longitudinal reinforcement location 1 and 2 Figure 3.8

The principal compression strain angle computed from the surface mounted strain gauge rosettes (Figure 3.9) was highly dependent on the location of the rosette with respect to the diagonal tension cracks, and was also affected by the inhomogeneity of the concrete. As a result there is significant variation between the four strain gauge rosettes; however the average angle computed from the four rosettes is similar to that predicted by the strut and tie analysis and illustrated in Figure 3.10. Each of the angle calculations produced an angle of principal compression strain that decreased from 90 degrees to between 33 and 43 degrees. This is due to the fact that tied arch behavior did not govern the load transfer mechanism of the specimen until shear cracking of the specimen occurred at a shear of approximately 40 kips, and the diagonal compression strut formed.

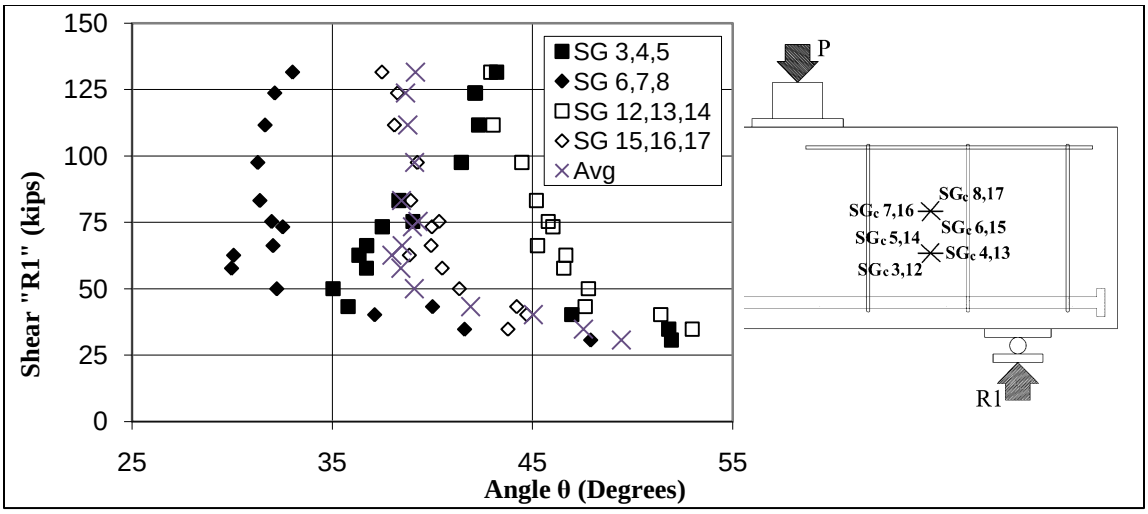

Figure 3.9 WP-E1 principal compression angle (SG rosettes)

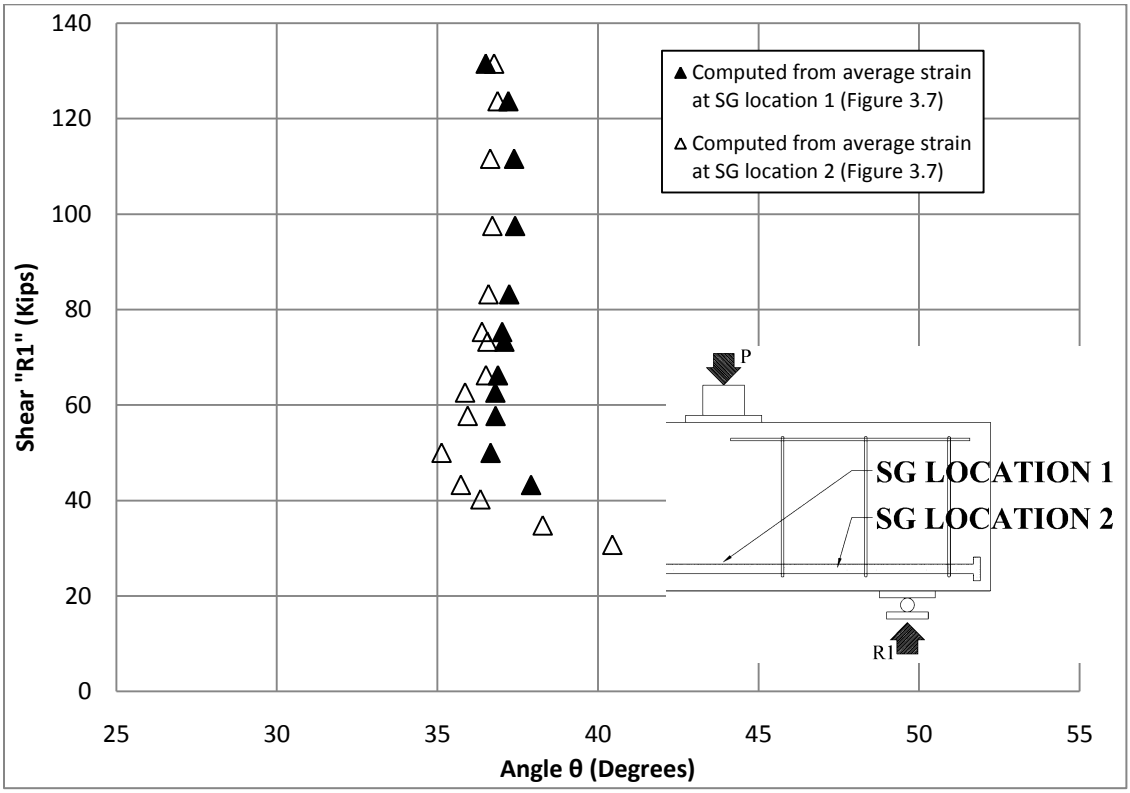

Figure 3.10 WP-E1 principal compression angle (SG bars)

3.5.5 Strain profile during test WP-E1

Strain profiles were developed using the strain gauges mounted on the concrete surface and the internal tension reinforcement. These profiles were located at the half-way point in the shear span between the column and support, 10.5 inches from the

support (Figure 3.11). Figure 3.11 illustrates a representative strain profile prior to cracking of the specimen. This profile was recorded when the shear in the test span was 20 kips, and appears to be approximately linear. Once cracking of the specimen occurs at a shear of approximately 40 kips, a tied arch mechanism is formed. This tied arch results in a constant strain in the tension tie between the load "P" and support "R1" (Figure 3.8), and changes the height of the centroid of the horizontal compression force between the load and support. This changing height of the centroid of horizontal compression force along the length of the specimen between the load and support, results in a non-linear strain profile through the depth of the specimen. Figure 3.12 illustrates the strains recorded at the centerline of the shear span at a shear of 73 kips.

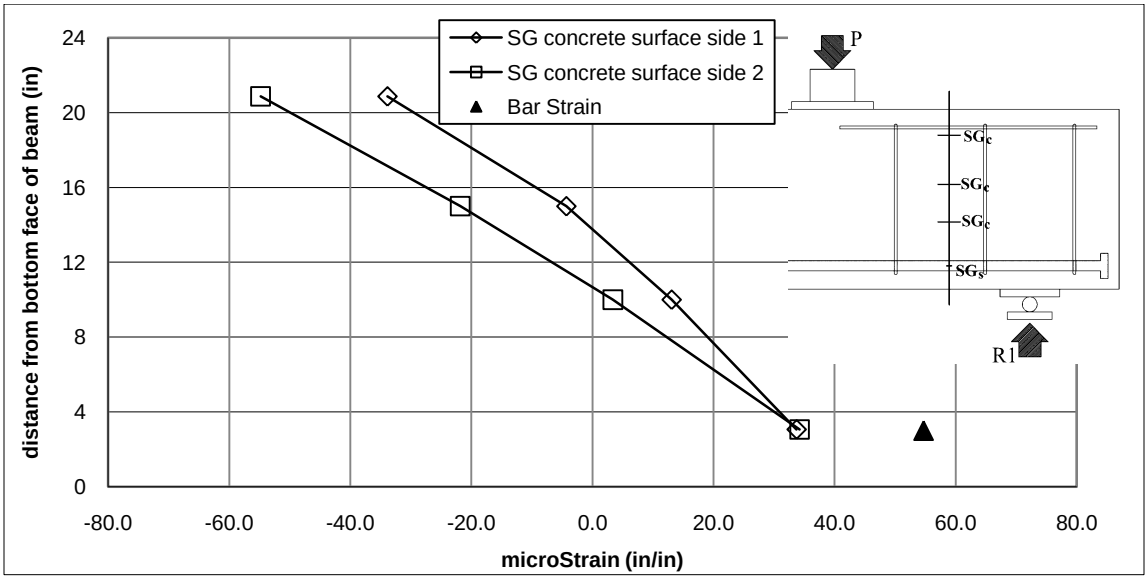

Figure 3.11 WP-E1 strain profile at center of shear span at shear "R1"of 20 kips

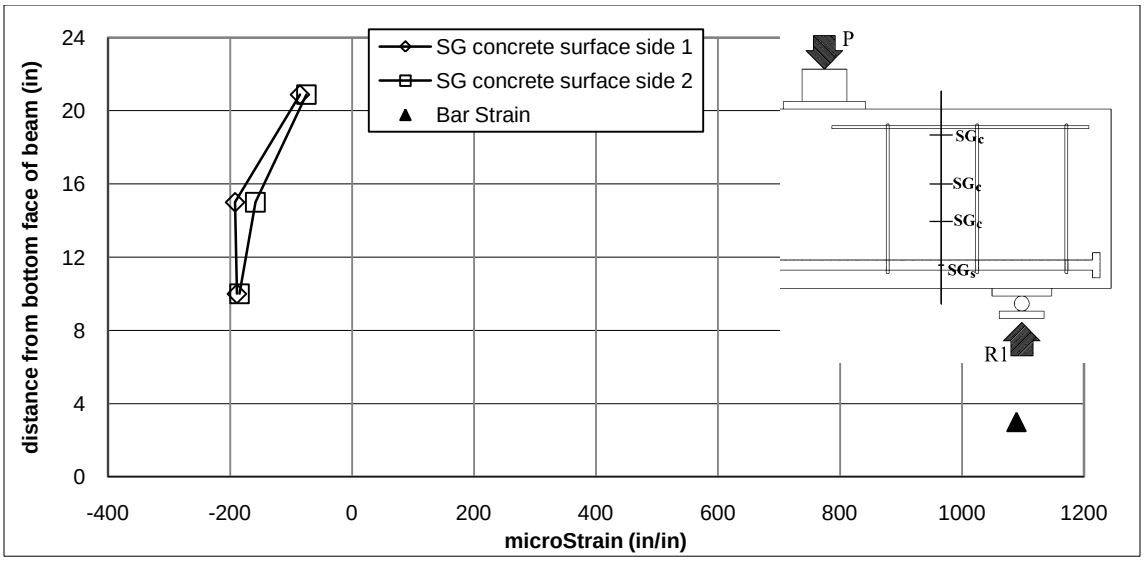

Figure 3.12 WP-E1 strain profile at center of shear span at shear "R1" of 73 kips

3.5.6 Cracking of the test specimen under loading during test WP-E1

Figure 3.13 illustrates the cracking pattern observed during test WP-E1. The specimen exhibited both diagonal tension and flexural cracks. The diagonal tension crack indicates the location of the lower edge of the compression strut or arch that formed between the load "P" and support "R1". During the loading process, the maximum crack width of the primary diagonal crack (crack A Figure 3.13) was measured on both faces of the beam. The crack width readings are presented in Table 3.4. As the shear increased a second diagonal tension crack B (Figure 3.13) was formed on both faces of the specimen and its width is also recorded in Table 3.4.

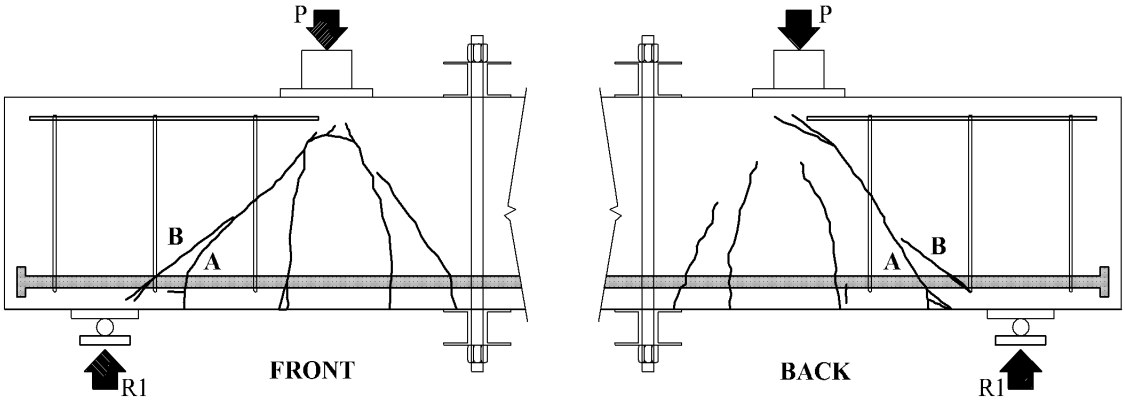

Figure 3.13 WP-E1 crack width measurement locations

Table 3.4 Test WP-E1 crack width measurements

Shear "R1" (kips)		49	55	62	65	73	82	97	111	121	130	0
Front	A (inches)	0.007	0.016	0.02	0.025	0.025	0.025	0.03	0.035	0.035	0.04	0.02
	B (inches)	-	-	-	-	-	0.005	0.01	0.016	0.02	0.03	0.009
Back	A (inches)	0.016	0.025	0.025	0.03	0.035	0.04	0.05	0.06	0.07	0.09	0.03
	B (inches)	-	-	-	-	-	-	-	0.005	0.009	0.02	0.005

3.6 Test WP-EI-PT

The retest of beam WP-E1 following rehabilitation with the application of a vertical external post-tensioning system as shown in Figure 3.14 (designated as WP-E1-PT) was performed after the test span was post-tensioned with a total force of 129 kips. The test was performed on the same end of the beam as test WP-E1, with initial cracks from test WP-E1. The specimen was loaded gradually until failure of the specimen occurred at a load "P" of 232 kips, which corresponds to a shear "R1" of 150 kips, at which point failure of the compression node under the load "P" occurred.

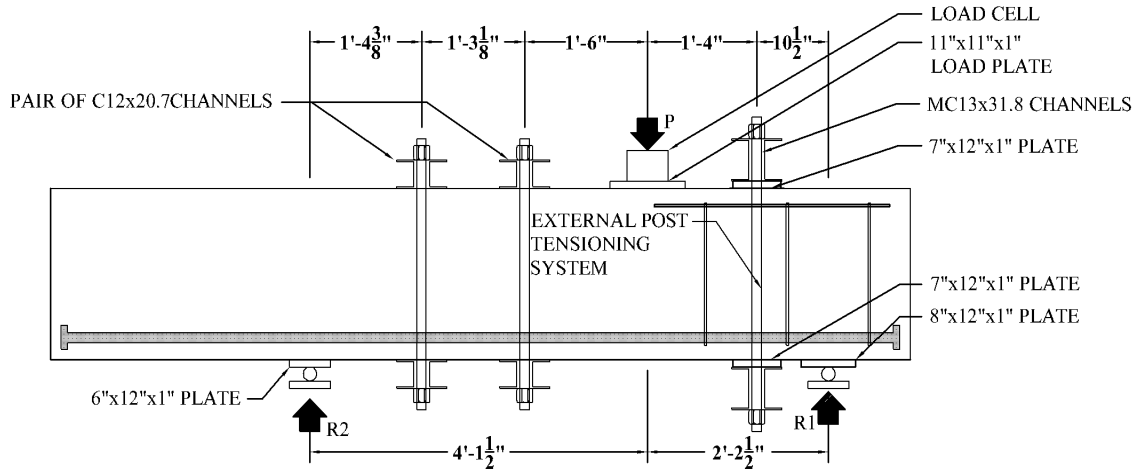

Figure 3.14 External post-tensioning system location

The external post tensioning force did not change significantly during test WP-E1-PT, and did not increase once "R1" exceeded the initial post-tensioning (Figure 3.15). As a result during test H-E1-PT it was decided to post-tension to a fraction of the expected shear capacity of the specimen to determine if the tension in the external bars would increase with the shear "R1." During the post-tensioning no accidental strain was measured in the horizontal tension reinforcement.

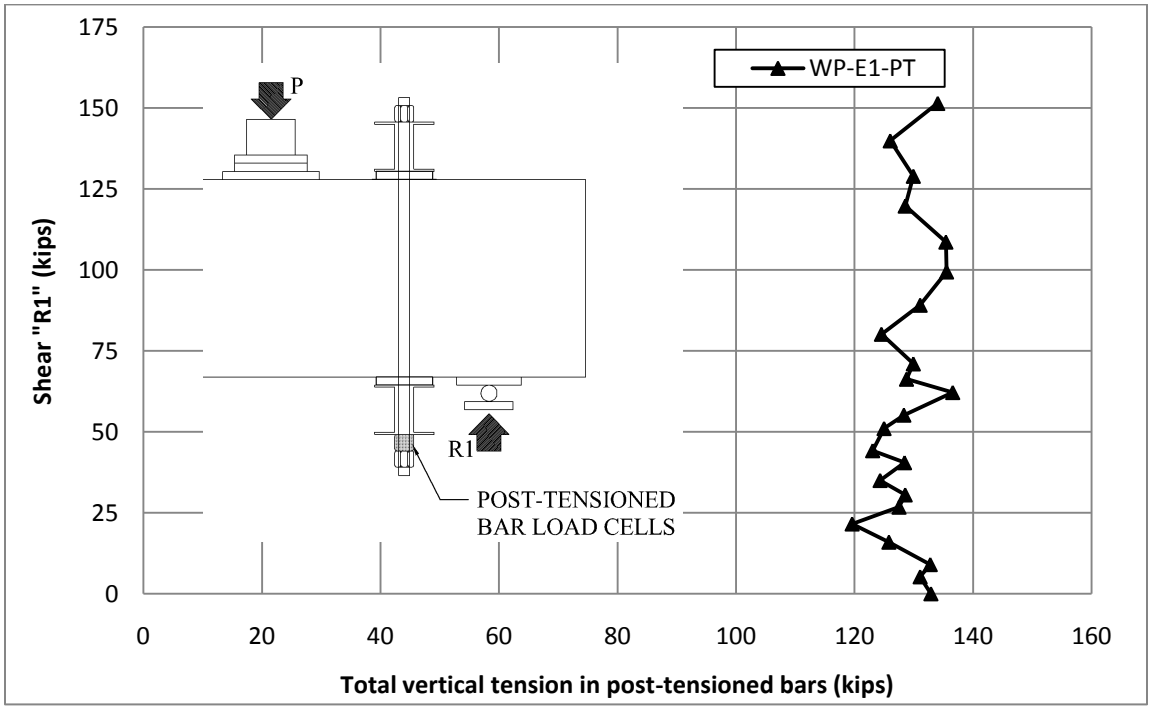

Figure 3.15 Tension in external post-tensioning during test WP-E1-PT

3.6.1 Instrumentation used during test WP-E1-PT

The same LVDT instrumentation scheme was used for experiment WP-E1-PT as in the original test, as shown in Figures 3.4. The same strain gauge instrumentation scheme as shown in Figure 3.3 was also used; however, the concrete surface-mounted strain gauges along the bottom edge of the beam were destroyed during experiment WP-E1 and thus could not be used during experiment WP-E1-PT.

3.6.2 Strain in the longitudinal reinforcement during test WP-E1-PT

The average measured strains in the reinforcing bars at SG location 1 and 2 are plotted against the shear in the test span in Figure 3.16. In contrast to experiment WP-E1, the average measured strains were not constant in the tension reinforcement. Due to the application of the post-tensioning system, a double strut mechanism (Figure 3.17), formed. The first strut developed in the specimen between the location of the load "P" and location where the post-tensioning system contacts the bottom of the specimen. The second diagonal compression strut formed between the location where the post-tensioning system contacts the top of the specimen and the reaction "R_1." Each strut transferred a force to the tension reinforcement separately, resulting in a jump in the strain at the location of the post-tensioning system.

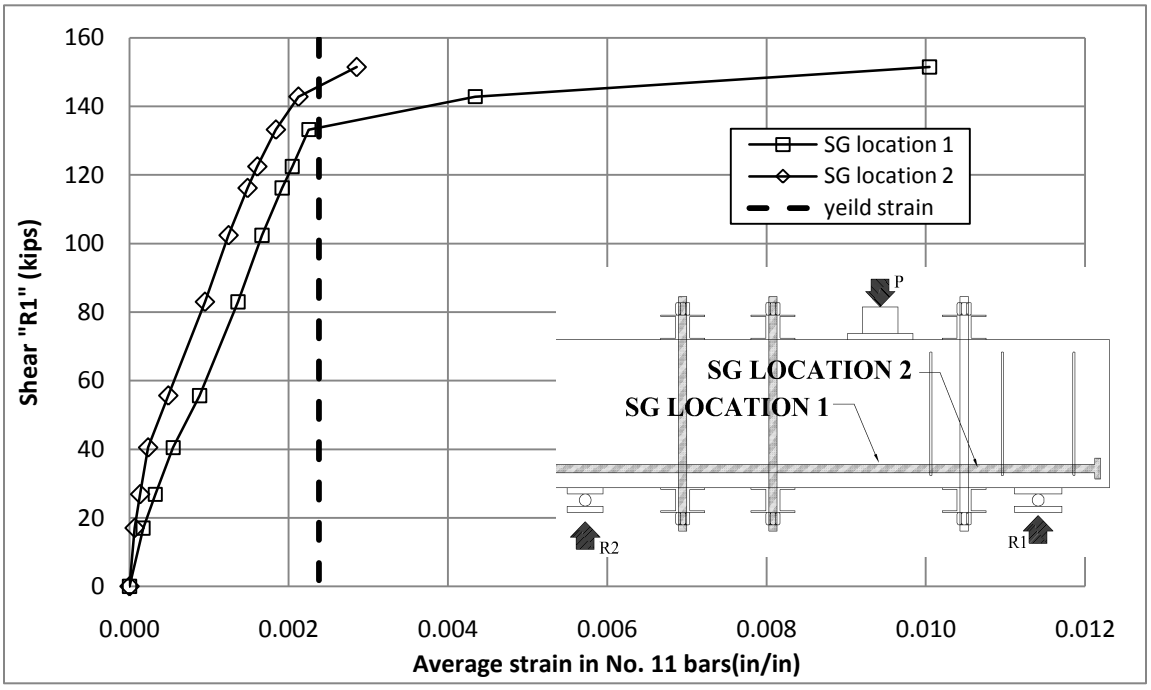

Figure 3.16 WP-E1-PT strain measurements from strain gauges mounted on bars

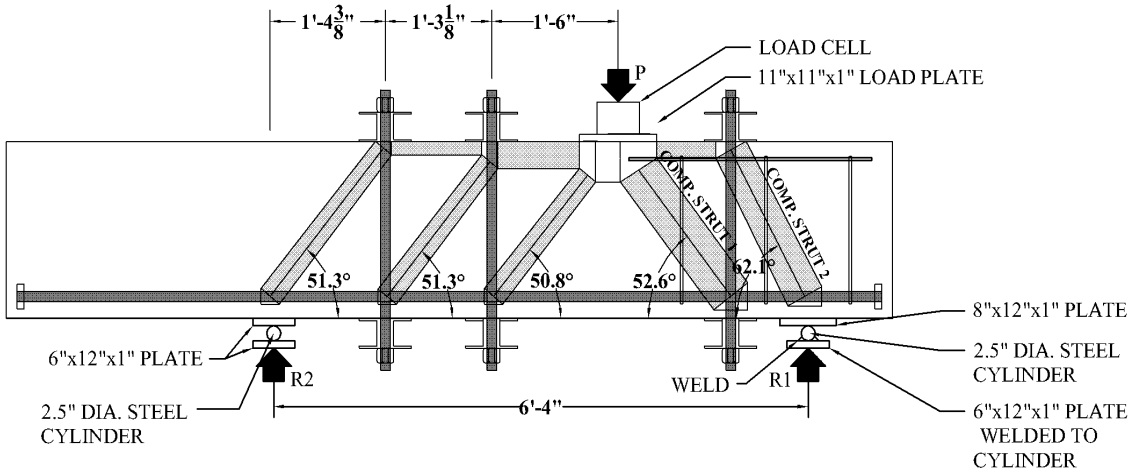

Figure 3.17 Double compression strut mechanism

3.6.3 Angle of inclination of the compression strut during WP-E1-PT

The techniques for computing the angle of principal compressive strain from a rosette of gauges presented in section 3.5.4 were used to compute the angle of principal compression strain from the surface mounted LVDTs and strain gauges. The angle of principal compression strain computed from the LVDT rosettes are shown in Figure 3.18,

and from the strain gauge rosettes in Figure 3.19 and Figure 3.20. The angle of principal compression strain was also computed from the measured strain in the tension reinforcement and the shear "R1" using the process outlined in section 3.5.4 and is shown in Figure 3.21. Unlike test WP-E1 there is no consistency in the angle of inclination of the compression struts obtained from the various strain measurements. A strut and tie analysis of the post-tensioned state of the specimen would indicate an angle of inclination of the compression struts between 50 and 60 degrees (Figure 3.17). While some of the computed strut angles fall within this range the majority are between 40 and 35 degrees. A possible cause for this lack of consistency is the location of the external post-tensioning; due to the 10 inch wide post-tensioning system and the short shear span (17 inches between the edge of the load plate at "P" and support plate at "R1" (Figure 3.17)), the external post-tensioning system could not fully cross the diagonal tension cracks. As a result the cracks at the location of the strain gauges opened, resulting in strain localizations in the bars and increases in measured strains, which decrease the computed compression strain strut angle. In addition, the externally mounted gauges crossed between the two compression struts and so were not able to provide the necessary information to compute the strain angle of either strut pictured in Figure 3.17.

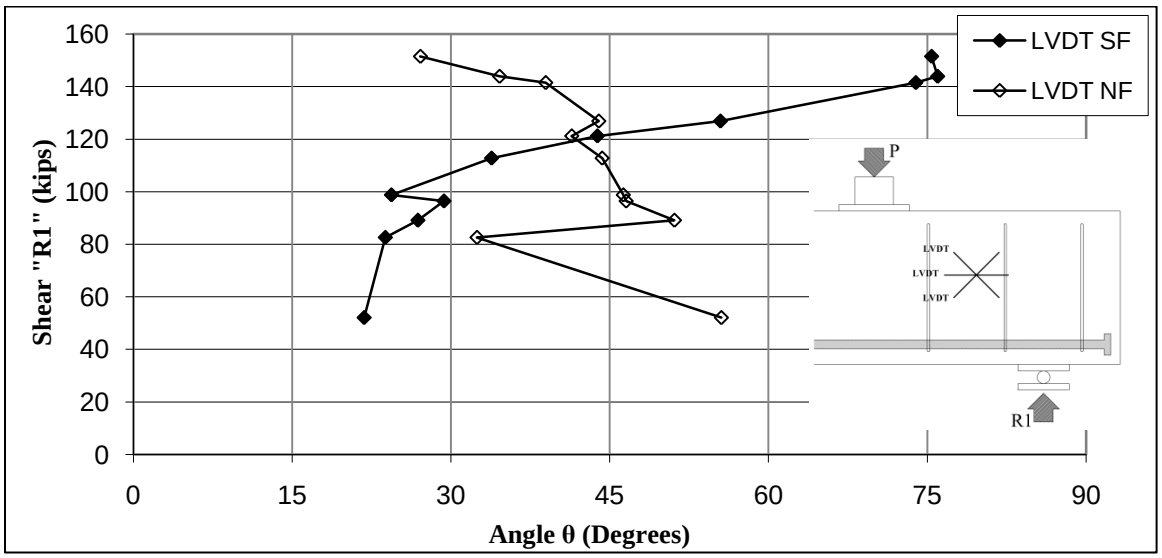

Figure 3.18 WP-E1-PT principal compression angle LVDTs (surface rosettes)

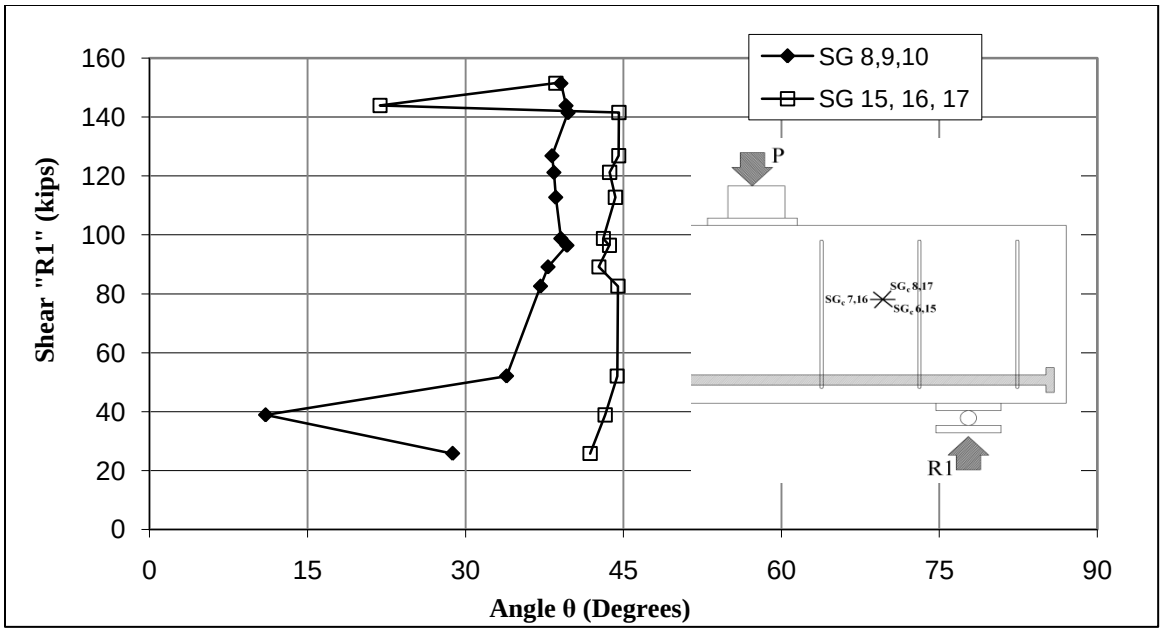

Figure 3.19 WP-E1-PT principal compression angles SG (surface rosettes)

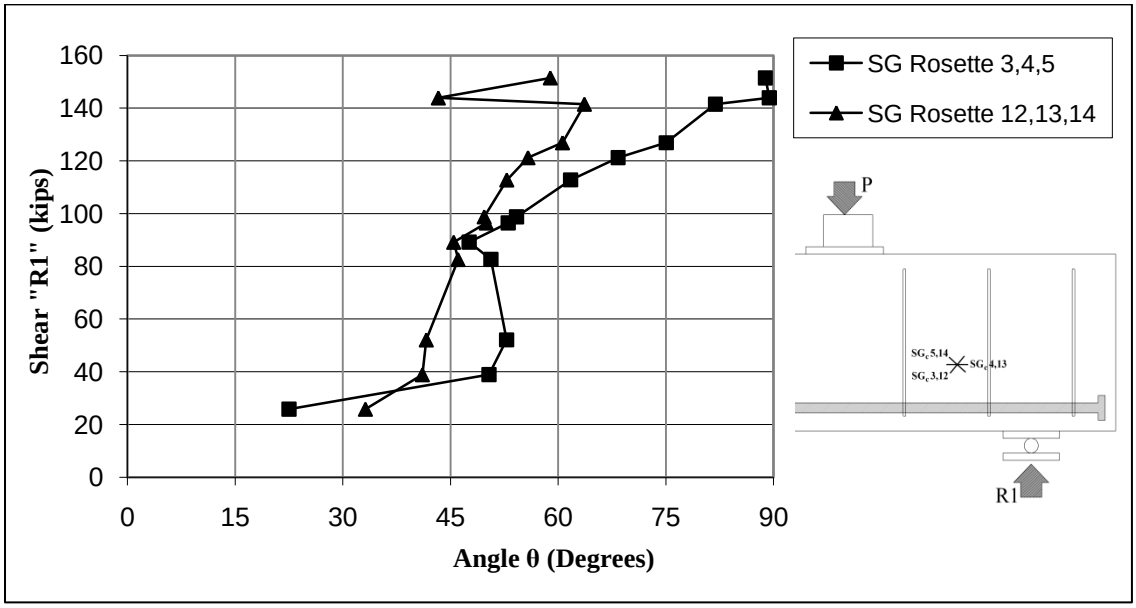

Figure 3.20 WP-E1-PT principal compression angles SG (surface rosettes)

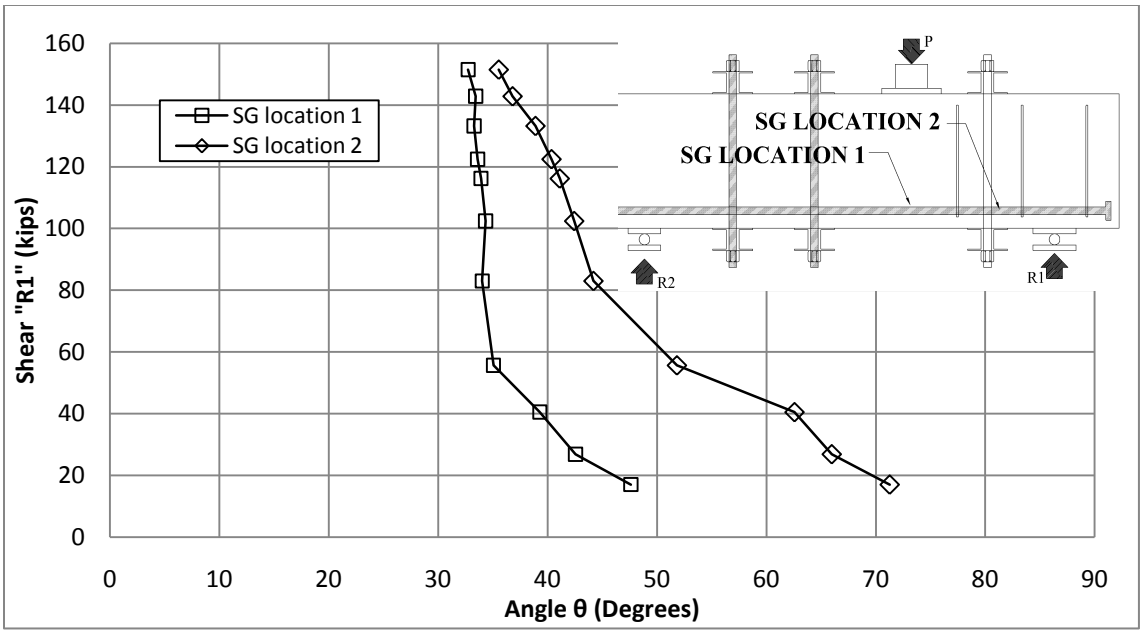

Figure 3.21 WP-E1-PT principal compression angle SG (tension reinforcement)

3.6.4 Cracking of the test specimen under loading during test WP-E1-PT

Figure 3.22 illustrates the additional cracking exhibited in specimen WP-E1-PT, beyond that which the specimen experienced during experiment WP-E1, and Table 3.5 lists the crack widths at various load levels. The new cracks formed during this experiment are highlighted in white in Figure 3.22, while the cracks that were formed during experiment WP-E1 prior to test WP-E1-PT are highlighted in black. A crushing failure of the concrete under the load plate limited the capacity of the specimen. Aguilar et al. (2002) also found that crushing failures occurred in the compression zone at the load plate in some of their deep beam shear tests. As a result, the test plan was modified so that specimens in the second phase were cast with a column stub segment to model the pier cap's boundary conditions.

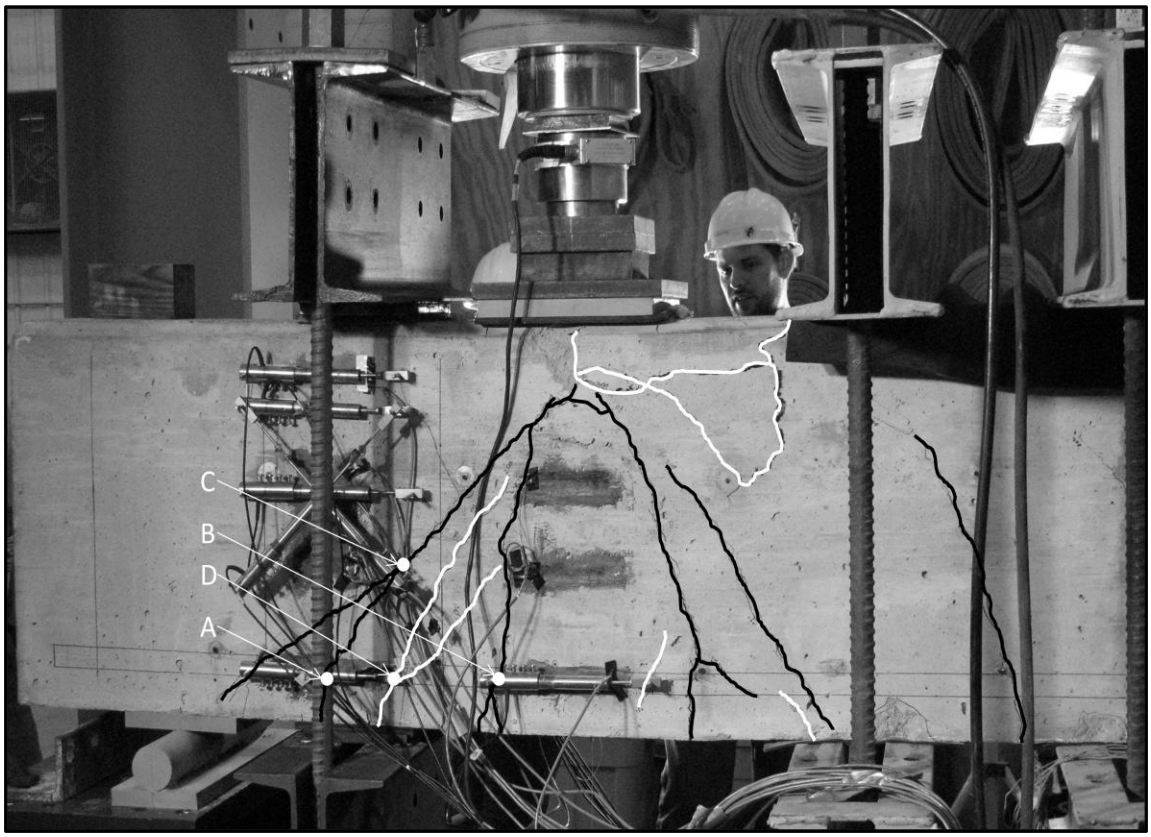

Figure 3.22 WP-E1-PT crack width measurement locations

Table 3.5 WP-E1-PT crack width measurements (inches)

	Side 1				Side 2			
Shear "R1" (kips)	**A**	**B**	**C**	**D**	**A**	**B**	**C**	**D**
16	0.011	0.007	0.005	-	0.007	0.003	0.011	-
27	0.011	0.007	0.005	-	0.007	0.003	0.011	-
39	0.011	0.007	0.005	-	0.007	0.007	0.013	-
54	0.013	0.009	0.007	-	0.007	0.0011	0.013	-
80	0.013	0.011	0.007	0.02	0.007	0.0013	0.016	0.005
101	0.013	0.011	0.009	0.025	0.007	0.02	0.016	0.013
115	0.013	0.013	0.009	0.03	0.007	0.02	0.016	0.025
132	0.013	0.016	0.009	0.035	0.007	0.02	0.016	0.03
111	0.013	0.016	0.009	0.06	0.007	0.05	0.016	0.06

3.7 Test WP-E2

Experiment WP-E2 was performed on the end of a beam having no stirrups (E2) and in which anchorage was provided by welded steel plates. Since the stirrup end (E1) of this specimen had already been tested (Experiments WP-E1 and WP-E1-PT), there was damage to the specimen outside of the test shear span which is outlined in Figure

3.23. This test differed from the previous tests, in that the length of the span between “P” and “R2” Figure 3.23, had to be shortened due to the existing damage to the specimen. To prevent a premature crushing failure under the load plate, as occurred in experiment WP-E1-PT, an 18 inch long load plate was used in place of the 11 inch long load plate used in the previous experiments. However, due to the initial damage to the specimen, failure of the specimen occurred at a 30% lower shear “R1” than was achieved during test WP-E1. Due to the extensive cracking of the specimen outside the test span illustrated in Figure 3.24 it was not possible to determine if the loss of shear resistance of the specimen initiated inside or outside of the test span. As a result of this test, the second end of the remaining specimens was not tested due to the complication of initial damage to the structure.

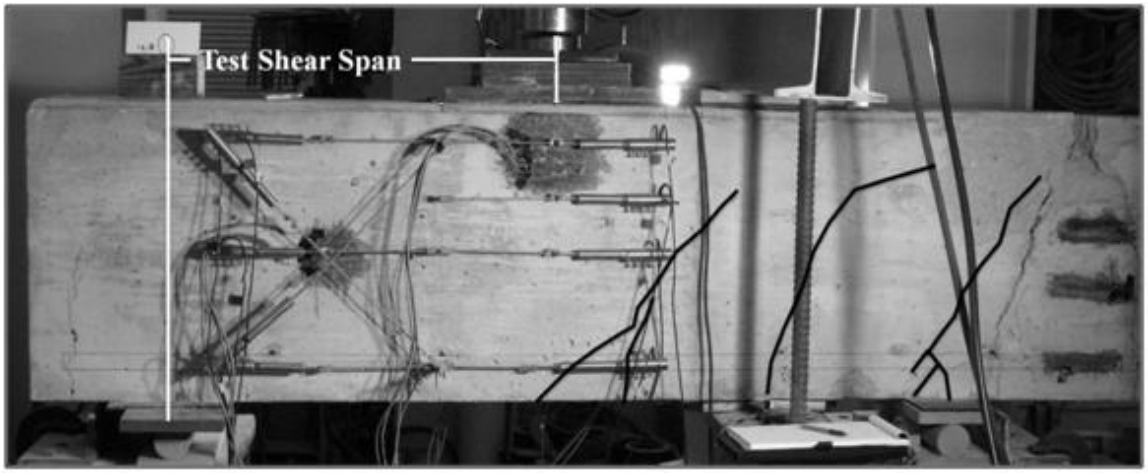

Figure 3.23 WP-E2 prior to loading

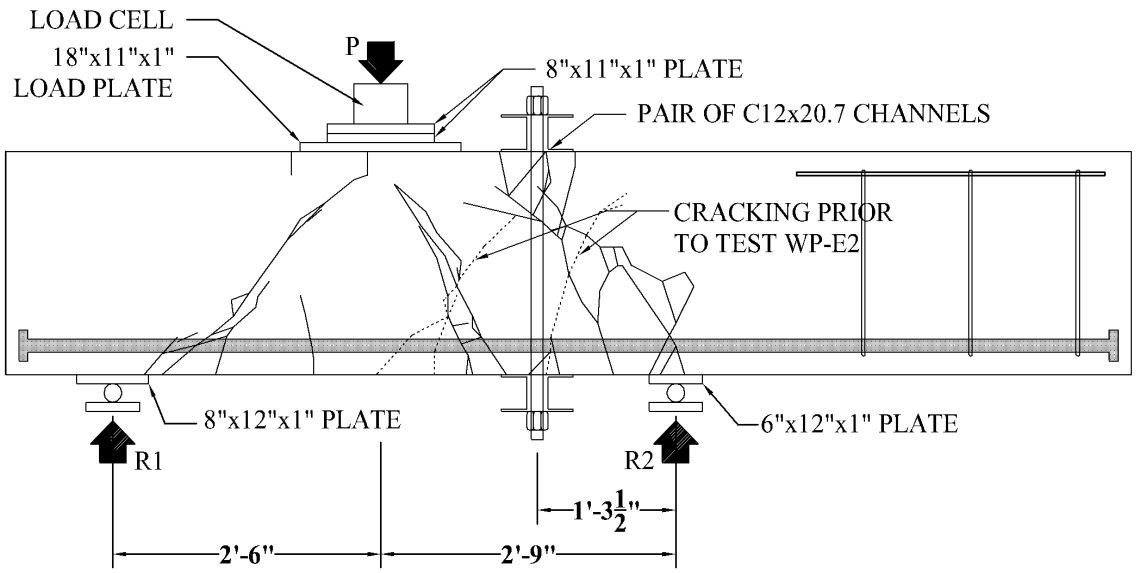

Figure 3.24 WP-E2 cracking pattern

3.8 Tests LT-E1, H-E1 and H-E1-PT

Each of the last three experiments discussed in this chapter utilized the same testing configuration, as shown in Figure 3.25. Test LT-E1 was performed on the specimen with threaded anchors to give a benchmark shear resistance of specimens H and LT. Test H-E1 was performed to crack the specimen with hooked anchorage prior to rehabilitation, and test H-E1-PT was performed to observe the effect of post-tensioning on this same beam. The post-tensioning force used on specimen H-E1-PT was intentionally below the predicted shear capacity of the specimen. This was done to determine if once the post-tensioning force was exceeded, the specimen would continue to carry shear through the two-strut mechanism illustrated in Figure 3.17, or if the load carrying mechanism would revert to a single diagonal compression strut between the load "P" and reaction "R1". As a result the specimen was only post-tensioned to one-half its predicted shear capacity (Chapter 6). Despite the fact that the shear "R1" exceeded two and a half times the initial external post tensioning of 79 kips, the tension in the external post-tensioning system did not increase significantly during the test (Figure 3-26). No

accidental strain was measured in the tension reinforcement during the post-tensioning process.

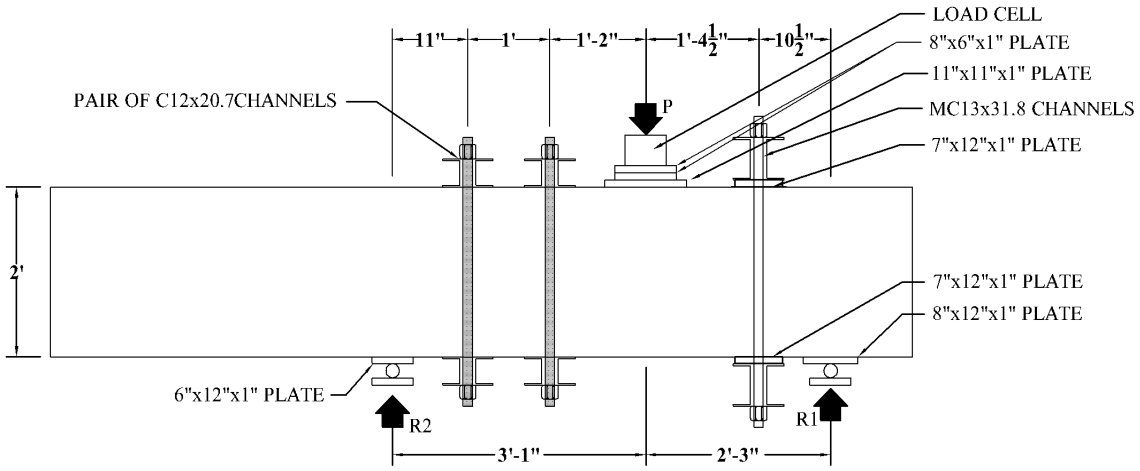

Figure 3.25 Test configuration of specimens LT-E1, H-E1 and H-E1-PT

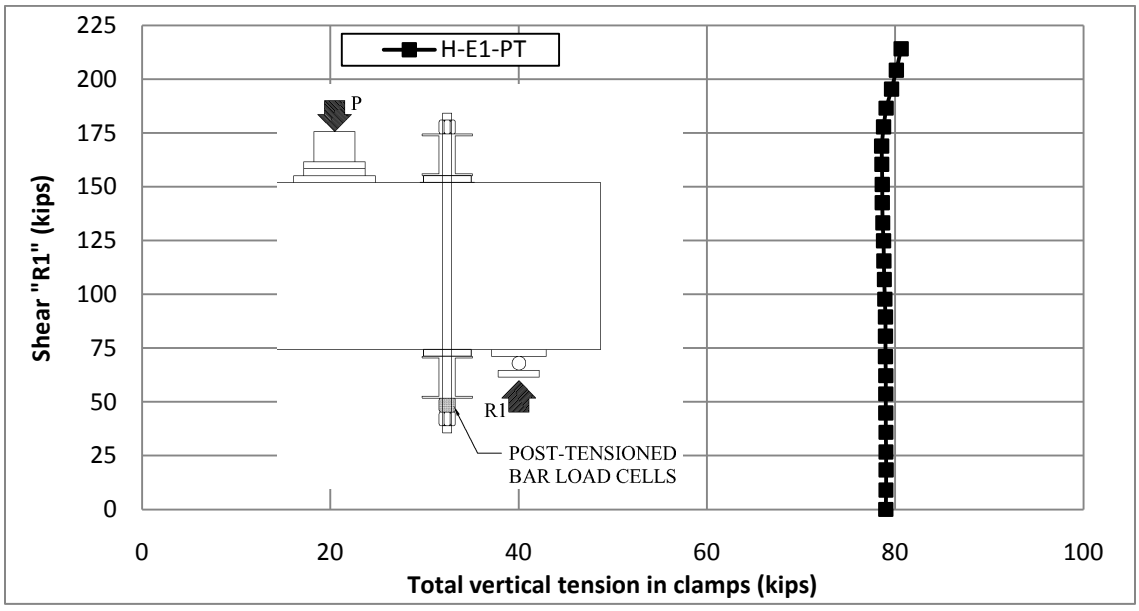

Figure 3.26 Tension in external post-tensioning system during test H-E1-PT

3.8.1 Instrumentation used during tests LT-E1, H-E1, and H-E1-PT

The surface-mounted strain gauges used in the previous experiments were eliminated in these final tests due to the fact that they provided too localized a measurement of strain to be useful when testing a non-homogeneous material. Additionally, the focus was shifted to monitoring the strain profile through the depth of

the compression strut as opposed to the depth of the beam, since the strain profiles through the depth were consistently nonlinear once cracking of the specimen occurred. On the other hand, the strain profile through the depth of the compression strut can be used to define the width of the strut and average compressive strain. The LVDT locations during experiment LT-E1are shown in Figure 3.27 and the LVDT locations during experiments H-E1 and H-E1-PT are shown in Figure 3.28.

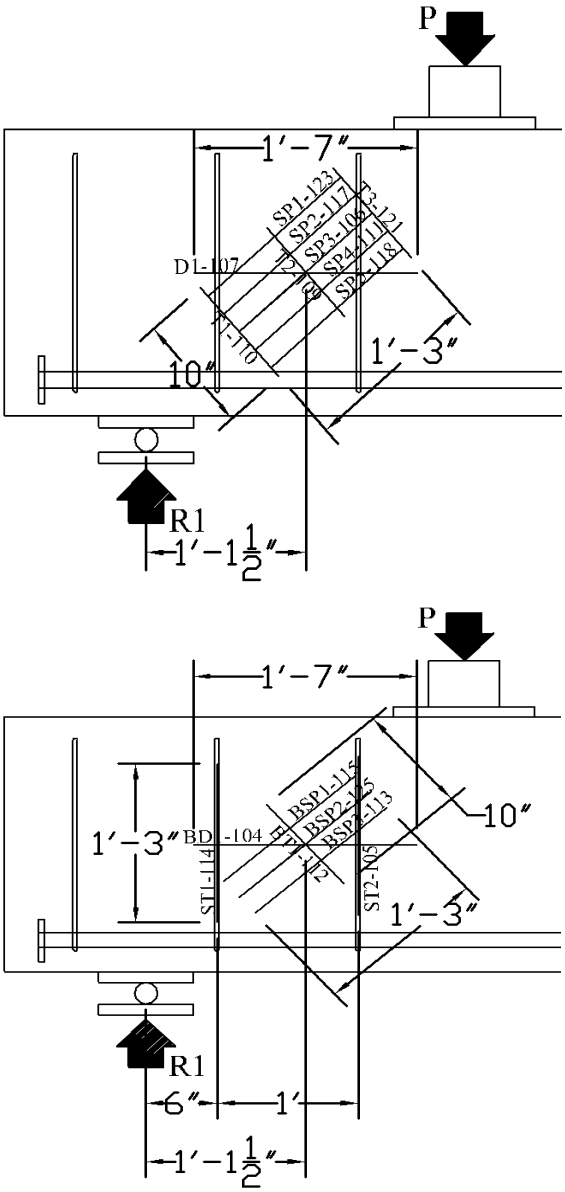

Figure 3.27 LVDT locations for specimen LT-E1

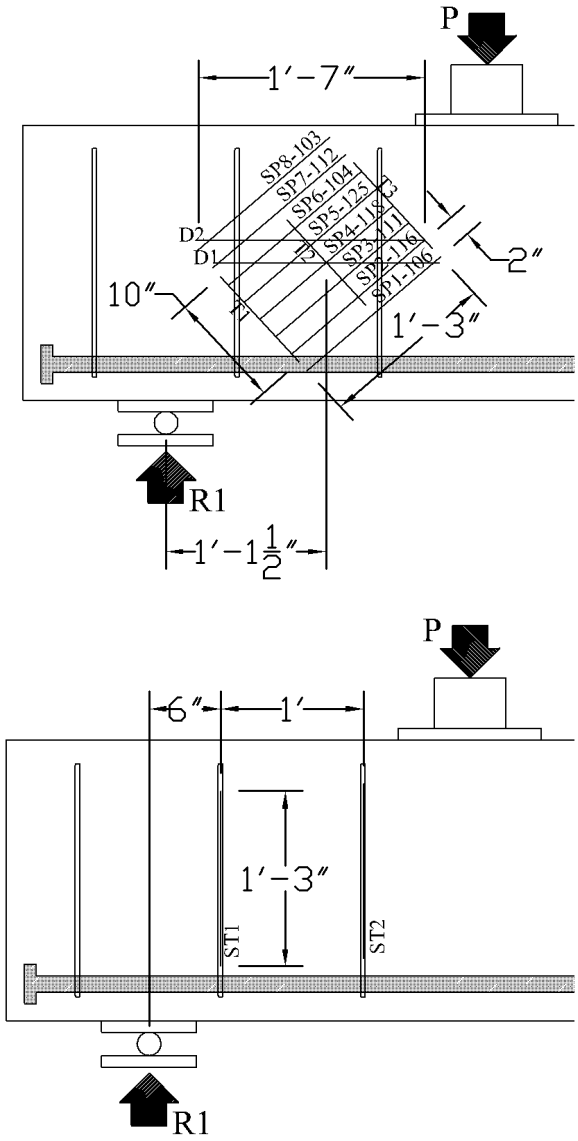

Figure 3.28 LVDT locations for specimens H-E1 and H-E1-PT

3.8.2 Displacement measured during tests LT-E1, H-E1, and H-E1-PT

The displacement response during each test was very similar, with yielding of the tension reinforcement occuring at a shear in the test span of between 180 and 190 kips (Figure 3.29). The test LT-E1 achieved a 6% higher capacity than test H-E1-PT, but its failure was more sudden. The failure of specimen LT-E1 was sudden and resulted in the loss of nearly 70% of the shear resistance of the specimen, which was accompanied by an increase in deflection of nearly 60%. This failure did not occur in the rehabiliated specimen due to the fact that the external post-tensioning system was able to hold the

beam together once failure occurred. However, the untimate capacity of both specimens was only reached after yielding of the tension reinforcement. In addition, both specimens exhibited significant deflections and very large diagonal crack widths prior to failure.

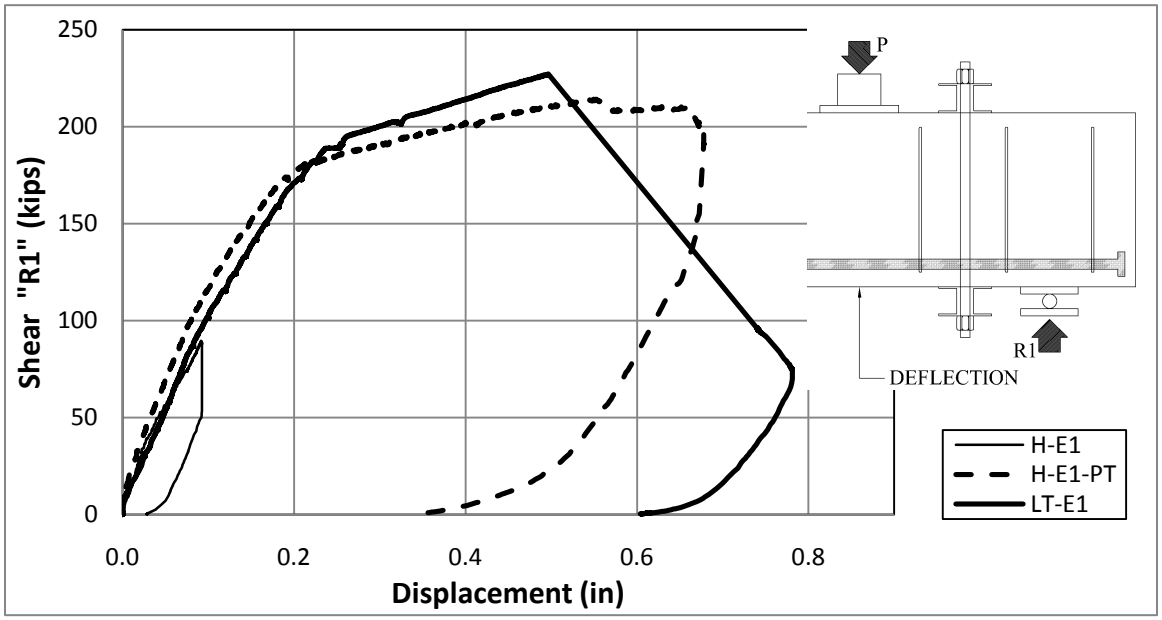

Figure 3.29 Load displacement comparison

3.8.3 Strain in the longitudinal reinforcement during tests LT-E1, H-E1, and H-E1-PT

The strain in the tension reinforcement was measured in the locations shown in Figure 3.3. The average strain measured below the load "P" (SG location 1) and at one-half the shear span (SG location 2) are presented in Figure 3.30. During Experiments LT-E1 and H-E1 when no external post-tensioning of the shear span was present, the strain at both locations was in excellent agreement throughout the tests. In test H-E1-PT there was a difference between the average measured strain of the tension reinforcement at SG locations 1 and 2. This difference is evidence that a double-strut (Figure 3.17) began to form in the test shear span; however the double strut did not fully develop because the post-tensioning force was too low. The shear in the test span exceeded the

initial post-tensioning of the rehabilitation, which makes up the vertical tension tie between the two struts in the test span; however the load cells measuring the force in the post-tensioned bars did not increase with increasing shear in the test span. As a result, a double-strut mechanism could not have been present once the shear in the test span exceeded 80 kips. In addition the existing crack which crosses the location of the strain gauge at SG location 2 was not kept closed by the post-tensioned clamp. The fact that this existing crack was able to open during loading caused strain localization in the rebar and increased the average measured strain at SG location 2.

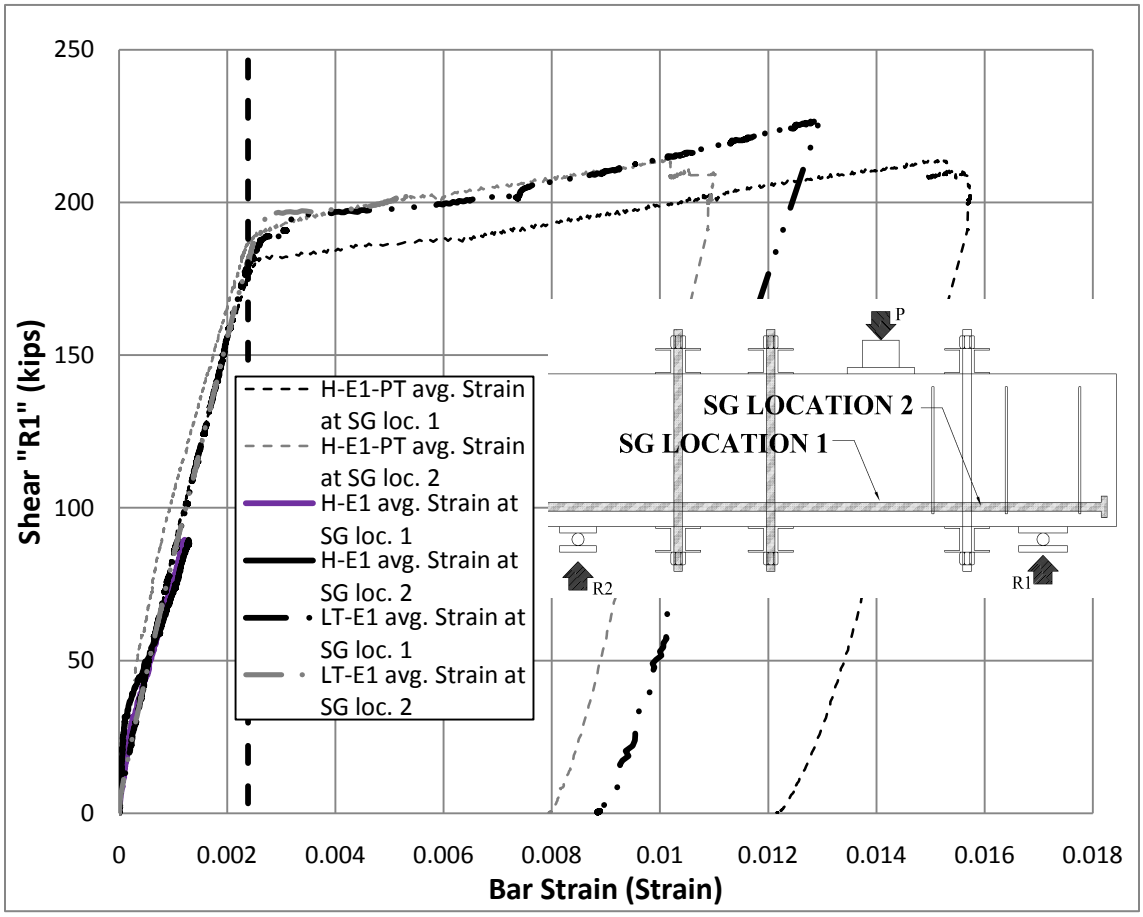

Figure 3.30 Longitudinal reinforcement strain comparison

3.8.4 Strain in concrete perpendicular to compression strut (H-E1 and H-E1-PT)

The LVDT readings presented in Figure 3.31 illustrate the effect of the rehabilitation when the test span is subjected to shear that is less than the post-tensioning

force. Figure 3.31 shows the average tension strain measured in the three LVDTs mounted perpendicular to the axis of the compression strut during experiments H-E1 and H-E1-PT. The average readings of these three gauges clearly show that the tension strain is reduced throughout the range of the experiment when the specimen has been post-tensioned prior to testing. Furthermore, until the specimen reaches a shear in the test span of 75 kips, the perpendicular tension strain in the compression strut is effectively zero. A total vertical pre-compression of 80 kips was applied through 2 bars on opposite faces of the specimen. One bar had a post-tensioning force of 37 kips and the other 43 kips, these bar forces remained constant throughout the experiment. Therefore, the bars did not offer resistance to the principal tension strain once the post-tensioning force was exceeded.

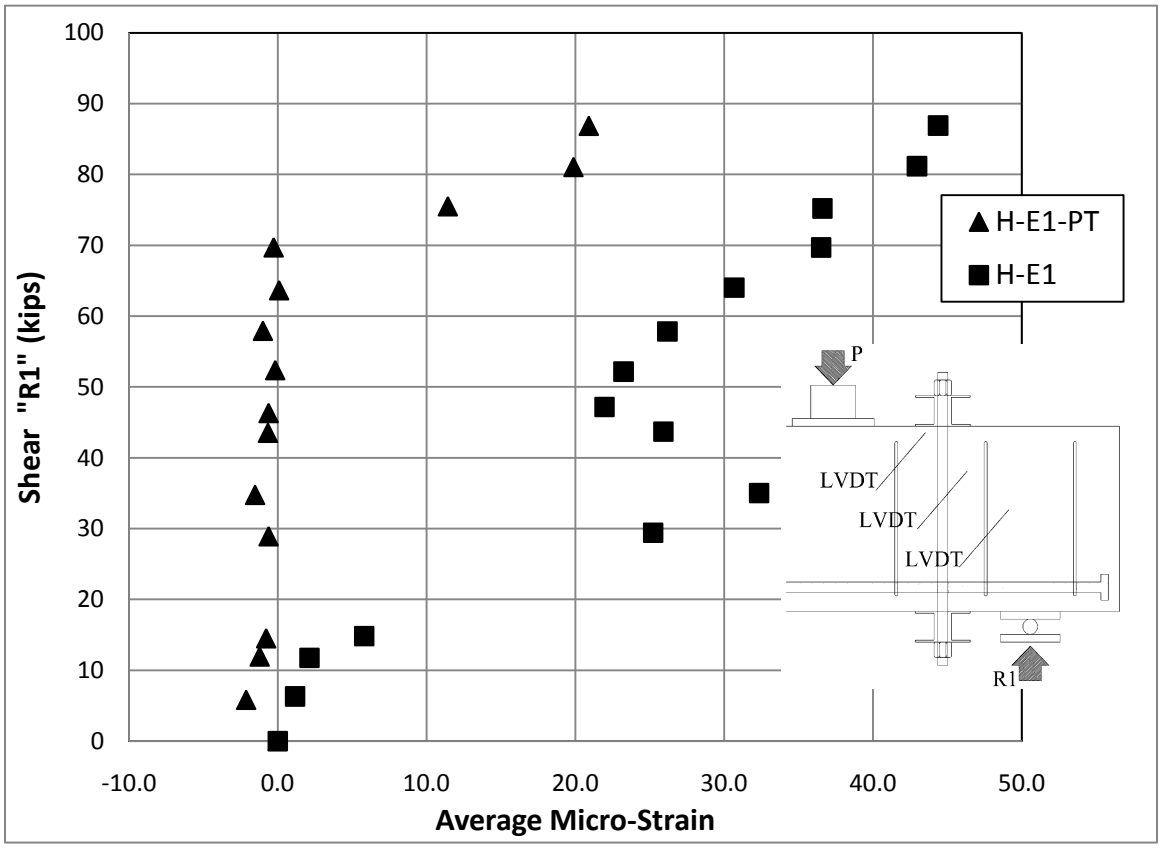

Figure 3.31 Tension strain perpendicular to compression strut

3.8.5 Strain profile compression strut measured during tests LT-E1, H-E1, and H-E1-PT

The array of LVDTs arranged parallel to the anticipated compression strut were used to produce strain profiles through the width of the compression strut. These profiles are plotted at various levels of shear "R1" in Figures 3.32 (LT-E1), 3.33 (H-E1), and 3.34 (H-E1-PT). The strain profiles corresponding to test LT-E1and H-E1 in Figures 3.32 and 3.33 show a uniform strain in the strut prior to the development of diagonal tension cracks. Tension strains develop in LVDTs SP5 (Figure 3.32) and SP 1 and 2 (Figure 3.33) because they are located below the diagonal tension crack that forms the boundary of the compression strut. All three tests show a trend of increasing compressive strain in the lower portion of the strut, up until failure. This suggests that the compression strut does not engage its full width but transfers most of the compression from the load "P" to the support along the bottom edge of the compression strut.

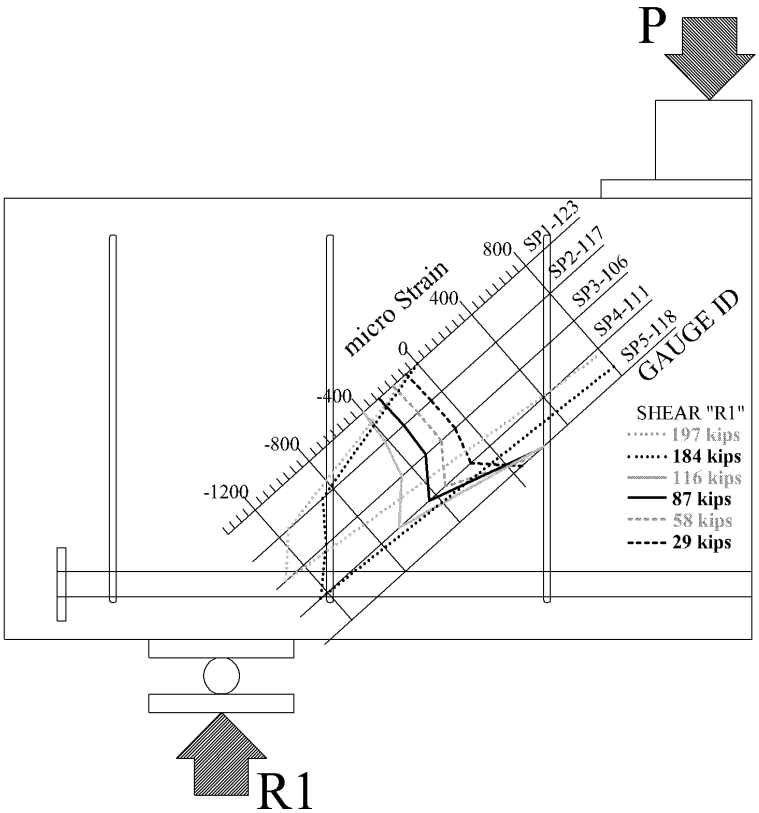

Figure 3.32 LT-E1 compression strut strain profile

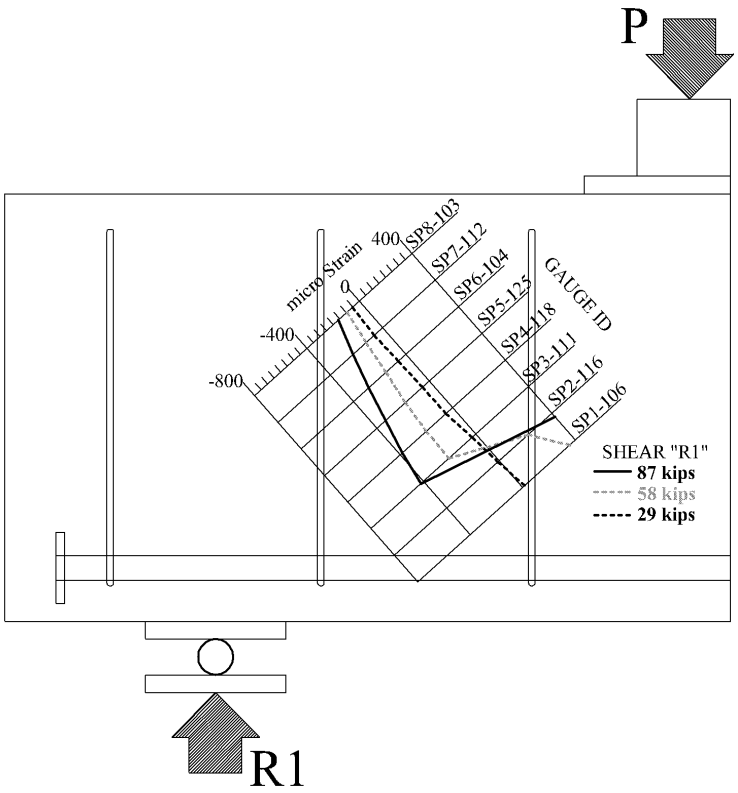

Figure 3.33 H-E1 compression strut strain profile

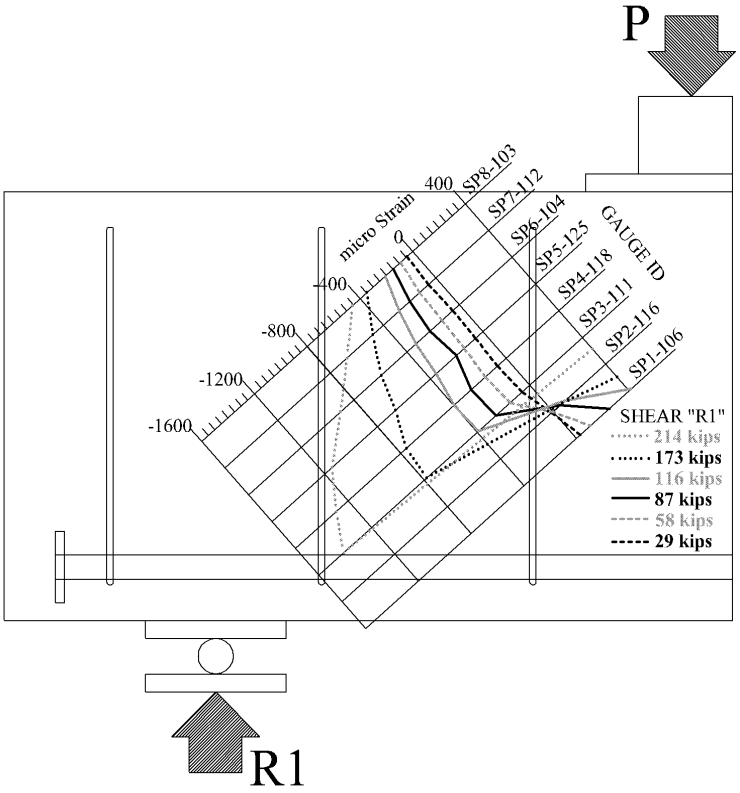

Figure 3.34 H-E1-PT compression strut strain profile

3.8.6 Angle of inclination of the compression strut during tests LT-E1, H-E1, and H-E1-PT

The angle of inclination of the compression strut was computed from the surface mounted LVDTs and is shown for each test in Figure 3.35. The LVDTs indicate an angle of inclination of between 40 and 45 degrees when the shear in the test span is less than 100 kips. As with previous tests, the angle of principal compression strain computed using the bar strain and shear in the test span is not as susceptible to localized strain effects as the LVDT rosettes and produces a more consistent angle of approximately 40 degrees for tests LT-E1 and H-E1 (Figure 3.36). From Figure 3.36 it can be seen that the strength increase of the specimen, once yielding of the tension reinforcement initiates, is achieved primarily through increasing the angle of the compression strut. To compute the angle of inclination of the compression strut after yielding of the tension reinforcement, the stress-strain curve obtained from bar tension tests was used to convert the measured strain to the strain in the bar. In test LT-E1, the compression strut angle increased by shrinking the node at the load plate until the node crushed and the failure propagated back through the compression strut to the support (Figure 3.37). Due to the fact that the shear in the test span exceeded the external post-tensioning in test H-E1-PT, the angle of principal compression strain is computed from the rebar mounted strain gauges as if a single strut formed between the load and support (Figure 3.36).

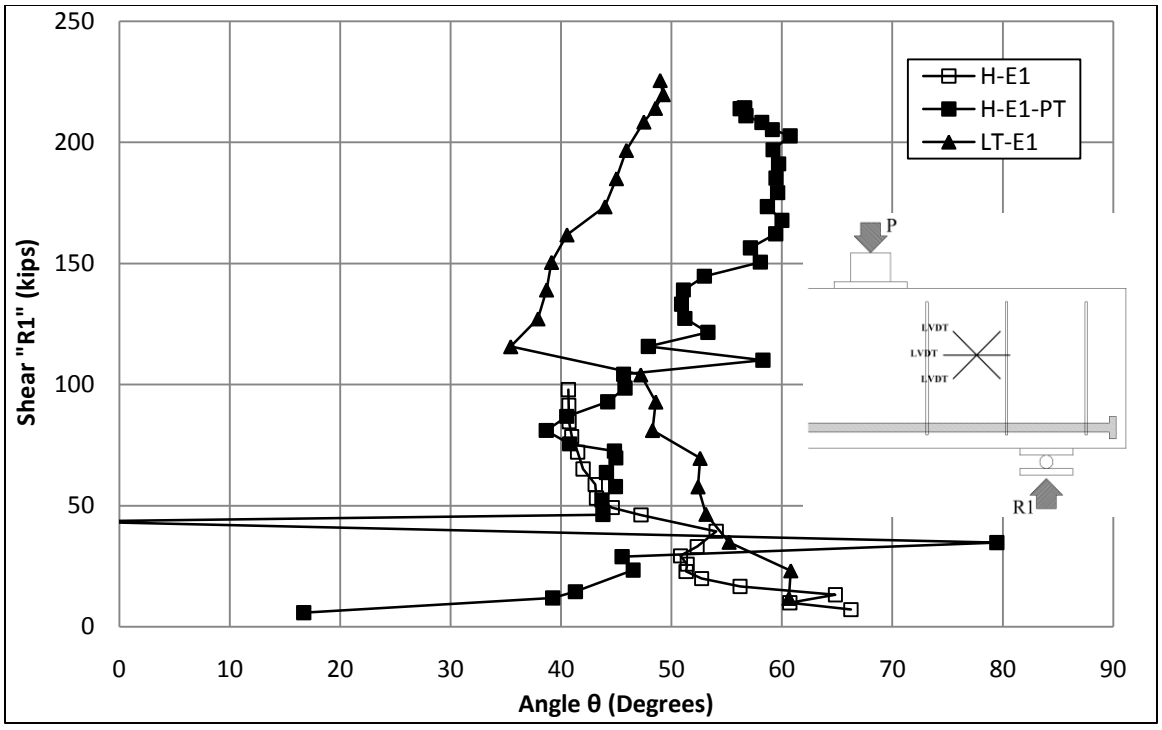

Figure 3.35 Angle of principal compression (computed from LVDTs)

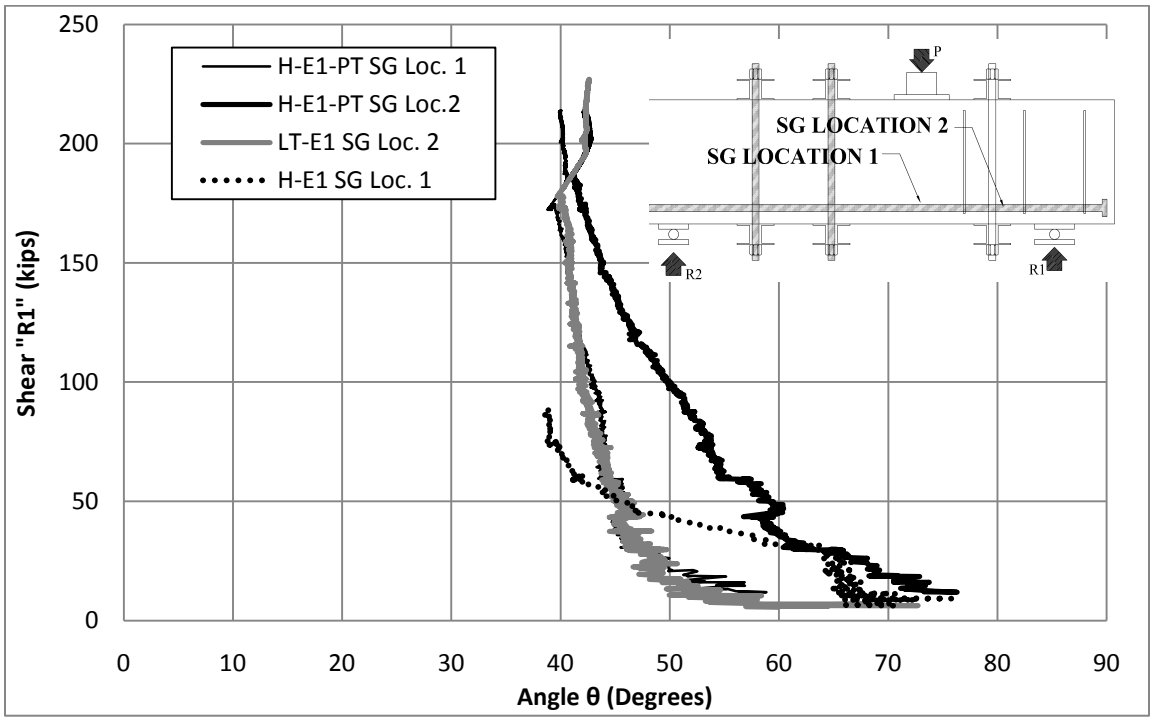

Figure 3.36 Angle of principal compression (computed from bar strain)

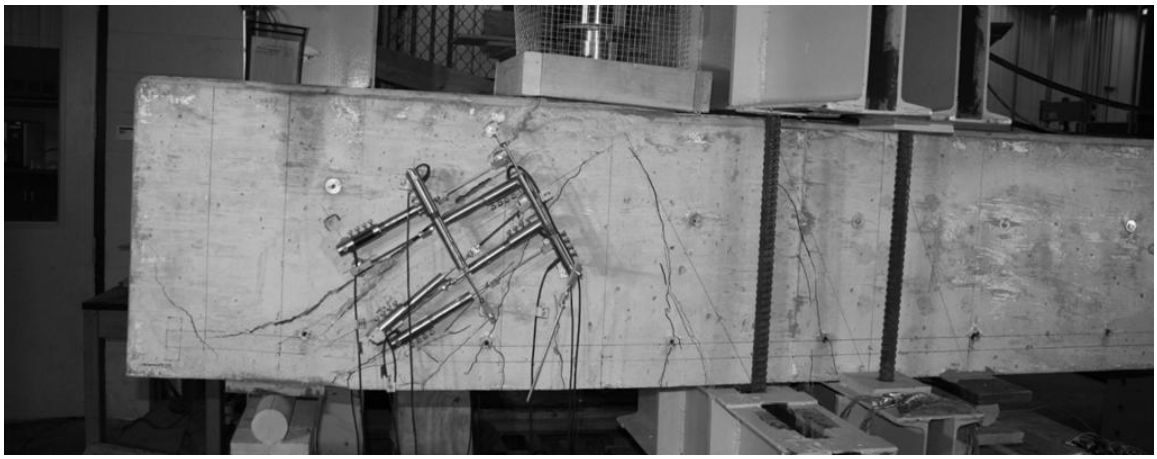

Figure 3.37 LT-E1 at ultimate load

3.8.7 Comparison of crack growth durring test LT-E1, H-E1, and H-E1-PT

Diagonal shear cracks were measured on both sides of the specimen durring tests H-E1 and H-E1-PT in order to evaluate the effectiveness of the rehabilitation in reducing the crack sizes. The crack locations are labeled A1-13 and C1-13 with the letter corresponding to the first initial of the person measuring the cracks. During both experiments the cracks were measured by the same two individuals. It was found that the cracking was not reduced by the external post-tensioning system in the case of specimen H-E1-PT. The most likely cause of the failure of the rehabitation to reduce the crack sizes is that due to the short length of the shear span, the post-tensioning system could not fully bridge the existing diagonal tension cracks. As a result, the diagonal tension cracks opened at a similar rate as test H-E1 and the overall behavior of specimen H-E1-PT was similar to test LT-E1.

3.8.8 Cracking of specimen under loading during tests H-E1 and H-E1-PT (side 1)

Figure 3.38 illustrates the locations of crack measurments A1-13 in both experiment H-E1 and H-E1-PT. The measurements are tabulated in Tables 3.6-3.8. There is little difference in the crack widths measured during experiment H-E1and H-E1-PT. When testing the pier cap specimens discussed in Chapter 4, it may be possible to

reduce the width of the crack that extends from A3-A6 due to the fact that the shear span is 50% longer and the rehabilitation can be moved to fully cross the diagonal tension crack A3-A6 .

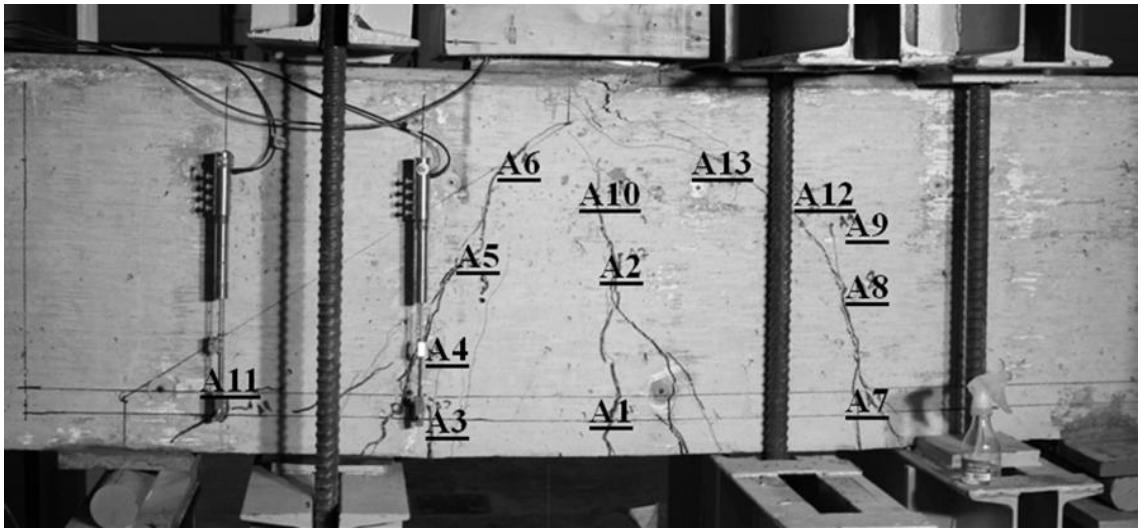

Figure 3.38 H-E1 and H-E1-PT crack width measurement locations (side 1)

Table 3.6 H-E1 crack width measurements

Shear "R1"	Crack Width (inches)										
kips	**A1**	**A2**	**A3**	**A4**	**A5**	**A6**	**A7**	**A8**	**A9**	**A10**	**A11**
29	0.003	<.003	0.003	<.003	<.003	-	-	-	-	-	-
43	0.011	<.003	0.007	0.009	0.003	<.003	-	-	-	-	-
58	0.013	0.003	0.007	0.013	0.009	<.003	-	-	-	-	-
72	0.016	0.003	0.025	0.02	0.016	0.003	-	-	-	-	-
87	0.02	0.007	0.03	0.025	0.02	0.003	0.007	0.003	<.003	<.003	0.003

Table 3.7 H-E1-PT crack width measurements (part1)

Shear "R1"	Crack Width (inches)							
kips	**A1**	**A2**	**A3**	**A4**	**A5**	**A6**	**A7**	
29	0.007	<.003	0.005	0.005	0.003	<.003	0.003	
43	0.011	0.003	0.007	0.009	0.007	<.003	0.005	
58	0.013	0.007	0.016	0.013	0.009	0.003	0.007	
72	0.011	0.007	0.02	0.02	0.011	0.003	0.007	
87	0.016	0.007	0.02	0.02	0.013	0.003	0.009	
116	0.016	0.009	0.025	0.03	0.016	0.005	0.011	0.011
145	0.02	0.013	0.03	0.035	0.02	0.009	0.007	0.013
173	0.02	0.013	0.04	0.05	0.03	0.011	0.02	0.005

Table 3.8 H-E1-PT crack width measurements (part 2)

Shear "R1"	Crack Width (inches)							
kips	A8	A9		A10	A11	A12		A13
29	<.003	<.003		<.003	<.003	-		-
43	0.003	<.003		<.003	<.003	-		-
58	0.003	<.003		<.003	<.003	-		-
72	0.003	<.003		<.003	<.003	-		-
87	0.003	<.003		<.003	<.003	-		-
116	0.009	0.005		<.003	<.003	-		-
145	0.016	0.005	0.009	<.003	<.003	0.003		-
173	0.025	0.005	0.013	0.003	<.003	0.016	0.003	0.009

3.8.9 Cracking of specimen under loading during tests H-E1 and H-E1-PT (side 1)

The cracking on side 2 of test H-E1 and H-E1-PT behaved similarly to side 1 and is labeled C1-C13 as illustrated in Figure 3.39, and tabulated in Tables 3.9-3.11.

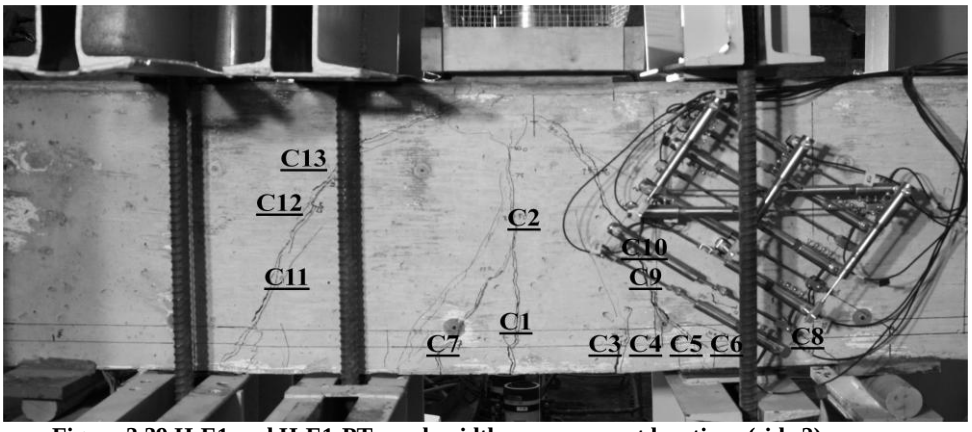

Figure 3.39 H-E1 and H-E1-PT crack width measurement locations (side 2)

Table 3.9 H-E1 crack width measurements

Shear "R1"	Crack Width (inches)									
kips	C1	C2	C3	C4	C5	C6	C7	C8	C9	C10
29	0.003	<.003	-	-	-	-	-	-	<.003	-
43	0.009	0.003	0.003	0.003	-	-	-	-	0.007	<.003
58	0.011	0.003	0.003	0.003	0.003	-	-	-	0.011	0.009
72	0.013	0.003	0.003	0.003	0.011	0.003	-	-	0.02	0.016
87	0.011	0.003	0.003	0.003	0.013	0.005	.007	.011	0.025	0.02

Table 3.10 H-E1-PT crack width measurements (part 1)

Shear "R1"	Crack Width (inches)							
kips	**C1**		**C2**	**C3**	**C4**	**C5**	**C6**	**C7**
29	0.005		<.003	<.003	<.003	0.003	<.003	<.003
43	0.009		0.003	0.003	<.003	0.005	<.003	0.003
58	0.011		0.003	0.003	<.003	0.007	<.003	0.005
72	0.011	0.003	0.005	0.007	<.003	0.009	<.003	0.007
87	0.011	0.003	0.005	0.009	<.003	0.011	<.003	0.009
116	0.013	0.007	0.005	0.013	<.003	0.02	<.003	0.016
145	0.013	0.009	0.007	0.02	<.003	0.03	<.003	0.02
173	0.016	0.009	0.013	0.25	<.003	0.06	<.003	0.025

Table 3.11 H-E1-PT crack width measurements (part 2)

Shear "R1"	Crack Width (inches)						
kips	**C8**	**C9**	**C10**	**C11**		**C12**	**C13**
29	<.003	0.005	0.003	<.003		-	-
43	<.003	0.011	0.009	0.003		0.003	-
58	<.003	0.016	0.011	0.005		0.005	-
72	0.003	0.02	0.016	0.007		0.007	-
87	0.003	0.025	0.02	0.009		0.009	-
116	0.005	0.03	0.025	0.005	0.005	0.013	-
145	0.005	0.04	0.04	0.005	0.016	0.02	-
173	0.005	0.06	0.05	0.005	0.05	0.03	0.02

3.9 Deep beam testing summary

The deep beam test specimens presented in this chapter were designed to have each end tested independently. However, it was observed that the damage to the specimen during testing of end 1 affected the behavior of the specimen during testing of end 2. As a result, the pier cap specimens whose designs are presented in Chapter 4 were not designed to test each end independently. Behavior of the deep beam specimens was affected by crushing of the concrete under the load plate; as a result, a study of the pier cap and column connection is presented in Chapter 4. The results of the deep beam testing will be further discussed and compared to the strut and tie analysis of the specimens as stipulated in AASHTO Article 5.6.3 in Chapter 6.

It was determined that surface mounted strain gauges provided too localized of a strain measurement. As a result the only surface mounted gauges used during the tests discussed in Chapters 4 and 5 were LVDTs and string potentiometers, because both were able to measure the average strain over larger gauge length than the strain gauges. In addition LVDTs and potentiometers were less likely to fail if a crack crosses the gauge location, and were more economical because they could be reused.

CHAPTER 4. PIER CAP EXPERIMENT DESIGN

This chapter discusses the design and experimental setup used for the testing of six 3 feet deep 1 foot wide by 11 feet long reinforced concrete pier caps, designed and cast to be representative of GDOT bridge pier caps. These designs utilized information gained in the initial testing phase involving three deep beams, as summarized in Chapter 3. Each pier cap included a 18 inches deep 1 foot wide by 3 feet long column segment. Each specimen had a shear span to depth ratio (a/d) of 1.53, where the shear span is defined as the distance from the center of the column to the center of the nearest girder, and the depth is the distance from the top of the beam to the centroid of the tension reinforcement. The pier caps were designed with typical longitudinal reinforcement ratios observed in GDOT pier caps constructed in the 1950's and 1960's. The experimental objectives were to evalute the effect of adding a column to the test structure, to determine if the strut and tie method as defined in AASHTO Article 5.6.3 (2007) is appropriate for analyzing existing pier caps regardless of whether they meet the minimum shear reinforcement requirement, and to evaluate the effectiveness of external post-tensioning at increasing the shear resistance and delaying crack propagation.

4.1 Selection of test specimen

To determine if a segment of the pier cap could be tested in place of the full structure, the force distribution within the full pier cap and column structure was analyzed. Bent number 3 of GDOT Bridge 085-00180-0 was used for the design of the model. GDOT Bridge 085-00180-0 is a two-lane bridge that carries state route 136 over the Etowah River, 5.7 miles east of Dawsonville, GA. The bridge was designed in 1963 for H-15 loading, and consists of four 49 foot spans. The bridge was one of those load-tested in the earlier research program (O'Malley, et al. 2009). The pier cap and supporting piers support four steel girders spaced at 8 feet on center, which in turn support the bridge deck. For the purpose of designing the test specimens, the pier cap

shown in Figure 4.1 was modeled as a fixed-fixed portal frame and the forces applied through the girders were determined from various pattern loadings of the current standard AASHTO HS-20 load, rather than the H-15 load (Figured 1.2) for which bridge 085-00180-0 was designed.

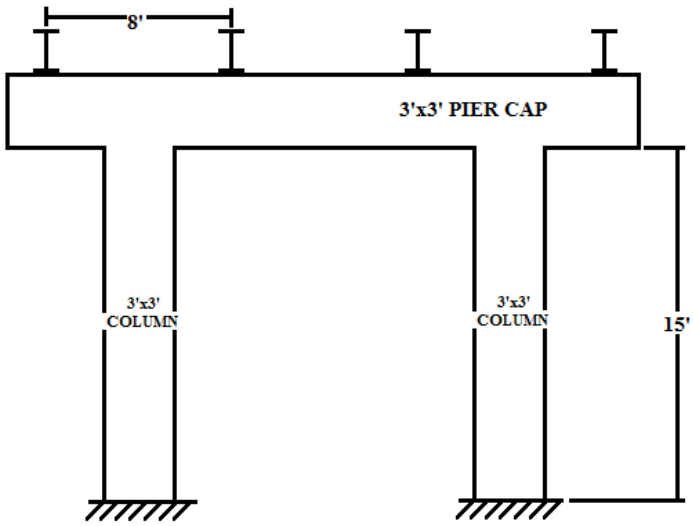

Figure 4.1 Typical pier cap and column

The pattern loading process consisted of placing multiple trucks across the width of the bridge spaced at a minimum of 4 feet between trucks and 2 feet from the curb. The deck of the bridge was then assumed to act as simply supported between adjacent girders, resulting in girder reaction forces for each load case. Each set of girder reaction forces was then applied to the pier cap and column model in order to find the critical load case. Through this analysis, the largest shear and moment loading combination in the pier cap was found to occur when the structure was loaded symmetrically (Figure 4.2). The region of highest shear is between the load points at the interior girders and the support at the adjacent column. The typical bridge girder spacing in Georgia during the 1950's and 1960's was 7 to 9 feet on center, resulting in an a/d ratio between 1 and 2.5.

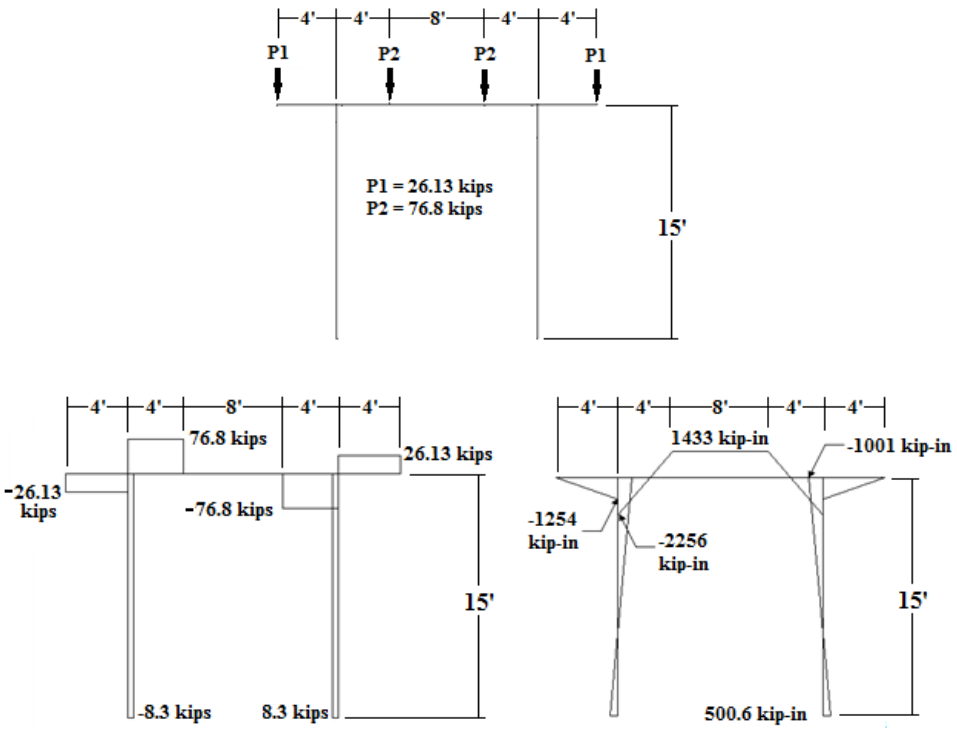

Figure 4.2 Pier cap and column loads (Top) shear diagram (right) moment diagram (left)

Due to the symmetric nature of both the structure and the load case that resulted in the highest shear, testing was performed on half of the full structure (Figure 4.3). This configuration allowed for a more economical testing procedure, due to the reduction in material cost and amount of instrumentation required. In addition, testing only half the pier cap reduced the number of load and reaction points from 6 to 3. The three remaining points are the location of the supporting column and the location of two girder supports, as shown in Figure 4.3. Furthermore, by inverting the structure it can be tested as a simply supported specimen, with the load applied through the column and simulated pin/roller supports at the location of the girders that frame into the pier cap (Figure 4.4). Both supports consisted of a 2.5 inch steel cylinder between 1 inch steel plates (Figure 4.5). The only difference between the two supports was that the cylinder was welded to the base plate in the simulated pin support. The load was applied by a hydraulic actuator through the load cell, a 1.5 inch thick socket, a 3 inch diameter ball, a 2 inch thick socket, and a stack of four 1 inch thick load plates (Figure 4.6).

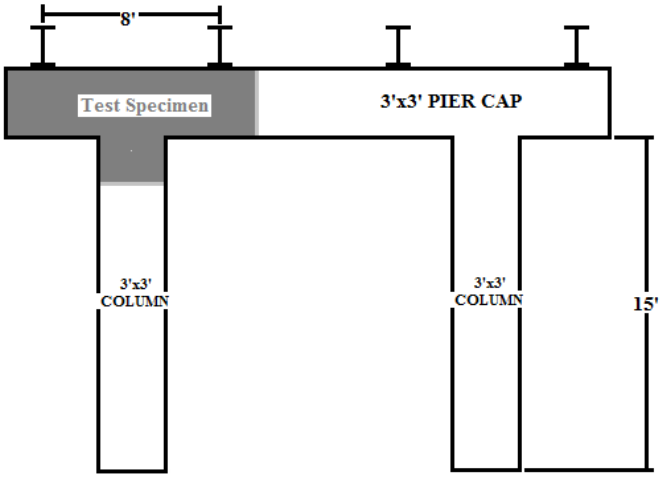

Figure 4.3 Test specimen design

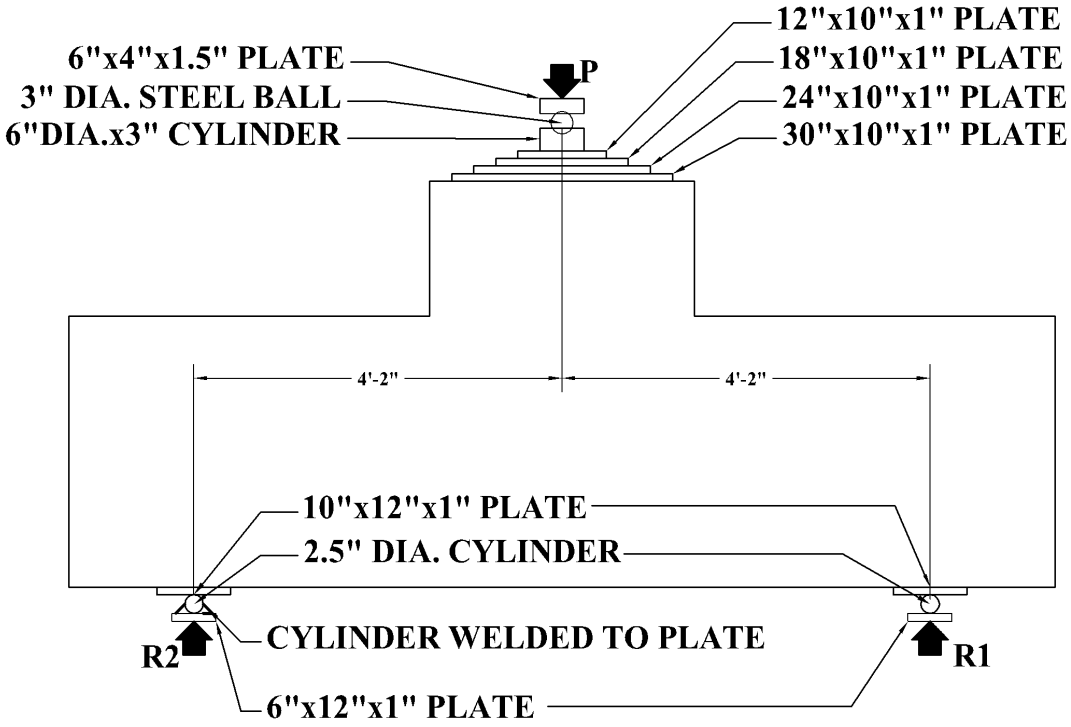

Figure 4.4 Test configuration for pier cap model

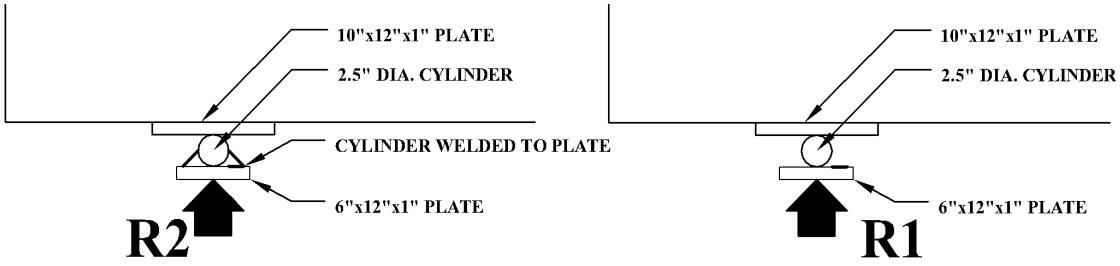

Figure 4.5 Support details simulated pin (left) simulated roller (right)

Figure 4.6 Loading assembly

4.2 Comparison of pier cap specimens with and without an integral column segment

4.2.1 Bearing tests performed on segments of deep beam WP

In experiments WP-E1-PT and WP-E2 (discussed in Chapter 3), bearing failures were observed under the load plate (Figure 4.7), which may have caused the failure of the specimen. As a result, a series of bearing tests (B1, B2, and B3) were performed on the segments of specimen WP that remained largely intact after experiments WP-E1, WP-E1-PT and WP-E2. The results of the three bearing tests are presented in Table 4.1. Under the load plate, the width of the beam was reduced from 12 to 11 inches due to the ½ inch chamfer on both sides of the beam. During each bearing experiment the load was applied to the specimen by a hydraulic jack through a different size bearing plate dimensioned in Figure 4.8. During bearing experiments B1 and B2 the load plate was oriented to extend over the full 11 inch width of the beam, along two different lengths (Figure 4.8). Failure of the specimen during bearing experiments B1 and B2 occurred at a bearing stress between the load plate and specimen of 2,800 to 2,900 psi. However, during bearing test B3 the load plate was rotated so that only the center 8 inches of the specimen was loaded, and a bearing stress of 4,300 psi was achieved prior to bearing failure. Bearing test B3

resulted in a 50% increase in bearing capacity as compared to test B1 and B2 by eliminating any edge loading. The rotation of the bearing plate proved to be a viable alternative as typical pier cap designs have a girder bearing plate inset from the face of the pier cap. As a result, the remaining tests of LT-E1 H-E1 and H-E1-PT were performed using the new bearing plate configuration.

Figure 4.7 WP-E1-PT failure

Table 4.1 Bearing test results

	Size	Load (kips)	Bearing stress (psi)
B1	11 inches x11 inches	344	2,800
B2	8 inches x11 inches	255	2,900
B3	12inches x8 inches	417	4,300

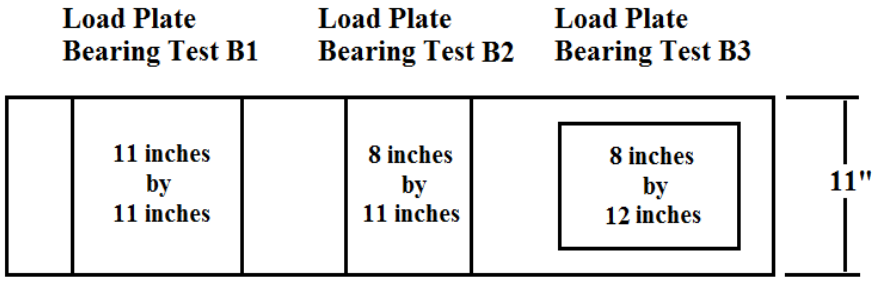

Figure 4.8 Bearing test load plates

4.2.2 Analysis of pier cap specimens with load applied through an integral column segment and through a load plate

With the importance of the bearing condition established, an elastic finite element analysis was employed to study the bearing conditions in the bridge structure where the pier cap is attached to a column, and to develop a comparable test specimen design. The development and location of diagonal tension cracks within the specimen governed the formation of tied arch behavior as well as the capacity of the tied arch mechanism. As a result of the importance of the development and physical location of the diagonal tension cracks an inelastic finite element model that could predict the response of the pier cap specimens was not possible. Instead an elastic finite element model that demonstrated the overall stress distribution within the specimen prior to cracking was constructed. A 3-D solid model was constructed using ABAQUS to represent a full pier cap structure with embedded steel reinforcing bars. Three bearing conditions were analyzed, including one with a 15 foot long column, one with the column replaced with an 18 inch tall column stub and one with the column replaced by a 2" steel plate.

For the ABAQUS model with the steel plate (Figures 4.9 and 4.10), the load was uniformly distributed over the steel plate having the same area as the column. A right hand coordinate system was utilized to present the results in these figures, where the 1 direction is horizontal in-plane, the 2 direction is vertical in-plane and the 3 direction is out of plane. This model resulted in an increase in the stresses in the horizontal or S11 direction in the tension region of the specimen (top of Figure 4.9) when compared to the model that included the column stub (Figure 4.11) at the same load level. This increase is due to the fact that the elimination of the column causes the horizontal compression block to extend further into the beam, reducing the moment arm between the specimen centroids of compression and tension forces.

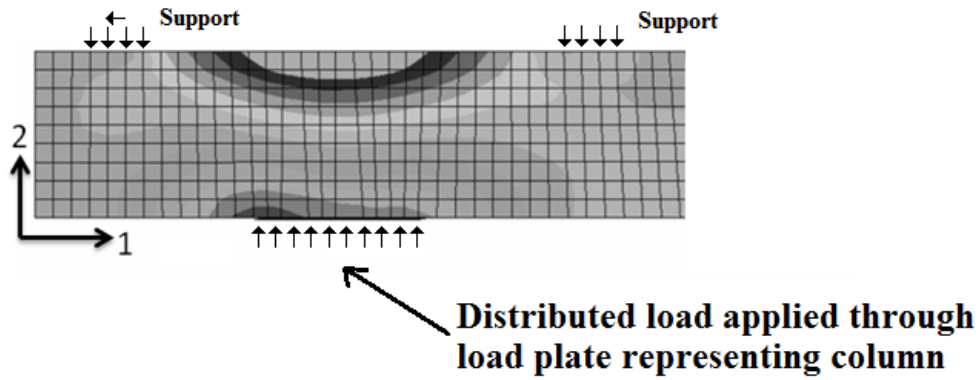

Figure 4.9 Column replaced with steel plate (S11-horizontal stress)

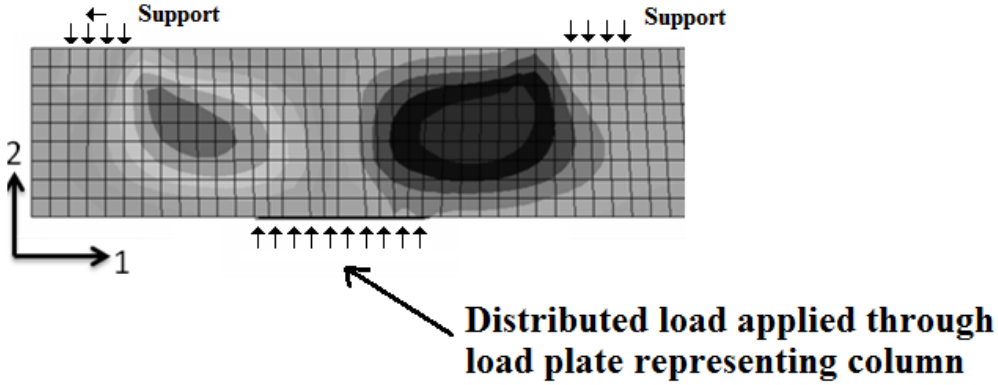

Figure 4.10 Column replaced with steel plate (S12-shear stress)

The ABAQUS model that included an 18-inch high integral column segment is illustrated in Figure 4.11 and 4.12. Unlike the model of the pier cap without an integral column, this model shows that the two compression struts extend into the column. As a result, localized stress concentrations occur around the pier cap and column interface; these stress concentrations are highlighted in Figure 4.12. These stress concentrations at the beam column interface were not present in the model that did not include an integral column segment (Figure 4.10). Both the ABAQUS model presented here and the experimental results in Chapter 5, described subsequently, revealed that proper modeling of the stress concentrations at the interface between the pier cap and column is crucial when analyzing or testing such structures. As a result of the ABAQUS analysis, the test specimen was selected as shown in Figure 4.3, which includes the integral 18 inch tall stub column.

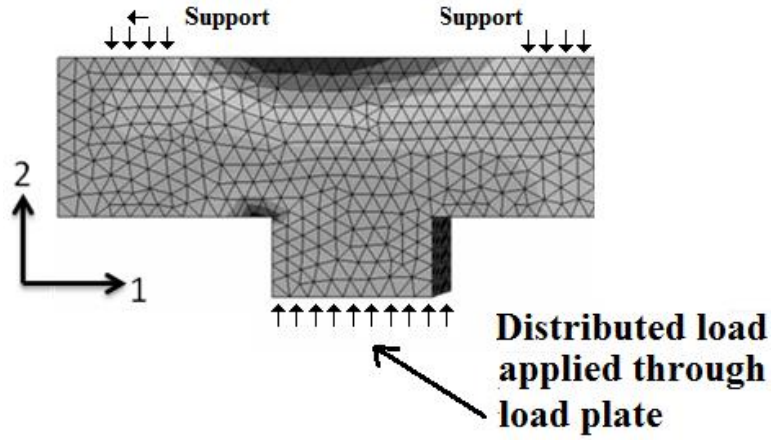

Figure 4.11 Column replaced with 18 inch stub column (S11-horizontal stress)

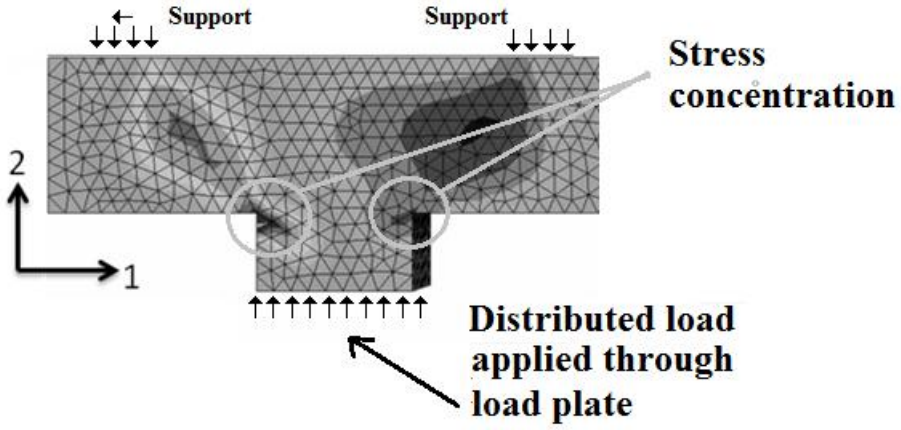

Figure 4.12 Column replaced with 18 inch stub column (S12 -shear stress)

4.3 Pier cap specimen design

4.3.1 Existing GDOT pier cap designs

Pier caps from six different GDOT bridges were evaluated prior to designing the experimental specimens. The first criterion for designing the pier cap specimens was the tension reinforcement ratio in the bridges, which was found to range between 0.97 and 0.56 percent in the section of the pier cap under evaluation (Table 4.2). The highest possible reinforcement ratio was selected in order to ensure that the flexural resistance of the pier cap specimens was greater than the shear resistance of the specimens. A ratio of 0.91 was selected for the experimental program, because it was at the high end of the

range of typical GDOT pier cap reinforcement ratios. The next criterion was the overall dimensions of the pier cap, the GDOT pier caps ranged from a depth of 2 feet 6 inches square to 3 feet 6 inches square. A depth of 3 feet was selected, because it was the average GDOT pier cap depth. The width of the specimens was selected to be 12 inches, which made the testing more economical and allowed for the construction of more specimens. This width reduction was possible because, as discussed in Chapter 2, specimens can be scaled in width without affecting their response.

Table 4.2 GDOT typical pier cap reinforcement ratios

Bridge Identification	Year Designed	Longitudinal Reinforcement Ratio	
		Top	Bottom
GDOT ID# 083-0016-0	1959	0.56	0.76
Gordon County Bridge over Camp Creek	1960	0.89	0.78
GDOT ID# 097-0032-0	1960	0.94	0.31
GDOT ID# 085-0018-0	1964	0.59	0.43
North Fulton Expressway S-bound over Abernathy Rd.	1967	0.67	0.67
GDOT ID# 067-0172-0	1979	0.97	0.71

4.3.2 Design of pier cap specimens with internal shear reinforcement that meets AASHTO LRFD bridge design specifications (2007)

Six pier cap specimens were tested in this phase. Pier caps 1, 2 and 3 were designed with a reinforcement ratio of 0.91% and shear reinforcement in compliance with the 2007 AASHTO LRFD Bridge Design Specifications. As per Article 5.8.1.2 of the AASHTO LRFD Bridge Design Specifications (2007), the pier cap-column structure is considered to be a region involving discontinuities and thus was designed and analyzed using the Strut and Tie provisions of Article 5.6.3. In addition, Article 5.8.1.2 requires that the detailing requirements for deep beams as specified in Article 5.13.2 be followed.

Pier cap 1 was intended to be loaded to failure without any retrofit technique applied, providing a baseline for comparing the behavior of pier caps 2 and 3, which were tested with the external post-tensioning retrofit. The specimens were reinforced with two layers of No. 8 bars as tension reinforcement, the first layer consisting of three bars at a

depth of 33.5 inches, and the second layer consisting of two bars at a depth of 31.5 inches (Figure 4.13). The cross sections of the specimen with internal shear reinforcement (S) shown in Figure 4.13 are shown in Figure 4.14.

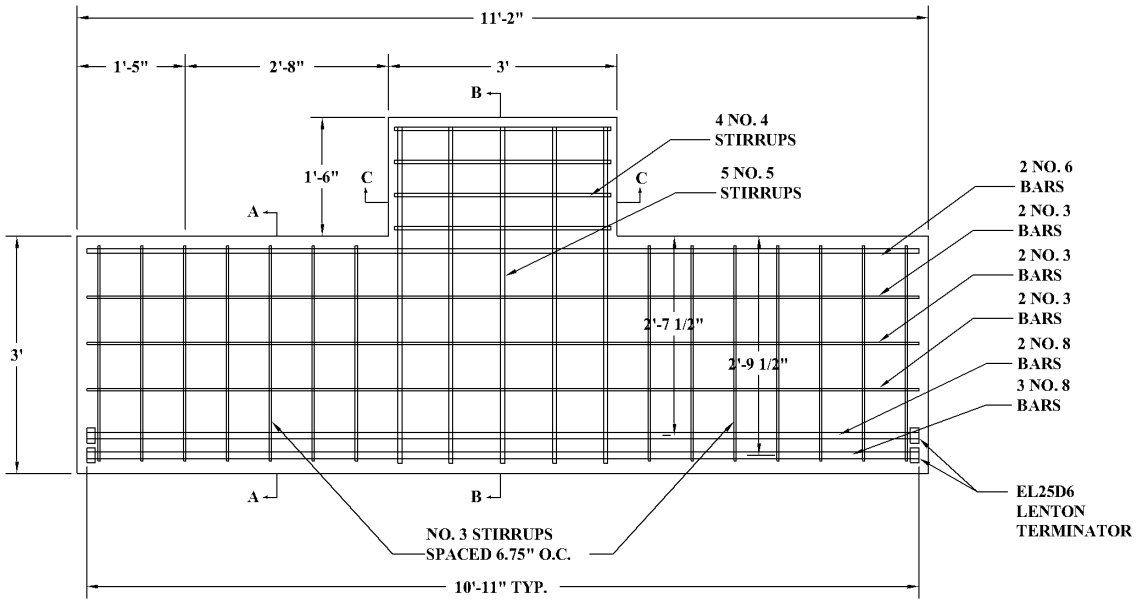

Figure 4.13 Design drawing of specimens with shear (S) reinforcement meeting Article 5.13.2.3 of AASHTO LRFD Specifications (2007)

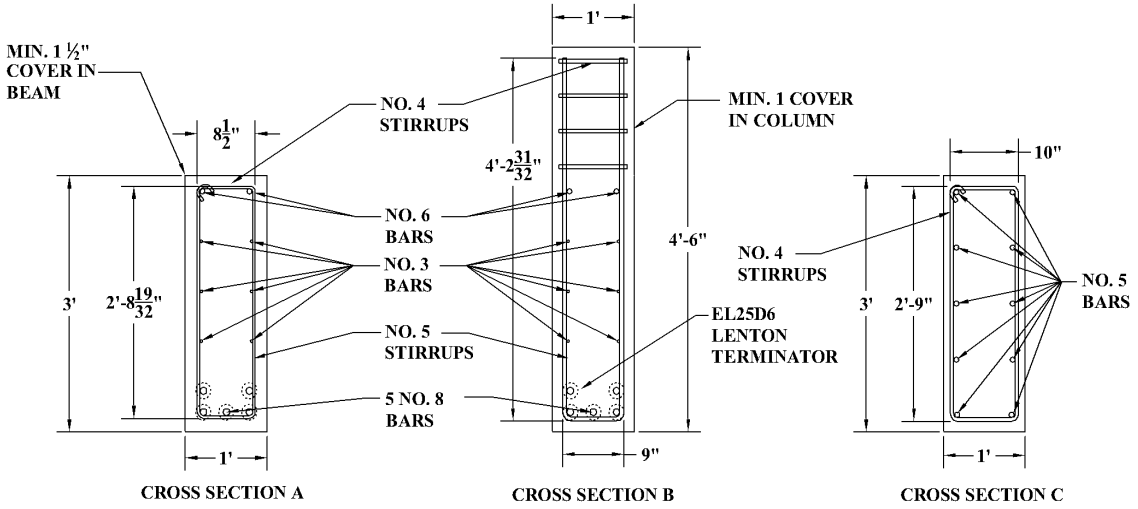

Figure 4.14 Cross sections of specimens shown in Figure 4.13

Compression reinforcement was provided by two No. 6 bars. Horizontal shear reinforcement was provided by No. 3 bars spaced 7 inches on-center on each face of the

specimen, in compliance with AASHTO LRFD Bridge Design Specification (2007) Article 5.13.2.3 "Detailing requirement for deep beams." The same article governs the vertical shear reinforcement in the specimen, which consisted of No. 3 stirrups spaced 6.75 inches on-center. The column reinforcement consisted of five vertical No. 5 stirrups, selected to represent one-third of the axial reinforcement of a typical column since the pier cap specimens are one-third of the width of a typical pier cap. Four horizontal No. 4 stirrups were equally spaced in the 18 inch column stub in order to provide confinement. A photo of the fabrication of the specimen is shown in Figure 4.15, the stirrups in the column are hidden by the formwork.

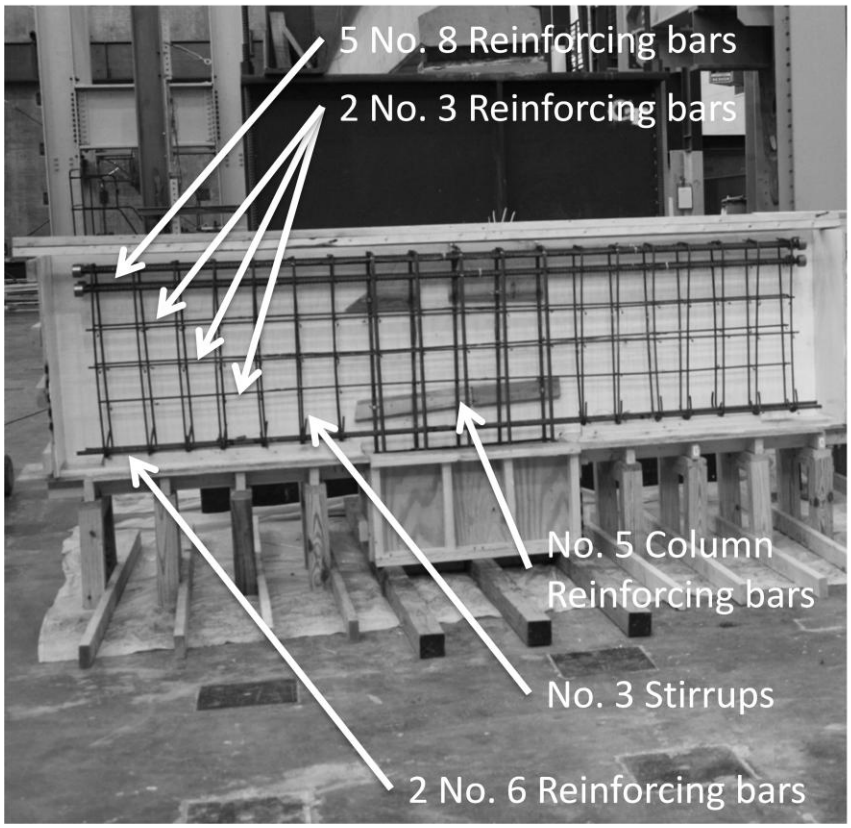

Figure 4.15 Specimen reinforcement meeting AASHTO LRFD Bridge Design Specification (2007)

4.3.3 Design of pier cap specimens without shear reinforcement

Pier caps 4, 5 and 6 were also designed with a reinforcement ratio of 0.91% but with no shear reinforcement in the shear span. Bridge design standards have changed

greatly between 1944 and 2007. The changes to the minimum shear stirrup spacing in that period are outlined in Table 4.3. In the pier cap geometry outlined in Figure 4.1, the 1944 and 1953 minimum spacing requirements result in a minimum of one stirrup in the pier cap in the shear span between the column and girder. Since pier caps built to the minimum specifications of 1944, 1953, or 1977 do not meet current requirements for the use of the strut and tie method it was decided to test the two extremes: specimens that meet the 2007 requirement for the use of the strut and tie method and specimens without any shear reinforcement in the shear span. These test specimens allow for the determination of whether the strut and tie method can be effectively applied to existing bridge pier cap structures that do not meet the current stirrup requirements.

Table 4.3 Sample of historical bridge design shear requirements

Code	Year	Min. stirrup spacing	Requirement
Standard specifications for highway bridges 4th edition	1944	$s = \frac{3}{4}d$	1st stirrup is $\frac{1}{4}d$ from the face of support
Standard specifications for highway bridge 6th edition	1953	$s = \frac{3}{4}d$	1st stirrup is $\frac{1}{4}d$ from the face of support
Standard specifications for highway bridges 12th edition	1977	$s = \frac{1}{2}d$	$A_{vmin} = \frac{50 b_w s}{f_y}$
AASHTO LRFD bridge design specifications 4th edition	2007	Article 5.6.3.6, 5.8.1.2, and 5.13.2.3	

The resulting pier cap reinforcement details for pier caps 4 - 6 include the same tension and compression reinforcement as in pier caps 1 - 3. In place of the five stirrups used in pier caps 1 – 3, ten vertical No. 5 bars representing the column axial reinforcement were used. Four No. 4 stirrups were used to confine the 18 inch integral column segment. In addition, three No. 3 stirrups were used at the location of each support for confinement of the bearing area. Figure 4.16 is the design drawing of the pier cap specimens without internal shear reinforcement (NS), and Figure 4.17 is a drawing of the cross sections A, B, and C identified in Figure 4.16. Figure 4.18 is a photo of the specimens without internal reinforcement (NS) during fabrication, the stirrups in the

column are hidden by the form work. In all six specimens, the pier cap and column segment were cast separately with a cold joint between them.

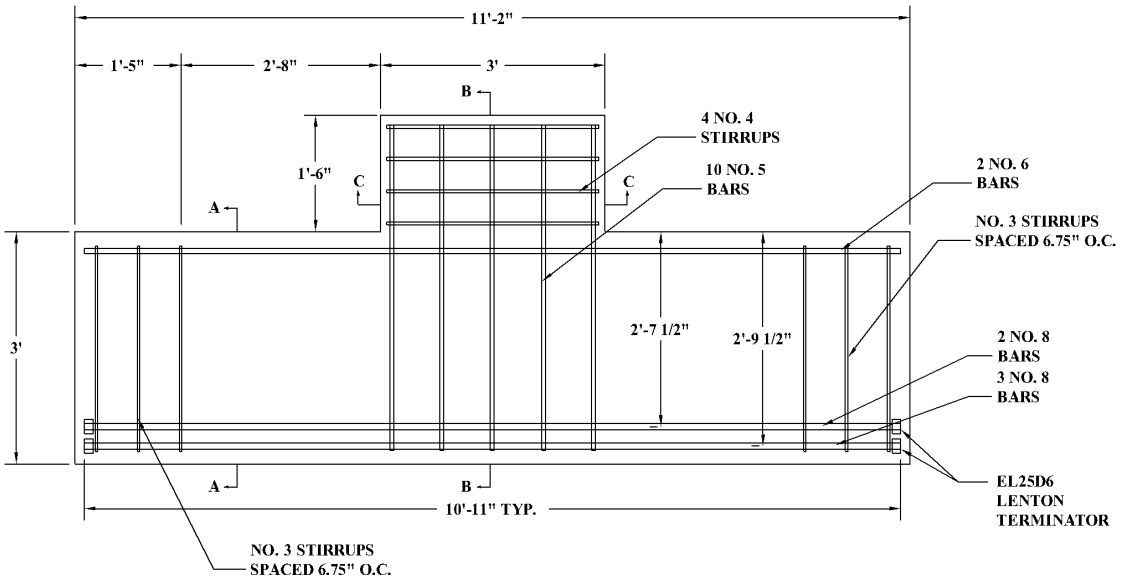

Figure 4.16 Design drawing of specimens with no internal shear reinforcement

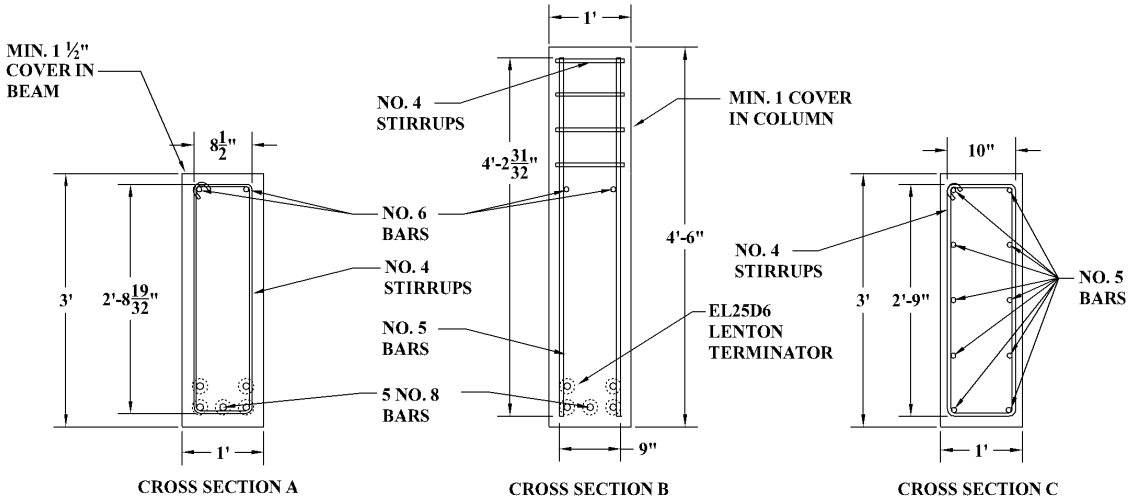

Figure 4.17 Cross sections of specimens shown in Figure 4.16

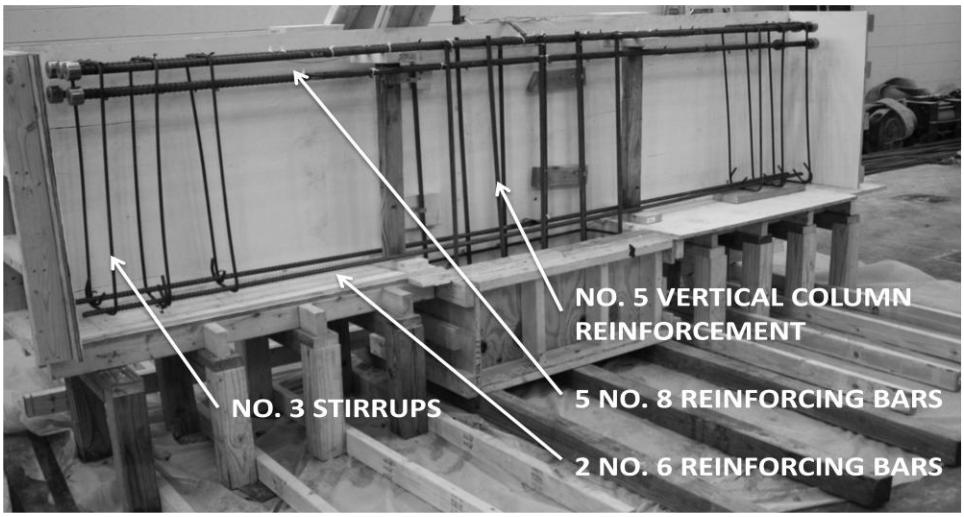

Figure 4.18 Specimen without internal shear reinforcement in the shear span

4.4 Details of pier cap specimens

The specimen details and tests performed on each pier cap are outlined in Table 4.4. The fabriction drawing used to construct specimens 1 - 3 is shown in Figure 4.13, and the fabrication drawing for specimens 4 - 6 is shown in Figure 4.16. The test ID numbers identify the the order of the test, whether the test specimen had stirrups (S) or did not have stirrups (NS), and whether the test specimen was cracked before being post-tensioned (CR-PT) or was post tensioned without any intial damage (PT).

Table 4.4 Detail of pier cap specimens

Pier cap	Test ID	Description	Test type
1	1-S	Control with internal stirrups	Loaded to failure
4	2-NS	Control without internal stirrups	Loaded to failure
6	6-NS	Control without internal stirrups	Loaded to failure
5	4-NS	Crack specimen prior to post-tensioning	Loaded to shear in the test span of 100 kips
3	5-S	Crack specimen prior to post-tensioning	Loaded to shear in the test span of 100 kips
2	3-S-PT	Post-tensioned specimen with internal stirrups	Loaded to failure
5	4-NS-CR-PT	Test specimen without internal reinforcement and with post-tensioning	Loaded to failure
3	5-S-CR-PT	Test specimen with internal reinforcement and with post-tensioning	Loaded to yielding of the tension reinforcement
3	5-S-CR-PT2	Test specimen with internal reinforcement and with post-tensioning	Loaded to failure

Post-tensioning of the pier caps consisted of installing the post-tensioning assembly in each span of the pier cap (ie. between "P" and "R1" and between "P" and "R2"). Each external post-tensioning assembly consisted of four vertical bars that were post-tensioning to approximately the same level. The tension in each bar and the total post tensioning in each assembly can be found in Table 4.5.

Table 4.5 External post-tensioning

	Span from "P" to "R1"(Figure 4.4) (kips)					Span from "P" to "R2"(Figure 4.4) (kips)				
	Bar 1	Bar 2	Bar 3	Bar 4	Total	Bar 5	Bar 6	Bar 7	Bar 8	Total
3-S-PT	70	64	62	69	265	60	65	60	71	256
4-NS-CR-PT	60	45	50	55	210	53	49	53	58	213
5-S-CR-PT	55	52	61	55	223	56	53	54	49	212
5-S-CR-PT2										

4.5 Instrumentation of pier cap specimens

Each pier cap was instrumented to verify the behavior predicted by the strut and tie model. The primary components of a strut and tie analysis include the tension ties, the concrete compression struts, and the nodes where they intersect. In order to validate the ability of the strut and tie methods to predict the specimen's behavior as well as its capacity, it was necessary to confirm the geometry and forces within the various struts and ties. Since it was not practical or feasible to measure the forces in each strut and tie in each test, a sufficient number of struts and ties were monitored in order to evaluate the strut and tie model's predictions.

Due to the non-homogeneity of concrete, it was decided to focus on measuring the forces in the tension ties and to use statics and the geometry of the specimen in conjunction with the applied load to compute the forces within the compression struts and their angle of inclination. This angle of inclination was also verified independently by a Mohr's Circle analysis of the strain measured by an array of three LVDTs mounted externally on the specimen. LVDTs also were used to provide strain profiles vertically under the load in order to confirm the location of a horizontal compression strut in the stub column observed in the ABAQUS model (Figure 4.11).

4.5.1 Strain gauge locations during pier cap specimen tests

Strain gauges were used exclusively on the internal reinforcing bars. Vishay 350 Ohm electrical resistance strain gauges were used. Specimens with and without internal shear reinforcement were instrumented with strain gauges on the five No.8 bars that comprised the main tension reinforcement. The gauges were installed at the center of the pier cap and the centerline of the shear span (Figures 4.19 and 4.21). Additionally, in specimens 1-3, strain gauges 9-19 (Figure 4.19) and in specimens 4-6 strain gauges 5-12 (Figure 4.21), were used to produce a strain profile through the depth of the specimen. Also, at the centerline of the shear span, strain gauges 0-8 and 28-36 (Figure 4.19) were used to measure the strain profile in specimens 1-3. Finally, the vertical stirrups in the shear span were instrumented at mid-depth using strain gauges 20-27 (Figure 4.20) in specimens 1-3.

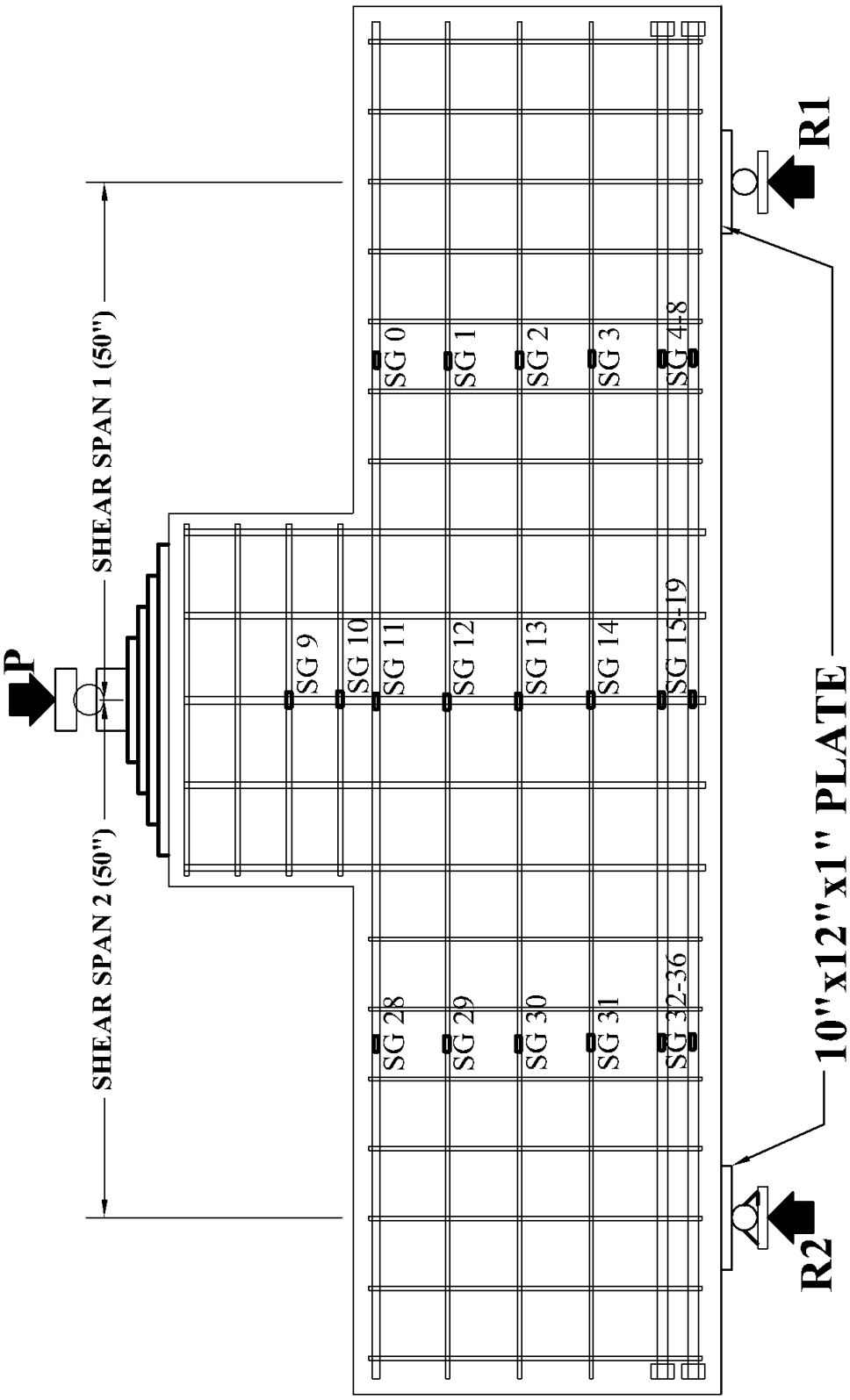

Figure 4.19 Location of strain gauges on reinforcement in specimens with internal shear reinforcement

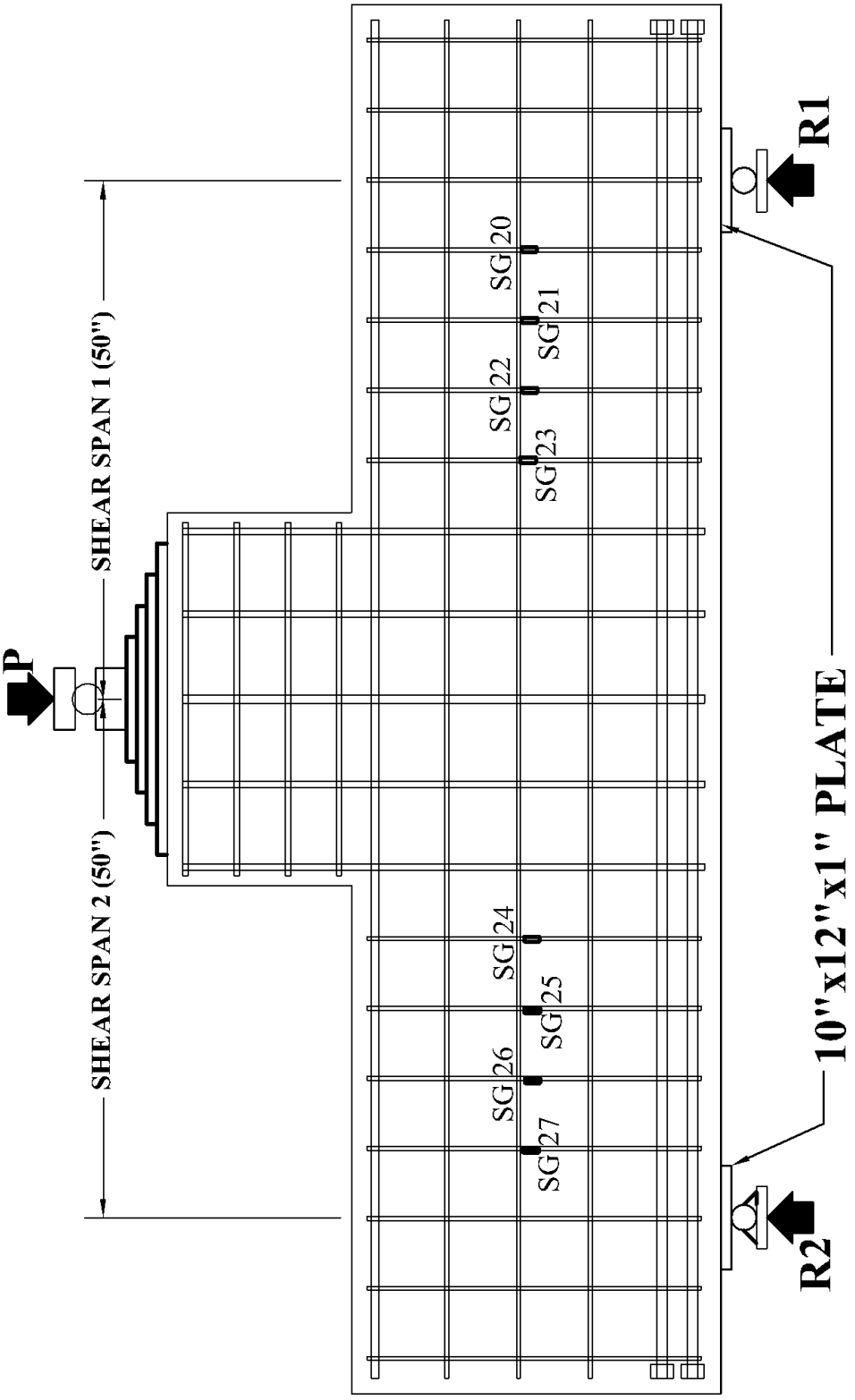

Figure 4.20 Location of strain gauges on shear reinforcement in specimens with internal shear reinforcement

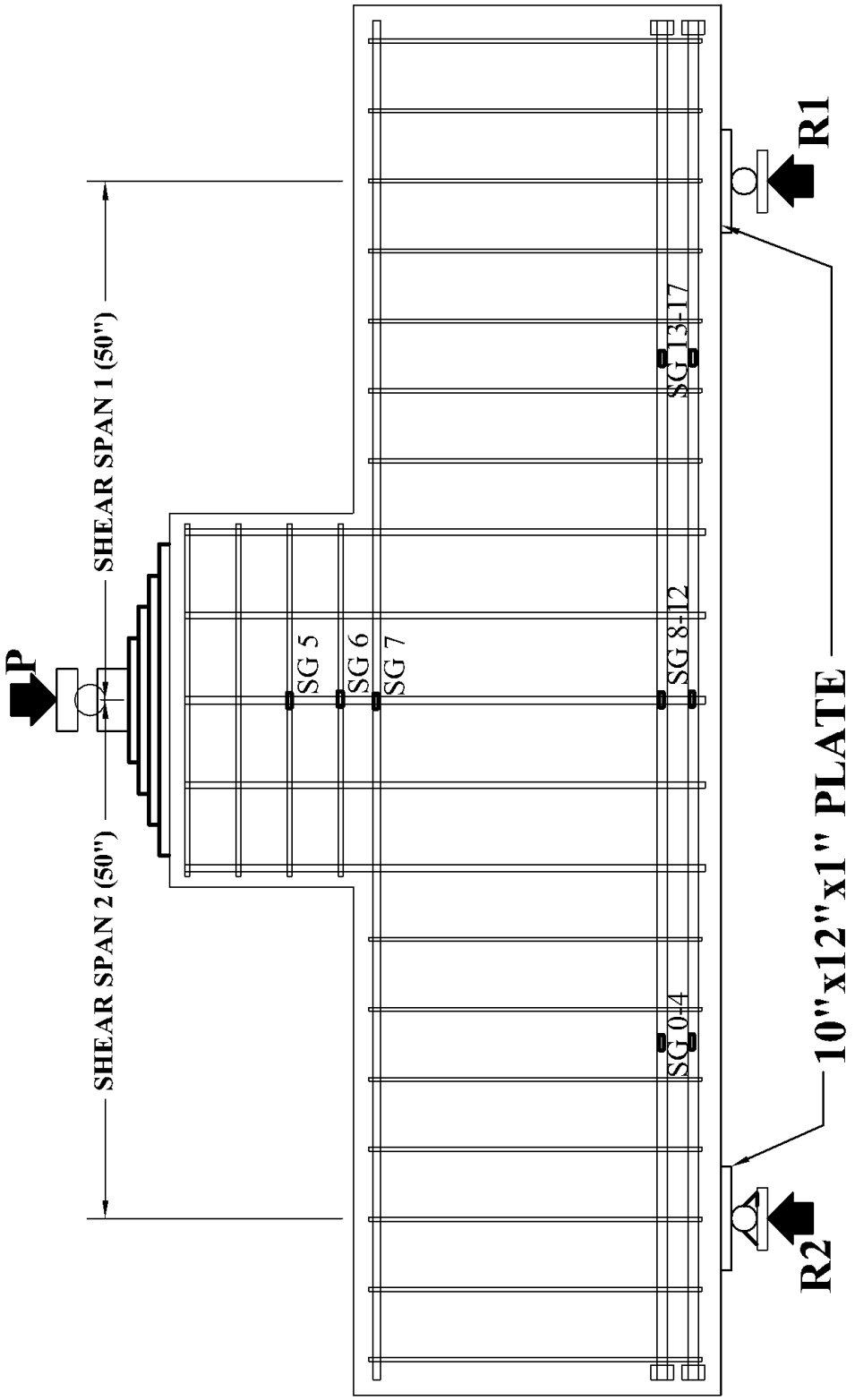

Figure 4.21 Location of strain gauges on reinforcement in specimens without internal shear reinforcement

4.5.2 LVDT locations during pier cap specimen tests

LVDT's were used to measure average strains in the concrete over various gauge lengths (Table 4.6). Due to the inhomogeneity of concrete and stress concentrations that arise in the reinforcement around cracks, average strain values over the length of the compression struts and tension ties were found to be a more reliable method of monitoring the specimen's performance than localized strain readings. The same general LVDT instrumentation techniques were used for specimens with and without internal shear reinforcement. However, the instrumentation locations were changed between the control specimen tests 1-S, 2-NS, and 6-NS (Table 4.4); and the post-tensioned test specimens 3-S-PT, 4-NS-CR-PT, and 5-S-CR-PT, as described below.

Table 4.6 LVDT gauge length

Pier cap tests (Figure 4.22)		**Post-tensioned pier cap tests (Figure 4.24)**	
LVDT 1	15 inches	LVDT 1	15 inches
LVDT 2	15 inches	LVDT 2	15 inches
LVDT 3	15 inches	LVDT 3	15 inches
LVDT 4	15 inches	LVDT 4	15 inches
LVDT 5	10 inches	LVDT 5	15 inches
LVDT 6	10 inches	LVDT 6	10 inches
LVDT 7	15 inches	LVDT 7	8 inches
LVDT 8	15 inches	LVDT 8	8 inches
LVDT 9	15 inches	LVDT 9	8 inches
LVDT 10	15 inches	LVDT 10	12 inches
LVDT 11	10 inches	LVDT 11	12 inches
LVDT 12	10 inches	LVDT 12	12 inches
LVDT 13	12 inches	LVDT 13	12 inches
LVDT 14	12 inches	LVDT 14	12 inches
LVDT 15	12 inches	LVDT 15	12 inches
LVDT 16	12 inches	LVDT 16	12 inches
LVDT 17	30 inches	LVDT 17	17 inches
LVDT 19	30 inches	LVDT 18	66 inches
String Potentiometer (19)	100 inches	LVDT 19	17 inches

For the control tests, the LVDTs were mounted on the surface of the specimen at the depth of the centroid of the 5 No. 8 bars that made up the main tension reinforcement (32.25 inches from the top of the specimen) in order to provide an average strain in the steel tension tie (String potentiometer Figure 4.22). Due to the formation of multiple

diagonal compression struts cause by the vertical post-tensioning of the specimen, the strain in the main tension reinforcement (Figure 4.23) was not constant over its length during the tests on post-tensioned specimens. During the post-tensioned specimen tests, the strain in the horizontal tension tie was monitored in three segments by LVDTs 17, 18, and 19 (Figure 4.24). The force in the tension tie was computed by converting the measured strain in the tension tie to stress through stress/strain curves created by performing tension tests on samples of the No. 8 reinforcement (Chapter 5). The force in the tension tie was then used in conjunction with the applied load to compute the angle of principal compression.

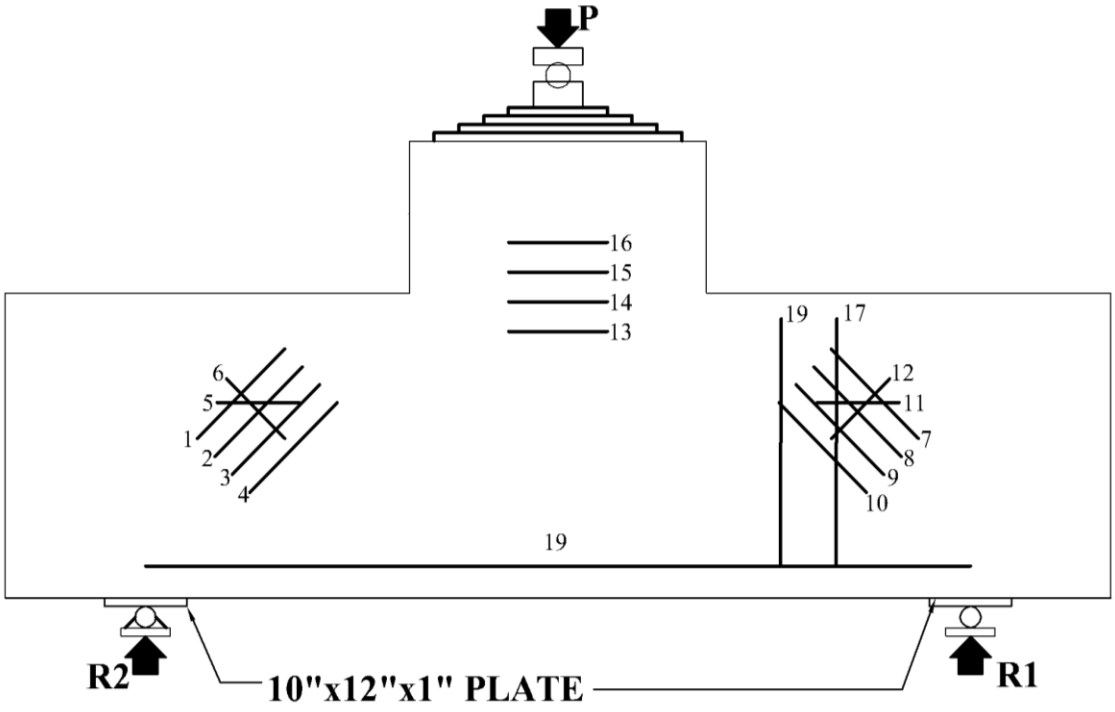

Figure 4.22 LVDT locations during pier cap tests

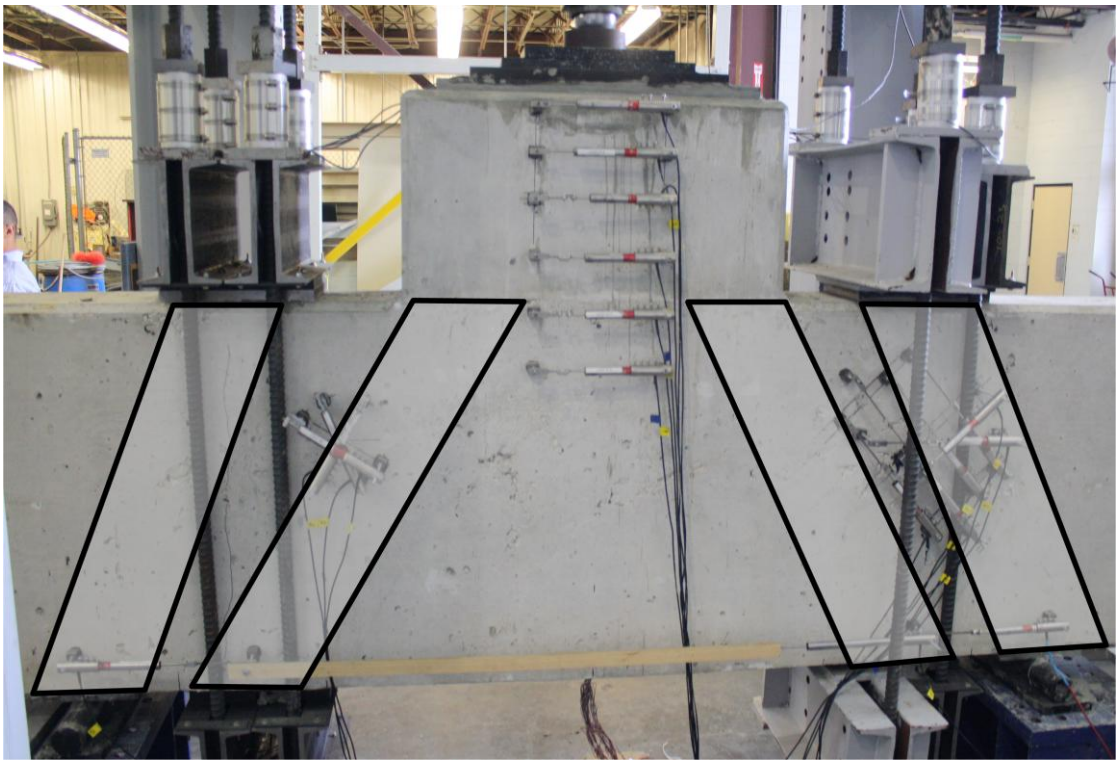

Figure 4.23 Post-tensioned specimen diagonal compression struts

For the control specimens, a rosette of three LVDTs was mounted in each shear span LVDTs 2-5-6 and 8-11-12 (Figure 4.22). For the rehabilitated specimens, LVDTs 2-5-6 were mounted in the same location to confirm that the rehabilitation altered the strut and tie mechanism, and did not simply provide confinement and limit cracking. Additionally, in shear span 1, LVDTs 7-8-9 (Figure 4.24) were oriented to measure the strain in the strut resulting from the rehabilitation. The readings from these LVDT rosettes were used to perform Mohr's Circle analyses in order to determine the angles of principal compressive strain in the compression struts. The angle computed using Mohr's Circle was then compared to the angle computed using the average strain in the tension ties and the applied load. Additionally, LVDTs were mounted parallel to the anticipated compression strut in the control specimens (LVDTs 1-4, and 7-10 Figure 4.22). These LVDTs were used to obtain a strain profile through the compression strut and to estimate its width.

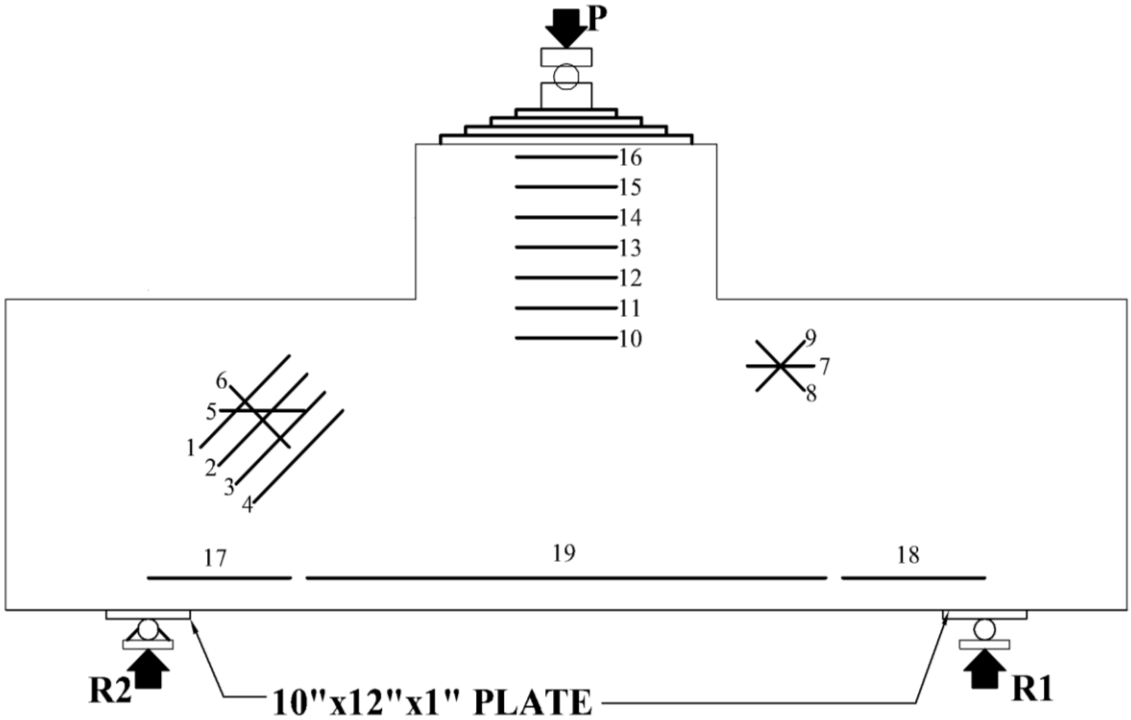

Figure 4.24 LVDT locations during post-tensioned pier cap tests

4.5.3 Potentiometer locations during pier cap specimen tests

String potentiometers were used to measure the vertical displacement of the specimen at mid-span (Figure 4.25). The rotation of the specimen was computed by measuring the horizontal in-plane displacement at the top and bottom of the specimen at each end (Figure 4.25). The rotation was computed by dividing the difference in horizontal displacement between potentiometers 1 and 2 by 35 inches (Figure 4.25)

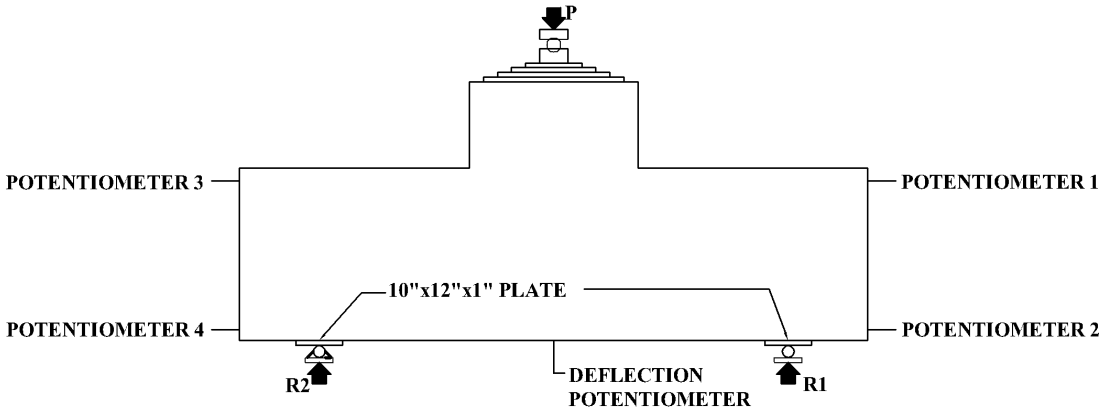

Figure 4.25 Potentiometer locations

4.5.4 Load cells used during pier cap specimen tests

The load cell shown in Figure 4.26 was used to measure the force applied to the specimen by the hydraulic jack. In addition for the specimens where external post-tensioning was used, the force in each of the DWYIDAG bars was measured by a load cell (Figure 4.26).

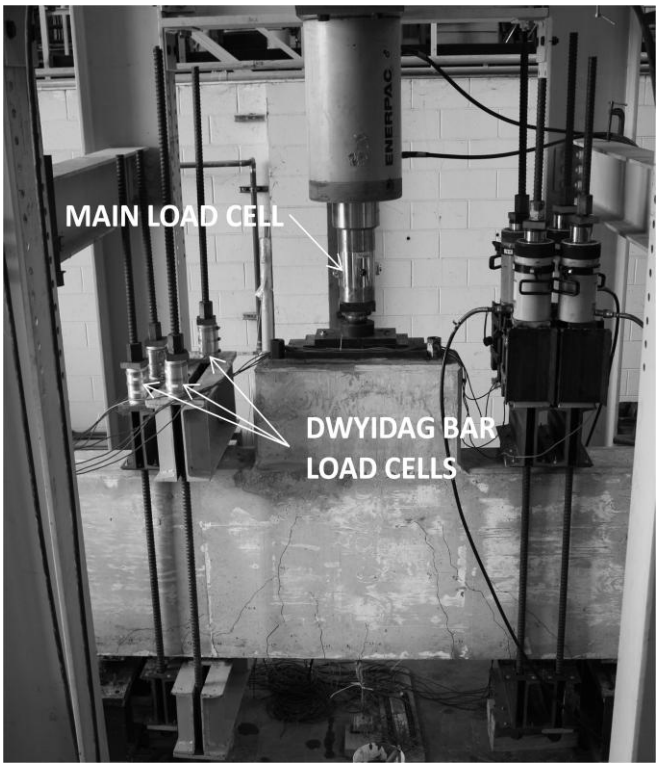

Figure 4.26 Load cell locations

CHAPTER 5. **PIER CAP SPECIMEN TESTS**

This chapter summarizes the nine tests performed on the six pier cap specimens described in Chapter 4 and summarized in Table 4.4. In this chapter, response of the test specimens with and without internal shear reinforcement are compared to each other; and the strengthening effect of the external post-tensioning system is examined.

Unlike the deep beam tests discussed in Chapter 3, the failure in each of the pier cap tests initiated at the corner of the pier cap-column interface. Failure of the specimens initiated at this location due to the stress concentration formed, by the discontinuity of the specimen's geometry. The external post-tensioning system shifted the diagonal compression struts away from the stress concentration, resulting in increased strength and the overall deflection of the specimen at its ultimate capacity (Section 5.2); however, ultimately failure of the specimen still initiated at the pier cap column corner.

5.1 External post-tensioning

The total tension force in the external post-tensioning system did not change significantly during any of the pier cap tests where it system was used. Figure 5.1 shows the total post-tensioning force in each of the clamps throughout tests 3-S-PT, 4-NS-CR-PT, 5-S-CR-PT, and 5-S-CR-PT2. The total post-tensioning force did increase significantly during each test and was not able to reach the shear force R1. The fact that the tension in the external bars did not increase with "R1" is the same as the behavior observed in the deep beam tests presented in chapter 3. Additionally no significant accidental strain in the internal No. 8 reinforcing bars was measured during the post-tensioning process. During the post-tensioning of 3-S-PT accidental horizontal tension strain developed in the concrete sufficient to crack the specimen vertically, as a result the total post-tensioning force was reduced slightly for tests 4-NS-CR-PT, 5-S-CR-PT, and 5-S-CR-PT2 (Table 4.5). The cracking of specimen 3-S-PT during post-tensioning is further discussed in Section 6.3.

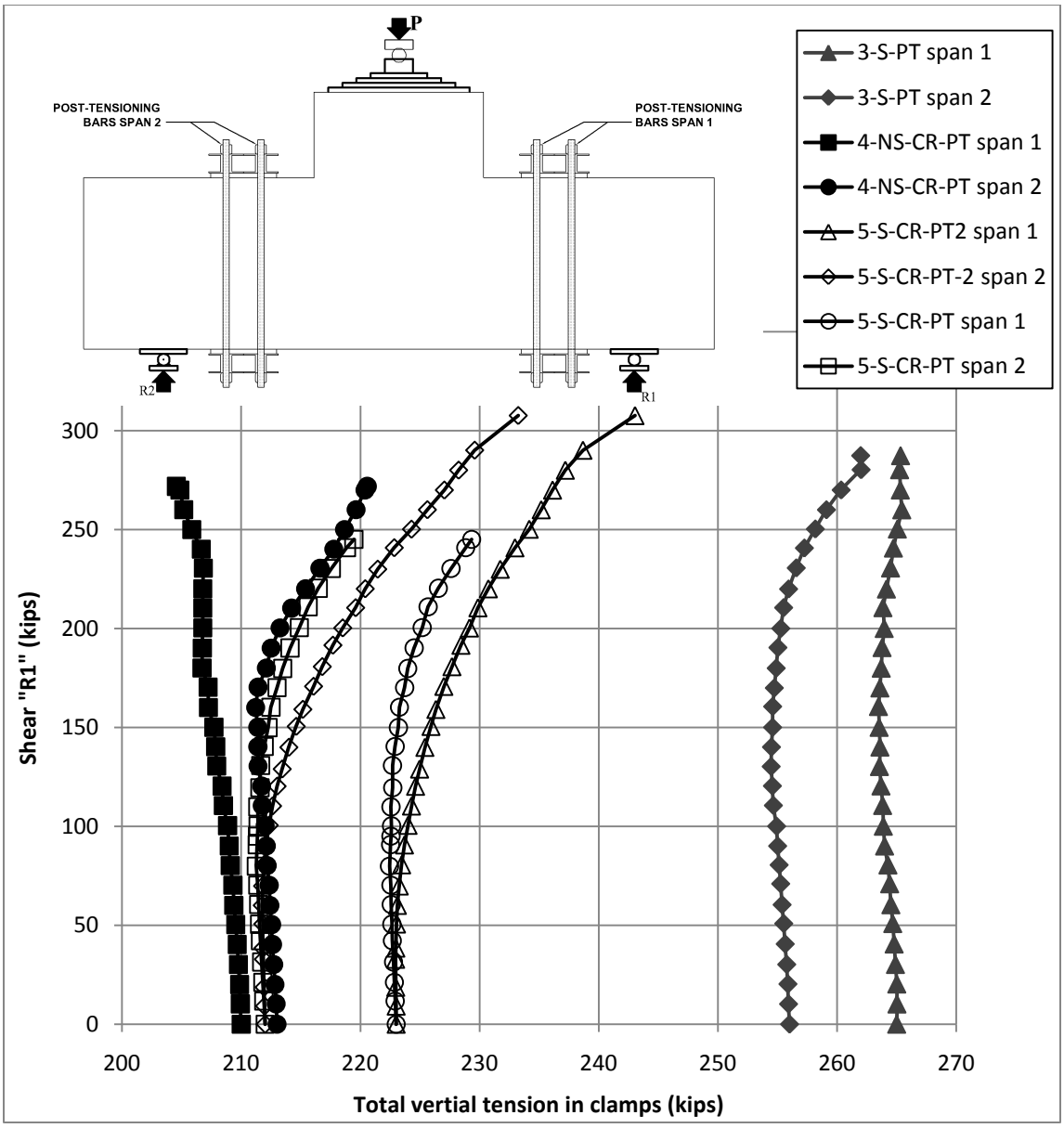

Figure 5.1 Tension in external post-tensioning system during tests

5.2 Displacement of pier cap specimens under loading

The vertical displacement of each specimen was recorded at mid-span during the pier cap tests. Two failure modes were observed during the pier cap tests; the first was a sudden loss of shear resistance at or before yielding of the main tension reinforcement. The sudden failure of the pier cap is considered to be undesirable because it gives little warning of impending failure and the specimen does not maintain its capacity once

yielding of the tension reinforcement occurs. The second failure mode was one in which the specimens were capable of sustaining both shear resistance and displacement after yielding of the tension reinforcement. For purposes of comparison of the measured displacements, the tests have been separated into two categories: tests performed without, and with the external post-tensioning system.

5.2.1 Displacement of specimens without post-tensioning (1-S, 2-NS, 4-NS, 5-S, 6-NS (Table 4.4))

Five tests were performed without the external post-tensioning system. During pier cap tests 1-S, 2-NS, and 6-NS, the specimens were loaded to failure. Pier cap tests 4-NS and 5-S were performed to pre-crack the specimens prior to application of the external post-tensioning. Accordingly, the tests were stopped and the load was removed when the shear in the test span reached approximately 100 kips. The decision to stop the testing when the shear in the test span reached 100 kips was made based on the results of tests 1-S and 2-NS. During tests 1-S and 2-NS diagonal cracking of the pier cap was observed visually prior to a shear "R1" of 100 kips; however, yielding of the tension reinforcement did not occurred until after "R1" exceeded 100 kips (Section 5.4).

Prior to yielding of the tension reinforcement, the shear versus displacement plot (Figure 5.2) of the specimens with (S) and without (NS) internal shear reinforcement are in good agreement. The control test for pier caps with internal shear reinforcement was test 1-S, which was conducted to failure of the specimen. During test 1-S, the specimen failed by crushing of the compression node and stress concentration located at the pier cap - column interface (Figure 5.3). This failure occurred at a shear "R1" of 196 kips and a centerline displacement of 0.25 inches. The hydraulic jack that applied load to the pier cap was extended after failure of the pier cap to determine if the damaged structure was capable of maintaining its shear resistance. As the jack was extended the specimen continued to deflect but was not capable of maintaining its shear resistance.

The control test for specimens without internal shear reinforcement was test 6-NS and was also conducted to failure. The test 2-NS was conducted to determine the effect of removing composite action between the pier cap and column. During test 2-NS de-bonding of the pier cap and column interface occurred because a 4 mil. visqueen plastic sheet was placed between the pier cap and column prior to casting of the pier cap. Specimen 2-NS exhibited larger deflections at lower shears than specimen 1-S and 6-NS; after reaching a shear "R1" of 139 kips and a displacement of 0.25 inches, specimen 2-NS continued to deflect with only a minor loss of shear resistance until it reached a shear "R1" of 122 kips and a deflection of 0.42 inches. This behavior differed from test 1-S and 6-NS because de-bonding of the pier cap – column interface (Figure 5.4) occurred prior to crushing of the concrete at the stress concentration at the pier cap – column joint (Figure 4.12).

The initial slope of the shear "R1" displacement curve for the tests with and without internal reinforcement 1-S and 6-NS was similar, with the sudden loss of shear resistance of the specimens occurring at a shear "R1" of 195 kips for specimen 1-S and 252 kips for specimen 6-NS. This difference in the shear resistance of the two specimens can be traced back to the available size of the diagonal compression strut and the compression capacity of the concrete. The cross sectional area of the diagonal compression strut was limited by the distance from the corner at the beam column connection to the nearest diagonal tension crack. In the case of test 1-S, this distance was 3 inches (Figure 5.3), while in the case of test 6-NS (Figure 5.5), it was 5 inches. These widths resulted in an area of the diagonal compression strut of 36 and 60 square inches for tests 1-S and 6-NS respectively, and average compression stress in the diagonal compression strut at failure of the specimens of 5.42 ksi and 4.20 ksi. The concrete compression strength obtained from cylinder compression tests were similar for tests 1-S (3.43 ksi), and 6-NS (3.46 ksi); however the diagonal compression strut in specimen 1-S was able to withstand a higher compression stress before failure due to the confinement

of the concrete provided by the internal shear reinforcement. Despite the effect of the confinement created by internal shear reinforcement specimen 1-S failed at a lower total compression force in the diagonal compression strut due to the fact that the diagonal compression strut had a smaller cross section during test 1-S than test 6-NS. Due to the fact that the diagonal compression strut failed at a lower total compression force in test 1-S than test 6-NS, a lower shear resistance "R1" was achieved by specimen 1-S than 6-NS.

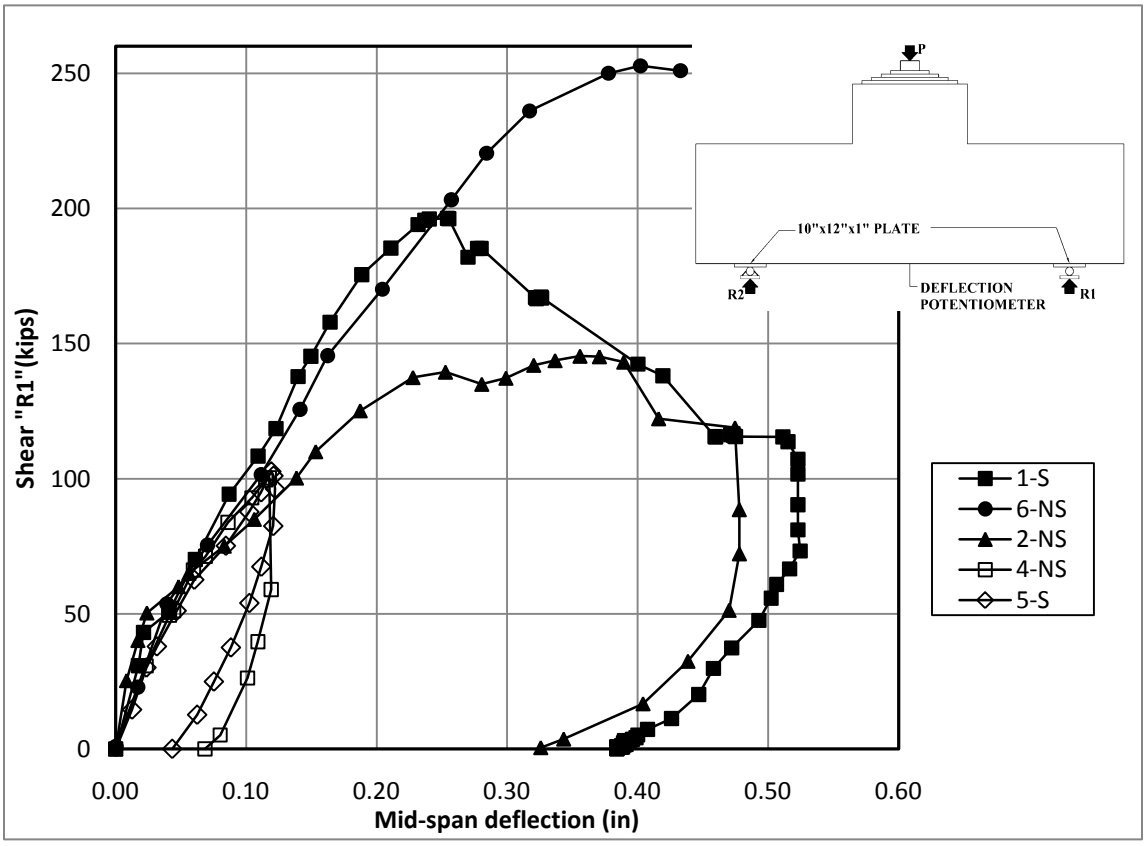

Figure 5.2 Mid-span deflection of pier cap specimens

Figure 5.3 Test 1-S compression strut width

Figure 5.4 Test 2-NS de-bonding

Figure 5.5 Test 6-NS compression strut width

5.2.2 Deflection of post-tensioned specimens (3-S-PT, 4-NS-CR-PT, 5-S-CR-PT)

Four tests were performed on pier caps with the exterior post-tensioning system in place. Test 3-S-PT was performed on a specimen without any initial cracking, whereas tests 4-NS-CR-PT, 5-S-CR-PT, and 5-S-CR-PT-2 were performed on specimens that had been initially cracked. During test 5-S-CR-PT, the specimen was loaded to the point of yielding of the tension reinforcement and then unloaded in order to evaluate the behavior of the pier cap after an extreme overload event. During test 5-S-CR-PT-2 the specimen loaded during test 5-S-CR-PT was loaded to failure.

The shear-displacement plots of all three tests on specimens that included internal shear reinforcement are in good agreement through yielding of the tension reinforcement and up to a shear "R1" of 287 kips (Figure 5.6). After the average strain in the tension reinforcement exceeded the yield strain of the bars all pier cap specimens that were externally post-tensioned were able to sustain increasing shear and deflection. The post tensioned pier caps sustained deflections after yielding of the tension reinforcement, between 1.4 and 5 times their deflection prior to yielding of the tension reinforcement.

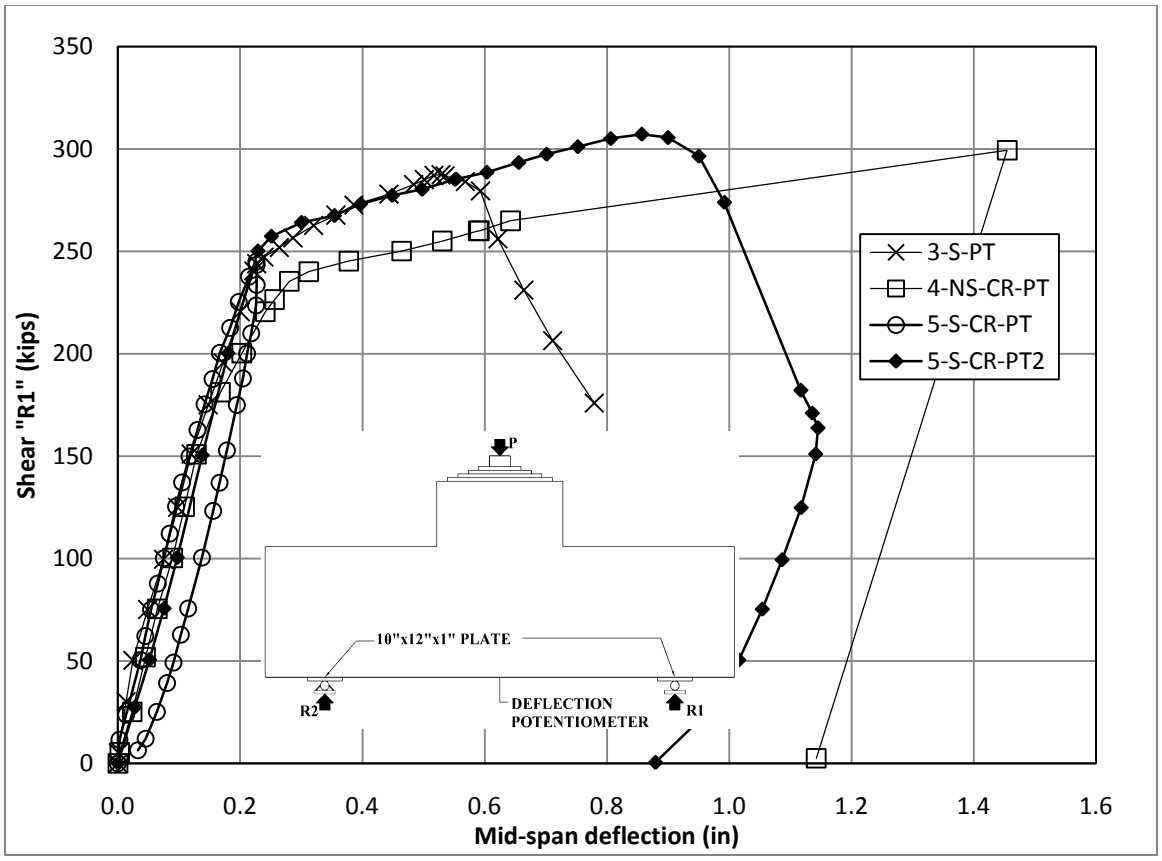

Figure 5.6 Mid-span deflection of post-tensioned pier cap specimens

5.3 End rotation of pier caps under loading

The horizontal in-plane end displacement at the top and bottom of the specimen was measured and the difference between the two was used to compute the end rotation of the pier cap specimens.

5.3.1 Rotation of pier caps without post-tensioning (1-S, 2-NS, 4-NS, 5-S, 6-NS)

The plot of shear "R1" versus end rotation (Figure 5.7) shows a continuous drop in shear after yielding of the tension reinforcement occurred during test 1-S, and a plateau in the case of test 2-NS.

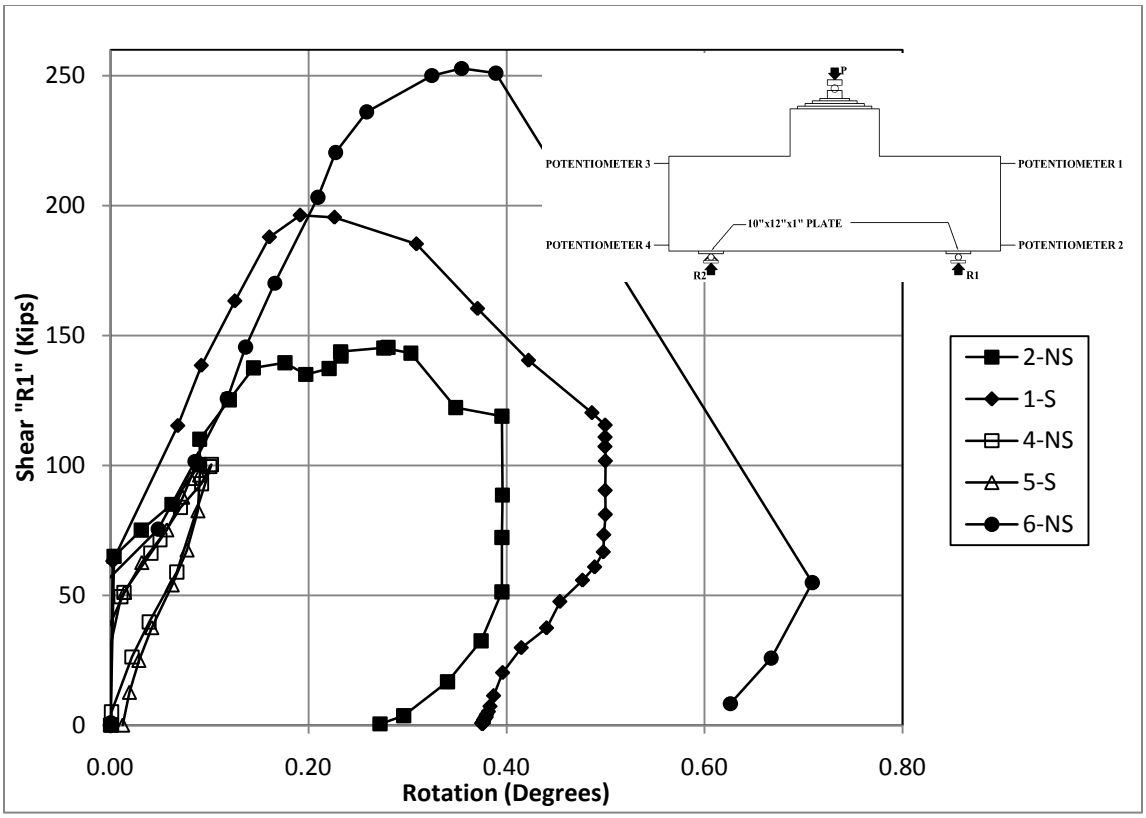

Figure 5.7 Pier cap end rotations

5.3.2 Rotation of pier caps with post-tensioning (3-S-PT, 4-NS-CR-PT, 5-S-CR-PT (Table 4.4))

The end rotation of the specimens that were externally post-tensioned is plotted versus the shear "R1" in Figure 5.8. The externally post-tensioned specimens were able to sustain ultimate rotations between 1.6 and 5.5 times their rotations at yielding of the tension reinforcement. The increased rotation capacity as compared to the specimens without the external post-tensioning system was due to the fact that the external post-tensioning system moved the diagonal compression struts away from the stress concentration at the corner of the pier cap and column.

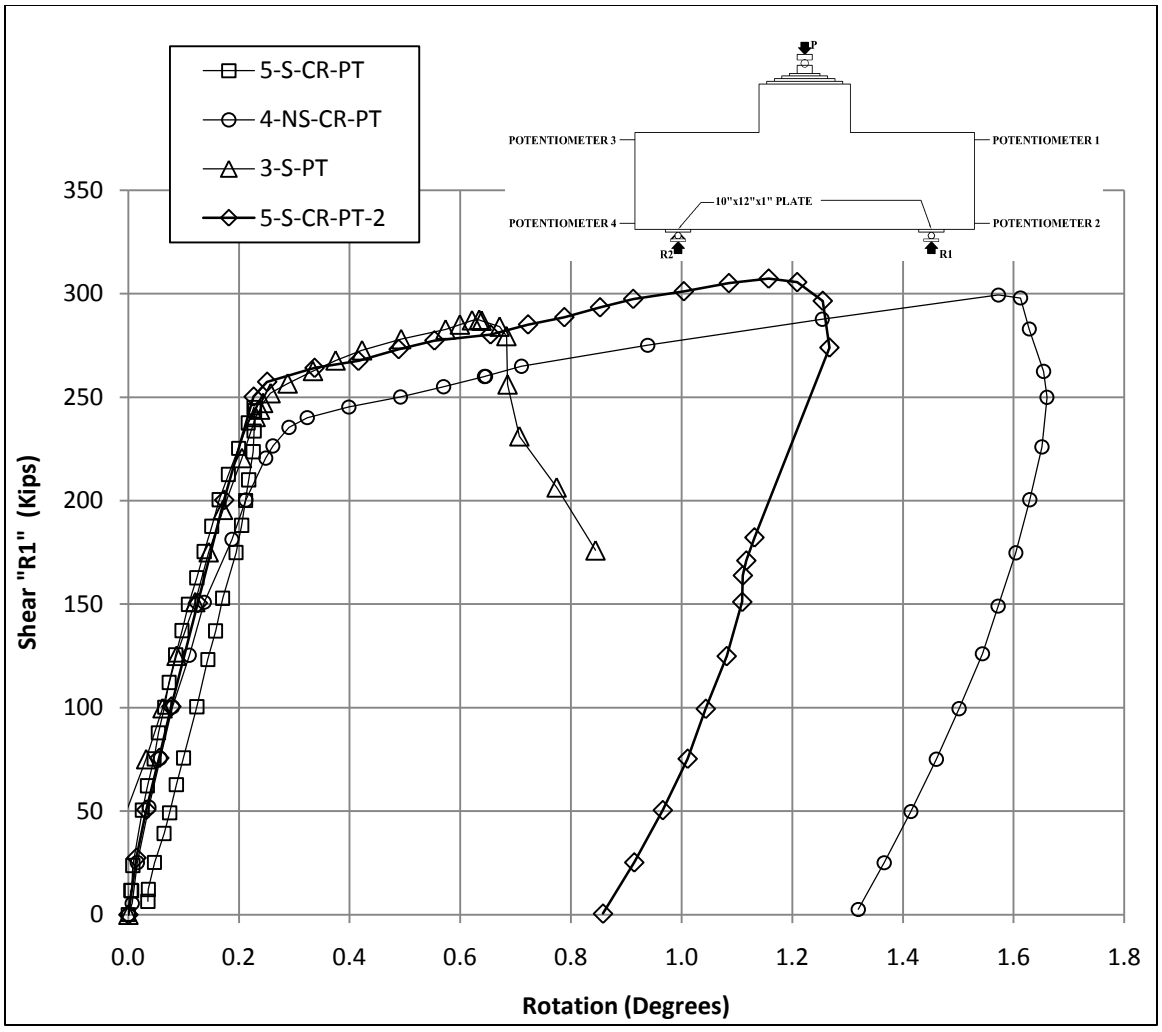

Figure 5.8 Post-tensioned pier cap end rotations

5.4 Strain in the tension reinforcement under loading

5.4.1 Strain in the tension reinforcement during tests on pier caps without external post-tensioning (1-S, 2-NS, 6-NS)

During test 2-NS, the average strain in the tension reinforcement between the two supports was computed by taking the displacement measured by the string potentiometer mounted on the specimen at the effective depth of the tension reinforcement (32.25 inches from the top of the specimen) (Figure 4.22) and dividing it by the gauge length of 100 inches. This computed strain response is illustrated in Figure 5.9, and labeled "String Potentiometer" The average strain measured in the tension reinforcement at each of the

gauge points was plotted in Figure 5.9; the center of each shear span (SG 0-4, 13-17 Figure 4.21), and the center of the overall span (SG 8-12 Figure 4.21).

Shear cracking of the specimen was visible on the surface of the specimen between a shear of 60 and 65 kips, between those shears, the strain in the tension reinforcement becomes uniform, suggesting that tied arch behavior governs the behavior of the specimen from that point onward (Figure 5.9, 5.10 and 5.11). The strain measured by the bar mounted strain gauges were susceptible to strain localizations depending on the proximity of the gauges to the nearest crack. The average strain over the length of the shear span measured by the externally mounted potentiometer; however, was not affected by the strain localization caused by the cracking of the specimen.

During test 1-S, when shear cracks formed at shear in the test spans of 62 and 70 kips, the measured strains approached a constant value indicating the formation of a tied arch within the specimen (Figure 5.10). During test 6-NS the diagonal shear cracks crossed the tension reinforcement at the locations of the strain gauges 0-4 and 8-12. As a result of the cracks crossing the tension reinforcement at those gauges locations, during test 6-NS, the strain gauges 0-4 and 8-12 measured higher strains than the average bar strain (Figure 5.11).

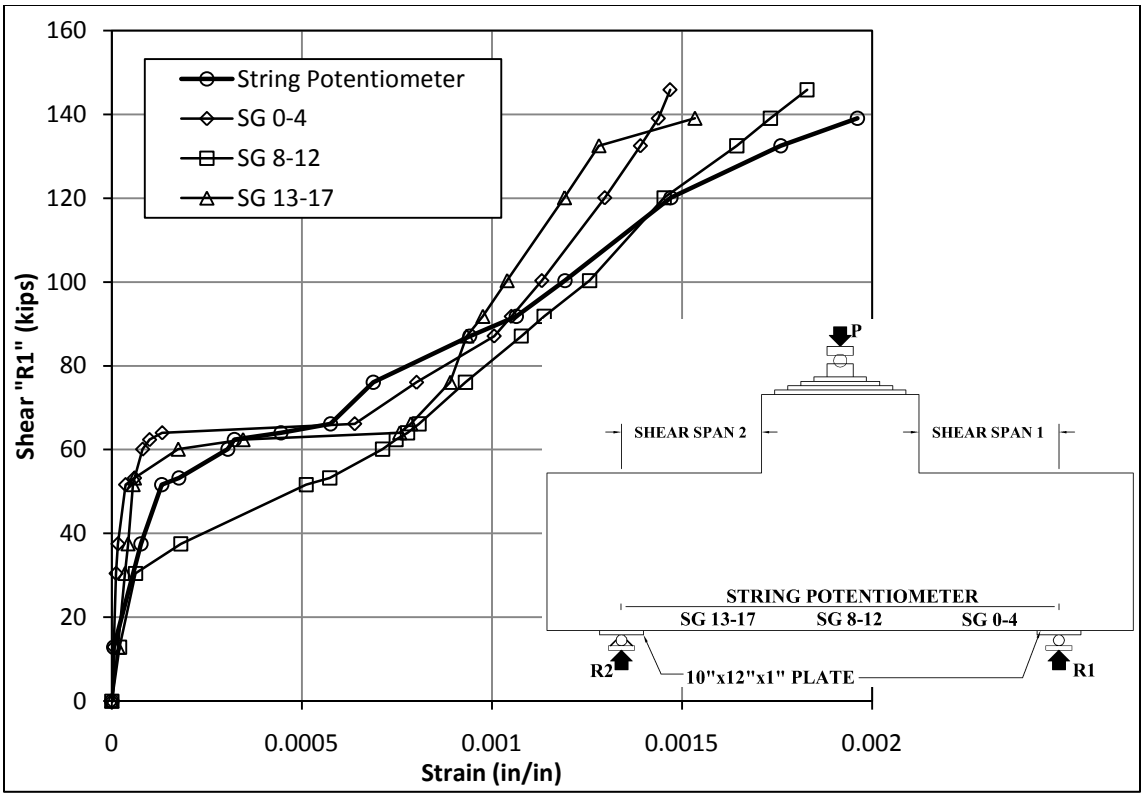

Figure 5.9 Test 2-NS tension reinforcement strains

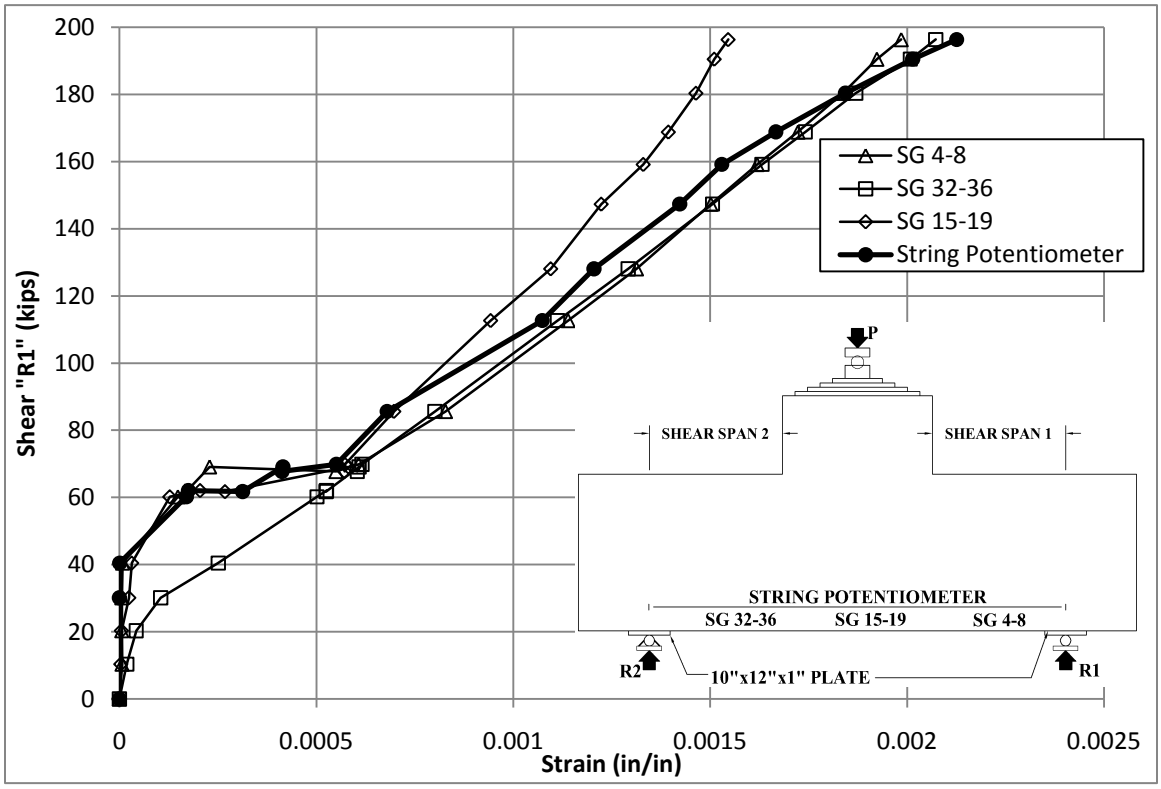

Figure 5.10 Test 1-S tension reinforcement strains

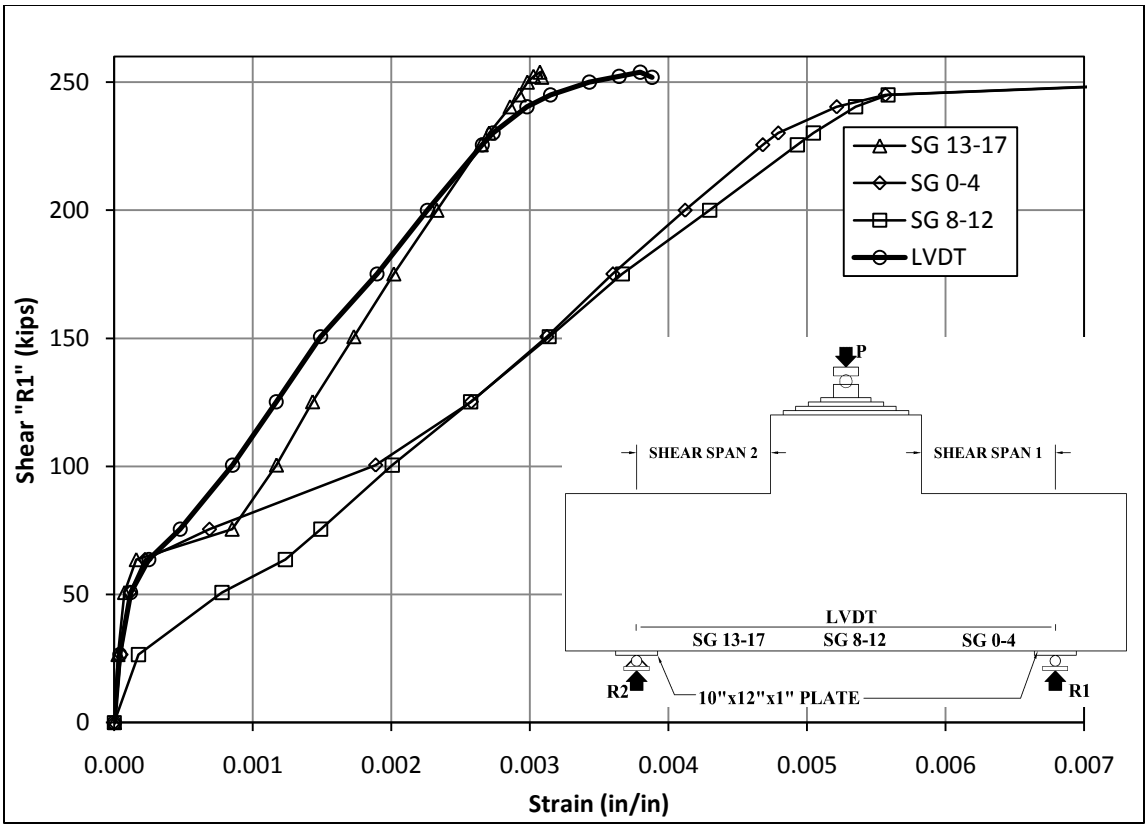

Figure 5.11 Test 6-NS tension reinforcement strains

Aguilar et al. (2002) tested twelve inch wide thirty six inch deep reinforced concrete beams with varying degrees of internal shear reinforcement. Aguilar et al. (2002) found that the lack of internal shear reinforcement only reduced the capacity of the specimen by 1%. The pier cap tests 1-S and 6-NS showed that the presence of internal shear reinforcement had no effect on primary load carrying mechanism present within the pier caps, tied arch behavior. Cracking of the specimens and the initiation of tied arch behavior occurs at the change in the slope of the shear "R1" versus strain response pictured in Figure 5.12 (around "R1" = 50-60 kips). The average strain in the tension reinforcement throughout the loading process is in excellent agreement in the specimens with and without internal reinforcement (Figure 5.12). However, the ultimate capacity of the two specimens 1-S and 6-NS differs by 22% due to the effect of the stress concentration at the reentrant corner between the beam and column. The presence of this reentrant corner had a profound effect on the development of the diagonal compression

strut, which had been ignored by experimental testing that replaced the column with a distributed load. The location of the diagonal tension cracks in specimen's 1-S and 6-NS differed significantly, with the diagonal tension cracks 40% closer to the stress concentration in the case of test 1-S. The degree to which the location of the diagonal tension crack is governed by the presence of internal shear reinforcement and the random location of voids within the specimen cannot currently be determined due to the lack of experimental testing on deep beams specimens with composite columns.

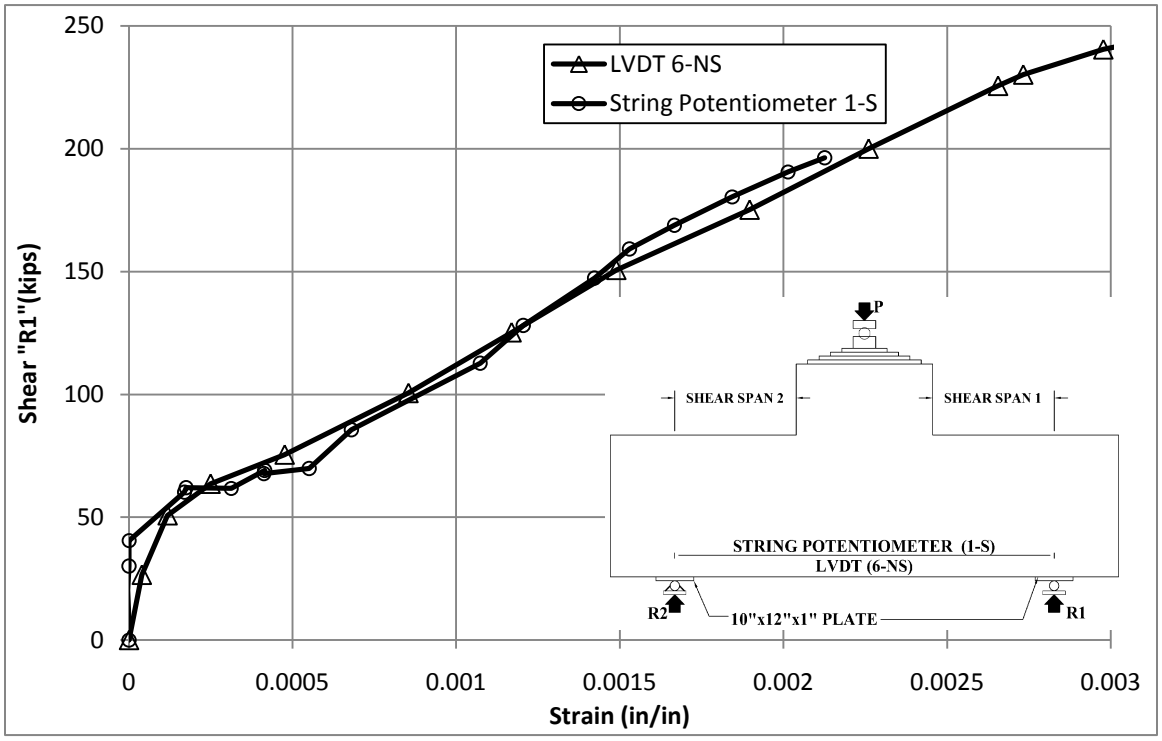

Figure 5.12 Average strain in tension reinforcement (tests 1-S and 6-NS)

5.4.2 Strain in the tension reinforcement during post-tensioned pier cap tests (3-S-PT, 4-NS-CR-PT, and 5-S-CR-PT)

During test 3-S-PT, the strain in the tension reinforcement was measured by strain gauges (SG 4-8, 15-19, and 32-36) on the tension reinforcement in the same locations as in test 1-S (Figure 4.19). However the average strain over the span was measured in by LVDTs in three separate locations shown in Figure 4.24 (LVDTs 17-19). Each of the

three LVDTs was mounted at the effective depth of the tension reinforcement (32.25 inches from the top of the specimen). LVDTs 17 and 18 are used to compute the average strain in the tension steel between the center of the support and the post-tensioning clamps, while LVDT 19 was used to compute the average strain in the tension steel between the two post-tensioned clamps. The average tension strain recorded at the location of each set of strain gauges and LVDT was plotted in Figure 5.13. Unlike tests 1-S, 2-NS, and 6-NS, the strain in the tension reinforcement was not constant between the supports. The jump in strain observed between that measured at the center of the specimen and that measured from the support to the post-tensioned clamps occurs because of the formation of two diagonal compression struts in each shear span (Figure 4.23) of the specimen. In Figure 5.13, several of the gauges stopped working before the ultimate shear resistance of the specimen was reached. Similar evidence of double-strut behavior was present in each of the tests conducted on post-tensioned pier caps 4-NS-CR-PT (Figure 5.14), and 5-S-CR-PT (Figure 5.15).

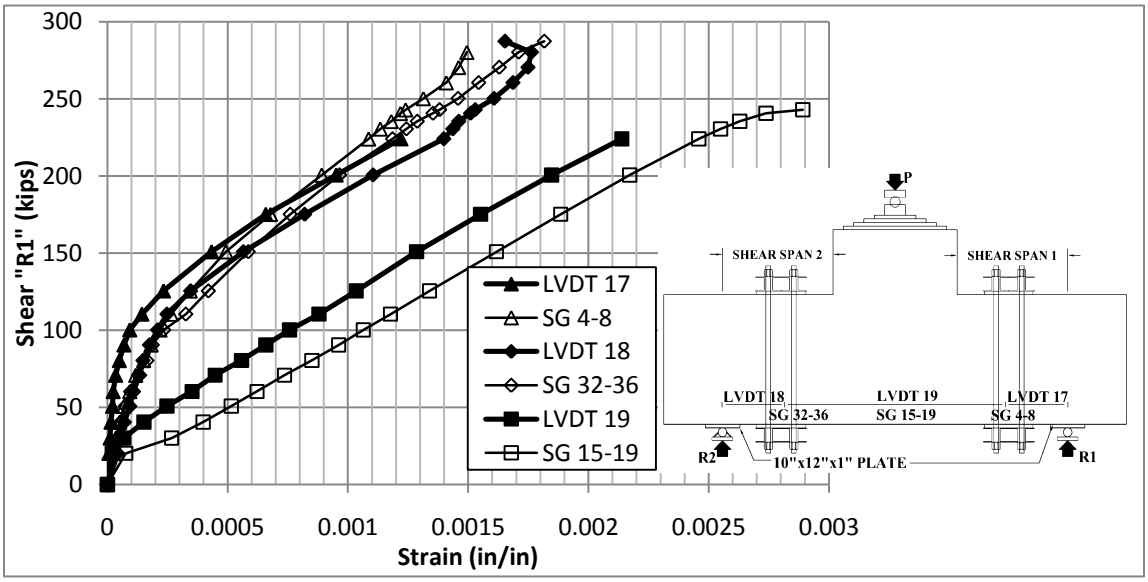

Figure 5.13 Test 3-S-PT tension reinforcement strain

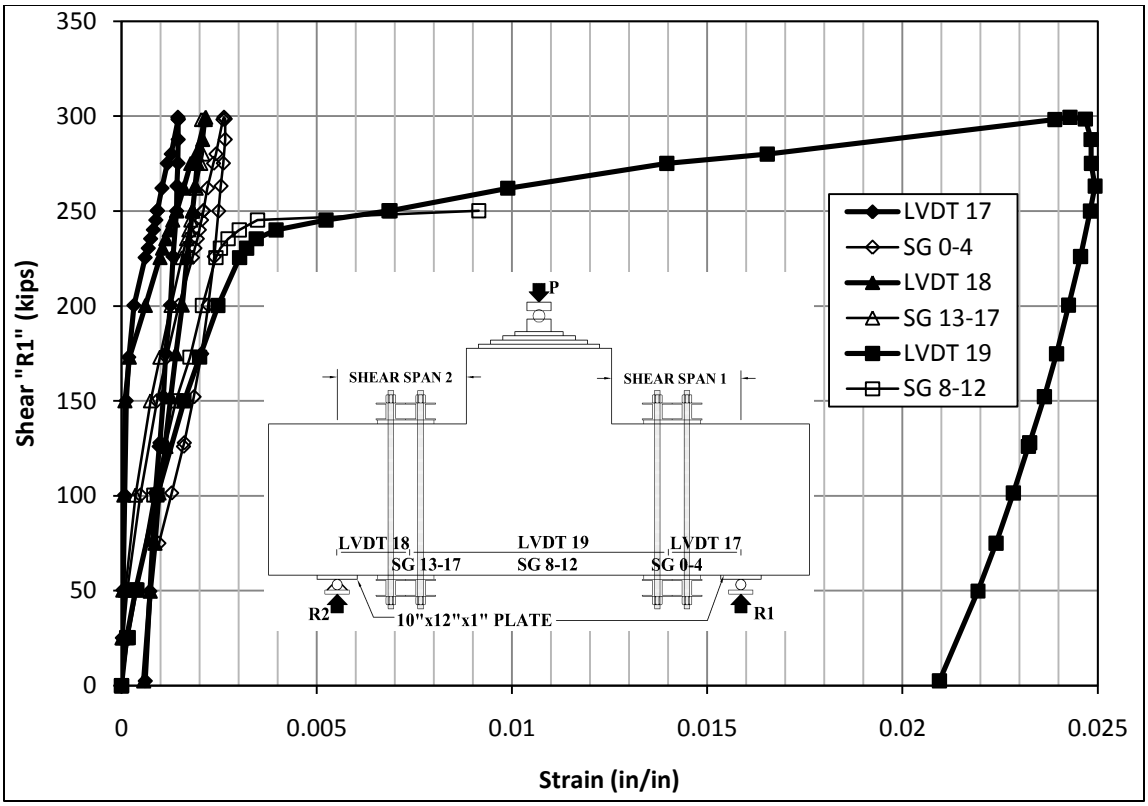

Figure 5.14 Test 4-NS-CR-PT reinforcement strain

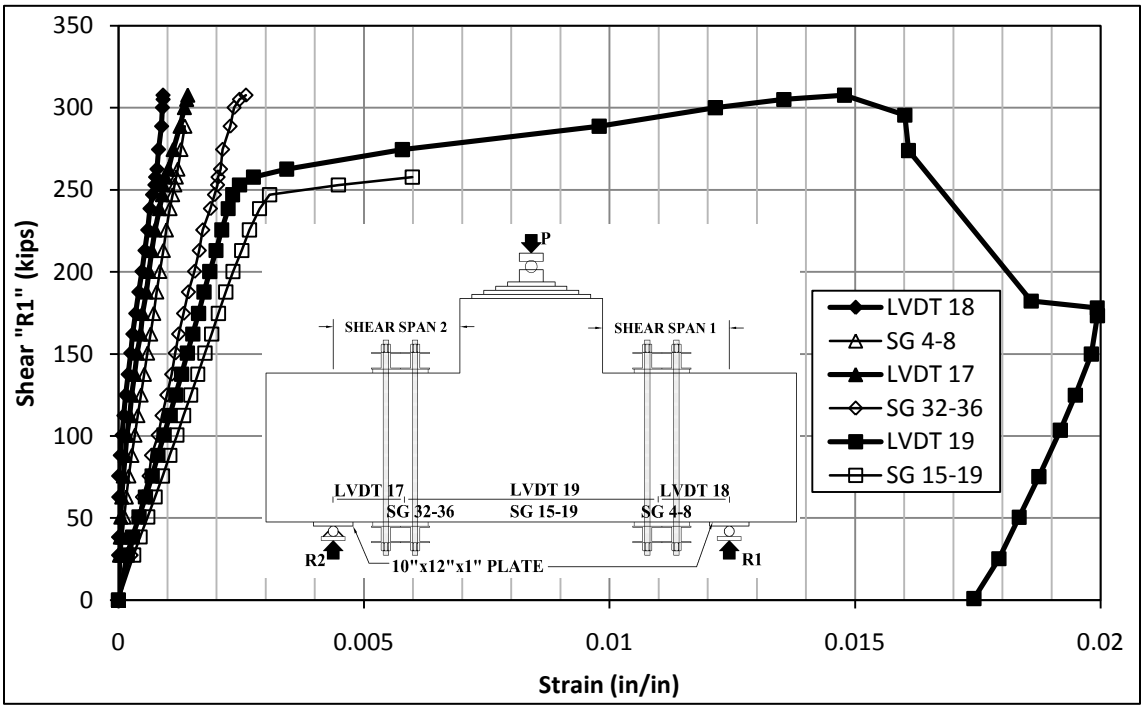

Figure 5.15 Test 5-S-CR-PT-2 reinforcement strains

5.5 Angle of compression strut

5.5.1 Angle of compression strut during pier cap tests without post-tensioning (1-S, 2-NS, 4-NS, 5-S, and 6-NS)

The angle of inclination of the principal compression strut in the shear span was computed from the average measured strain in the tension reinforcement and the shear in the test span. The method used to compute the compression strut angle was outlined in Section 3.5.4 and in Equation 3.3. The results of this computation are plotted in Figures 5.16 through 5.20 for tests 1-S, 2-NS, 4-NS, 5-S, and 6-NS. The angle of inclination of the compression strut was also computed for each test using the strain readings from the external LVDT rosettes, and is plotted in Figure 5.21. The angle of principal compression strain was computed from the LVDT rosettes using the same technique outlined in section 3.5.4. As was found in Chapter 3, the angle computed from the rosette readings is highly dependent on the location of the rosette relative to the diagonal tension cracks within the specimen. The angle computed from the average strain in the strain gauges mounted on the tension reinforcement is also highly dependent on the distance of the gauge from the nearest crack, as shown in Figure 5.16, 5.18 and 5.20, where the angle computed from the average strain measured by one of the sets of strain gauges differs from the other two and the angle computed using the average bar strain measured by either the LVDT or String Potentiometer. During experiments 4-NS and 5-S, the average strain in the tension reinforcement was computed by dividing the total elongation measured from LVDTs 17, 18 and 19, by 100 inches. Three LVDTs were used to measure the elongation along the length of the tension reinforcement during test 4-NS and 5-S so that they would be in place for tests 4-NS-CR-PT and 5-S-CR-PT, during which the strain varied along the length of the tension reinforcement. The computed compression strut angle tends to lie between 40 and 50 degrees once the dominant inclined shear cracking occurs, for all of the tests on pier caps without the external post-

tensioning system. When the shear in the test span was less than 30 kips, the computed angle of the principal compression strut fell between 75 and 90 degrees. These calculated angles are inaccurate, however, because prior to 30 kips, flexural cracking of the specimen had not occurred and the concrete was carrying a portion of the horizontal tension strain rather than the steel carrying all of the tension, as assumed in the calculation. Between a shear of 30 kips and 70 kips, the flexural cracking of the specimen continued to propagate and the diagonal tension cracks developed. Once these cracks develop, the specimen transfers load through tied arch behavior and the 5 No. 8 bars that make up the tension reinforcement carried all of the horizontal tension force and the angle of inclination of the diagonal compression strut can be calculated from the strain in the tension reinforcement.

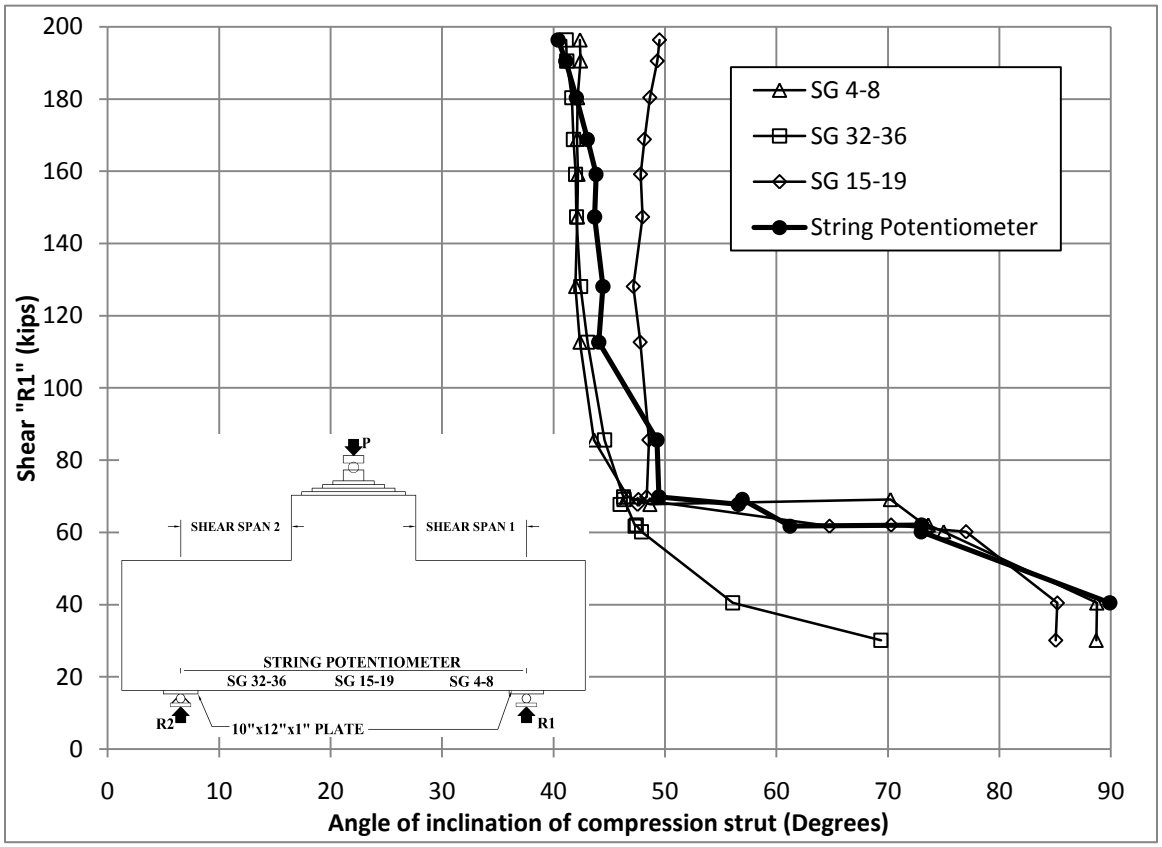

Figure 5.16 Test 1-S compression strut angle (computed using average measured bar strain)

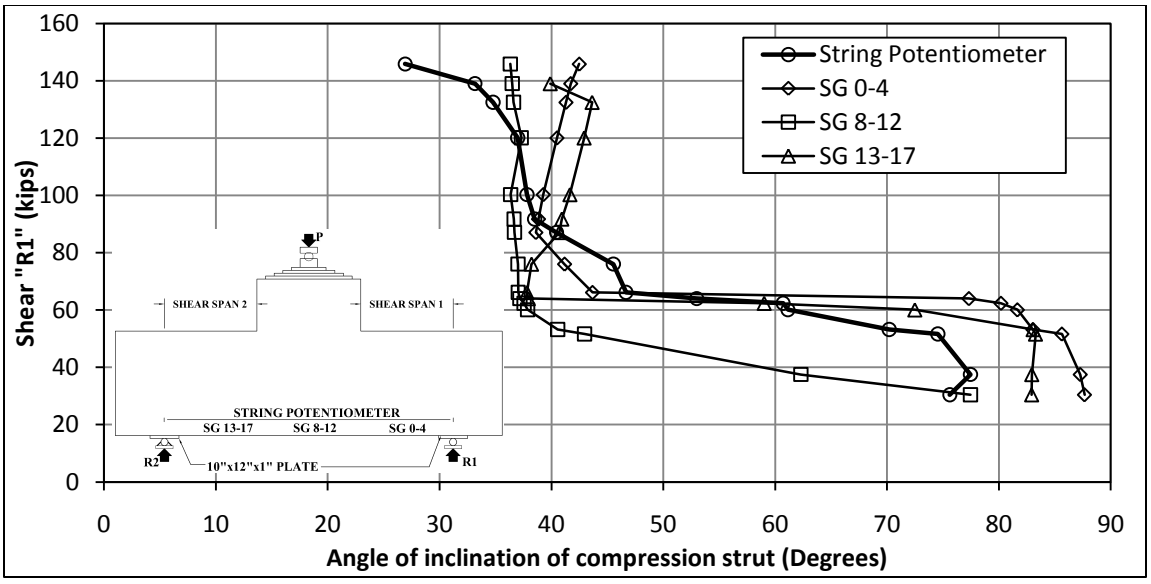

Figure 5.17 Test 2-NS compression strut angle (computed using average measured bar strain)

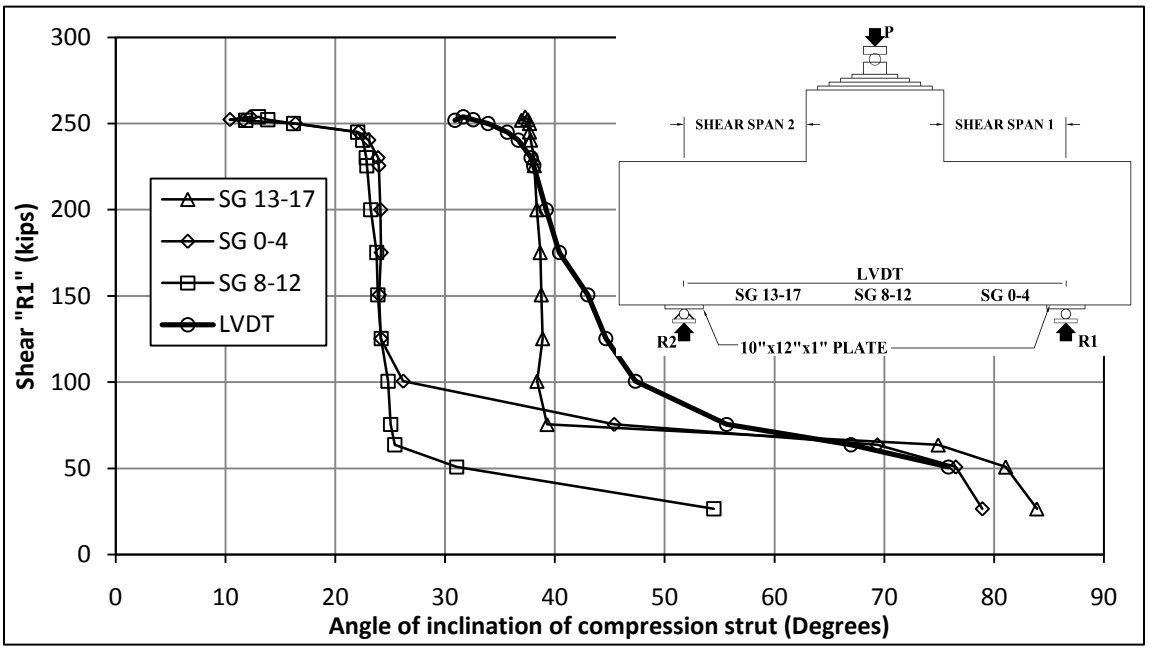

Figure 5.18 Test 6-NS compression strut angle (computed using average measured bar strain)

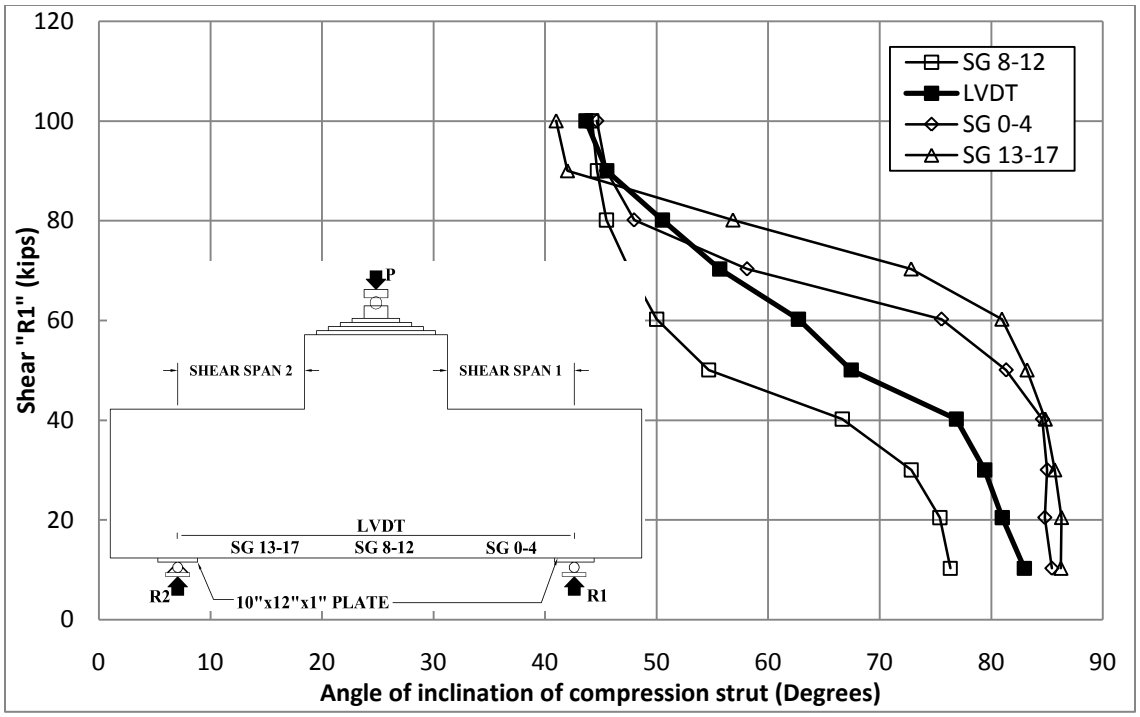

Figure 5.19 Test 4-NS compression strut angle (computed using average measured bar strain)

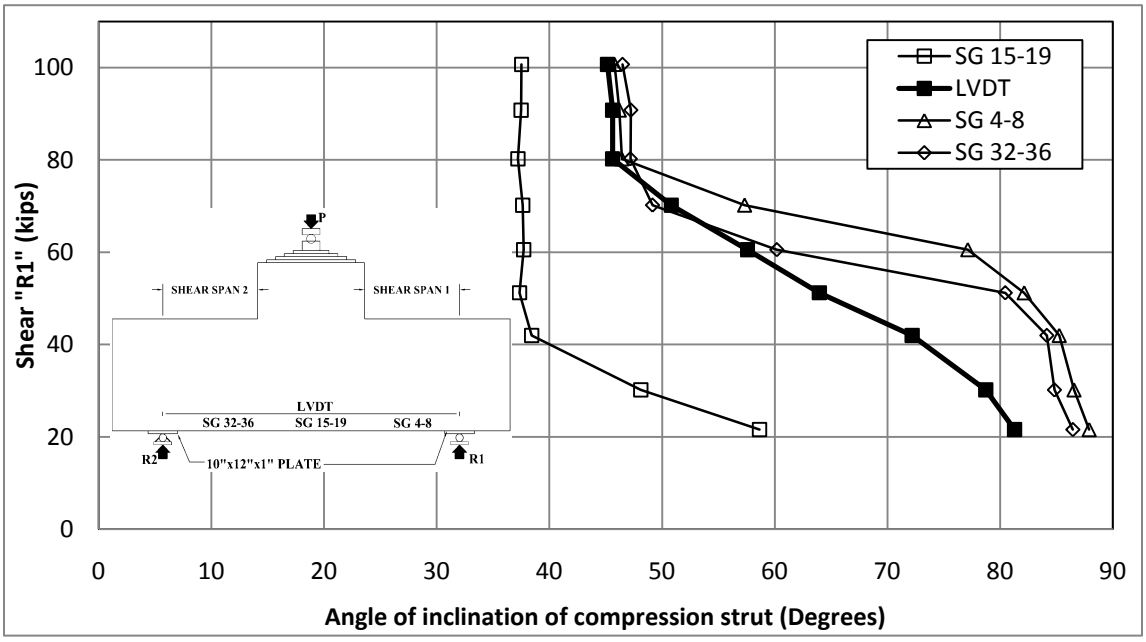

Figure 5.20 Test 5-S compression strut angle (computed using average measured bar strain)

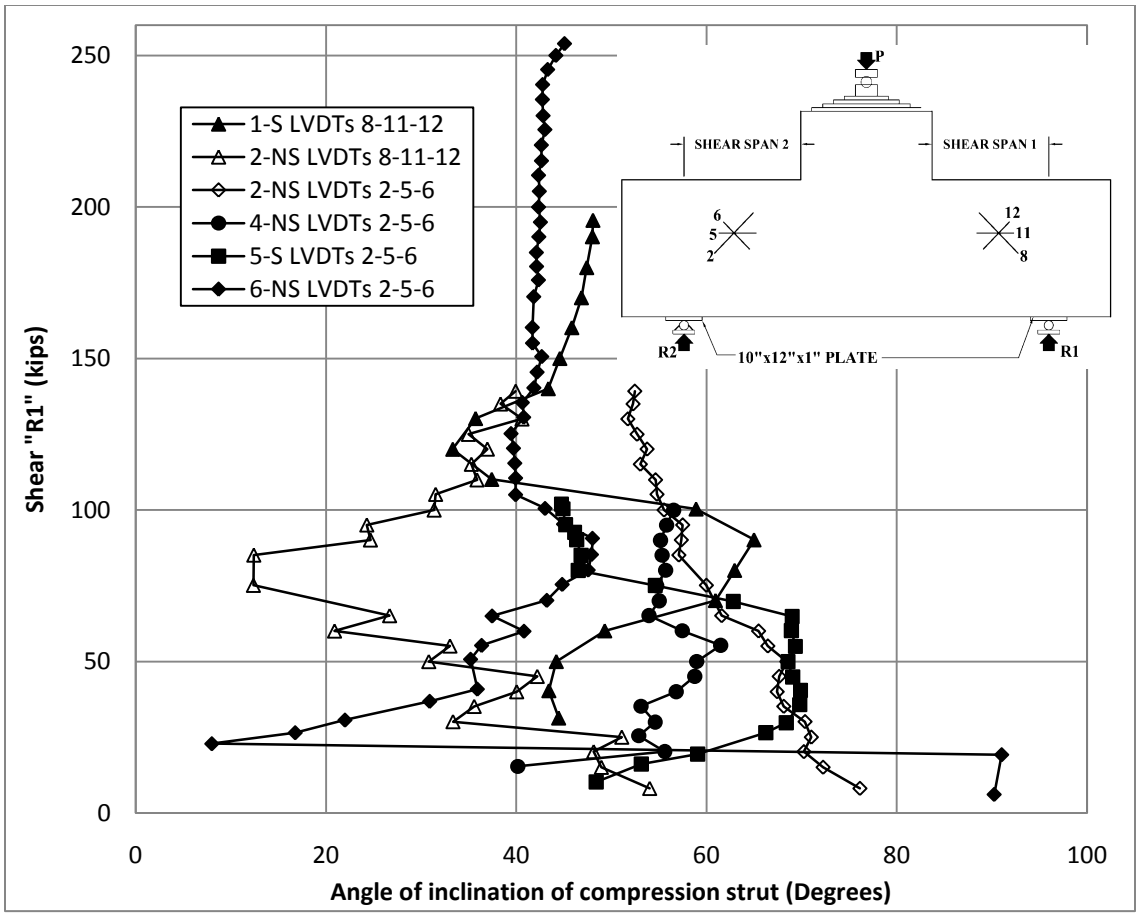

Figure 5.21 Angle of inclination of compression strut in pier caps (computed from external rosette measurements)

5.5.2 Angle of compression strut in pier cap test with external post-tensioning (Test 3-S, 4-NS-CR-PT, and 5-S-CR-PT)

The angle of the compression strut computed from the measured responses of the pier cap specimens with the external post-tensioning systems are presented in Figures 5.22 through 5.25. These plots indicate that two struts are formed in each test span at between 55 and 70 degrees, when the external post-tensioning system is employed. They also show that the center strut computed from LVDT 19 initially forms at an angle of 40-50 degrees and then increases until the strut approaches the reentrant corner between the pier cap and column. Once the compression strut approaches the reentrant corner, each of the pier cap specimens fails due to crushing of the concrete at the stress concentration

at that corner. In the specimens without the post-tensioning, the initial location of the diagonal compression struts passed through the stress concentration. In comparison, in the specimens with external post-tensioning, the diagonal compression struts initially were aligned with the center of the column away from the stress concentration at the beam column corner. From their initial direction, however, the diagonal compression struts in the specimens with external post-tensioning then shifted direction toward the beam-column corner once the horizontal tension steel reached the yield point.

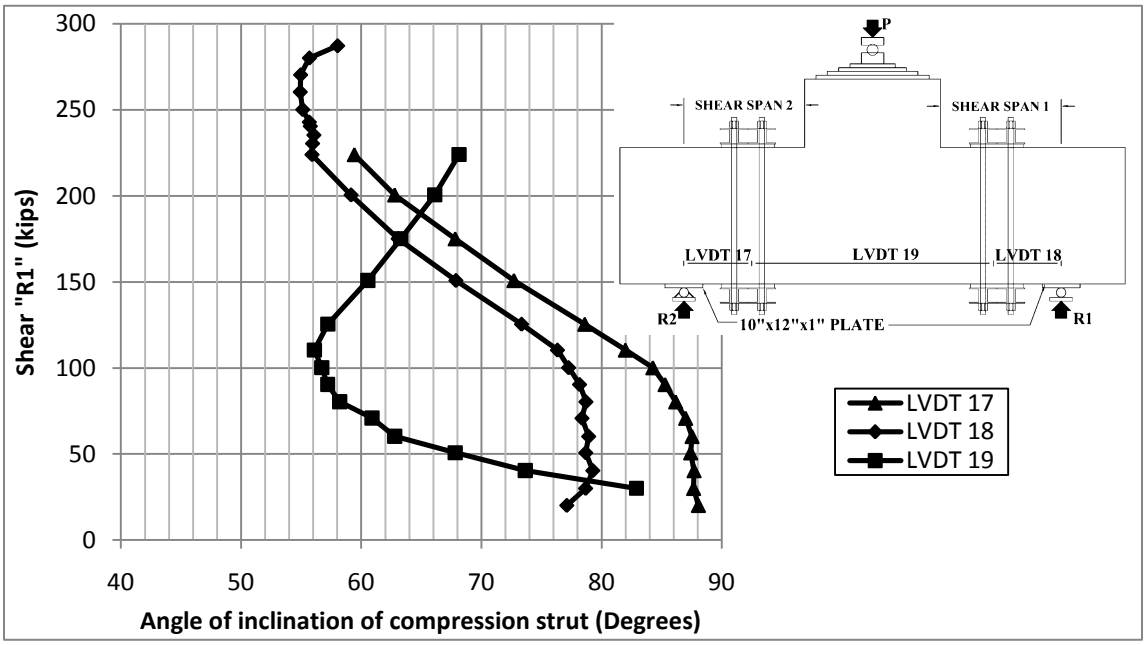

Figure 5.22 Test 3-S-PT compression strut angle (computed from bar strain)

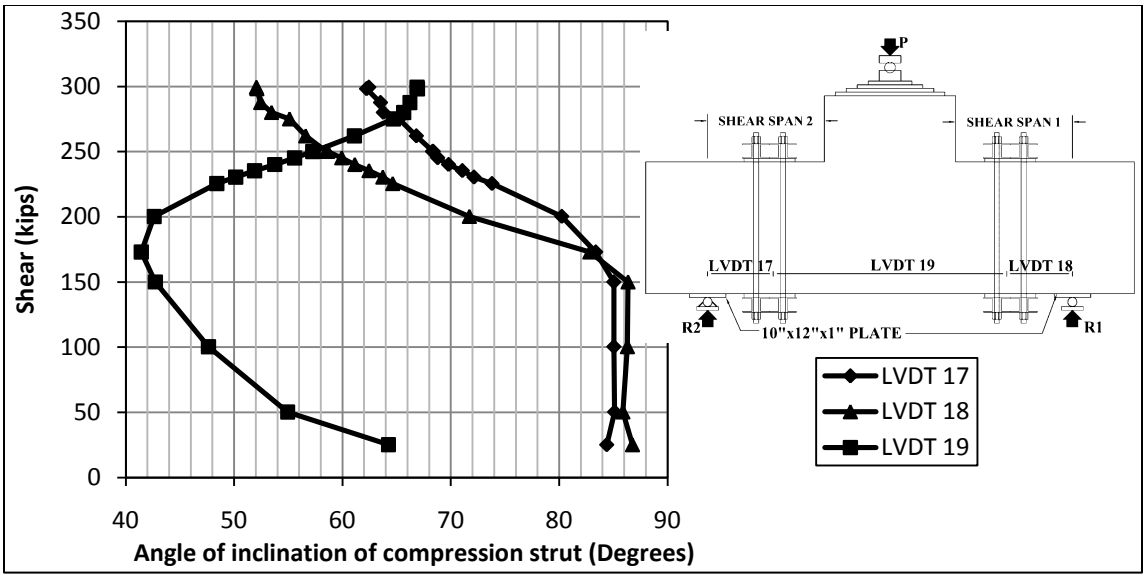

Figure 5.23 Test 4-NS-CR-PT compression strut angle (computed from bar strain)

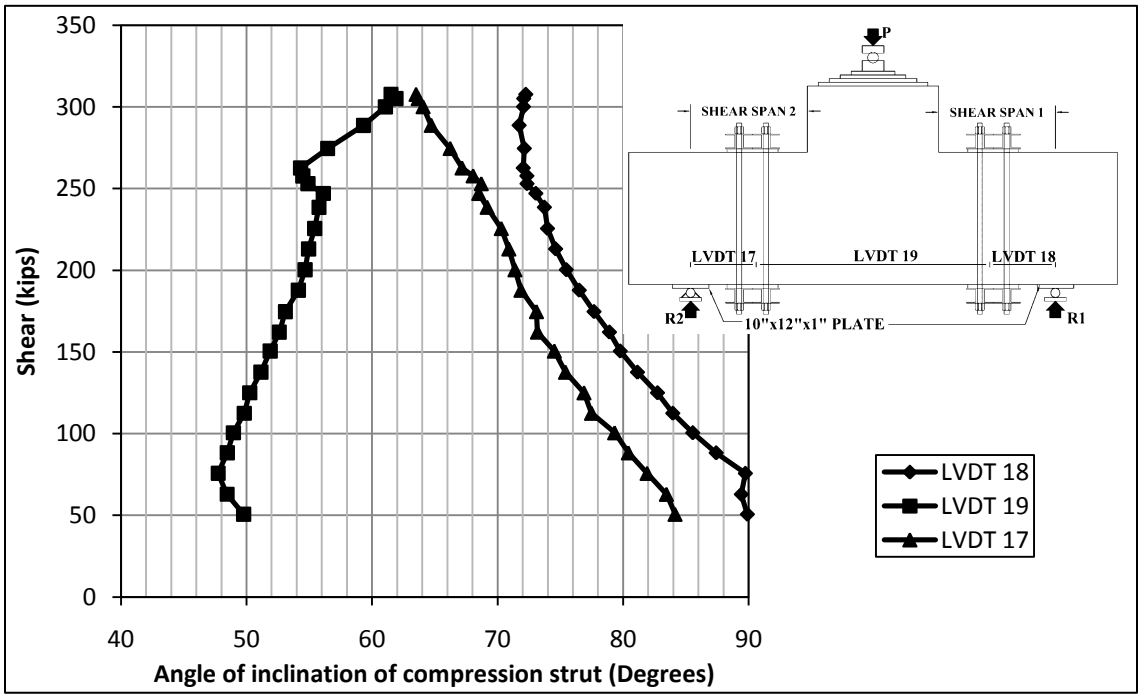

Figure 5.24 Test 5-S-CR-PT-2 compression strut angle

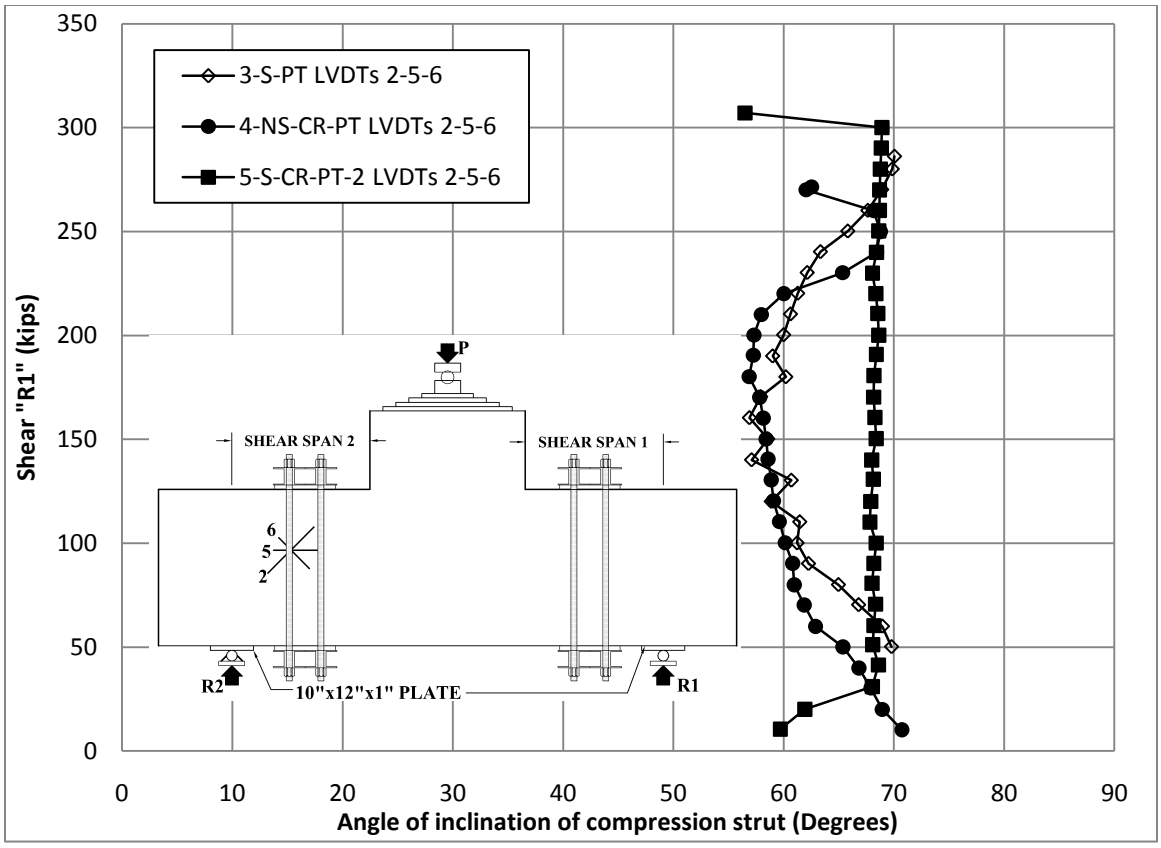

Figure 5.25 Angle of inclination of compression strut (computed for LVDT rosettes)

5.6 Strain profile of compression strut

The measured strain profiles are plotted for four levels of "R1" in Figure 5.26 for test 1-S. The strain profiles show a uniform strain in the strut prior to when the primary shear cracks were observed at a shear in the test spans of 65 kips. In shear span 1 on the right of Figure 5.26 the strain measured in LVDT 4 drops to zero once the shear crack in that span forms at 65 kips due to the fact that the crack passes above the gauge. Alternatively, LVDT 10 was located in the same location in shear span 2 on the left of Figure 5.26. However the crack in shear span 2 developed below LVDT 10 so it continued to measure compression strain throughout the loading process.

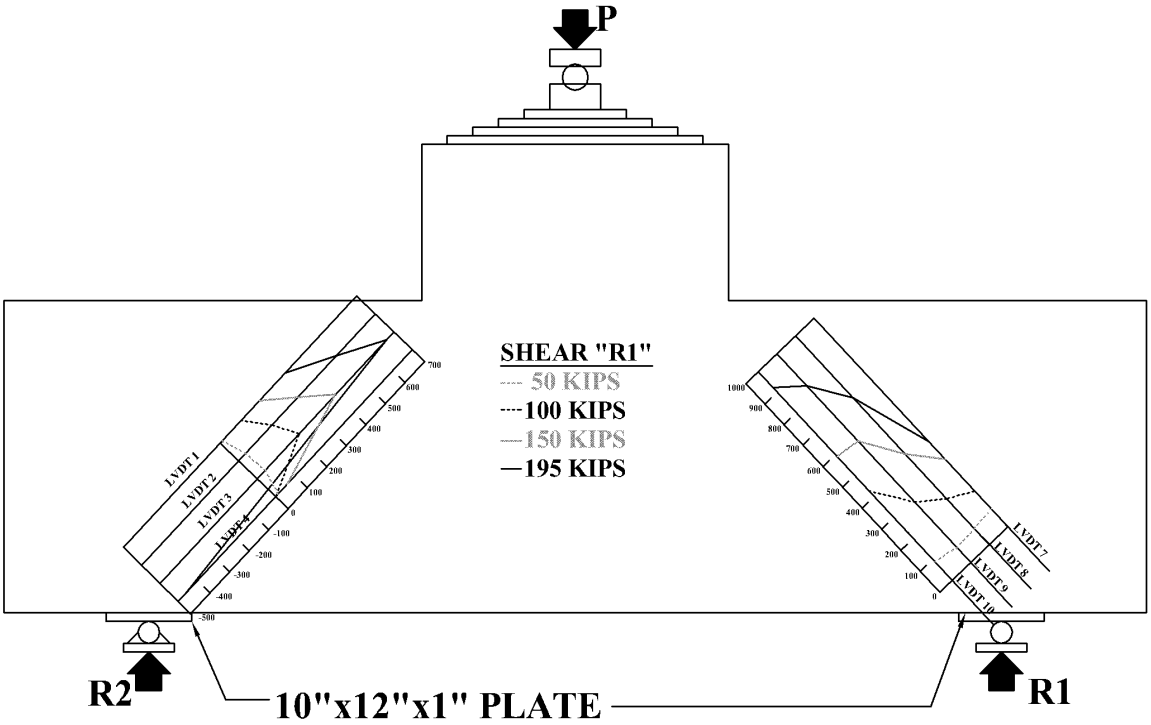

Figure 5.26 1-S Micro-strain measured in compression strut at given shear "R1"

The measured strain profile is plotted for four levels of "R1" in Figures 5.27 for test 2-NS. The strain profiles show a uniform strain in the strut prior to when the primary shear cracks were observed at a shear in the shear spans 70 kips.

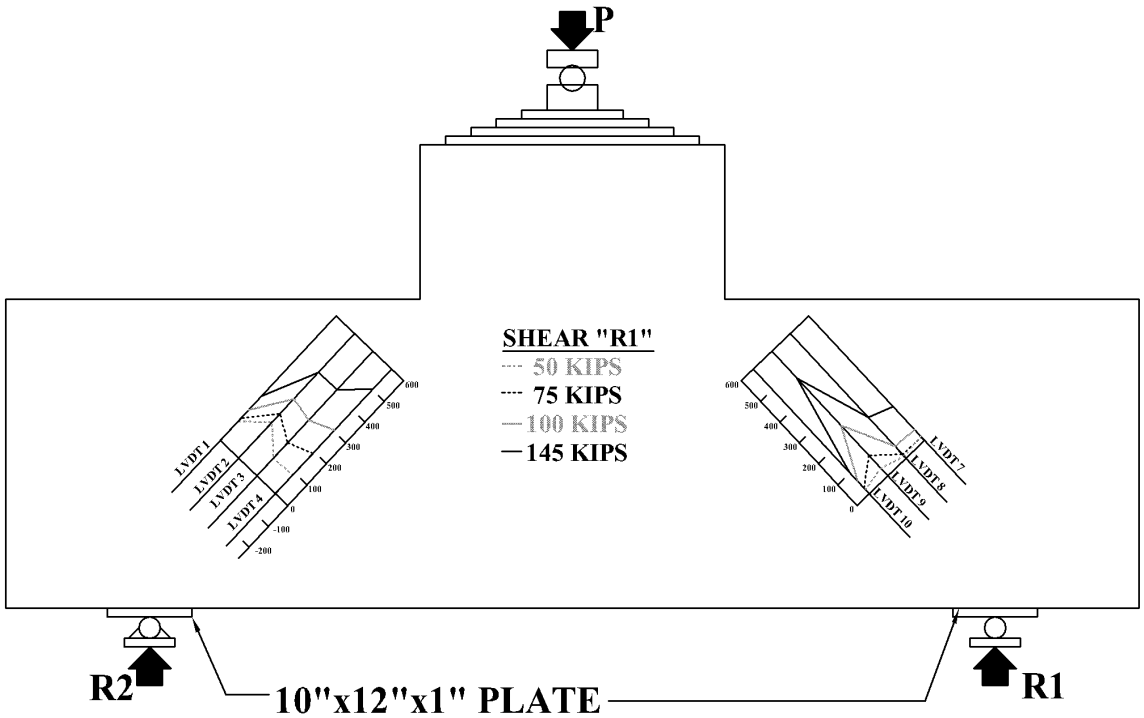

Figure 5.27 2-NS Micro-strain measured in compression strut at given shear "R1"

Figures 5.26 and 5.27 illustrate that the compression strain in the diagonal compression strut peaks just above the crack location and decreases the farther away from the crack the gauge is mounted. This indicated that the majority of the compression in the strut is carried by the compression strut between the lower three LVDTs (ie. 2-4, and 8-10). Since the spacing of the LVDTs was 3 inches the strut width can be approximated as being between 6 and 9 inches, which is smaller than the strut width predicted by the strut and tie method presented in Chapter 6.

5.7 Summary of pier cap specimen tests

The pier cap test program summarized in this chapter revealed the importance of the stress concentration at the interface between the pier cap and column joint. It was observed that failure of the specimens initiates at this stress concentration, and that by applying external vertical post-tensioning to the pier cap structure it is possible to shift the compression struts away from the region of the stress concentration. By shifting the

compression struts away from the stress concentration, both the strength and ductility of the pier cap structure can be significantly increased.

The presence of internal shear reinforcement did not significantly impact the behavior of post-tensioned specimens, since the capacity of the internal shear reinforcement was negligible when compared to the external post-tensioning. In the case of specimens without the external post-tensioning the presence of internal shear reinforcement had an unexpected impact. While it provided confinement and increased the ultimate compression stress of the concrete in the diagonal compression struts, overall it decreased the compression force that could be transferred through the diagonal compression struts. This reduction in shear capacity occurred because the location of the diagonal tension cracks was closer to the stress concentration at the pier cap column corner and the area of the compression strut was reduced by approximately 50%.

The results of the pier cap testing will be further discussed and compared to the strut and tie analysis of the pier caps stipulated in AASHTO Article 5.6.3 in Chapter 6.

CHAPTER 6. ANALYSIS OF DEEP BEAM AND PIER CAP SPECIMEN TEST RESULTS

Each deep beam test from Chapter 3 and pier cap test from Chapter 5 was analyzed with the strut and tie method (STM) provisions found in Articles 5.6.3 and the general shear provisions found in Article 5.8.3.4.1 of AASHTO LRFD Bridge Design Specifications (2007). All specimens discussed in this chapter were designed to be representative of existing bridge components constructed prior to the current specifications. The STM provisions of Article 5.6.3 have been used to calculate the capacity of all of the specimens as a means of assessing the applicability of using Article 5.6.3 when performing a bridge rating calculation on bridge components that do not meet current shear reinforcement requirements. Minimum longitudinal and transverse crack control reinforcement requirements are found in Articles 5.6.3.6 and 5.13.2.3. According to Article 5.8.1.2, these requirements must be met when designing a reinforced concrete member with the strut and tie method, as detailed in Article 5.6.3 of the AASHTO LRFD Bridge Design Specifications (2007). The general simplified resistance procedure, as outlined in Article 5.8.3.4.1 of the AASHTO LRFD Bridge Design Specification (2007), was also applied to each specimen discussed in this chapter.

6.1 Comparison of deep beam specimen experiments and analysis

This section compares the results of the experimental testing of beam specimens presented in Chapter 3 to the results of analysis of the specimens using the AASHTO LRFD Bridge Design Specifications (2007).

6.1.1 Shear resistance of deep beam specimens per Article 5.8.3.4.1 of AASHTO (2007)

The simplified procedure for non-prestressed sections, as defined in Article 5.8.3.4.1 of AASHTO LRFD (2007), was used to calculate the capacity of each of the

deep beams that was tested in the first phase of the experiment program. The only test that did not meet the minimum transverse reinforcement requirements (Article 5.8.2.5) for the use of this method was test WP-E2. Equations 6.1-6.3 and terms used in this method, as defined in Article 5.8.3.4.1, are:

$$V_n = V_c + V_s + V_P \qquad \text{Eq. 6.1}$$

$$V_c = 0.0316\beta\sqrt{f_c'}\,b_v d_v \qquad \text{Eq. 6.2}$$

$$V_s = \frac{A_v f_y d_v (\cot\theta + \cot\alpha)\sin\alpha}{s} \qquad \text{Eq. 6.3}$$

β = Factor indicating ability of diagonally cracked concrete to transmit tension as specified in Article 5.8.3.4
θ = Angle of inclination of diagonal compressive stress (taken as 45^o when using the simplified procedure)
α =Angle of inclination of transverse reinforcement to longitudinal axis (^{o}) (90^o in this case of test specimens)
f_c' = Compressive strength of concrete (ksi)
b_v = Effective web width taken as the minimum web width within the depth d_v as determined in Article 5.8.2.9 (in.) (12 in. in the case of test specimens)
d_v = Effective shear depth as determined in Article 5.8.2.9 (in.) (21 in. in the case of test specimens)
A_v = Area of shear reinforcement within distance s (in.^{2}) ($0.22 in.^2$ in the case of test specimens)
f_y = Specified minimum yield strength of reinforcing bars (ksi)
s = spacing of stirrups (in.) ($12\ in.$ in the case of end 1 of test specimens)

The shear resistance of the test span computed for each test case using AASHTO 5.8.3.4.1 is presented in Table 6.1.

Table 6.1 Shear resistance of phase 1 deep beam specimens per Article 5.8.3.4.1 of AASHTO (2007)

Test ID	f_t' (ksi)	f_c' (ksi)	$V_{article\ 5.8.3.4.1}$ (Kips)	Post-tensioning (kips)
WP-E1	0.49	3.58	45.5	-
WP-E1-PT	0.407	3.83	46.6	129
WP-E2	0.393	3.32	29.0	-
LT-E1	0.455	3.71	46.1	-
H-E1	0.506	3.42	44.9	-
H-E1-PT	0.506	3.42	44.9	79

6.1.2 Shear resistance of deep beam specimens per Article 5.6.3 of AASHTO (2007)

The angle of the principal compression strut or struts in the test shear span, as well as the strain in the tension reinforcement at the computed specimen shear resistance

as per Article 5.6.3 (AASHTO 2007), are presented in Tables 6.2 and 6.3. Table 6.2 lists the analysis of each specimen based on a single strut and tie mechanism, whereas Table 6.3 list the analysis results for an assumed double-strut mechanism for each of the specimens when the external post-tensioning system was applied to the test shear span. Table 6.4 summarizes the ratio of the experimental capacity of the specimens to the computed capacity utilizing both the method outlined in Section 6.1.1 and the strut and tie method. Test WP-E1-PT experienced a crushing failure at the load plate prior to the predicted tension steel yielding. This failure resulted in a redesign of the load plate configuration in later tests. The interpretations of the results of experiment WP-E2 are complicated by the extensive damage toWP-E2. The single strut mechanism capacity of specimen H-E1-PT is presented in Table 6.4 because the external post-tensioning system was only tensioned to 49 percent of the shear resistance of the specimen, and during testing the force in the post-tensioning bars did not increase with the shear in the test span once the test span shear exceeded the initial post-tensioning.

Table 6.2 Single strut deep beam specimen models (terms defined Figure 6.1) (AASHTO LRFD 2007 Article 5.6.3)

Test ID	f'_t (ksi)	f'_c (ksi)	load plate	Theta (degrees)	e	V (kips)	Shift (in.)	Limit State
WP-E1	0.49	3.58	12"	37	0.00148	101	-0.635	Strut crushing
WP-E2	0.393	3.32	18"	37	0.00141	96	-1.3	Strut crushing
LT-E1	0.455	3.71	12"	37	0.00152	104	-0.675	Strut crushing
H-E1	0.406	3.42	12"	37	0.00144	98	-0.675	Strut crushing

$f'_t = split\ cylinder\ tension\ strength\ of\ 6"\ dia.\ concrete\ cylinders\ (ksi)$

$f'_c = compression\ strength\ of\ 6"\ dia.\ concrete\ cylinders\ (ksi)$

$V = R_1 = shear\ resistance\ (kips)$

Table 6.3 Double strut deep beam specimen models (terms defined Figure 6.2) (AASHTO LRFD 2007 Article 5.6.3)

Test ID	f'_t (ksi)	f'_c (ksi)	load plate	Theta 1 (degrees)	e_1	Theta 2 (degrees)	e_2	V (kips)	Shift (in.)	Limit State
H-E1-PT	0.506	3.42	12"	62	0.00095	51	0.00238	161	-0.05	Steel yield
WP-E1-PT	0.407	3.83	11"	62	0.00097	53	0.00238	166	0.26	Steel yield

Table 6.4 Ratio of computed shear resistance to shear at deep beam specimen failure

Test ID	$V_{article\ 5.6.3}$ (Kips)	$V_{article\ 5.8.3.4.1}$ (Kips)	$V_{ult.exp}$ (Kips)	$V_{ult.exp}$/ $V_{article\ 5.6.3}$	$V_{ult.exp}$/$V_{article\ 5.8.3.4.1}$
WP-E2	96	29.0	98	1.02	3.38
LT-E1	104	46.1	227	2.18	4.92
H-E1-PT	98	44.9	214	2.18	4.77
WP-E1-PT	166	46.6	150	0.90	3.22

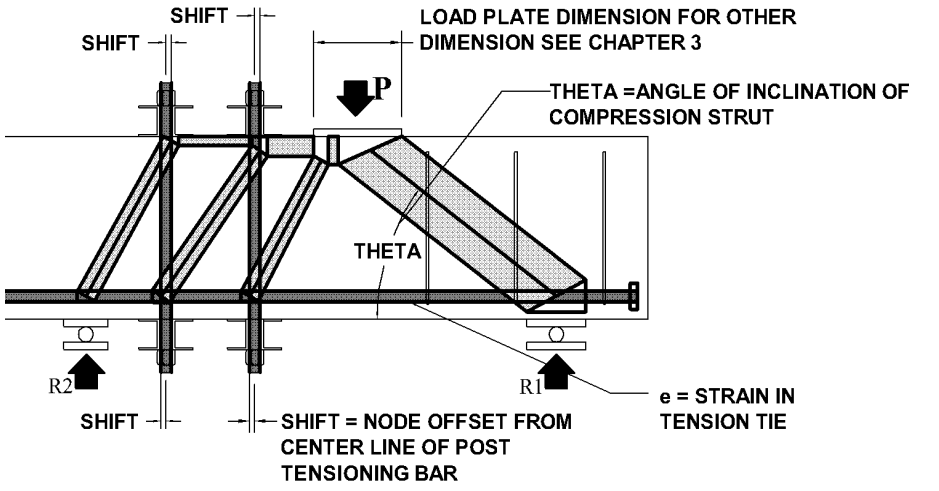

Figure 6.1 Definition of terms used in Table 6.2

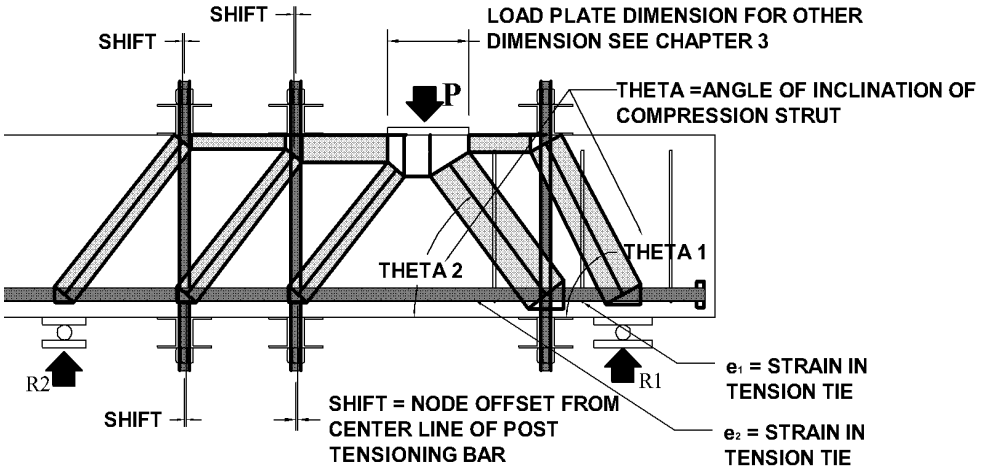

Figure 6.2 Definition of terms used in Table 6.3

6.1.3 Single strut mechanism computation of deep beam specimens (AASHTO LRFD 2007 Article 5.6.3)

The result of the (AASHTO LRFD 2007 Article 5.6.3) strut and tie analysis of test WP-E1 (Table 3.4) estimated the angle of inclination of the compression strut in the

test span to be 37 degrees. The strut and tie analysis also estimated the shear resistance of the test span to be 98 kips and a constant strain in horizontal tension tie no. 1 (Figure 6.3) of 0.00144 strain when that shear was reached. The angle of inclination of the compression strut computed from the surface mounted strain gauge rosette ranged between 30 and 45 degrees (Figure 3.9). This is due to the in-homogeneity of the concrete. However, the angle of inclination of the compression strut was shown to vary from 37 to 38 degrees when the strain gauges mounted on the horizontal tension reinforcement were used in the analysis. (Figure 3.10). The measured strain in the tension reinforcement was 0.00145 when the shear in the test span equaled 97.5 kips (Figure 3.8). The measured strain and angle of the compression strut are in good agreement with the strut and tie analysis prediction of 0.00144 strain in the tension reinforcement at 98 kips of shear in the test span, and a compression strut angle of 37 degrees. However the test was stopped prior to failure in order to post-tension and to retest the specimen.

The fact that the specimen was loaded to the predicted strut and tie capacity and then retested with the post-tensioning system during test WP-E1-PT meant that there was extensive cracking damage to the system prior to application of the post-tensioning system. This extensive cracking prevented the specimen from receiving the full benefit of the post-tensioning system. As a result subsequent tests, such as H-E1, performed in order to crack a deep beam or pier cap prior to application of post-tensioning system were loaded to only 49 percent of their predicted strut and tie capacity.

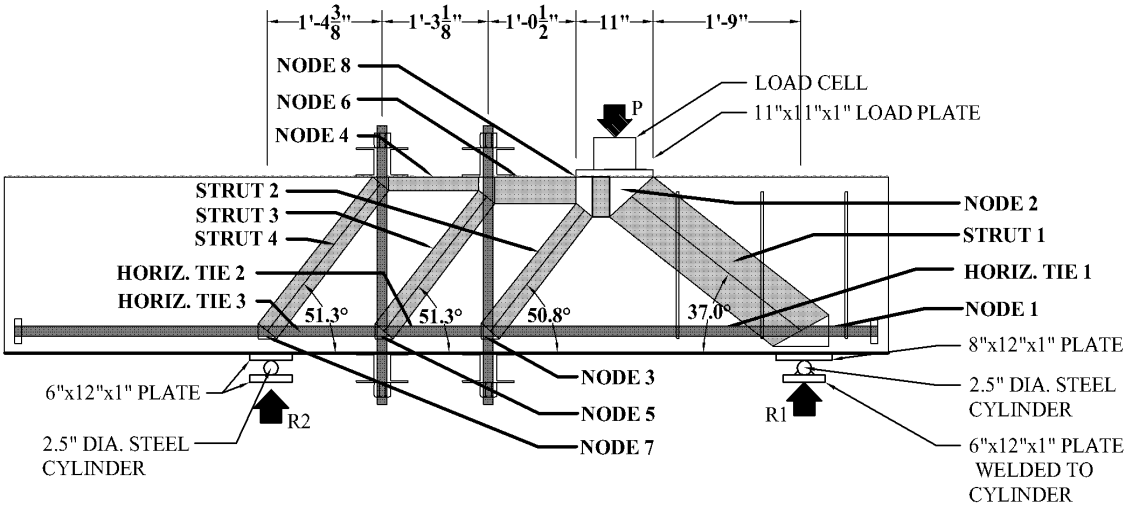

Figure 6.3 WP-E1 strut and tie mechanism (AASHTO LRFD 2007 Article 5.6.3)

The measured angle of inclination of the compression strut in tests LT-E1, H-E1 and H-E1-PT was between 35 and 45 degrees in all three cases. This indicates that each test behaved as if a single compression strut formed in the test span between the load "P" and support "R1". Similar to the test results for beam WP-E1, these beams did not fail at the predicted shear because the compression strut had a larger capacity than what was predicted by the strength reduction equation in Article 5.6.3 (Table 6.4). Sample strut and tie calculations following the Article 5.6.3 standards are presented in Appendix A1.

6.1.4 Deep beam test WP-E1-PT

The strut and tie analysis results outlined in Table 6.3 indicated a shear resistance for the test span of 166 kips; however, the specimen failed at a shear of 150 kips (Table 6.4) by means of concrete crushing under the load plate. The first possible explanation for the difference is that the crushing failure occurred due to the limited bearing area under the load plate. The second possible explanation is that the extent of diagonal cracking during test WP-E1 limited the size of the compression strut. During experiment WP-E1, the diagonal tension crack progressed to within 3 inches of the top face of the specimen, which is less than the 5.5 inches (Appendix A) required by the strut and tie analysis to anchor the compression strut.

The strut and tie analysis of test WP-E1-PT predicted that two struts would form in the test span: the first at 62 and the second at 54 degrees (Figure 6.4). The surface-mounted strain gauges and LVDTs were not able to capture the angle of inclination of the compression struts due to the fact that they were located between the two struts or bridged across them. The angle of the diagonal compression struts, STRUT 1 and STRUT 2 in Figure 6.4, could also not be computed from the strain gauges mounted on the rebar due to the fact that both strain gauges were mounted on the same tension tie instead of on either side of the vertical post-tensioning system.

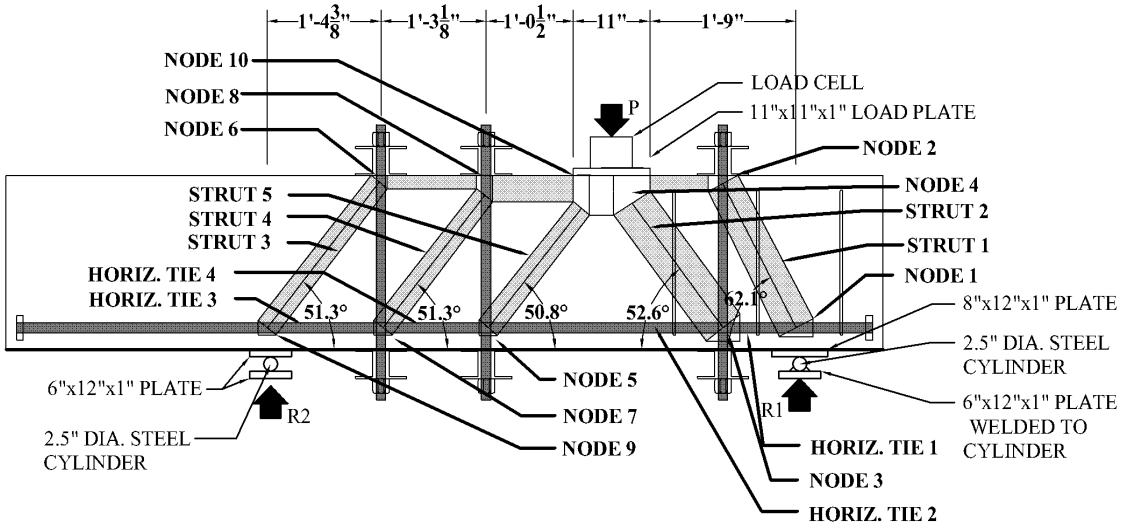

Figure 6.4 WP-E1-PT strut and tie mechanism

6.1.5 Deep beam tests LT-E1, H-E1, and H-E1-PT

As discussed in Chapter 3, the post-tensioning force used in test H-E1-PT was only 50 percent of the computed shear capacity of the double strut mechanism. As a result once the shear in the test span exceeded the pre-compression force, the specimen's response reverted to the single strut mechanism presented in Figure 6.3, and there was no benefit provided by the external post-tensioning system.

6.2 Comparison of pier cap specimen experiments and analysis

This section compares the results of the experimental testing of pier cap specimens presented in Chapter 5 to the results of analysis of the specimens using the AASHTO LRFD Bridge Design Specifications (2007).

6.2.1 Shear resistance of pier cap specimens per Article 5.8.3.4.1 of AASHTO (2007)

The simplified procedure for non-prestressed sections, as defined in Article 5.8.3.4.1of AASHTO LRFD (2007), was used to calculate the capacity of each of the pier cap tests. The specimens that did not meet the minimum transverse reinforcement requirements (Article 5.8.2.5) were specimens 2-NS, 4-NS, 4-NS-CR-PT, and 6-NS. The results of the analysis using equations 6.1 - 6.3, as defined in Section 6.1.1, are presented in Table 6.5.

Table 6.5 Pier cap shear resistance per Article 5.8.3.4.1 of AASHTO (2007)

Test ID	f_t' (ksi)	f_c' (ksi)	$V_{article\ 5.8.3.4.1}$ (Kips)	Post-tensioning (kips)	
				Span 1	Span 2
1-S	0.333	3.43	80.7	-	
2-NS	0.326	3.18	43.6	-	
3-S-PT	0.381	3.55	81.6	265	256
4-NS	0.338	3.08	42.9	-	
4-NS-CR-PT	0.338	3.08	42.9	210	213
5-S	0.360	3.51	81.3	-	
5-S-CR-PT	0.415	3.53	81.4	223	212
5-S-CR-PT2	0.386	3.64	82.2	223	212
6-NS	0.427	3.46	45.5	-	

6.2.2 Shear resistance of pier cap specimens per Article 5.6.3 of AASHTO (2007)

The angle of the principal compression strut or struts in the test shear span and the strain in the tension reinforcement at computed specimen shear resistance as per Article 5.6.3 (AASHTO 2007) are presented in Tables 6.6 and 6.7. Table 6.6 lists the analysis of each specimen based on a single strut and tie mechanism, whereas Table 6.7 list the analysis results for an assumed double strut mechanism when the external post-tensioning system was applied to the test shear span.

Table 6.6 Single strut pier cap models (terms defined Figure 6.5) (AASHTO LRFD 2007 Article 5.6.3)

Test ID	f'_c (ksi)	f'_c (ksi)	Theta 1 (Degrees)	e	V (kips)	Limit State
1-S	0.333	3.43	38.6	0.00155	134	Strut crushing
2-NS	0.326	3.18	38.5	0.00147	127	Strut crushing
4-NS	0.338	3.08	38.5	0.00144	124	Strut crushing
5-S	0.360	3.51	38.6	0.00157	136	Strut crushing
6-NS	0.427	3.46	38.6	0.00156	135	Strut crushing

$f_t' = split\ cylinder\ tension\ strength\ of\ 6"\ dia.concrete\ cylinders\ (ksi)$

$f_c' = compression\ strength\ of\ 6"\ dia.concrete\ cylinders\ (ksi)$

$V = R_1 = shear\ resistance\ (kips)$

Table 6.7 Double strut pier cap models (terms defined Figure 6.6) (AASHTO LRFD 2007 Article 5.6.3)

Test ID	f'_t (ksi)	f'_c (ksi)	Theta 1 (Degrees)	e_1	Theta 2 (Degrees)	e_2	V (kips)	Limit State
3-S-PT	0.381	3.55	60.9	0.00117	54.7	0.00266	228	Steel yield
4-NS-CR-PT	0.338	3.08	60.7	0.00113	52.9	0.00266	219	Steel yield
5-S-CR-PT	0.415	3.53	60.9	0.00117	54.6	0.00266	227	Steel yield
5-S-CR-PT2	0.386	3.64	60.9	0.00118	55.0	0.00266	229	Steel yield

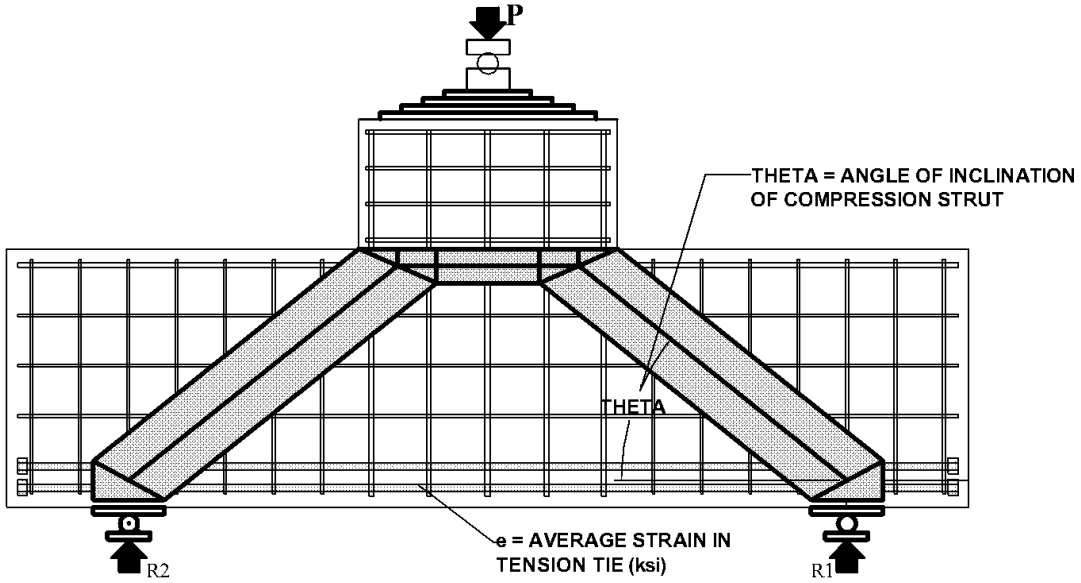

Figure 6.5 Definition of terms used in Table 6.6

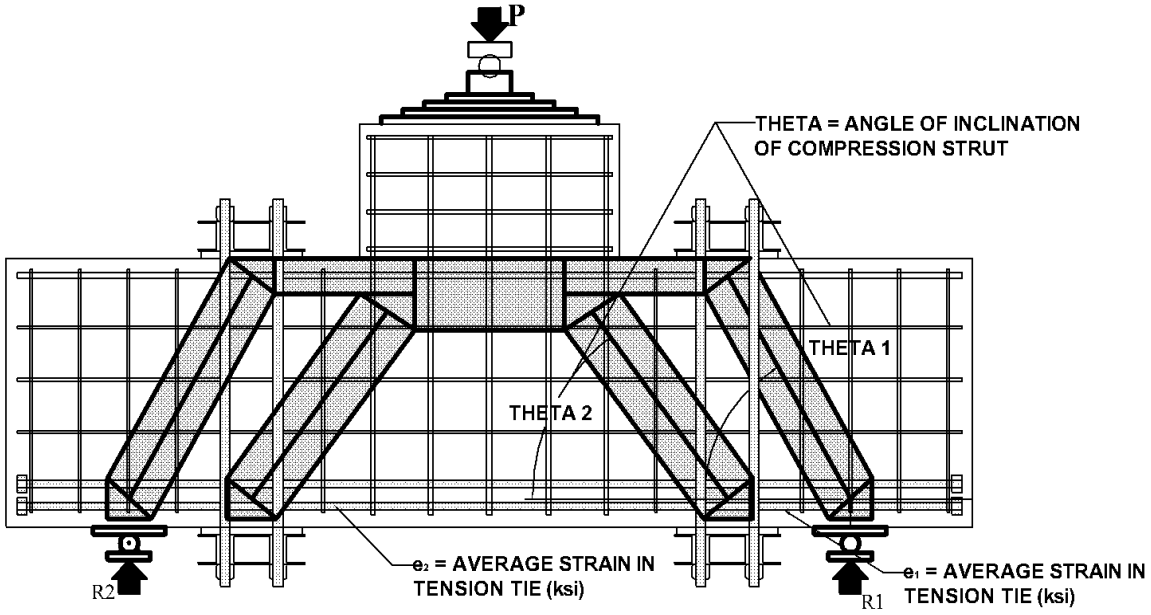

Figure 6.6 Definition of terms used in Table 6.7

6.2.3 Pier cap test specimens without post-tensioning (1-S, 2-NS, and 6-NS)

The ratios of experimental to computed capacity for the specimens loaded to failure without the external post-tensioning system are presented in Table 6.8. The shear resistance computed according to AASHTO LRFD 2007 Article 5.8.3.4.1 in all cases resulted in a conservative assessment of the resistance of the specimen.

Table 6.8 Ratio of test shear capacity to computed shear capacity (pier cap specimens)

Test ID	$V_{article\ 5.6.3}$ (kips)	$V_{article\ 5.8.3.4.1}$ (kips)	$V_{ult.exp}$ (kips)	$V_{ult.exp}/V_{article\ 5.6.3}$	$V_{ult.exp}/V_{article\ 5.8.3.4.1}$
1-S	134	80.7	195	1.45	2.42
2-NS	127	43.6	145	1.14	3.33
6-NS	135	45.5	252	1.87	5.54

In the case of test 1-S, the AASHTO strut and tie analysis performed in accordance with Article 5.6.3 underestimated the capacity of the test specimen by 45 percent. The reason this method underestimated the capacity of the specimen was due to the compression strut strength reduction equations 6.4 and 6.5, which predict failure of the compression strut at the pier cap supports when the strain in the tension reinforcement reached 58 percent of the yield strain. During testing, however, failure of the pier cap specimen 1-S occurred by crushing of the compression strut at the reentrant corner

between the pier cap and column when the strain in the tension reinforcement reached 80 percent of the yield strain.

The strut and tie analysis of the test 6-NS specimen also under predicted the shear resistance due to the compression strut strength reduction equations. Like test 1-S, the predicted shear resistance of the specimen was governed by the width of the compression strut at the supports while the experimental capacity of the specimen was governed by crushing of the compression strut at the reentrant corner of the pier cap and column. Unlike test 1-S, crushing of the compression strut did not occur until the shear in the test span reached 252 kips, which is after the tension reinforcement yielded at a shear in the test span of 225 kips. The reason the specimen did not fail prior to yielding of the tension reinforcement during test 6-NS was the location of the diagonal tension crack in reference to the corner between the pier cap and column. During test 1-S the diagonal tension crack occurred 3 inches from the corner, whereas in test 6-NS the diagonal tension crack occurred 5 inches from the corner, allowing a wider compression strut to form. By comparison, the strut and tie analysis predicted the width of the compression strut during tests 1-S and 6-NS to be 10.5 inches. In conclusion, during tests 1-S and 6-NS the specimens were able to achieve a higher shear resistance than predicted by the Article 5.6.3 (AASHTO 2007) strut and tie specifications, with a narrower strut than predicted. Additionally the lack of horizontal and vertical tension reinforcement did not adversely affect the shear resistance of the pier cap specimen 6-NS.

Test 2-NS differed from tests 1-S and 6-NS in that lack of bond between the beam and column prevented them from acting in a composite fashion. Unlike any of the other specimens, the horizontal compression block at the top of specimen 2-NS was confined to the beam and did not extend into the column. This behavior was observed by measurements of the externally mounted LVDTs in the column, which measured horizontal compression in the column 3 inches above the top of the beam in all tests except 2-NS. Additionally a horizontal crack occurred at the beam and column interface

and the diagonal tension cracks turned horizontal as they approached the top of the beam, neither of these cracking patterns were observed in any specimens other than 2-NS (Figure 6.3).

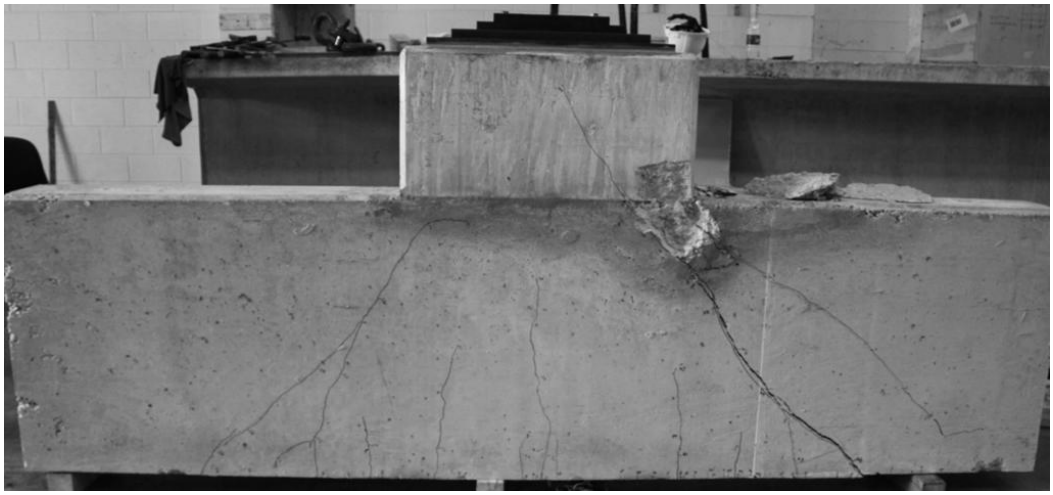

Figure 6.7 Test 2-NS failed specimen

As a result of this non-composite behavior of specimen 2-NS, the diagonal compression strut did not bypass the stress concentration at the reentrant corner and form a compression node in the column; instead, a compression node was formed at the stress concentration. As a result of the compression node forming at the stress concentration, the horizontal compression force at the top of the pier cap was added to the stress concentration and caused the pier cap to fail at a lower shear than it would have if the specimen had acted in a composite fashion. Consequently, the ratio of experimental to predicted shear resistance (Table 6.8) of specimen 2-NS is closer to 1 than any of the other specimens tested without the external post-tensioning system. The fact that experimental capacity of 2-NS was the closest to its predicted resistance should be expected since the majority of the tests conducted to develop the STM were performed on beams without a composite column.

6.2.4 Pier Cap specimens with post-tensioning (3-S-PT, 4-NS-CR-PT, and 5-S-CR-PT-2)

The three tests of specimens for which the external post-tensioning system was employed all produced similar responses, as summarized in Table 6.9.

Table 6.9 Ratio of test shear capacity to predicted shear capacity (post-tensioned pier caps)

	$V_{article\ 5.6.3}$ (Kips)	$V_{article\ 5.8.3.4.1}$ (Kips)	$V_{ult.exp}$ (Kips)	$V_{ult.exp}/V_{article\ 5.6.3}$	$V_{ult.exp}/V_{article\ 5.8.3.4.1}$
3-S-PT	228	81.6	287	1.26	3.52
4-NS-CR-PT	219	42.9	299	1.37	6.97
5-S-CR-PT2	229	82.2	307	1.34	3.73

Each test resulted in a ratio of shear at specimen failure to shear resistance computed by the strut and tie method (Article 5.6.3 AASHTO 2007) between 1.26 and 1.37. The three post-tensioned specimens included specimens that were cracked, 4-NS-CR-PT and 5-S-CR-PT2, as well as a specimen that was not cracked, 3-S-PT, prior to application of the retrofit. Additionally specimens 3-S-PT and 5-S-CR-PT2 had internal shear reinforcement in the test span whereas specimen 4-NS-CR-PT did not. Since the ultimate shear resistance of all three specimens was within 6 percent of each other, the effect of internal shear reinforcement appeared to be negligible when the external post-tensioning system was employed. It was also concluded that vertical external post-tensioning of pier caps was just as effective when used on specimens that have experienced diagonal tension cracking as when used on specimens that have not experienced diagonal tension cracking. Specimen 5-S-CR-PT2 was loaded until yielding of the tension reinforcement occurred, unloaded, and then reloaded until failure of the specimen occurred. Test 5-S-CR-PT2 shows that the external post-tensioning system remains effective after an overload event. This means the external post-tensioning system could be designed to increase the strength of a pier cap for a permit or other overload situation, in addition to its current use by GDOT for emergency repair of damaged pier caps.

6.3 Design of post-tensioning for rehabilitation of pier cap specimens

The post-tensioned specimens were observed to have higher capacity and ductility than the specimens that are not post-tensioned due to the formation of a double strut mechanism (Figure 6.8). This double strut mechanism shifted the diagonal compression strut away from the stress concentration at the corner of the pier cap and column interface.

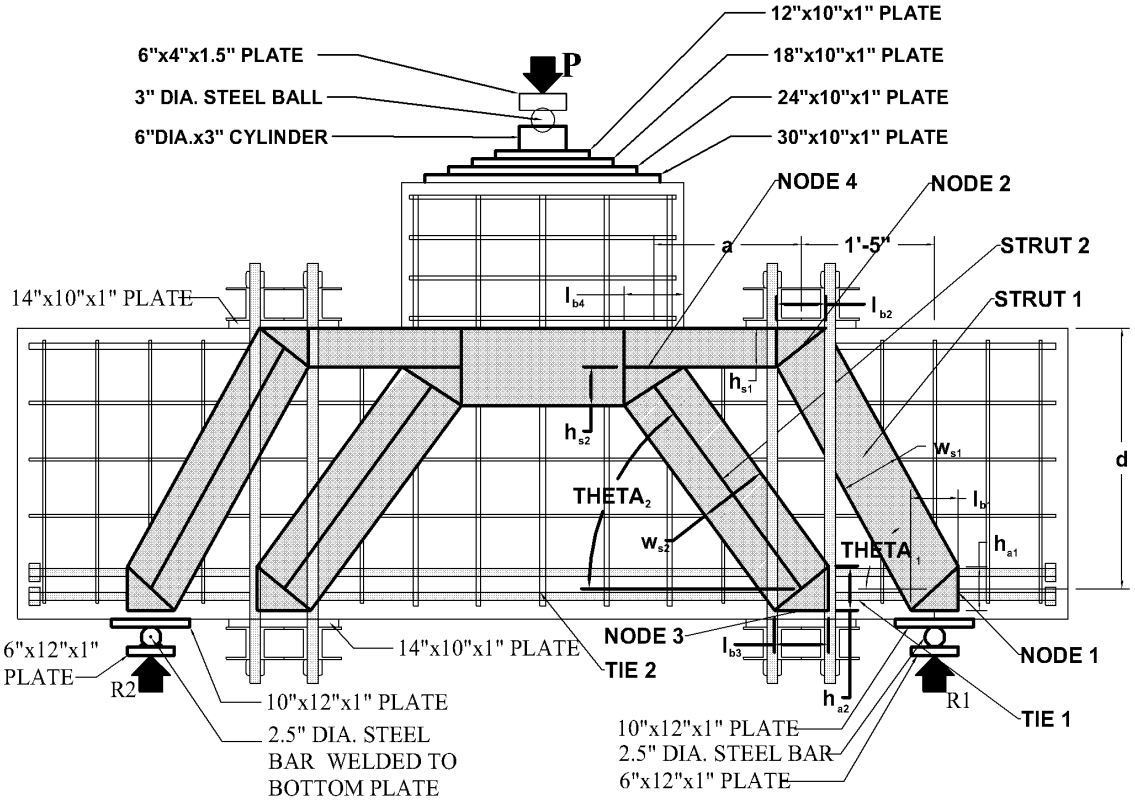

Figure 6.8 Pier cap double strut mechanism (AASHTO LRFD 2007 Article 5.6.3)

The shifting of the diagonal compression struts away from the pier cap-column corner enabled the formation of wider struts than those formed in a single strut mechanism (Figure 6.9). As a result of the wider struts, the specimens transferring load through a double strut mechanism were able to reach yield of the tension reinforcement prior to failure of the specimen. Consequently, the external post-tensioning system should be designed so that a double strut mechanism is formed within the pier cap. To

design the post-tensioning system so that a double strut mechanism is formed, two strut and tie analyses were first performed, one on the specimen using a single strut mechanism Table 6.6 (Appendix A-3), and one on the specimen using a double strut mechanism Table 6.7 (Appendix A-4).

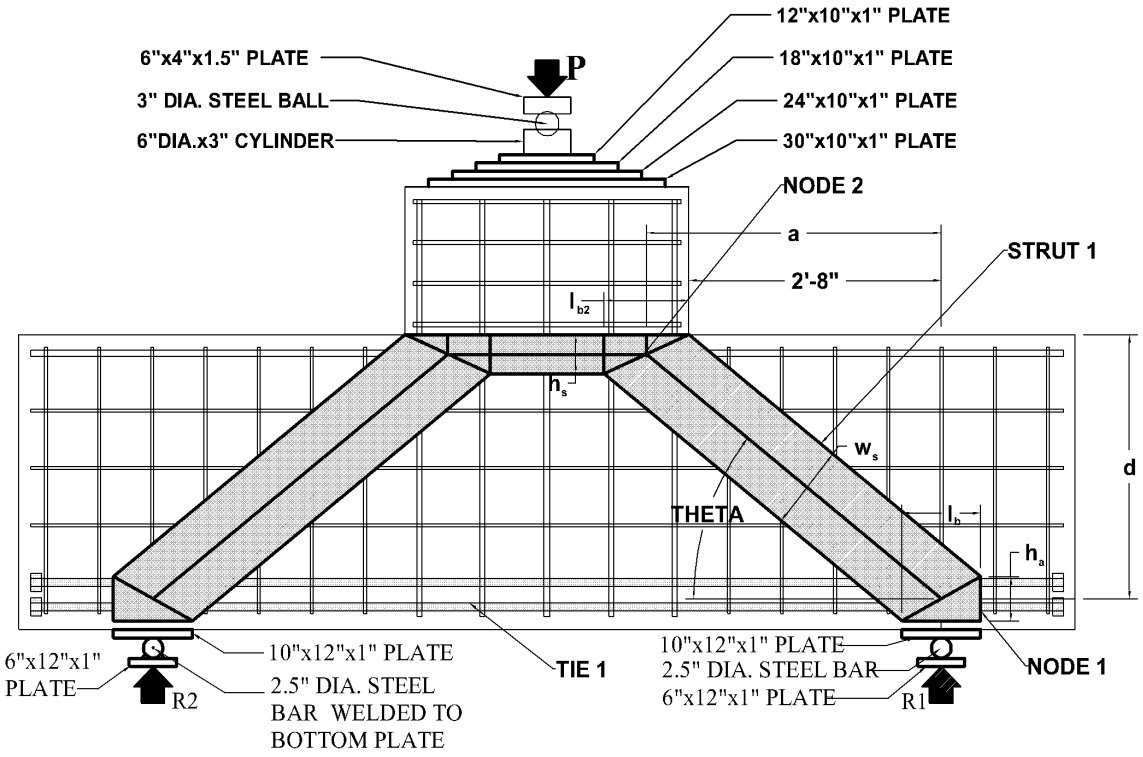

Figure 6.9 Pier cap single compression strut mechanism (AASHTO LRFD 2007 Article 5.6.3)

In order to determine which strut and tie mechanism forms within a structure, a strain energy analysis must be performed on all possible strut and tie mechanisms. The mechanism with the lowest strain energy is the mechanism that will form, since it requires the least amount of energy. The total energy of a strut and tie mechanism is computed by summing the strain energy of each strut and tie that comprises the total mechanism. The individual strain energies for each strut and tie are calculated using Eq. 6.6.

$$u = \frac{F^2 l}{E\,A} \qquad \text{(Eq. 6.6)}$$

$u =$ strain energy in single strut or tie (kip-inches)

$F =$ force in single strut or tie (kips)
$l =$ length of single strut or tie (inches)
$E =$ modulus of elasticity of strut or tie material (ksi)
$A =$ cross sectional area of single strut or tie (square inches)

By comparing the strain energy of the single and double strut and tie mechanisms (Appendix B), the single strut mechanism was determined to require 16 percent less strain energy. Therefore, in order to force the double strut mechanism to occur, additional strain energy had to be imparted into the system. This additional strain energy was imparted to the system through post-tensioning the external tension tie, which placed the concrete in pre-compression. Once post-tensioned, when load is applied to the specimen, rather than creating tension strain in the external tie, the pre-compression in the concrete was relieved. As a result of the post-tensioning, the total strain energy of the double compression strut mechanism was lower than the single strut mechanism. The results of the strain energy computation presented in Appendix B concluded that the post-tensioning force must be greater than 78 percent of the shear in the test span for the double strut mechanism to form; otherwise the strut and tie mechanism will revert to the single strut mechanism.

After post-tensioning of the specimen 3-S-PT prior to test, vertical cracks were found in the specimen in the center of the pre-compressed region (Figure 6.10). The cracks occurred overnight between the time the post-tensioning was applied to the specimen and when test 3-S-PT was conducted.

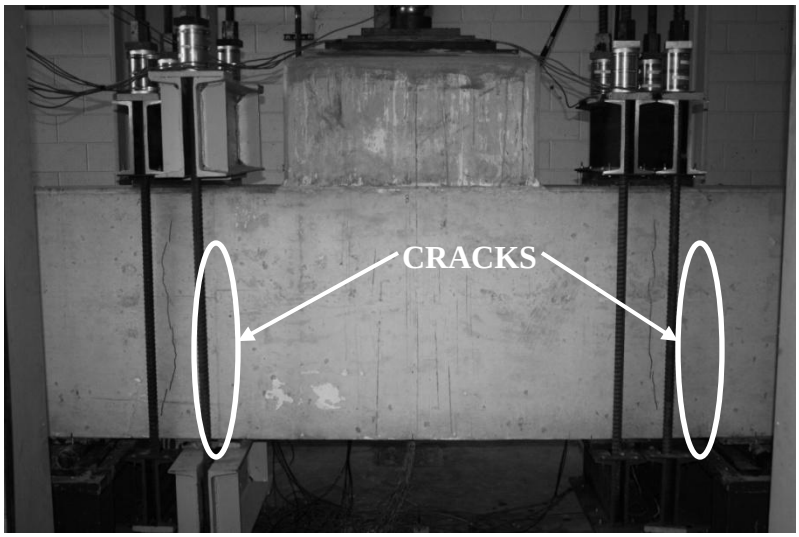

Figure 6.10 Test 3-S-PT post-tensioning cracks

The cracks were unexpected because the level of post-tensioning was less than the bearing capacity of the concrete. To identify the cause of the cracking and determine the maximum post-tensioning that could be used without inducing damage to the specimen, an ABAQUS finite element model of the test specimen was performed. In the finite element model the post-tensioning force was applied to the top and bottom of the specimen as a uniformly distributed load over a one inch thick 14 x 10 inch steel plate (Figure 6.11).

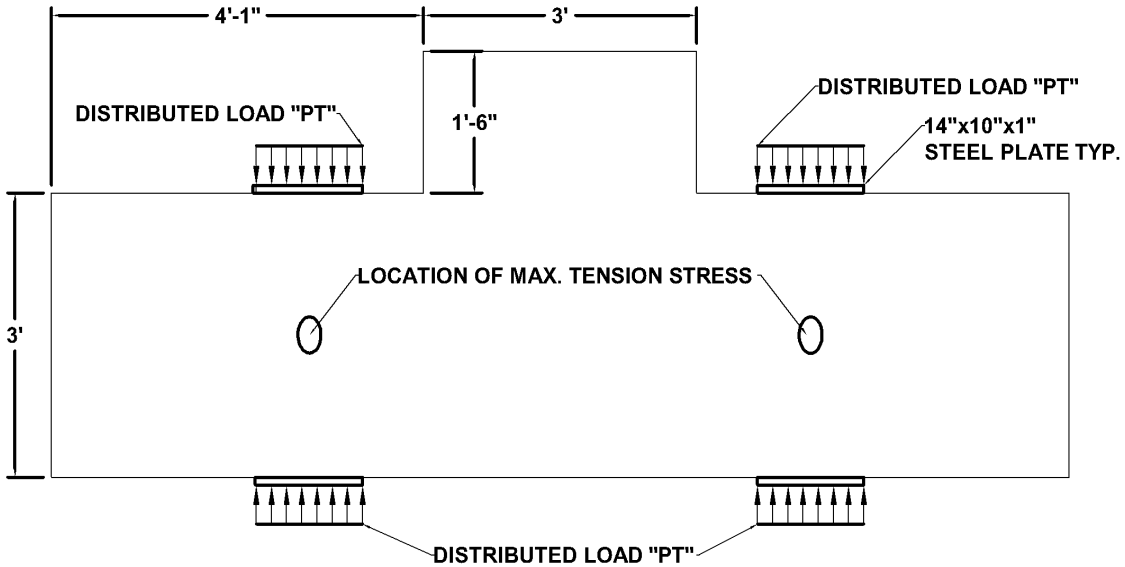

Figure 6.11 ABAQUS finite element model of post-tensioning

The analysis showed a maximum horizontal tension stress occurring at mid-depth of the specimen, with a linear relationship between the post-tensioning force and resulting horizontal tension stress (Equation 6.7).

$$\sigma_t = \left(\frac{0.9\,psi}{kip}\right) \times (PT) \qquad \text{(Eq. 6.7)}$$

$\sigma_t = \text{horizontal tension stress at mid} - \text{depth of the specimen in psi}$
$PT = \text{vertical post} - \text{tensioning force in kips}$

The tension strength of the concrete σ_t was determined to be between 348 and 442 psi by performing three split cylinder tests. According to the ABAQUS analysis, the post-tensioning force required to reach a horizontal tension stress of 350 psi, was 389 kips or 97 kips in each of the post-tensioning bars. The post-tensioning force in the specimen 3-S-PT was 64 kips; however the specimen was post-tensioned to approximately 100 kips in each bar in order to achieve 64 kips after the hydraulic jacks were released. Accordingly, it was concluded that cracking of the specimen 3-S-PT was initiated during the post-tensioning process.

6.4 Summary of comparison of experimental results and analysis

Through comparing the results of the deep beam tests and pier cap tests to AASHTO LRFD (2007) analysis tools, it was determined that Article 5.6.3 of that Specification is suitable for the analysis of existing bridge pier caps, regardless of whether or not internal shear reinforcement is present. In addition, Article 5.6.3 specifications in conjunction with a strain energy analysis of the possible strut geometries can be used to design the post-tensioning system. Finally, when installing the post-tensioning system to strengthen the pier cap, care must be taken not to overload the pier cap and induce damage to the structure.

CHAPTER 7. **CONCLUSIONS**

The objectives of the research that is reported in this dissertation were to:

- Evaluate the effectiveness of the external post-tensioning system currently used by GDOT as a rehabilitation technique for strengthening reinforced concrete bridge pier caps.
- Determine whether the AASHTO LRFD 2007 Article 5.6.3 strut and tie provisions are an appropriate means of performing a strength assessment of existing pier cap structures that do not meet AASHTO's minimum shear reinforcement requirements.
- Evaluate whether the AASHTO LRFD 2007 Article 5.6.3 strut and tie provisions are an appropriate means of designing the external post-tensioning strengthening system.
- Compare the behavior of a deep beam to the behavior of a pier cap in which the beam section is cast composite with the pier (column).

To achieve the research objectives, three deep beam and six pier cap specimens, which included a segment of the column, were designed fabricated, instrumented and tested. Six tests were performed on the three deep beam specimens, including three tests where the external post-tensioning system was applied to the specimen. Nine tests were performed on the pier cap specimens, including four tests where the external post-tensioning system was applied the specimens. These tests were aimed at providing a better understanding of pier cap and column assemblies and to determine the benefits, if any, of external post-tensioning as a rehabilitation strategy aimed at increasing their *in situ* strength. The tests revealed that the ultimate capacity and load carrying mechanism of each of the specimens was governed by tied arch rather than classical beam behavior and that their load-carrying capacity could be conservatively estimated using the AASHTO (2007) strut and tie analysis provisions.

7.1 Deep beam specimen tests

Failure of the deep beam specimens was governed by crushing failure at the compression node under the load plate where the load (from the pier) was applied. It was also observed that the behavior and failure during test WP-E1-PT was affected by the damage caused to the specimen during test WP-E1, conducted to crack the specimen prior to post-tensioning. During subsequent tests performed to crack specimens prior to application of the external post-tensioning systems, the specimens were loaded to only 80% of the ultimate capacity predicted by the AASHTO strut and tie procedure. Test WP-E2 was affected by the damage caused to the specimen during tests WP-E1 and WP-E1-PT, and as a result, only one end of each subsequent specimen was tested. The addition of the external post-tensioning system was found to alter the geometry of the strut and tie load-carrying mechanism within the deep beam specimens up to the point where the shear in the test span exceeded the initial compression induced by the post-tensioning. This finding is supported by the strain energy analysis in Appendix B, which suggested that the single strut geometry is the most efficient load carrying mechanism when the a/d ratio of the specimen is less than 1.5, unless there is sufficient post-tensioning to force the formation of a double strut mechanism.

7.2 Pier cap specimen tests

During the pier cap testing it was observed that the failure of each specimen, regardless of whether or not external post-tensioning was present, occurred by crushing of the concrete in compression at the reentrant corner between the pier cap and the column. Failure occurred at this location due to the stress concentration that arises when the diagonal compression strut passes through that point. It was also observed that post-tensioning causes a double strut mechanism to form. The double strut mechanism was successful in increasing the capacity of the specimens and allowed the specimen to sustain increasing load and deflection after yielding of the tension reinforcement, this

behavior was not observed in the beams without the rehabilitation. This improvement in behavior occurred because the post-tensioning moved the compression strut away from the reentrant corner, allowing the specimen to develop the full yield strength of the horizontal tension reinforcement prior to failure. Once the tension reinforcement yielded, the test specimens continued to carry increased load by means of raising the angle of the compression struts until they approached the reentrant corner and failed due to the stress concentration at that corner.

The pier cap testing also revealed that the presence of internal shear reinforcement in either the horizontal or longitudinal direction had a negligible effect of the behavior of pier caps that were externally post-tensioned. The internal sheer reinforcement's lack of influence on the behavior of the specimen was because the relative stiffness and capacity of the internal No. 3 bars used to provide shear reinforcement was only a fraction of that of the four No. 11 DWYDAG bars used in the external post-tensioning system. It was observed in tests 1-S and 6-NS that the diagonal compression strut formed at approximately the same angle regardless of the presence of internal shear reinforcement. However, the location of the diagonal tension crack was shifted between tests 1-S and 6-NS. During test 1-S, the diagonal tension crack occurred directly below the diagonal compression strut, whereas during test 6-NS the diagonal tension crack occurred 2 inches lower. As a result, during test 6-NS there was a larger area of concrete for the stress concentration to distribute over at the reentrant corner of the beam column connection, enabling the 6-NS specimen to achieve a higher capacity.

Test 2-NS differed from all the other tests in that composite action between the beam and column did not develop. In the tests where the beam and column acted in an integrated fashion, the diagonal compression strut bypassed the stress concentration at the reentrant corner between the beam and column, enabling a compression node to form in the column. However, in test 2-NS due to the non-composite behavior of the specimen, the compression node formed at the reentrant corner between the beam and column

causing the failure of the specimen to occur at a lower load than the specimens that had composite action (1-S and 6-NS).

The pier cap tests conducted in support of this dissertation showed that the integral column segment caused a stress concentration at the reentrant corner between the beam and column. The presence of this reentrant corner had a profound effect on the development of the diagonal compression strut, which had been ignored by all experimental testing that replaces the column with a distributed load. The study by Aguilar et al. (2002), tested twelve inch wide thirty six inch deep reinforced concrete beams with an a/d ratio of 1, the beams had more tension reinforcement than the pier cap tests presented in chapters 4-6 and did not have an integral column. Aguilar et al. (2002) found that the lack of internal shear reinforcement only reduced the capacity of the specimen by 1%. The pier cap tests results from experiment 1-S and 6-NS showed that the location of the diagonal tension crack shifted in the absence of internal shear reinforcement and that the shift in crack location affected the capacity of the specimen by 22%. In order for the AASHTO strut and tie provisions to accurately represent the mechanics of deep beams a method of predicting the compression strength of concrete in regions with discontinuities is required. In addition a method of predicting the available width of the diagonal compression strut at such discontinuities is also needed. In order to develop a method of predicting the strength and width of diagonal compression struts that cross discontinuities further testing of deep reinforced concrete beams, with discontinuities is required.

This dissertation shows that the current AASHTO strut and tie provisions predict wider compression struts than are actually formed within the specimen. Wider struts than occurred during the experiment were predicted due the compression strut strength reduction equation presented in AASHTO Article 5.6.3.3.3. The compression strut strength reduction equation reduces the strength of the strut based on the tension strain in the tension reinforcement and angle at which the tension reinforcement crosses the

compression strut. The experimental tests conducted to support this dissertation found no evidence that the strain in the horizontal tension tie reduced the strength of the diagonal compression struts. Further testing is needed to determine in what cases, if any, the strain in the tension tie affects the strength of the compression strut and in what cases the strength reduction factor should and should not be used.

During the post-tensioning of specimen 3-S-PT prior to the test, vertical cracking of the specimen occurred due to over compressing the specimen. As a result, the post-tensioning process was revised in subsequent tests. The post-tensioning process applied to 3-S-PT consisted of tensioning the system with hydraulic jack, tightening the nuts on each of the post-tensioned steel rods, and removing the hydraulic jacks. The revised post-tensioning process involved using a larger wrench to tighten the nuts, which reduced the post-tensioning losses when the hydraulic jacks were removed. The post-tensioning force was also reduced by 18% in order to ensure cracking did not occur during the post-tensioning process. This revised post-tensioning process did not affect the capacity of the strengthened pier caps. The total post-tensioning force was sized at 90 percent of the shear in the test span, and not any specific percent of the yield strength of the DWYDAG bars. The post-tensioning force was sized by performing a strain energy analysis of the post-tensioned structure to determine the level of post-tensioning force required to force the double strut geometry to occur in the specimen at yielding of the tension reinforcement (Appendix B). For long term application of the post-tensioning system the size of the post-tensioned bars should be selected so that the desired force can be achieved using established post-tensioning and strain relaxation guidelines for the material in use.

7.3 Assessment of AASHTO strut and tie provisions

The AASHTO 2007 Article 5.6.3 provisions were used to construct strut and tie models of each test specimen. The research performed in this study showed that the strut

and tie models, represent the overall tied arch behavior of the specimens and provide a conservative strength assessment regardless of the presence of internal shear reinforcement. However, the AASHTO strut and tie provisions fall short of providing a fundamental mechanics based assessment of pier cap capacity, due to the method's inability to deal with stress concentrations within diagonal compression struts, the use of a compression strut strength reduction factor, and the method's inability to predict the width of diagonal compression struts.

While the strut and tie provisions do not capture the proper failure mode of pier cap specimens, which involves crushing of the concrete at the stress concentration, the provisions are nonetheless able to provide conservative predictions of strength and, combined with a strain energy evaluation, can be used to design an effective external post-tensioning rehabilitation. The external post-tensioning rehabilitation succeeded in increasing the strength and ductility of the pier cap specimens, by creating a double strut mechanism. The double strut mechanism shifted the diagonal compression struts away from the stress concentration at the reentrant corner of the pier cap and column connection. The strain energy analysis found that the formation of a single compression strut mechanism required less energy than a double strut mechanism. However, by post-tensioning the specimen, a double strut mechanism was formed, as detailed in Chapter 6, if the post-tensioning force is at least 78% of the shear transferred through the pier cap between the column and support. Furthermore, the external post-tensioning system can be effectively used to increase both the strength and ductility of the typical pier caps constructed for GDOT during the 1950's and 1960's, as well as those designed to current AASHTO specifications.

The strut and tie analysis as stipulated in Article 5.6.3 (AASHTO 2007) had some limitations. These included an inability to address the effect of the stress concentration which occurred at the pier cap-column reentrant corner. In addition, the compression strut strength reduction equations caused the width of the predicted diagonal compression

struts to be larger than observed. The strut strength reduction equations predicted that the compression strut would fail in pier cap specimens 1-S, 2-NS, and 6-NS at the base of the compression strut prior to yield of the tension reinforcement. The strength reduction equations predicted this failure would occur due to the tension strain in the rebar that crossed the compression strut at the support. Instead, the three specimens failed due to crushing of the compression strut at the stress concentration at the reentrant corner. As a result, the strut and tie method predicted a compression strut failure for the wrong reasons and at the wrong location, but provided a conservative strength assessment.

The strut and tie models of the pier caps with the external post-tensioning system, 3-S-PT, 4-NS-CR-PT, and 5-S-CR-PT, predicted the specimens to reach yielding of the tension reinforcement prior to failure. During the testing of these three specimens, however, yielding occurred at a load 5 to 10 percent higher than that predicted by the strut and tie method. All three specimens failed by crushing of the compression strut *after* yielding of the tension reinforcement. It can be concluded that the strut and tie method provides a conservative analysis of the post-tensioned specimens and accurately predicts the mechanics of the specimens up to the point of yielding of the tension reinforcement. Comparison of the predicted width of the diagonal compression struts and the cracking pattern of the specimens showed that narrower struts formed during testing than those predicted.

7.4 Recommendations

All pier caps should be analyzed using the provisions in Article 5.6.3 of the AASHTO LRFD Bridge Design Specifications 2007. New pier caps should be designed to meet the AASHTO minimum shear reinforcement requirement. However, the strut and tie method should also be used to assess existing pier caps that do not meet current minimum shear reinforcement requirements, since it provides a conservative strength estimate. In addition, new pier caps should be designed to prevent a stress concentration

from forming at the reentrant corner between the pier cap and column since this was found to be the limiting factor in the strength of the pier cap specimens.

This study found that Lenton terminators were capable of fully developing the tension reinforcement within the pier cap specimens, in addition to producing a similar response of the specimen to 180 hooked bars. The reason Lenton terminators were selected for the specimens tested in support of this dissertation was the relative ease of fabrication compared to 180 degree hooked bars as well as the increased ability to ensure confinement of the concrete around the tension reinforcement. Both of these reasons for selecting Lenton terminators as the means of bar anchorage would also benefit field construction, and based on the results of the test presented in this dissertation as well as the study conducted by Aguilar et al. (2002), Lenton terminators are able to fully develop a pier cap or there deep beam's tension reinforcement, up to and beyond the point of yielding of the tension reinforcement.

7.5 Recommended future research

This research program revealed that the boundary conditions of deep reinforced concrete beams have a profound and non-negligible effect on their behavior and load carrying capacity. As a result, it is recommended that during any experimental study attempting to strengthen deep reinforced concrete members, the boundary conditions of the specimen in an actual bridge or building be modeled as closely as possible. Component tests on simply supported deep beams are insufficient in terms of assessing the effectiveness of strengthening techniques on member that act compositely with a column or other structural element in a bridge or building. Even if the deep beam is designed to act in a non-composite fashion with the column, if it is cast in a manner that composite action could be achieved, that action must be considered. The presence of composite action between the deep beam and column is likely to be the limiting

parameter in the strength of pier cap-like structures, as was found to be the case in the pier cap tests presented in Chapters 5 and 6.

Since it was impractical to construct full length columns over all possible lengths, an elastic finite element analysis was used to determine at what point the length of the column no longer affects the stress concentration at the reentrant corner between the beam and column. An inelastic finite element model was not constructed, because the location of the diagonal tension cracked affected the behavior and capacity of the specimen, and a cracking model that accurately predicted the damage and behavior of the structure could not be found. The elastic model determined that a similar size and location for the stress concentration occurred in a specimen with an 18 inch long column as did in a specimen with a 15 foot long column. Since the elastic analysis was only able to determine that the length of the integral column segment could be reduced to 18 inches (one half the column width), without affecting the formation of the stress concentration under elastic analysis. Experimental testing to determine what effect lengthening the column to the width or twice the width of the column would have on the ultimate response of the specimen would be beneficial.

A parametric study to determine the appropriate design of the beam and column connection in order to eliminate the stress concentration at the reentrant corner between the two should be conducted. The study should begin with an elastic finite element study to determine if a chamfer between the beam and column is sufficient to eliminate the stress concentration, and if so how large of a chamfer is required or if a hammer head pier cap is required. A specimen or specimens should then be constructed as a proof of concept for the proposed modifications to standard pier cap design.

In order to properly assess the ability of analysis tools such as the strut and tie method, more information needs to be gathered during an experiment than the ultimate capacity of the member (Hawkins et al. 2005). To determine if the specimen is transferring load in the same manner as predicted by a strut and tie analysis, the angle and

width of the compression struts are also needed. The angle and location of the compression struts should be measured by a combination of techniques since the inhomogeneity of the concrete makes reliance on a single gauge or technique unreliable.

For the AASHTO strut and tie provisions to be a fundamental mechanics based method that accurately predicts the response of the full range of reinforced concrete members, an extensive experimental study designed to determine the width of diagonal compression struts is required. The experimental study must include specimens with discontinuities such as beam with integral column. Once an accurate method of predicting the width of diagonal compression strut is established a compression strut stress concentration factor can be proposed. The test 1-S and 6-NS on specimens with an integral column segment found the compression strut widths two be significantly smaller than those predicted by the AASHTO strut and tie procedure and the compression strength of the strut at failure to be between 1.2 and 1.58 times f_c'. However, these two tests alone are not sufficient to develop a method of predicting diagonal compression strut width, so further testing is required to develop the strut and tie method into a fundamental mechanics based method capable of assessing all reinforced concrete members.

7.6 Summary

This research program demonstrated that the behavior of a composite pier cap and column differed significantly from the behavior of a deep beam or even a non-composite pier cap and column. This observation is significant since the majority of existing experimental data on the behavior of deep beams has been obtained from tests conducted on simply supported deep beams in either three or four point bending. In contrast, this program showed that failures of the pier cap specimens were governed by the interaction of the pier cap and column. In addition, the success of the external post-tensioning system was due to its ability to shift the location of the diagonal compression strut away

from the reentrant corner at the pier cap and column interface. It was concluded from the pier cap tests that for any rehabilitation or strengthening technique to be effective at increasing the strength and/or ductility of similar pier caps it must address the presence of the stress concentration at the reentrant corner where the pier cap and column meet. Any strengthening technique that is focused only on increasing the shear resistance of the pier cap would have a minimal effect on the ultimate capacity of the pier cap-column assembly.

The strut and tie method, as outlined in AASHTO 2007, provides a conservative assessment of the strength of bridge pier caps regardless of the presence of internal shear reinforcement. The strut and tie method accurately predicts the behavior of externally post-tensioned pier cap specimens up to the point of yielding of the tension reinforcement, which the AASHTO strut and tie analysis considers a limit state. The strut and tie method, however, is not capable of predicting the presence or effect of the stress concentration at the reentrant corner of the pier cap and column.

A strain energy analysis was used to compare the strut and tie models of a pier cap, with an a/d ratio of 1.53, with and without the external post-tensioning system. This strain energy analysis determined that the single strut mechanism forms at an angle of 45 degrees, because it requires lower strain energy than a multiple strut mechanism. Multiple struts can be formed at larger angles of inclination only by post-tensioning the specimen to 78% or more of the force transferred through the pier cap between the column and support. This finding was observed both in the strain energy analysis of the pier cap specimens and the tests on deep beam H-E1-PT. It can be concluded for any strengthening technique to be effective at altering the strut mechanism within a pier cap with an a/d ratio of 1.5 or less, it must input energy into the load carrying system. Any purely passive strengthening technique that relies of the deformation of the pier cap to engage it will be ineffective at altering the internal strut and tie mechanism.

APPENDIX A EXAMPLE STRUT AND TIE CALCULATIONS

A.1 Example of single strut calculation for beam specimens

The following computation was performed on the specimen configuration of test H-E1 outlined in Figure A.1. The steps of the strut and tie analysis performed in accordance with Article 5.6.3 of the AASHTO LRFD Bridge Design Specification 2007, include sizing of each of the nodes, and checking the capacity of each of the concrete strut and steel ties. Only the final iteration of this process is outlined here. The capacity of the strut and tie model was found to be governed by the strength of the compression strut. The resulting strut and tie analysis presented below produced the geometry illustrated in Figure A.1.

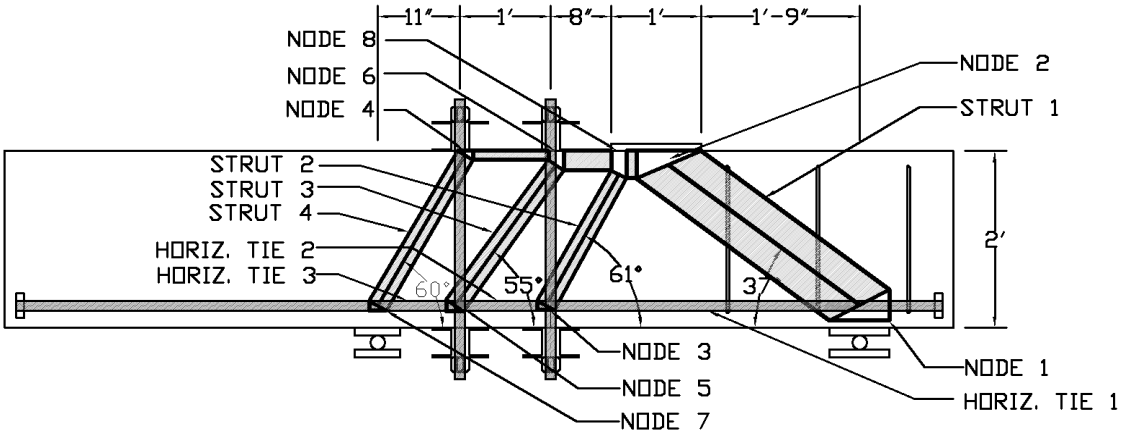

Figure A.1 Test H-E1 strut and tie model

Given:

$A_s = area\ steel\ in\ tie\ 1 = 3.12\ in.^2$
$f_y = yeild\ strength\ steel\ in\ tie\ 1 = 68.8ksi$
$E_s = elastic\ modulus\ steel\ in\ tie\ 1 = 28{,}890\ ksi$
$f_c' = concrete\ compressive\ strength = \ 3.42\ ksi$
$h = height\ of\ specimens = 24\ in.$
$d = depth\ to\ centroid\ of\ tie\ 1 = h - 3 = 21\ in.$
$a = horizontal\ distance\ bettween\ node\ 1\ and\ 2 = 21 + \frac{l_{b2}}{2}$
$b = secimen\ width = 12\ in.$

Assume:

$$l_b = length\ of\ node\ 1 = 8\ in.$$
$$\varepsilon_s = strain\ in\ steel\ tie\ 1 = 0.00144$$

Calculate:

$$f_{cu1} = compression\ strength\ node\ 1 = 0.75 f_c' = 2.57\ ksi$$
$$f_{cu2} = compression\ strength\ node\ 2 = 0.85 f_c' = 2.91\ ksi$$

$$H = horizontal\ force\ in\ strut\ 1 = A_s E_s \varepsilon_s = 130\ kips$$
$$h_a = height\ of\ node\ 1 = \frac{H}{f_{cu1} b} = 4.21\ in.$$
$$h_s = height\ of\ node\ 2 = \frac{H}{f_{cu2} b} = 3.71\ in.$$

Solve for l_{b2} and θ:

$$l_{b2} = length\ of\ node\ 2$$
$$w_s = width\ of\ strut\ 1 = l_b \sin(\theta) + h_a \cos(\theta)$$
$$w_s = l_{b2} \sin(\theta) + h_s \cos(\theta)$$
$$\theta = angle\ of\ inclination\ of\ strut\ 1 = \tan^{-1}\left(\frac{d - \frac{h_s}{2}}{a}\right)$$
$$l_{b2} = 8.66 \text{ in.} \qquad \theta = 37.1° \qquad w_s = 8.18\ in.$$

Compression strut strength:

$$\varepsilon_{s1} = \varepsilon_s + (0.002 + \varepsilon_s)\left(\frac{1}{\tan(\theta)}\right)^2 = 0.00746$$
$$f_{cu3} = compression\ strength\ of\ strut\ 1 =$$
$$min\left[\left(\frac{f_c'}{(0.8 + 170\varepsilon_{s1})}\right), (.85 f_c')\right] = 1.65\ ksi$$

Check strut width then adjust ε_s and l_b :

$$F_s = force\ in\ strut\ 1 = \frac{H}{\cos(\theta)} = 162\ kips$$
$$w_s = \frac{F_s}{f_{cu3} b} = 8.18\ in.$$

Compute shear capacity:

$$V = vetical\ force\ in\ strut\ 1 = H \tan(\theta) = 98\ kips$$

The same analysis is then applied to the rest of the nodes, ties, and struts in the specimen computing the node size and angle of inclination of each strut. The final step

is to check that the horizontal and vertical forces within the specimen are in equilibrium. In the example above, there was a 6% difference in the force in the tension reinforcement between the left and right spans in Figure A.1. This difference was eliminated by shifting the locations of nodes 3 and 5 (Figure A.1) 0.68 inches to the left, and the locations of nodes 4 and 6 0.68 inches to the right. This was done to reduce the angle of the diagonal compression struts 2, 3, and 4; increasing the horizontal force component in each strut and balancing then against diagonal compression strut 1. The justification for shifting the nodes horizontally was because the struts were smaller than the beam plates used on the top and bottom of the specimen, so it was possible for the struts to shift from the center of the plates.

A.2 Example of double strut calculation for beam specimens

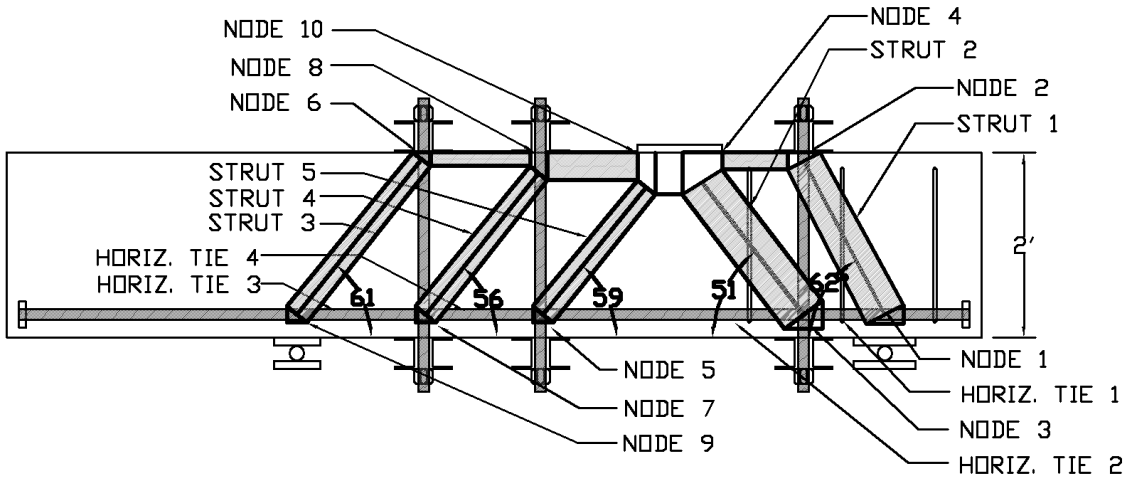

Figure A.2 Test H-E1-PT strut and tie model

Given:

$A_s = area\ steel\ in\ tie\ 1\ and\ 2 = 3.12\ in.^2$
$f_y = yeild\ strength\ steel\ in\ tie\ 1\ and\ 2 = 68.8\ ksi$
$E_s = elastic\ modulus\ steel\ in\ tie\ 1\ and\ 2 = 28{,}890\ ksi$
$f_c' = concrete\ compressive\ strength = \ 3.42\ ksi$
$h = height\ of\ specimens = 24\ in.$
$d = depth\ to\ centroid\ of\ tie\ 1 = h - 3 = 21\ in.$

$a = horizontal\ distance\ bettween\ node\ 3\ and\ 4 = 10.5 + \frac{l_{b4}}{2}$

$b = secimen\ width = 12\ in.$

Assume:

$$l_{b1} = length\ of\ node\ 1 = 4.43\ in.$$
$$\varepsilon_{si} = steel\ strain\ strut\ 1 = 0.000946$$
$$l_{b3} = length\ of\ node 3 = 5.28\ in.$$
$$\varepsilon_{sii} = steel\ strain\ strut\ 2 = 0.00238$$

Calculate:

$$f_{cu1} = compressive\ strength\ node\ 1\ and\ 3 = 0.75f_c' = 2.57\ ksi$$
$$f_{cu2} = compressive\ strength\ node\ 2\ and\ 4 = 0.85f_c' = 2.91\ ksi$$
$$H_1 = horizontal\ force\ strut\ 1 = A_s E_s \varepsilon_{si} = 85\ kips$$
$$h_{a1} = height\ of\ node\ 1 = \frac{H_1}{f_{cu1} b} = 2.77\ in.$$
$$h_{s1} = height\ of\ node\ 2 = \frac{H_1}{f_{cu2} b} = 2.44\ in.$$
$$H_2 = horizontal\ force\ strut\ 2 = A_s E_s (\varepsilon_{sii} - \varepsilon_{si}) = 130\ kips$$
$$h_{a2} = height\ node\ 3 = \frac{H_2}{f_{cu1} b} = 4.21\ in.$$
$$h_{s2} = height\ node\ 4 = \frac{H_2}{f_{cu2} b} = 3.72\ in.$$

Solve for l_{b2}, θ_1, l_{b4} and θ_2:

$$l_{b2} = length\ of\ node\ 2$$
$$w_{s1} = width\ strut\ 1 = l_{b1} \sin(\theta_1) + h_{a1} \cos(\theta_1)$$
$$w_{s1} = l_{b2} \sin(\theta_1) + h_{s1} \cos(\theta_1)$$
$$\theta_1 = angle\ of\ inclination\ strut\ 1 = \tan^{-1}\left(\frac{d - \frac{h_{s1}}{2}}{10.5}\right)$$

$$l_{b4} = length\ of\ node\ 4$$
$$w_{s2} = width\ strut\ 2 = l_{b3} \sin(\theta_2) + (h_{a2} + h_{a1}) \cos(\theta_2)$$
$$w_{s2} = l_{b4} \sin(\theta_2) + (h_{s2} + h_{s1}) \cos(\theta_2)$$
$$\theta_2 = angle\ of\ inclination\ strut\ 2 = \tan^{-1}\left(\frac{d - \frac{h_{s2}}{2} - h_{s1}}{10.5 + \frac{l_{b4}}{2}}\right)$$

$l_{b2} = 4.60$ in. $\quad \theta_1 = 62.0° \quad w_{s1} = 5.2\ in.$

$l_{b4} = 5.95$ in. $\quad \theta_2 = 51.1° \quad w_{s2} = 8.5\ in.$

Compression strut strength:

$$\varepsilon_{s1i} = \varepsilon_{si} + (0.002 + \varepsilon_{si})\left(\frac{1}{\tan(\theta_1)}\right)^2 = 0.00178$$

$$f_{cu3} = compression\ strength\ of\ strut\ 1 = min\left[\left(\frac{f_c'}{(0.8 + 170\varepsilon_{s1i})}\right), (.85f_c')\right] = 2.91\ ksi$$

$$\varepsilon_{s1ii} = \varepsilon_{sii} + (0.002 + \varepsilon_{sii})\left(\frac{1}{\tan(\theta_2)}\right)^2 = 0.00523$$

$$f_{cu4} = compression\ strength\ of\ strut\ 2 = min\left[\left(\frac{f_c'}{(0.8 + 170\varepsilon_{s1ii})}\right), (.85f_c')\right] = 2.02\ ksi$$

Check strut width then adjust ε_s and l_b :

$$F_{s1} = force\ in\ strut\ 1 = \frac{H_1}{\cos(\theta_1)} = 182\ kips$$

$$w_{s1} = \frac{F_{s1}}{f_{cu3}b} = 5.2\ in.$$

$$F_{s2} = force\ in\ strut\ 2 = \frac{H_2}{\cos(\theta_2)} = 206\ kips$$

$$w_{s2} = \frac{F_{s2}}{f_{cu4}b} = 8.5\ in.$$

Compute shear capacity:

$$V_1 = vertical\ force\ in\ strut\ 1 = H_1 \tan(\theta_1) = 161\ kips$$

$$V_2 = vertical\ force\ in\ strut\ 2 = H_2 \tan(\theta_2) = 161\ kips$$

The same analysis is then applied to the rest of the nodes, ties, and struts in the specimen computing the node size and angle of inclination of each strut. The final step is to check that the horizontal and vertical forces within the specimen are in equilibrium. In the example above, there was a 0.8% difference in the force in the tension reinforcement between the left and right spans in Figure A.2. This difference was eliminated by shifting the locations of nodes 6 and 8 (Figure A.1) 0.05 inches to the left, and the locations of nodes 5 and 7 0.05 inches to the right. This was done to increase the angle of diagonal compression struts 2, 3, and 4; decreasing the horizontal force

component in each strut and balancing then against the horizontal force in compression strut 1 and 2. The justification for shifting the nodes horizontally was because the struts were smaller than the beam plates used on the top and bottom of the specimen, so it was possible for the struts to shift from the center of the plates.

A.3 Example of single strut calculation for pier cap specimens

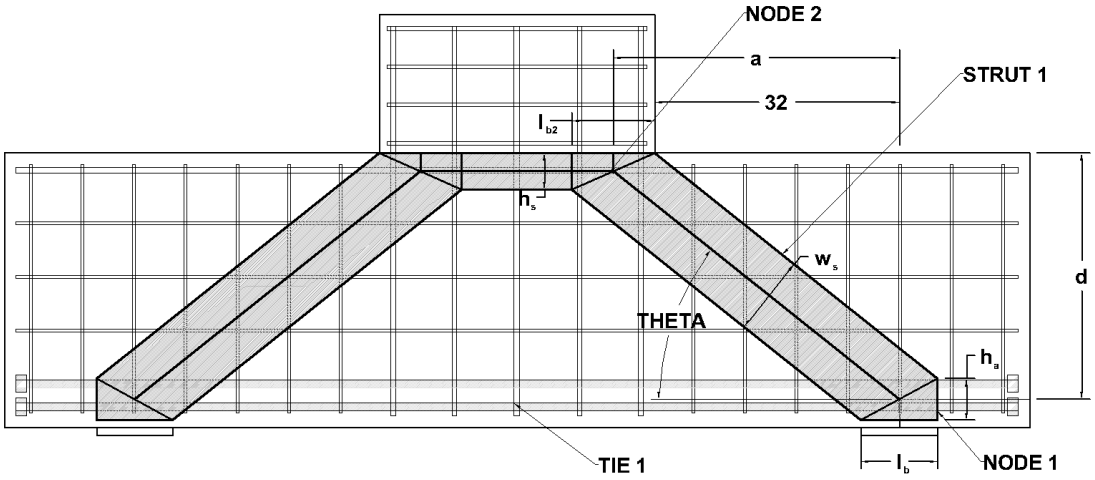

Figure A.3 Pier cap specimen strut and tie mechanism

Given:

$A_s = area\ steel\ in\ tie\ 1 = 3.95\ in.^2$
$f_y = yeild\ strength\ steel\ in\ tie\ 1 = 73\ ksi$
$E_s = elastic\ modulus\ steel\ in\ tie\ 1 = 27{,}460\ ksi$
$f_c' = concrete\ compressive\ strength = \ 3.43\ ksi$
$h = height\ of\ specimens = 36\ in.$
$d = depth\ to\ centroid\ of\ tie\ 1 = h - 3.75 = 32.25\ in.$
$a = horizontal\ distance\ bettween\ node\ 1\ and\ 2 = 32 + \frac{l_{b2}}{2}$
$b = secimen\ width = 12\ in.$

Assume:

$$l_b = length\ of\ node\ 1 = 10\ in.$$
$$\varepsilon_s = strain\ in\ steel\ tie\ 1 = 0.001548$$

Calculate:

$$f_{cu1} = compression\ strength\ node\ 1 = 0.75 f_c' = 2.57\ ksi$$
$$f_{cu2} = compression\ strength\ node\ 2 = 0.85 f_c' = 2.92\ ksi$$

$$H = horizontal\ force\ in\ strut\ 1 = A_s E_s \varepsilon_s = 168\ kips$$

$$h_a = height\ of\ node\ 1 = \frac{H}{f_{cu1} b} = 5.45\ in.$$
$$h_s = height\ of\ node\ 2 = \frac{H}{f_{cu2} b} = 4.79\ in.$$

Solve for l_{b2} and θ:

$$l_{b2} = length\ of\ node\ 2$$
$$w_s = width\ of\ strut\ 1 = l_b \sin(\theta) + h_a \cos(\theta)$$
$$w_s = l_{b2} \sin(\theta) + h_s \cos(\theta)$$
$$\theta = angle\ of\ inclination\ of\ strut\ 1 = \tan^{-1}\left(\frac{d - \frac{h_s}{2}}{a}\right)$$
$$l_{b2} = 10.8 \text{ in.} \qquad \theta = 38.6° \qquad w_s = 10.5\ in.$$

Compression strut strength:

$$\varepsilon_{s1} = \varepsilon_s + (0.002 + \varepsilon_s)\left(\frac{1}{\tan(\theta)}\right)^2 = 0.00712$$
$$f_{cu3} = compression\ strength\ of\ strut\ 1 =$$
$$min\left[\left(\frac{f_c'}{(0.8 + 170\varepsilon_{s1})}\right), (.85 f_c')\right] = 1.71 ksi$$

Check strut width then adjust ε_s and l_b :

$$F_s = force\ in\ strut\ 1 = \frac{H}{\cos(\theta)} = 215 kips$$
$$w_s = \frac{F_s}{f_{cu3} b} = 10.5\ in.$$

Compute shear capacity:

$$V = vetical\ force\ in\ strut\ 1 = H \tan(\theta) = 134\ kips$$

A.4 Example of double strut calculation for pier cap specimens

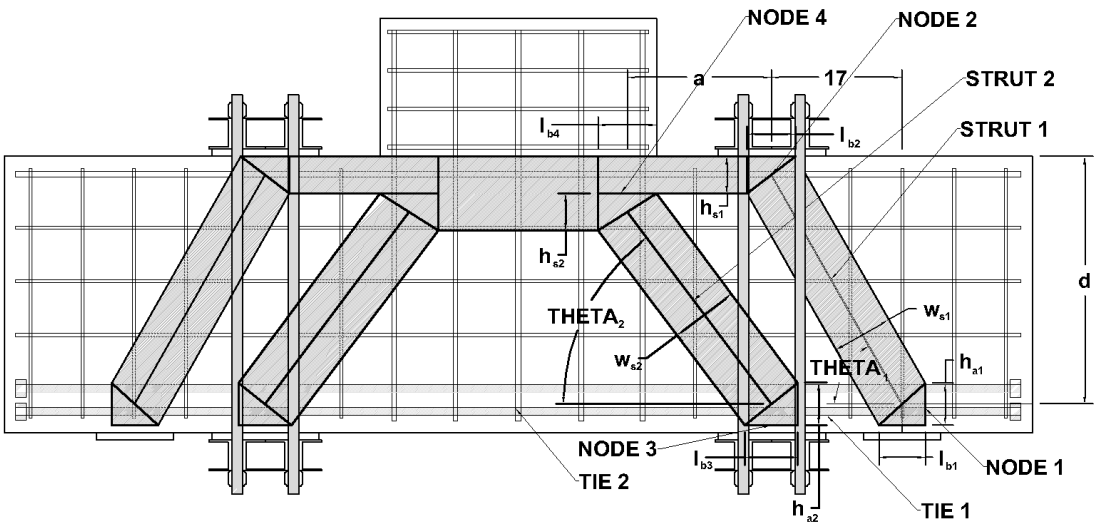

Figure A.4 Post-tensioned pier cap specimen strut and tie mechanism

Given:

$A_s = area\ steel\ in\ tie\ 1\ and\ 2 = 3.95\ in.^2$
$f_y = yeild\ strength\ steel\ in\ tie\ 1\ and\ 2 = 73\ ksi$
$E_s = elastic\ modulus\ steel\ in\ tie\ 1\ and\ 2 = 27{,}460\ ksi$
$f_c' = concrete\ compressive\ strength = \ 3.55\ ksi$
$h = height\ of\ specimens = 36\ in.$
$d = depth\ to\ centroid\ of\ tie\ 1 = h - 3.75 = 32.25\ in.$
$a = horizontal\ distance\ bettween\ node\ 3\ and\ 4 = 17 + \frac{l_{b4}}{2}$
$b = secimen\ width = 12\ in.$

Assume:

$$l_{b1} = length\ of\ node\ 1 = 6.03\ in.$$
$$\varepsilon_{si} = steel\ strain\ strut\ 1 = 0.00117$$
$$l_{b3} = length\ of\ node3 = 6.86\ in.$$
$$\varepsilon_{sii} = steel\ strain\ strut\ 2 = 0.002658$$

Calculate:

$$f_{cu1} = compressive\ strength\ node\ 1\ and\ 3 = 0.75f_c' = 2.66\ ksi$$
$$f_{cu2} = compressive\ strength\ node\ 2\ and\ 4 = 0.85f_c' = 3.02\ ksi$$
$$H_1 = horizontal\ force\ strut\ 1 = A_sE_s\varepsilon_{si} = 127\ kips$$
$$h_{a1} = height\ of\ node\ 1 = \frac{H_1}{f_{cu1}b} = 3.98\ in.$$
$$h_{s1} = height\ of\ node\ 2 = \frac{H_1}{f_{cu2}b} = 3.50\ in.$$
$$H_2 = horizontal\ force\ strut\ 2 = A_sE_s(\varepsilon_{sii} - \varepsilon_{si}) = 161\ kips$$

$$h_{a2} = height\ node\ 3 = \frac{H_2}{f_{cu1} b} = 5.04\ in.$$

$$h_{s2} = height\ node\ 4 = \frac{H_2}{f_{cu2} b} = 4.44\ in.$$

Solve for l_{b2}, θ_1, l_{b4} and θ_2:

$$l_{b2} = length\ of\ node\ 2$$

$$w_{s1} = width\ strut\ 1 = l_{b1} \sin(\theta_1) + (h_{a1}) \cos(\theta_1)$$

$$w_{s1} = l_{b2} \sin(\theta_1) + h_{s1} \cos(\theta_1)$$

$$\theta_1 = angle\ of\ inclination\ strut\ 1 = \tan^{-1}\left(\frac{d - \frac{h_{s1}}{2}}{17}\right)$$

$$l_{b4} = length\ of\ node\ 4$$

$$w_{s2} = width\ strut\ 2 = l_{b3} \sin(\theta_2) + (h_{a2} + h_{a1}) \cos(\theta_2)$$

$$w_{s2} = l_{b4} \sin(\theta_2) + (h_{s2} + h_{s1}) \cos(\theta_2)$$

$$\theta_2 = angle\ of\ inclination\ strut\ 2 = \tan^{-1}\left(\frac{d - \frac{h_{s2}}{2} - h_{s1}}{15 + \frac{l_{b4}}{2}}\right)$$

$l_{b2} = 6.29$ in. $\quad \theta_1 = 60.9° \quad w_{s1} = 7.2\ in.$

$l_{b4} = 7.61$ in. $\quad \theta_2 = 54.7° \quad w_{s2} = 10.8\ in.$

Compression strut strength:

$$\varepsilon_{s1i} = \varepsilon_{si} + (0.002 + \varepsilon_{si})\left(\frac{1}{\tan(\theta_1)}\right)^2 = 0.00216$$

$$f_{cu3} = compression\ strength\ of\ strut\ 1 =$$

$$min\left[\left(\frac{f_c'}{(0.8 + 170\varepsilon_{s1i})}\right), (.85 f_c')\right] = 3.02 ksi$$

$$\varepsilon_{s1ii} = \varepsilon_{sii} + (0.002 + \varepsilon_{sii})\left(\frac{1}{\tan(\theta_2)}\right)^2 = 0.005$$

$$f_{cu4} = compression\ strength\ of\ strut\ 2 =$$

$$min\left[\left(\frac{f_c'}{(0.8 + 170\varepsilon_{s1ii})}\right), (.85 f_c')\right] = 2.15 ksi$$

Check strut width then adjust ε_s and l_b :

$$F_{s1} = force\ in\ strut\ 1 = \frac{H_1}{\cos(\theta_1)} = 261 kips$$

$$w_{s1} = \frac{F_{s1}}{f_{cu3} b} = 7.2\ in.$$

$$F_{s2} = force\ in\ strut\ 2 = \frac{H_2}{\cos(\theta_2)} = 279 kips$$

$$w_{s2} = \frac{F_{s2}}{f_{cu4} b} = 10.8\ in.$$

Compute shear capacity:

$$V_1 = vertical\ force\ in\ strut\ 1 = H_1 \tan(\theta_1) = 228\ kips$$

$$V_2 = vertical\ force\ in\ strut\ 2 = H_2 \tan(\theta_2) = 228\ kips$$

APPENDIX B STRUT AND TIE STRAIN ENERGY ANALYSIS

Strut and Tie Strain Energy Analysis Un-Rehabilitated Specimen

$P = 390\ kips$
$f_c' = 3.5\ ksi$
$E_c = 3370\ ksi$
$b_w = 12\ in$
$d = 32.75\ in$
$h = 36\ in$
$\theta = 40°$
$E_s = 29000\ ksi$
$A_s = 5 * .79 = 3.95\ in^2$

Compression strut node size at ultimate load

Vertical size

$$w_v = \frac{V}{0.85 f_c' b_w} = \frac{195}{0.85(3.5)12} = 5.5\ in$$

Horizontal size

$$w_h = \frac{\frac{V}{\tan\theta}}{0.85 f_c' b_w} = \frac{\frac{195}{\tan 40}}{0.85(3.5)12} = 6.5\ in$$

Diagonal Strut Width

$$w_s = \sqrt{5.5^2 + 6.5^2} = 8.5\ in$$

Diagonal Strut Length

$$l_s = \sqrt{28^2 + 33.4^2} = 43.6\ in$$

Compute Strain Energy in Terms of Shear V = P/2

Compression Struts

Diagonal Strut (total of 2)

$$F_{strut} = \frac{V}{\sin\theta} = 1.556V$$

$$U_{st} = 2\frac{(F_{strut})^2 l_s}{E_c b_w w_s} = 2\frac{(1.556V)^2 43.6}{3370(12)8.5} = 6.1419 \times 10^{-4} V^2$$

Horizontal Compression Strut

$$l_h = 32\ in$$

$$F_h = \frac{V}{\tan\theta} = \frac{V}{\tan 40} = 1.192V$$

$$U_h = \frac{(F_h)^2 l_h}{E_c b_w w_h} = \frac{(1.192V)^2 32}{3370(12)6.5} = 1.7297 \times 10^{-4} V^2$$

Tension Tie

$$l_{tie} = 100\ in$$

$$F_{tie} = \frac{V}{\tan\theta} = \frac{V}{\tan 40} = 1.192V$$

$$U_t = \frac{(F_{tie})^2 l_{tie}}{E_s A_s} = \frac{(1.192V)^2 100}{29000(3.95)} = 12.4039 \times 10^{-4} V^2$$

Strain Energy Computation

$$U = U_t + U_h + 2 \times U_{st}$$

$$U = 12.4039 \times 10^{-4} V^2 + 1.7297 \times 10^{-4} V^2 + 6.1419 \times 10^{-4} V^2 = 20.28 \times 10^{-4} V^2$$

Strut and Tie Strain Energy Analysis Rehabilitated Specimen

$P = 500\ kips$
$f_c' = 3.5\ ksi$
$E_c = 3370\ ksi$
$b_w = 12\ in$
$d = 32.75\ in$
$h = 36\ in$
$\theta = 60°$
$E_s = 29000\ ksi$
$A_s = 5 * .79 = 3.95\ in^2$

Compression strut node size at ultimate load

Vertical size

$$w_v = \frac{V}{0.85 f_c' b_w} = \frac{195}{0.85(3.5)12} = 5.5\ in$$

Horizontal size

$$w_h = \frac{\frac{V}{\tan\theta}}{0.85 f_c' b_w} = \frac{\frac{195}{\tan 60}}{0.85(3.5)12} = 3.2\ in$$

Diagonal Strut Width

$$w_s = \sqrt{5.5^2 + 3.2^2} = 6.4\ in$$

Diagonal Strut Length

$$l_s = \sqrt{30^2 + 17^2} = 34.5\ in$$

Compute Strain Energy in Terms of Shear V = P/2

Compression Struts

Diagonal Strut (total of 4)

$$F_{strut} = \frac{V}{\sin\theta} = \frac{V}{\sin 60} = 1.15V$$

$$U_{st} = 4\frac{(F_{strut})^2 l_s}{E_c b_w w_s} = 4\frac{(1.15V)^2 34.5}{3370(12)6.4} = 7.0515 \times 10^{-4}V^2$$

Horizontal Compression Strut 1 (total of 2)

$$w_{h1} = w_h = 3.2in$$

$$l_{h1} = 17\ in$$

$$F_{h1} = \frac{V}{\tan\theta} = \frac{V}{\tan 60} = 0.577V$$

$$U_{h1} = 2\frac{(F_{h1})^2 l_{h1}}{E_c b_w w_{h1}} = 2\frac{(0.577V)^2 17}{3370(12)3.2} = 0.8747 \times 10^{-4}V^2$$

Horizontal Compression Strut 2

$$l_{h2} = 32\ in$$

$$w_{h2} = w_{h1} + w_h = 6.4\ in$$

$$F_{h2} = \frac{V}{\tan\theta} + F_{h1} = \frac{V}{\tan 60} + 0.577V = 1.154V$$

$$U_{h2} = \frac{(F_{h2})^2 l_{h2}}{E_c b_w w_{h2}} = \frac{(1.154V)^2 32}{3370(12)6.4} = 1.6465 \times 10^{-4}V^2$$

Tension Tie 1 (total of 2)

$$l_{tie1} = 17\ in$$

$$F_{tie1} = \frac{V}{\tan\theta} = \frac{V}{\tan 60} = 0.577V$$

$$U_{t1} = 2\frac{(F_{tie1})^2 l_{tie1}}{E_s A_s} = 2\frac{(0.577V)^2 17}{29000(3.95)} = 0.9882 \times 10^{-4}V^2$$

Tension Tie 2

$$l_{tie2} = 66\ in$$

$$F_{tie2} = \frac{V}{\tan\theta} + F_{tie1} = \frac{V}{\tan 60} + 0.577V = 1.154V$$

$$U_{t2} = \frac{(F_{tie2})^2 l_{tie2}}{E_s A_s} = \frac{(1.154V)^2 66}{29000(3.95)} = 7.6729 \times 10^{-4} V^2$$

Post-Tensioned Vertical Strut (The load case of interest occurs when the shear V exceeds the pre-compression F_{pc})

$$U_{pc} = \frac{-(F_{pc})^2 36}{3370(12)14} + \frac{(V)^2 36}{3370(12)14} + \frac{-(F_{pc})^2 69}{29000(5.08)} + \frac{(V)^2 69}{29000(5.08)}$$

$$= 5.3195 \times 10^{-4} V^2 - 5.3195 \times 10^{-4} F_{pc}^2$$

Total

$$U = 7.6729 \times 10^{-4} V^2 + 0.9882 \times 10^{-4} V^2 + 1.6465 \times 10^{-4} V^2$$

$$+0.8747 \times 10^{-4} V^2 + 7.0515 \times 10^{-4} V^2 + 5.3195 \times 10^{-4} V^2 - 5.3195 \times 10^{-4} F_{pc}^2$$

$$= 23.5533 \times 10^{-4} V^2 - 5.3195 \times 10^{-4} F_{pc}^2$$

Set Equal to Un-Rehabilitated Specimen and Solve for Pre-Compression

$$20.28 \times 10^{-4} V^2 = 23.5533 \times 10^{-4} V^2 - 5.3195 \times 10^{-4} F_{pc}^2$$

$$\sqrt{F_{pc}^2} = \sqrt{\frac{23.5533 \times 10^{-4} V^2 - 20.28 \times 10^{-4} V^2}{5.3195 \times 10^{-4}}}$$

$$F_{pc} = \sqrt{0.6153 V^2} = 0.78V$$

REFERENCES

American Concrete Institute (ACI) Committee 318 (2002). "Building code requirements for reinforced concrete," ACI 318-02. Farmington Hills, Mich.

American Concrete Institute (ACI) Committee 318 (1999). "Building code requirements for reinforced concrete," ACI 318-99. Farmington Hills, Mich.

American Society of Civil Engineers-American Concrete Institute (ASCE-ACI) Committee 426. (1973). "The shear strength of reinforced concrete members," J. Struct. Div. ASCE, 99, No, 1091-1187.

Aguilar, Gerardo Matamoros, Adolfo B. Parra-Montesinos, Gustavo J. Ramirez, Julio A. Wight, James K. (2002). "Experimental Evaluation of Design Procedures for Shear Strength of Deep Reinforced Concrete Beams," ACI Struct. J., 99(S56). 539-548

AASHTO Load and Resistance Factor Design (LRFD) Bridge Design Specification Third Edition. (2004). Am. Assoc. of State Highway and Transp. Officials, Washington, D.C.

AASHTO Load and Resistance Factor Design (LRFD) Bridge Design Specification Fourth Edition. (2007). Am. Assoc. of State Highway and Transp. Officials, Washington, D.C.

AASHTO Manual for Condition Evaluation of Bridges Second Edition. (1994). Am. Assoc. of State Highway and Transp. Officials, Washington, D.C.

AASHTO Standard Specifications for Highway Bridges Fifteenth Edition. (1992). Am. Assoc. of State Highway and Transp. Officials, Washington, D.C.

AASHTO Standard Specifications for Highway Bridges Twelfth Edition. (1977). Am. Assoc. of State Highway and Transp. Officials, Washington, D.C.

Bentz, E.C. (2000). "Sectional analysis of reinforced concrete members." Ph.D. Thesis, Dept. of Civil Eng., The University of Toronto, Toronto, Ontario.

Bollo, M. E., Mahin, S. A., Moehle, J. P., Stephen, R. M., and Qi, X. (1990). "Observations and implication of test on the Cypress Street viaduct test structure." *Rep. No. UCB/EERC-90/21*, University of California, Berkeley, Calif.

Canadian Standards Association (CSA). (1994). "Design of concrete structures: Structures (design)-A national standard of Canada." CAN-A23.3-94, Clause 11.1.2, Toronto.

CEB-FIP MC90. (1993). CEB-FIP model code 1990, Thomas Telford, London, 1993.

Collins, M. P., Bentz, E. C., Sherwood, E. G. (In Publication). "Where is shear reinforcement required? A review of research results and design procedures," Submitted to ACI Struct. J., March 12, 2007.

Ellingwood, B. R., Zureick, A.H., Wang, N., O'Malley, C. (2009). "Condition assessment of
existing bridge structures: Report of Task 4 - Development of guidelines for condition assessment, evaluation and rating of bridges in Georgia." Report of Project GDOT No. RP05-01, Georgia Department of Transportation, Atlanta, GA

Federal Highway Administration. (1995). *FHWA Seismic Retrofitting Manual*, Federal Highway Administration, U.S. Dept. of Transportation, Washington, D.C.

GDOT, Division of Permits and Operations, Office of Maintenance, "Georgia Legal Loads," Oct. 2005

Hawkins, N. M., Kuchma, D. A., Mast, R. F., Marsh, M. L., Reineck, K.-H., (2005). NCHRP Report 549: Simplified Shear Design of Structural Concrete Members, Transportation Research Board, Washington, D.C.

Kani, G. N. J. (1964). "The riddle of shear failure and its solution," *Journal of the American Concrete Institute,* 61(4), 441-467.

Kani, G. N. J. (1967). "How safe are our large, reinforced concrete beams?" *ACI Struct. J.,* 64(3), 128-141.

Kong, F. K. Robins, P. J. Cole, D. F. (1970) "Web reinforcement effects on deep beams," *ACI. J.,* 67(73), 1010-1017.

Kong, F. K. Robins, P. J. Kirby, D. P., Short, D. R. (1972a) "Deep beams with inclined web reinforcement," *ACI. J.,* 69(16), 172-176.

Kong, F. K. Robins, P. J., Singh, A., Sharp, G. R. (1972b) "Shear analysis and design of reinforced concrete deep beams," *Struct. Eng., 50(10), 405-409.*

Loov, R. (1998). "Review of A23.3-94 simplified method of shear design and comparision with results using shear friction." Canadian Journal of Civil Engineering, 25, 437-449.

O'Malley, C., Wang, N., Ellingwood, B. R., Zureick, A.H. (2009). "Condition assessment of
existing bridge structures: Report of Task 2 and 3 – Bridge Testing Program." Report of Project GDOT No. RP05-01, Georgia Department of Transportation, Atlanta, GA

Peng, L. (1999). "Shear strength of beams by shear friction." M.A.Sc. thesis, the University of Calgary, Calgary Alberta.

Schiessl, Peter; Raupach, Michael (1997). "Laboratory studies and calculations on the influence of crack width on chloride-induced corrosion of steel in concrete," *ACI Materials Journal*, 94(1), 56-62.

Saatcioglu, M., Yalcin, C. (2003). "External prestressing concrete columns for improved seismic shear resistance," *J. Struct. Engrg.,* ASCE 129(8), 1057-1070.

Smith, K. H., Vabtsiotis, A. S. (1982) "Shear strength of deep beams," *ACI. J.*, 79(22), 201-213.

Somo, S., Hong, H. P. (2006). "Modeling error analysis of shear predicting models for RC beams," Structural Safety, 28(3), 217-230.

Standard Specifications for Highway Bridges Fourth Edition. (1944). Am. Assoc. of State Highway Officials, Washington, D.C.

Standard Specifications for Highway Bridges Sixth Edition. (1953). Am. Assoc. of State Highway Officials, Washington, D.C.

Tan, K. H., Cheng, G. H. (2006). "Size effect on shear strength of deep beams: Investigating with strut-and-tie model," *J. Struct. Engrg.,* ASCE 132(5), 673-685.

Tan, K. H., Cheng, G. H., and Cheong, H. K. (2003). "Size effect in shear strength of large beams – Behavior and finite element modeling," *Mag. Concrete Res*., to be published.

Tan, K.H., Lu, H. Y. (1999). "Shear behavior of large reinforced concrete deep beams and code comparisons," *ACI Struct. J.*, 96(5), 836-845.

Tan, K. H., Tong, K., Tang, C. Y. (1995) "High-strength concrete deep beams with effective span and shear span variations," *ACI Struct. J.*, 92(S37), 395-405.

Tang, C. Y., Tan, K. H. (2004). "Interactive mechanical model for shear strength of deep beams," *J. Struct. Engrg.,* ASCE 130(10), 1534-1544.

Tonias, Demetrios E. P.E., Zhao, Jim J. P.E. (2007) Bridge Engineering Second Edition, McGraw-Hill Companies, Inc. Pg. 98-99

Vecchio F. J., Collins, M. P. (1986) "Modified compression field theory for reinforced concrete elements subjected to shear," *ACI Struct. J.*, 83(2), 219-231.

Zhang, Zhichao, Hsu, Cheng-Tzu Thomas, Moren, Jon (2004). "Shear strengthening of reinforced concrete deep beams using carbon fiber reinforced polymer laminates." Journal *J. Compos. for Constr.,* ASCE, 8(5), 403-414.

Zsutty, T. C., 1986. “Beam shear strength prediction by analysis of existing data.” ACI Journal, 45(11), 943-951.

Zsutty, T. C., 1971. “Beam shear strength prediction for separate categories of simple beam tests.” ACI Journal, 68(2), 138-143.